DEVELOPMENT OF OPTIMAL TOTAL HIP JOINT REPLACEMENT

MOHAMMAD RABBANI

Dissertation for the degree of

Doctor of Philosophy

School of Engineering

& the Built Environment

2018

In The Name Of God

Acknowledgment

This project is certainly the most significant academic accomplishment of my life, and without the wonderful people who have supported and believed in me, this thesis would not have been possible.

It is with great pleasure that I sincerely thank those who have helped me on this journey. Firstly, I would also like to thank Professor Michal Krzyzanowski, my senior supervisor at the school of engineering and the built environment for his contribution and suggestions that made a difference. I'd like to express my sincere appreciation to Professor Hanifa Shah, my second supervisor. I am very grateful for her guidance, intensive supervision, and trust through my candidature. Her energy and enthusiasm in research have been a major source of motivation to me.

I extend my sincere appreciation to Professor Hossein Saidpour through my Ph.D. candidature. His knowledge and advice contributed enormously to my journey through the research world. This thesis would likely not have matured had it not been for his support and inspiration.

I have the deepest gratitude to my lovely parents, wonderful brother and also my uncle Dr. Masoud Rabbani, who continue to offer their unwavering support, love and encouragement to keep me moving forward throughout my entire education. I love you all.

I dedicate this work to my kind and lovely parents. There's no doubt in my mind that, without your constant love, endless encouragement and support, I would not have achieved this outcome.

List of publications

- Rabbani, M and Saidpour, H (2015) “Stress analysis of a cementless hip join replacement subjected to realistic loading conditions” Journal of Robotics and Mechanical Engineering Research.
- Rabbani, M and Saidpour, H (2012) “Stress analysis of a cementless hip prosthesis under nine heavy-loading and frequent activities of daily living” Proceedings of Advances in Computing and Technology 7th Annual Conference.
- Rabbani, M and Saidpour, H (2011) ‘Finite element simulation of the hip joint’ Proceedings of Advances in Computing and Technology 6th Annual Conference, ISBN 978-0-9564747-1-1, pp 116-127, http://hdl.handle.net/10552/1344.
- Rabbani, M. and Saidpour, H. (2010) ‘Optimum design of artificial hip joints’, Proceedings of Advances in Computing and Technology, pp.127-134, 27, ISBN 978-0-9564747-0-4.

Abstract

Total hip replacement (THR) is a surgical process in which the hip joint is replaced by a hip prosthesis. It is one of the most popular and cost effective surgery. In particular in 2014, 83,125 primary procedures were recorded. Some of these operations need to be carried out again for different reasons after sometime. These are called revision (replacement of the prosthesis) procedures. Important studies and statistics suggest that the number of THR procedures is projected to increase by almost 175% by 2030.

Aseptic loosening appears to be the most significant cause of failure in THR. Aseptic loosening might lead to revision surgery and in turn can be avoided by enhancing the stability and durability of the hip replacement. Primary stability attained after surgery is a determinant issue for the long-term stability of cementless hip arthroplasty. Primary stability is the level of relative micromotion between the femur and the prosthesis induced via the physiological joint forces following the surgery. The hip prosthesis is also exposed to dynamic loadings and activities of daily living, which can induce the stress distribution on the prosthesis of the hip joint model and affect the durability of the implant.

The aim of this study is to develop an optimal total hip replacement (THR) implant with new and improved design features to achieve stability and durability. The micromotion between bone and implant interface and the stress distribution on the prosthesis and femur assembly has been reviewed and investigated.

The laboratory testing were carried out on the femur including the compression, torsion and Brinell hardness testing. A compression testing using strain gauge technique done on the hip implant. Finite element analysis software used to simulate all compression and torsion testing assuming the same boundary and loading conditions and subsequently the computational results were compared with the earlier experimental data to verify the experiments and models used.

The comparative micromotion studies and findings of other researchers were used beside the clinical follow-up reports on success or failure rates of related hip designs, to justify the best solutions for design factors. In this computational approach researchers usually use finite element methodology to calculate micromotion of elements, sometimes known as migration. The elements exceeding the threshold limit would simulate the migration and subsequently eliminated from the assembly. This procedure recurs until reaching the convergence that derives a stable mechanical equilibrium.

One of the restrictions of micromotion analysis was the inability to divide the final results into axial and rotational components. Therefore it would have been inappropriate to eventually conclude the best femoral stem, without considering the sustaining torsional loadings. Another limitation was that the micromotion analysis would not reflect the stress distribution on the hip prosthesis and consequently would ignore the potential high stress concentration that is associated with post operative pain as well as low durability and long-term stability. For these reasons stress analysis was carried out under dynamic loadings of nine different activities to examine the von Mises stress, shear stress and principal stress distribution of a cementless hip implant. In each activity realistic boundary and loading conditions of a complete assembly of femur and hip implant were investigated which includes defining of many variables including different geometry, material properties, boundary conditions, forces and moments of varying magnitude and orientation over specific time intervals. The critical points and areas that were developed in the entire 3D model were evaluated and explained.

The finite element analysis which verified by experimental testing and hold the clinical relevance were used to decide the best optimal hip stem design amongst different presented design concepts. This was accompanied and improved with further stress analysis of different design factors to get the final optimal model. High offset stem option is a unique feature that helps tightening the abductor and boosts the hip implant stability with the ability to adjust neck and offset. It gives a surgeon more options to fix the most accurate offset and do the operation more effectively. The final optimal design and its advantages were presented in the last chapter.

Table of Contents

List of figures

List of tables

Glossary

Ansys, Catia, Solidworks	Computer software for engineering modelling and simulation.
Arthroplasty	The surgical repairing or replacement of a joint.
Cancellous Bone	The spongy bone found at the end of long bones consisting of regularly ordered mineralized collagen fibres in a looser array than in the lamellar bone of the shaft.
Cortical Bone	Dense or compact bone, found mainly in the shafts (diaphyses) of long bones, accounting for about 80% of total body bone.
Coxa	Scientific name for hip joint.
Diaphyseal	The shaft or midsection of femur.
Endoprosthesis (*plural* Endoprostheses)	A synthetic insert or prosthesis placed within the body.
Flexion, Abduction, Adduction, Extension, Rotation,Circumduction	Anatomical motions.
Gluteus maximus	The very powerful, large buttock gluteal muscle, which has its origins on the pelvic girdle and has its insertion on the gluteal tuberosity of the femur and via a strong tendon on the iliotibial band. The primary actions of it are extension and lateral rotation of the femur.
Gluteus Medius	A thick buttock muscle covered by the gluteus maximus. Its origin is on the lateral, posterior surface of the ilium, and its insertion is on the lateral aspect of the greater trochanter of the femur. Its primary actions are abduction and medial rotation of the femur.
Gluteus Minimus	The smallest and deepest of the buttock muscles. It has its origin on the lateral, posterior surface of the ilium, and its insertion on the anterior surface of the greater trochanter. Its primary actions are abduction and medial rotation of the femur.
Greater Trochanter	Quadrilateral protuberances on the proximal femur.
Ilio-Tibial Band	Fibrous tissue of hip & thigh.
Iliofemoral Ligament	Ligament of hip joint.
In vitro	Tests or observations implemented in a controlled situation outside a living organism.
In vivo	Tests or observations implemented inside a living organism.
Ischiofemoral Ligament	Ligament of hip joint.
Lesser Trochanter	Conical protuberances on the proximal femur.

Medial	Toward the midline of the body.
Lateral	Away from the midline of the body.
Anterior	Toward the front of the body.
Posterior	Toward the back of the body.
Proximal	Closer to the trunk or the origin of a structure.
Distal	Away from the midline of the trunk of a structure.
Inferior	Lower in the body in relation to another structure or surface.
Superior	Upper in the body in relation to another structure or surface.
Orthopaedics	Medical specialty in musculoskeletal system.
Osteolysis	Resorption of bone tissue.
Periprosthetic Bone	Bone Infection or fracture around an implant.
Pubofemoral Ligament	Ligament on the inferior side of the hip joint.
Sagittal	One of the three cardinal planes which runs longitudinally down the body, dividing it into right and left halves.
Frontal	One of the three cardinal planes which divides the body from left to right into front (anterior) and back (posterior) halves.
Transverse	A cardinal plane which runs horizontally at right angles to the longitudinal axis of the body, dividing it into superior (top) and inferior (bottom) halves.
Sawbone ®	Composite bone using a mixture of short glass fibers and epoxy resin.
S-N Curve	Wöhler curve representing the fatigue life of an object.
Tensor Fascia Latae	Muscle of hip & thigh.
Tribology	Study of interacting surfaces in relative motion considering friction, lubrication and wear.
Wolff's Law	Self-adaptation of bone under different loads through increasing or decreasing (stress shielding) of the bone density.

Nomenclature

ASTM	International Standards Organisation
CAD	Computer Aided Design
CJRR	Canadian Joint Replacement Registry
CMM	Coordinate Measuring Machine
CoCrMo	Cobalt Alloy (Cobalt-Chromium-Molybdenum)
DOF	Degree Of Freedom
FEA	Finite Element Analysis
FEM	Finite Element Method
FGM	Functionally Graded Material
FS	Fatemi-Socie
HA	Hydroxyapatite
HB	Brinell Hardness test unit
IPA	Isopropyl Alcohol
ISO	International Standards Organisation
JRU	Swedish Hip Arthroplasty Register
NJR	England and Wales National Joint Registry
PEEK	Polyetheretherketone
PMMA	Poly Methylmethacrylate
ROM	Range of Motion
SED	Strain Energy Density
SWT	Smith-Watson-Topper
THA	Total Hip Arthroplasty
THR	Total Hip Replacement

Ti-6Al-4V	Titanium Alloy (Titanium-6%Aluminium-4%Vanadium)
Ti-6Al-7Nb	Titanium Alloy/ Timetal 367 (Titanium-6%Aluminium-7%Niobium)
UHMWPE	Ultra High Molecular Weight Polyethylene

Chapter 1

Introduction

Total hip replacement (THR) is one of the most common orthopaedic operations performed worldwide. Detailed data for procedures in England and Wales are documented in National Joint Registry and show that during the year from 2003 to 2014 there were 708,311 primary hip replacements carried out in total (National Joint Registry 2015). In particular in 2014, 83,125 primary (first time) procedures were recorded. Some of these operations need to be carried out again for different reasons after sometime which are called revision (replacement of the prosthesis) procedures. In other countries there are also a high number of THRs procedures performed. In 2014, the Swedish Joint Registry recorded about 23,518 THRs procedures that indicates more than 100% increase from 1992. This breaks down into 16,565 primary and 6953 revision operations (Swedish JRU 2014). Similarly in the same year, 35,645 THR were performed in Canada (CJRR 2014) showing 16.5% growth from 2009 for all type of hip operations. More than 193,000 THRs were carried out per annum in the United States of America (USA) where the cost was estimated as $5 billion (Graver 2010).

Important studies and statistics suggest that the number of THR procedures is projected to increase by almost 175% by 2030. Likewise, the number of revision THR procedures can be expected to increase significantly (Kurtz et al., 2007). To meet the above demands and to reduce the number of revision THR surgeries, the implant design and performance must be improved. However, hip prostheses will bear composite effects including tension, pressure, torsion, interfacial shear force, fatigue, wear and corrosion when the artificial hip joint is implanted in the human body. Aseptic loosening appears to be the most significant cause of failure in THR (Shaik et al., 2012 and Kai et al., 2014).

Aseptic loosening might lead to revision surgery and in turn can be avoided by enhancing the durability of the hip replacement. At present many primary hip replacements last less than 15 years, so patients who are relatively young at the time of primary replacement will require at least one revision over their lifetime. Revisions usually have a shorter life than primary replacements, so prolonging implant lifetime to allow younger and more active patients to benefit from the treatment is currently one of the major goals of research and development. It

has to be said that failure is not the only problem related to hip mechanics; some patients do not recover normal gait and others suffer dislocations.

1.1 Background

1.1.2 Latest research into the performance of THR

To review the performance of THR many researchers have investigated various aspects, including bio-compatibility of materials (Gepreel 2013, and Nakahara et al., 2013), musculoskeletal analysis and new techniques (Lewis and Sahrmann 2015, Martelli et al., 2013), the effect of geometrical parameters on the wear characteristics (Bhatt and Goswami, 2012), improvement of implant shape using various optimisation methods (Katoozian and Davy, 2000), and the long-term durability of the implant design (Bennett and Goswami, 2007, Senalp et al., 2007, Faizan et al., 2015). Katoozian and Davy (2000) carried out an FE based 3D shape optimisation study of cemented and uncemented implants. Two kinds of loading conditions were considered: a physiological loading, and a pure bending moment. The study assumed the bone to be an isotropic elastic material, and the interfaces between the bone and implant as well as the cement and implant to be perfectly bonded. The final optimized design predicted a wedge shaped proximal region (close to the head) and a tapered distal stem. However their assumptions are unrealistic, including an isotropic bone. They also did not considered the dynamic loadings and movements. Pyburn and Goswami (2004) investigated the stress distribution in hip implants for various cross sections in the presence of bone cement, utilizing FE simulations on idealized implant assemblies. A comparative analysis of stresses generated in the cement–implant interface for different cross sections of the implant was performed. Latham and Goswami (2004) studied the effect of geometric parameters such as neck angles, neck diameter and head diameters, on the stress distribution in the stem region. They concluded that larger head sizes led to lower stresses in the stem region. However, their study did not consider the interaction between the head and the stem.

Previous studies have suggested that the use of a larger sized femoral head reduces the incidence of dislocation compared to a smaller sized femoral head, provides improved stability of the femoral head within the acetabulum, and results in a larger range of motion (Cross et al., 2012, Theodorou et al., 2011, and Barnett et al., 2009). However, it is not clearly understood whether a larger femoral head could lead to higher stresses in the neck region of the implant,

and hence adversely affect its long-term durability. Neck fracture of the femoral stem due to fatigue has been reported in the literature for some cementless titanium alloy hip implants (Grivas et al., 2007). Although such fractures are not very common, it is important to understand the influence of a larger-sized femoral head on the long-term durability of the implant.

1.1.3 Current research and challenges

Studies on implanted femur revealed that prosthesis stiffness (rigidity) serves a crucial function in controlling stress shielding. Prosthesis stiffness has a bilateral effect on stress shielding and interface stress. Prostheses that are extremely stiff induce high levels of stress shielding in the proximal portion of the femur and low levels of stress on the interface of the implanted femur constituents. By contrast, prostheses with low stiffness decrease stress shielding and increase interface stress. Therefore, prosthesis designers aim to balance stress shielding and interface stress in THR by controlling prosthesis stiffness, which is a function of prosthesis geometry and material (Oshkour et al., 2014).

Considering the importance of dynamic loadings, the realistic boundary conditions of the hip joint have been lacking from significant research findings. Recently Shaik et al. (2012) have highlighted this feature and explained that in reality the hip implant is subjected to other loading patterns in addition to the single-stance phase, and the fatigue life is dependent on such loading. Therefore, another challenge for developing an optimal hip implant is to utilize a realistic models and boundary conditions of the hip joint.

In this research both 2D and 3D models of the ball-stem assembly of a generic hip implant using a standard and validated bone model, were studied under static load. The loading condition corresponds to the so-called single stance phase of gait, which represents the short periods of time during normal walking when only one leg bears the entire body weight. Also other loads have been considered including peak loads experienced from daily living, namely running, climbing upstairs and downstairs.

1.1.4 Project methodology and design optimization process

The initial stage of this project involved review of the literature on the performance of THR implants currently being used by Orthopaedic surgeons in England and Wales. It soon became clear that due to the lack of data on the existing implants, it was essential to test and examine closely the competing implants, in-vitro, in addition to a comprehensive literature review. Furthermore, according to NJR statistics recommends that further research into the success of these hip replacements and the rate of failure of both stem and cup is essential. In addition to redesigning the hip replacement, the application of different materials has been assessed. For this reason the variation of materials that are used for hip replacement models have been reviewed and the advantages and disadvantages of each material combination was evaluated.

An accurate assessment of the stress distribution in the implant-femur assembly is central to achieving the optimal results. This will consequently help in investigating the main causes of high stress and strain in an existing hip replacement. Stress analysis was carried out using a combination of practical experiments and computer simulation. The use of computer simulation in the form of finite element analysis (FEA) would suffice, however using this in conjunction with practical experiments provided a wider range of data. Furthermore, the FEA method required validation. It might be possible to make errors during the simulation if FE analysis was merely used. Nevertheless by comparing the simulated results to those obtained from an actual experiment a frame of reference was provided and the simulation could be validated. The hip replacement was then redesigned using CAD to improve upon the existing specifications.

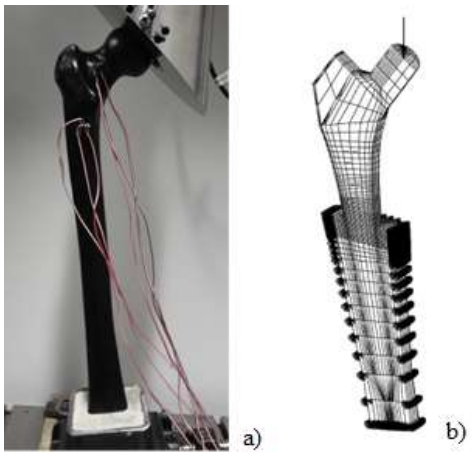

Figure 1.1- a) Cemented prosthetic femur with a load applied (Shah, 2012),
b) Diagram of a loaded prosthetic femur bone (Ploeg, 2009)

This modified design was tested, under the same condition, using FEA to compare the two designs. For this reason, to ensure an accurate comparison, validation of the FEA method was vital to this project. The experiments that were carried out to validate the FEA results include, strain gauges and photostress analysis. The ISO 7206 was utilized as a standard for laboratory tests that determine the endurance of femoral and hip components (Figure 1.1).

1.2 Aim of the investigation

The aim of this study is to develop and test an optimal total hip replacement (THR) implant with new and improved design features to achieve stability and durability.

1.2.1 Objectives of the investigation

The objectives of this research are:

- To investigate and analyse the performance of existing THR used by orthopaedic surgeons and to examine the particular features of individual prostheses which contribute to the reliability and durability of the implants.
- To propose new designs for femoral stem and femoral head which could potentially lead to a reduction in the risk of implant loosening, dislocation, early revision and painful experiences, by minimising the associated prosthesis-femur interfacial macromotions.
- To model, design and implement new implant-femur assembly using three dimensional analysis of the complete hip joint, by suitably adjusting the strength and stiffness in the prosthesis- femur assembly.
- To evaluate the stress and strain distribution in the implant-femur assembly using finite element analysis techniques.
- To improve the quality and durability of a THR by detecting the main causes of stress and other mechanical issues. After identifying potential areas for improvement, the THR was remodelled for improved and optimal performance.
- To test and validate the durability of the proposed implant using experimental techniques, including strain gauges.

The research breakdown structure is shown in Table 1.1.

Table 1.1- Breakdown of the research related to the objectives

Research Breakdown Structure			
Task No.	**Statement / Steps**	**Outputs**	**Objectives covered**
	Literature review and research context		
1.1	Research Scope and new developments	Classification	O1-6
1.2	Reviewing NJR for statistics, cost and data	Identifying the trends	O1
1.3	Classification of complications and failures	Defining problems	O1
1.4	Investigation of the current implants (Stryker, Zimmer, DePuy, Smith and Nephew companies)	Examine design features	O1
	Developing the initial implant design		
2.1	Evaluation of design requirements and factors	Examine design features	O2
2.2	Proposing the initial design using Modelling and FEA software (Ansys, Catia and SolidWorks)	Preliminary model	O2
	Realistic CAD models of the assembly		
3.1	Assessment of the anatomy of hip	Implant model	O3
3.2	Preparing standard 3D model of femur (Sawbone)	Bone model	O3
	Finite element analysis of the assembly		
4.1	Investigation of bone and implant materials	FEA results	O4,5
4.2	Study the effect of implant design on stability	FEA results	O4,5
4.3	Evaluation of the effect of different fixation	FEA results	O4,5
4.4	Kinetics and realistic boundary condition of hip under	FEA results	O4,5
	different daily life activities	FEA results	O4,5
4.4.1	Investigation of hip forces and moments	FEA results	O4,5
4.4.2	Study the flexion and extension data	FEA results	O4,5
	Outcome	Conference paper 1,2	
	Design optimisation process		
5.1	Detecting the main causes of micromotions and stress	Optimal design	O5
5.2	FE analysis and durability evaluation	Optimal design	O5
	Outcome	Conference paper 3	
	Laboratory tests and data validation		
6.1	Strain gauges test on femur and implant	Experimental results	O6
6.2	Brinell hardness test	Experimental results	O6
6.3	Data validation, FEA results with experimental data	Final results	O6
	Outcome	Journal paper 1,2	O6

Chapter 2

Literature Review

This section discussed the basic subjects related to THA. Firstly, the anatomy and forcing of the hip are explained, together with elements as well as mechanical properties of human bone tissue. In addition, femoral stem materials, designing factors as well as different techniques of fixation are also explained, and finally, the typical reasons and factors that promote the failure of hip prostheses stem are presented.

2. 1. The hip joint

2.1.1 Anatomy of human body

The hip that is coxal articulation joint, is actually a ball and socket mechanism created by the femoral head along with the acetabulum within the pelvis. The pelvis is made of 3 bone that merge with each other at the beginning of adulthood; these include the ilium, ischium and pubis. The proximal part of the femur bone comprises of the femoral head which is round in shape, the cylindrical femoral neck as well as two bony landmarks which are employed to get muscle connection, known as the greater and lesser trochanters. The actual structure of the proximal femur is demonstrated in Figure 2.1. The posterior view of femur on the left shows main part of femur including the femoral head and neck of femur. Also lesser trochanter and greater trochanter that are conical and quadrilateral protuberances on the proximal femur respectively. In a healthy hip, cartilage handles the top from the femoral head and the acetabulum. The collagenous cartilage provides shock reducing and a totally free moving articulating joint having a low friction surface area. The interior view of proximal femur includes ligamentous reinforcement of the hip. Three structures provide balance in the joint; these kinds of ligament are the iliofemoral, pubofemoral and also the ischiofemoral. The iliofemoral ligament links the ilium to the femur and provides the primary constraint within the hip combined. The ischiofemoral ligament ties the ischium to the femur on the rear side from the joint. The actual pubofemoral tendon connects the actual pubis along with the femur, additionally blending along with the iliofemoral ligament.

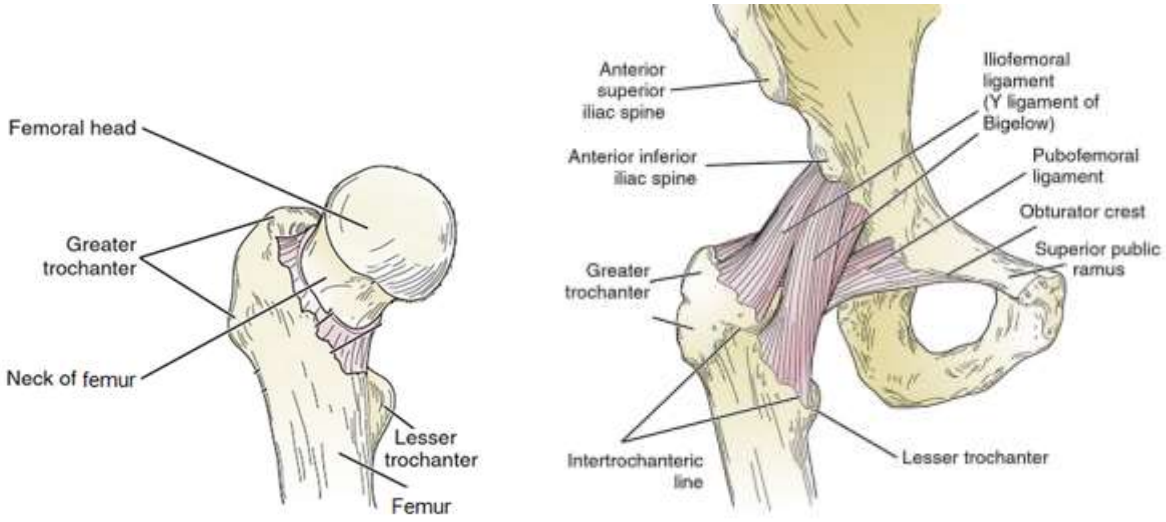

Figure 2.1 Anatomy of the proximal femur- posterior and anterior view (Reese and Bandy, 2016)

The muscles that involves with the hip are many and quite a few muscles are frequently engaged to supply any individual movement in the joint. The actual motions in the hip system are flexion, extension, abduction, adduction, rotation and circumduction, almost all of them are generally explained in relation to the anatomical planes of the body, which are demonstrated in Figure 2.2.

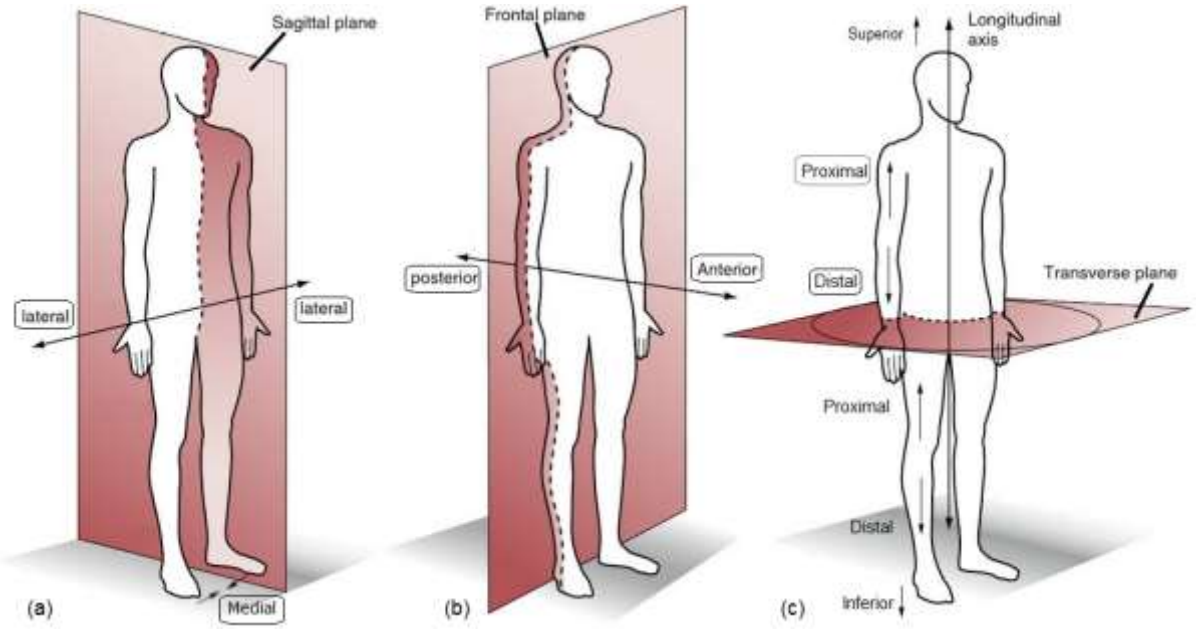

Figure 2.2- Anatomical planes (a) Sagittal plane (b) Frontal plane (c) Transverse plane (Reese and Bandy, 2016)

Three planes of the body include: 1- Sagittal plane 2- Frontal plane 3- Transverse plane. The anatomical directions that are described in accordance with these planes are as follow:

- Anterior: front or in front of,
- Posterior: back or in the back of,
- Lateral: towards the side of the body or away from the middle,
- Medial: towards the middle of the body,
- Proximal: nearest or close to the trunk of the body,
- Distal: farthest or away from the trunk of the body,
- Superior: upper or towards the head,
- Inferior: lower or towards the feet,
- Superficial: towards the outer surface,
- Deep: towards the inside.

For instance there are two different types of hip implant fixation, known as proximal fixation and distal fixation that refer to the location of hip implant inside the femur which can be either towards the head or shaft of femur. The implant fixation will be discussed in chapter 5. Nevertheless the actual motions in the hip joint system are explained in Figure 2.3.

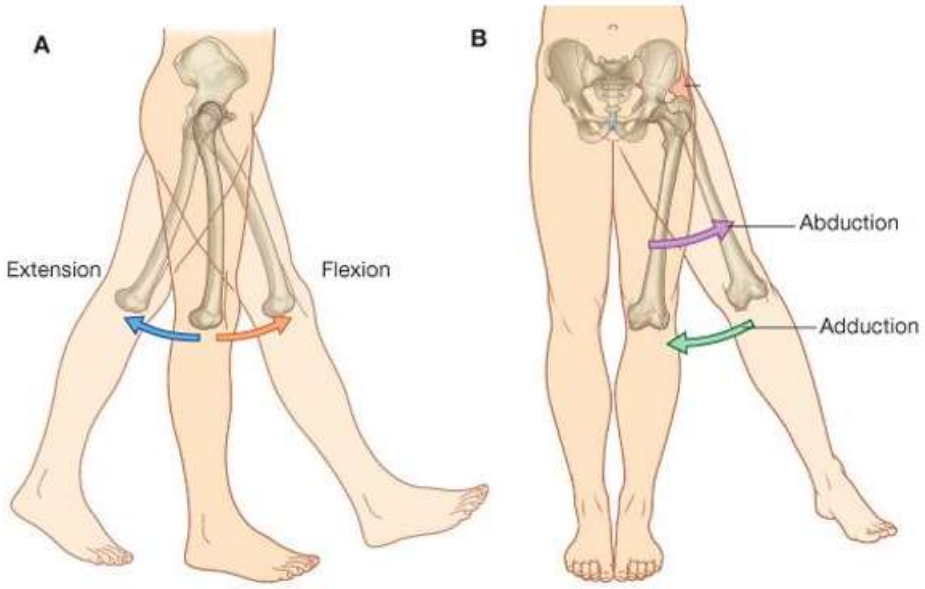

Figure 2.3- Hip motions (Patton, 2015)

- Flexion is the motion of the femur bone in the sagittal plane in the anterior direction, while extension is the motion of the femur in the posterior direction.

- Abduction would be the motion of the femur bone in the frontal plane laterally, while adduction is the motion of the femur medially.
- Rotation in the hip is a rotating activity of the anterior area of the femur in the longitudinal axis. Medial rotation takes place internally in the direction of the human body and lateral rotation is known as a motion away from the body.
- Circumduction is a mixture of flexion, extension, abduction and adduction.

2.1.2 Forces on the hip joint

Rohlmann et al. (1988) used a telemetrised artificial femoral stem to determine hip loads and to some degree started in vivo measuring. Subsequently, instrumented prostheses have been implemented to calculate hip loads when conducting common daily life. It is obvious that the amount of hip loads differs based on the type of exercises that are being carried out by the person (Bergmann et al., 1993; Bergmann et al., 2001; Heller et al., 2001). It has been estimated that the hip is actually exposed to in excess of 1 million gait cycles annually (Morlock et al., 2001). When walking typically in the one stance stage of gait, the average maximum hip reaction load has been noted to be around 2.5 times body weight (Bergmann et al., 2001). Heller et al. (2005) established a validated musculoskeletal technique as a way to produce a more precise assembly of in vivo loading scenarios and revealed that the abductor muscle produced a maximum load of around one's individual body weight when walking. Fisher and Duda have also presented similar gait and activity models while the Bergmann's model remains the most comprehensive. The Bergmann's model will be explained thoroughly later in chapter 6.

2.2 The shape and physical properties of bone

The quality and quantity of bone tissue intended for orthopaedic joint replacement is a crucial element that may decide the success of joint arthroplasty (Wirth et al., 2011). As a result, to be able to inspect the efficiency of orthopaedic prostheses, the features and movement of human bone must be recognized. Bones form the major element of our musculoskeletal structure, and their task is to bear body weight, resist physical loading, carry out motion and secure the body's internal organs. Furthermore, bones are essential for calcium metabolism and for supplying space to permit the creation of blood cells. Bone is a substance with a matrix composed of both

organic and inorganic parts. The organic part of bone is mainly made up of collagen I; this specifies the bone's shape and facilitates the resistance of tensile forcing. The inorganic resources are hydroxyapatites, usually composed of calcium phosphates that produce stability towards compressive loading.

The human skeleton includes two sorts of bone, cortical and cancellous or trabecular bone. The actual difference among these two sorts of bone tissue is dependent on density and porosity. It is believed that the changeover between cortical and cancellous bone takes place at around 30% porosity (Brown et al., 1998). In the human skeleton, cortical bone is typically discovered where the employed physical stresses are greater and cancellous bone in which the stresses tend to be lesser. Figure 2.4 indicates the cross section of a normal proximal femur, in which the distribution within the cortical and cancellous bone might be noticed. The specific trabeculae of the cancellous bone are normally aligned to optimize the force from the femoral head and neck towards the diaphysis or shaft of the femur. The diaphysis of the femur is made up of hollow round cross section of cortical bone tissue, which exchanges the load through the hip towards the knee.

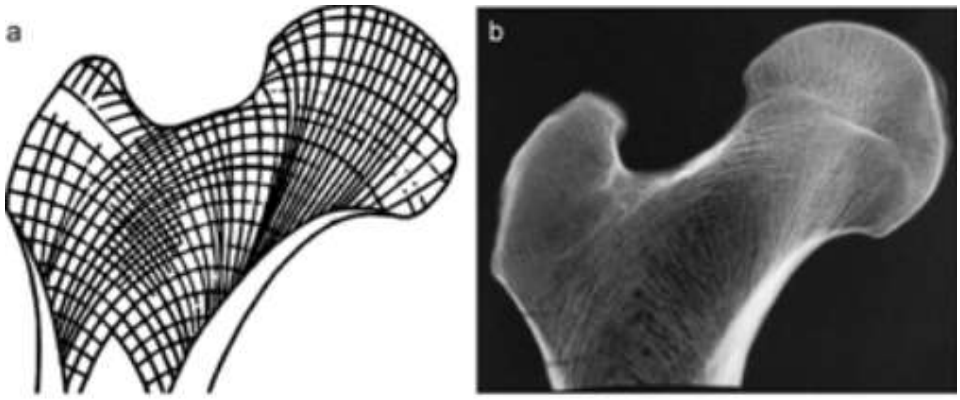

Figure 2.4- The frontal cross section of a natural proximal femur. a) Wolff's original analytical trajectory (Wolff, 1892), b) A natural proximal femur radiograph (Skedros and Baucom 2007).

2.2.1 Physical properties of bone

Bones should be sufficiently solid to avoid fracture under some situations so it could be categorised as regular physiological loading. The physical properties of bone tend to be based mostly upon the existence of the nutrient phase inside the material's matrix. The nutrient content as well as microstructure of bone tend to be distributed in a heterogeneous way, and

also the stress-strain laws of cortical as well as cancellous bone are sensitive to the bone's porosity and microstructural position. The elastic modulus for femoral cortical bone tissue has been claimed to be about 17 GPa in the longitudinal direction and 11. 5 GPa in the transverse path (Reilly and Burstein, 1975). The data displayed in Table 2.1 indicate that cortical bone is a substance which shows anisotropic behaviour.

Table- 2.1 Mechanical properties of cortical bone (Reilly and Burstein, 1975).

Mechanical property	**Longitudinal axis**	**Transverse axis**
Young modulus (GPa)	17	11.5
Ultimate tensile strength (MPa)	133	51
Ultimate compressive strength (MPa)	193	133
Ultimate strain (%)	3.1	0.7

The actual anisotropy within cortical bone tissue is a result of the positioning of osteons alongside the longitudinal axis of long bones including the femur, while the anisotropy of cancellous bone tissue depends upon the direction of the each trabecular. The elastic modulus of cancellous bone tissue is less predictable than the cortical bone and may vary between 0. 1 GPa and 4.5 GPa and is influenced by anatomical position (Turner et al., 1990).

2.3 Bone remodelling theory

Bone is actually a vascular system that reacts to specific hormonal and also mechanical signals. Consequently bone could functionally adjust to the environment that it is situated in. For that reason bone changes its mass and structures based on the physical forces that it is exposed to (Huiskes et al., 2000). Therefore, bone tissue remodelling has developed into an important issue of consideration related with the design, evaluation and performance of artificial femoral stems.

Wolff (1892) presented theory identified as 'Wolff's Law', explaining that bone modifies and adjusts based on the physical stresses and also strains applied to it, which means that new bone tissue is laid down wherever it is required and even resorbs where it is not required. The physical modifications in bone occur gradually because of the action of bone tissues. The

development of osteoblasts leads to bone apposition (formation of bone) and osteoclasts leads to bone tissue resorption (removal of bone). This event of bone tissue constantly modifying is referred to as bone remodelling and might be explained by either external or perhaps internal remodelling. External remodelling can be assessed with a modification within the geometry of the bone while internal remodelling can be calculated by a modification in bone tissue mineral density, and therefore porosity.

Following the original work by Wolff, there were several analyses carried out on bone remodelling. Cowin and Hegedus (1976) established one of the primary numerical models explaining exactly how bone remodelling might be predicted considering basic continuum mechanical principles. Deeper work in this field was carried out by Huiskes et al. (1987) and Weinans et al. (1992) who did bone remodelling mathematically utilizing the finite element technique. In both scenarios, finite element models had been employed to estimate bone tissue resorption within the femur by utilizing Strain Energy Density (SED) as the physical stimulus for feedback. This properties allowed the determination of bone shape and density adaptions in reaction to physical loading conditions. The technique of utilizing SED as the mechanical stimulation to replicate bone remodelling is common in the literature (Huiskes et al., 1992; Kuiper and Huiskes, 1997; Yan et al., 2011; Gong et al., 2012; Arabnejad and Pasini, 2013), where SED is equivalent to $u=\frac{1}{2}\sigma\varepsilon$, when σ is the stress vector and ε is the strain vector. Using this relationship, it could be noted that a raise in stress inside the periprosthetic bone tissue is good for raising the mechanical stimulus and therefore bone remodelling.

2.4 Femoral stem materials

Materials which are employed for orthopaedic programs are generally known as biomaterials. Any materials which are chosen for orthopaedic purposes should be biocompatible and have the ability to resist the mechanical forces applied to all of them throughout day to day activities. It is known that biomaterials should be capable of resisting damage from the body, without subjecting any kind of harm to the body itself. Orthopaedic implants are normally made of three categories of materials, these groups being metals, ceramics and polymers. Total joint

replacements are typically created with a combination of two or more of these kinds of materials groups.

Polymers in many cases are implemented for the articulating area of the acetabular part which is used in THA. The most typical polymer utilized for articulating surfaces is UHMWPE (Ultra High Molecular Weight Polyethylene). This is a highly cross-linked type of polyethylene which offers excellent wear features and also a low coefficient of friction. For this investigation, the focus has been employed to metals which are particularly applied for the production of femoral stems.

2.4.1 Metals

Stainless steel had been one of the primary metals being employed for orthopaedics, and the alloy 316L is the type most frequently used. During recent years, the application of this particular alloy for total joint replacement has reduced gradually because of its relatively lower strength and corrosion resistance in comparison with other biocompatible materials. Nevertheless from a financial point of view this particular alloy is superior to other metals and is used for fracture fixation products, screws as well as intramedullary nails (Gil et al., 2006).

Other typical metals employed for femoral stems are titanium and cobalt chrome structured alloys. Titanium alloys were initially formulated mainly for use within the aerospace industry and are now regularly used for biomedical purposes. The most typical titanium alloy employed within orthopaedics is actually Ti-6Al-4V. This particular alloy has developed into a popular material for orthopaedic prostheses as it is less dense and much more flexible compared to other implantable alloys. Usually, titanium as well as its alloys are favoured over other alloys including cobalt chrome and stainless steel for orthopaedic purposes because of their superior biocompatibility, overall flexibility, specific strength as well as corrosion resistance (Niinomi, 2002). Regardless of this, there are complications related to the use of titanium alloys when it comes to their weak wear qualities and notch sensitivity. Therefore, a solution that has been proposed for the application of titanium alloys is to stabilise the wear problem by utilising the oxide layers.

The most frequent cobalt chrome based alloy employed for the production of femoral stems is actually cobalt chromium molybdenum (CoCrMo). This alloy can be used in cast or wrought modes, with the latter frequently being favored for orthopaedic applications, because of its excellent strength and toughness (Marti, 2000). CoCrMo is regarded as the strongest, toughest and most fatigue resistant of all of the metals utilized for force bearing prostheses, but its fairly large elastic modulus of about 200 GPa is almost twice that of Ti-6Al-4V. This could result in a stiffness that is not compatible with femoral cortical bone and is greater by nearly twelve times. This stiffness mismatch stimulates the stress shielding phenomenon that is explained in section 2.7.3. Hence the implant stiffness is crucial when metallic alloys are to be employed and minimal amounts of stress shielding should be achieved (Niinomi, 2008). It is worth mentioning that Timetal 367 (Ti-6Al-7Nb) has been developed recently to avoid toxic substances in Ti-6Al-4V alloy.

2.4.2 Functionally graded and composite materials

The idea of a Functionally Graded Material (FGM) is to develop a composite through grading the microstructure of the material, or change the microstructure of one particular material to another over a particular gradient (Bever and Duwez, 1972). From a medical point of view, the idea of functional gradation is common in living cells including bone tissue. Bone includes a rigid dense external structure (cortical bone) with a structure which gradually modifies to a less rigid porous inner structure (cancellous bone). As a result, to be able to optimise the response of an orthopaedic prosthesis to external forcing it has previously been hypothesised that this optimal composition must have an identical gradation to bone (Pompe et al., 2003).

Functionally graded and composite femoral stems have been reviewed in theory utilizing the finite element technique. Simões and Marques (2005) suggested a stem with a CoCrMo core which was encircled with a flexible composite material, whilst Boudeau et al. (2012) suggested an alternative solution composed of a carbon fibre reinforced polyetheretherketone composite material. Each of these researches suggested that the force transfer towards the proximal femur was enhanced by the development of more versatile stiffness designs. Gong et al. (2012) employed a basic two dimensional axisymmetric finite element design and numerical optimization methods to investigate the efficiency of a titanium alloy-hydroxyapatite

functionally graded material. It was noticed that the elastic modulus in the hip implant stem can be axially graded to ensure that it was more rigid proximally whilst having a much lesser elastic modulus distally. This led to a decrease in proximal stress shielding without reducing the bone-implant interface stability. Lately, Oshkour et al. (2014) explored stainless steel-hydroxyapatite and titanium alloy-hydroxyapatite functionally graded hip prostheses, in which a 22% rise in SED was noted in the proximal femur.

The earlier researches have outlined the prospect of employing functionally graded and composite materials. Nevertheless, it might be regarded that the arrival of more adaptable femoral stems for medical usage has been delayed because of restrictions that have been related with conventional production techniques, and also because of the greater expenses that have traditionally been involved with the development of functionally graded and composite materials.

2.5 Femoral stem designs

2.5.1 Historical innovations

It is considered that the initial THA was carried out by Philip Wiles in 1938, utilizing stainless steel parts (Wiles, 1958). A hip stem was manually attached to the outside of the femur. But the outcomes were poor in this case as the parts which were utilized for connection purposes broke or started to be loose (Wiles, 1958). In the 1950's, Kenneth McKee initiated the use of monoblock Thomson prostheses. Stainless steel parts were employed at first and an important problem of loosening was observed to happen at large scale after just one year review (McKee and Watson-Farrah, 1966). After this, alternative materials were employed for the production of stems. In 1953, a revised Thomson implant with a reduced femoral head was made entirely with a cobalt chrome alloy and that showed relatively better performance as compared to its stainless steel alternatives (McKee and Watson-Farrah, 1966). Ring (1968) then presented what is considered to be the first cementless parts for THA. Nevertheless, in the 1970's, even though the McKee and Ring implants continued to work effectively, they were substituted with models that were produced by Sir John Charnley (Gomez and Morcuende, 2005).

2.5.2 Existing developments

Selecting hip stems for THA is eventually decided by the personal preference of the orthopaedic doctor and there is a large choice of cemented along with cementless total hip implants available worldwide. Developments have been documented in the National Joint Registry for England, Wales and Northern Ireland explaining the most famous cemented as well as cementless femoral stems which are employed with regard to primary THA. The Exeter V40 stem is the most preferred cemented implant and has completely dominated selection for the past Decade (National Joint Registry, 2015). The most famous cementless stem is actually the Depuy Corail completely hydroxyapatite coated titanium alloy stem. This particular stem continues to be employed in over little less than a half of the cementless arthroplasties carried out in the last five years throughout England, Wales and North Ireland (National Joint Registry, 2015).

2.5.3 Modular against monoblock implants

The appearance of hip implants has changed over the years and also to date continues to be influenced by the actual implant producer (Mai et al., 2010). To simplify issues femoral stems are referred to as either monoblock, in which the stem as well as head is a single item, or modular, in which the stem along with the head tend to be independent parts that can be interlocked mechanically with a taper junction, as demonstrated in Figure 2.5. Titanium alloys in many cases are selected as the favoured material for modular hip implants, because of the material's reasonably lower stiffness, and they are frequently joined with a cobalt chrome or even ceramic femoral head. But the weak wear characteristics associated with titanium alloys eliminate any kind of use for articulation and for that reason monoblock stems are typically made out of cobalt chrome metals. Modular stems provide the patient options and several level of customisation with regard to femoral head offset, version as well as leg length (Sporer and Paprosky, 2006). As opposed to this, latest problems have been related to modular models because of the physical failing of the taper junction (Sotereanos et al., 2013) and because of the recognition of negative reactions regarding soft tissue which have been associated with the metal on metal wear debris which is produced from the taper junction (Langton et al., 2012).

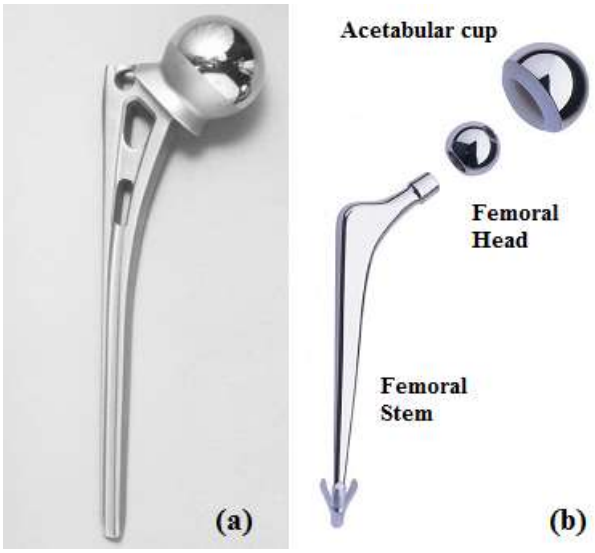

Figure 2.5- (a) A femoral stem with a monoblock design (Kharmanda 2016) (b) a femoral stem with a modular design (Stryker, 2016)

2.6 Femoral stem fixation

2.6.1 Cemented fixation

Hip implants could be cemented in to place utilising the acrylic polymethylmethacrylate (PMMA), that is prepared during surgery and it is used to develop a bond between implant along with the bone itself. This technique of fixation is effective for old and less active patients, with post-operative survivorship results as high as 20 years being revealed (Kavanaugh et al., 1994; Smith et al., 1998). The caveat is the fact that heat produced throughout the curing phase of the PMMA which can easily encourage a common condition called thermal necrosis, which could harm the periprosthetic cells and damage the stability of the implant.

2.6.2 Cementless fixation as well as bone tissue ingrowth

Cementless fixation is usually where the femoral stem is press fitted inside the bone as a way to build biological fixation by bone tissue ingrowth. This technique of fixation has in the past been favoured for younger, more energetic people who have sufficient bone tissue stock for the process (Dorr et al., 1990). In contrast, a more current research has pointed out that cementless fixation has got the possibilities to become a safe, practical choice for patients older than 75 years of age (Meftah et al., 2013). Femoral implants which are utilized for cementless fixation usually need a rough or porous area to be able to stimulate bone tissue ingrowth throughout the recovery stage. Porous substrates have traditionally been utilized to present

natural fixation in the bone- implant interface. Roughened titanium, titanium beads or even plasma sprayed titanium as well as cobalt chrome along with the adding the bioactive materials including hydroxyapatite (HA) have been employed to the area of hip implants. HA sprayed implants typically accomplish great results; with Aebli et al. (2003) explaining that HA coated implants create a connection with the host bone tissue which can achieve similar strength to cortical bone tissue. Regardless of this, there are issues with utilizing HA coatings when it comes to the brittleness of the materials, the effectiveness of connection among the HA and the metal hip stem, and because of the situation of the bone-implant interface after the resorption of the HA spraying (Manley et al., 1998). The resorption of the HA spraying could be challenging, since eventually the coating could be replaced by new bone tissue on the implant surface area and also the mechanical interlocking amongst the HA and the bone tissue could be minimal (Geesink et al., 1988).

2.6.3 Comparison between cemented and cementless fixation

Hearn et al. (1995) mentioned that cemented and cementless femoral stems utilized in THA performed with similar efficiency, and that the interest for shifting towards cementless implants was justified. Mont et al. (1999), in their 5-year follow up research also discovered that the efficiency of cementless femoral implants was similar to cemented. As opposed to this, Weidenhielm et al. (1995) discovered that cemented implants performed well for 14 years, while cementless implants often fail at about 5 years. Nevertheless, the stems investigated in this research were varied in materials and geometry that could happen to be a potential restriction. Lately, cemented femoral stems were observed to enjoy a 12- year success rate of 98. 3% (Aubault et al., 2013). Furthermore, throughout at least ten years follow-up research a success rate of 97. 2% was noticed at 16 years for cementless prostheses (Hwang et al., 2012).

Looking at hip implant fixation, it is still unclear from the assessed papers which technique brings optimal outcomes. But existing tendencies are generally favouring cementless fixation (National Joint Registry, 2015). This tendency is demonstrated in Figure 2.6, where it may be seen that the change from cemented to mainly cementless implants happened in 2009. This suggests that cementless fixation associated with femoral implants is the most popular solution in the United Kingdom, though this tendency is changing in recent years.

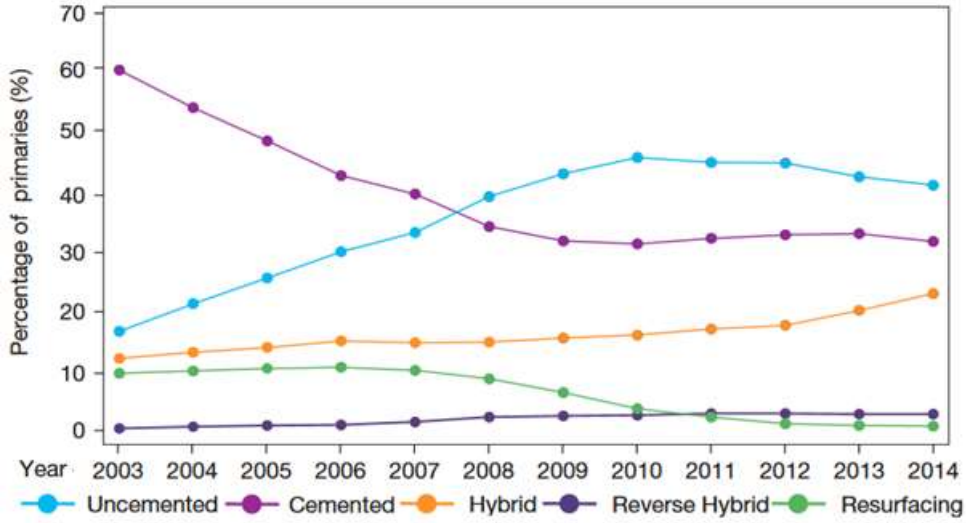

Figure 2.6- Types of THA procedures that have been performed in England, Wales and Northern Ireland between 2005 and 2014 (National Joint Registry, 2015)

2.7 Failure of femoral implant fixation

From an engineering point of view, the failing of THA is the result of the mechanical failure of implanted parts or from the failure of fixation. In addition there are surgical problems including infection, blood clots and nerve destruction that must be considered. But all these may not be enhanced from an engineering viewpoint; hence, they have not been investigated in this study. The complications of femoral implant fixation after the operation are due to several reasons; but it is usually thought that aseptic loosening is the central factor. Aseptic loosening may be generated by implant wear debris, caused relative small movements in the bone-implant interface together with the stress shielding effect on the periprosthetic bone.

Reason	Type of revision procedure Single stage (n=69,655)
Aseptic loosening	52.0%
Pain	23.6%
Lysis	15.8%
Dislocation/subluxation	15.0%
Infection	3.1%
Periprosthetic fracture	9.2%
Implant fracture	3.5%
Implant wear	14.0%
Malalignment	5.7%
Head-socket size mismatch	0.8%
Other indication	8.0%
Adverse reaction to particulate debris	10.4% n=51,815

Figure 2.7- Percentage of main reasons of hip revision procedures (National Joint Registry, 2015)

2.7.1 Aseptic loosening and micromotions

Aseptic loosening is the main reason for hip implant failure. In fact when the bone-implant interface is not fully attached, small motions would lead to loosening of the implant. Micromotions are actually the relative displacements which take place within the surface of the artificial implant and the bone tissue. The amounts of these displacements are closely related to the particular physiological forces that are placed on the implanted joint. It is believed that when the micromotions exceed threshold limit in the range of about 100 μm to 200 μm, the natural fixation of the implant will be affected, and fibrous tissue would be created in the bone-implant interface, instead of unique bone (Pilliar et al., 1986; Maloney et al., 1989). This kind of fibrous tissue has poor mechanical properties in comparison to bone and for that reason plays a role in the unwanted loosening of prostheses.

The stability between the bone and the implant could be categorised as primary and secondary stability. Primary stability relates to the stability at the bone-implant interface soon after operation and is based completely upon mechanical aspects (Viceconti et al., 2000). Secondary stability explains the biological stability of the hip implant when bone tissue ingrowth takes place. From the literature and papers, it is noticeable that inferior primary stability leads to fixation failure of cementless hip implants that are employed in THA (Maloney et al., 1989; Phillips et al, 1990). Therefore it is important to set up reasonable primary stability as a way to attain sufficient secondary stability via complete bone ingrowth along the bone-implant interface. From a medical point of view, the two principal elements that play a role for the stability of an orthopaedic hip prosthesis is the quality and also quantity of the bone tissue, along with the surgical fixation of the implant. Wirth et al. (2011) proved that implant stability is actually impacted by the microstructural quality of the periprosthetic cancellous bone tissue. Bertollo et al. (2011) examined the influence of medical fixation upon implant shear strength with regard to porous titanium and discovered that the average shear strength within cortical and cancellous bone tissue sites was greater in press fit in comparison with the 1mm clearance fit. This particularly signifies that making preliminary contact at the interface is crucial to be able to encourage bone tissue ingrowth and also optimise secondary stability.

2.7.2 Wear particles

In THA, UHWMPE is usually employed as the supporting surface to the acetabulum. The articulating movement of the hip implant triggers polymeric wear particles to be produced by fretting or fragmentation. These kinds of sub-micron debris may cause an inflammatory response inside the periprosthetic cells identified as osteolysis. The UHWMPE wear particles attracts the cell type identified as a macrophage which should absorb the actual particles which are developed; but at the same time the wear particles result in these kinds of cells dying and releasing additional digestive enzymes and chemical messengers into the body system. These enzymes and chemical messengers could potentially cause the gradual failure of the periprosthetic bone and also contribute to the loosening and ultimately lead to failure of the arthroplasty.

Along with polymeric wear particles, the deposition of cobalt and chromium ions inside the blood vessels may lead to aseptic loosening and may cause necrosis of the bone tissue and surrounding soft cells (Gruber et al., 2007). Damaging soft tissue reactions have been related to the metal-on-metal wear particles which are produced from the metal-on-metal bearings, this being common within big head metal on metal hip implants and modular designs (Langton et al., 2012).

2.7.3 Stress shielding

Stress shielding can be described as a phenomenon that is related to all different types of joint arthroplasty and is particularly common within the replacement of force bearing joints including the hip and knee. After the total hip replacement operation, the body weight force transfer towards the proximal femur is decreased when femoral stems having a noticeably greater stiffness compared to bone are inserted. Therefore, the femoral stem of hip implant bears a fraction of the force that was previously completely carried with the periprosthetic bone. This phenomenon leads to a decrease in the stress distributed inside the remaining host bone, which means that the periprosthetic bone can become inadequately loaded and therefore will not be remodelled. Stress shielding phenomenon in this case may eventually influence the durability of THA and in turn, enhance the need for revision operation.

Stress shielding may also lead to the unwanted failure of THA via femoral stem migration or fractures in the bone (Kröger et al., 1998). Stress shielding following THA is particularly common in the proximal-medial femur and the area of the calcar and lesser trochanter of the femur bone is often worse affected (Karachalios et al., 2004; Stiehl, 2009). In clinical circumstances, radiographic assessments are carried out to evaluate and measure the influences of stress shielding through dividing the femur bone into what are referenced as Gruen's zones as displayed in Figure 2.8. These zones are generally used to determine periprosthetic bone density after the total hip replacement and consequently provide suggestions of exactly where stress shielding may happen (Gruen et al., 1979).

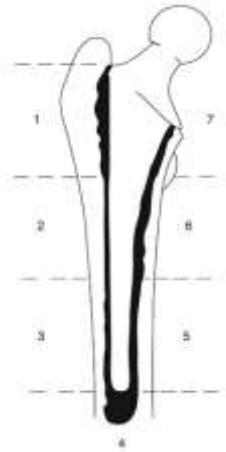

Figure 2.8- Gruens zones intended to calculate periprosthetic bone density (Gruen, 1979)

2.8 Durability of hip prosthesis

Investigation during the last 3 decades have attempted to theoretically and practically improve the development of orthopaedic endoprostheses durability, via modifications as well as by altering their applied principle. These kinds of enhancements could be assessed and reviewed with laboratory fatigue testing and FE study.

In the beginning, the level of revision was greater because of physical and biological issues. A number of these stimulated the proximal aseptic loosening, the situation in which the stem works as a ‘‘cantilever beam’’, raising the stress level therefore causing the stem to break over a long period of time. Although some studies were undertaken to solve this problem, there is still a considerable rate of revision operations after few years. Specifically, the development of

the strength fatigue standard ISO 7206-4 within the 1980s, to some extent led to decrease in the failure levels. Using this experiment, the researcher can measure the material response in addition to other elements which could boost the failure chance of the stem exposed to an extreme situation of the proximal aseptic loosening.

In relation to the loading scenarios, orthopaedic prostheses encounter significant cyclic forces, and pre-clinical evaluation is carried out to guarantee they could endure numerous forcing cycles. Fatigue strength assessment requires a number of verifications using the full range of regular and distressing physiological loading conditions, with associated boundary conditions as well as an associate environment. The fracture and fatigue durability of innovative joint replacement prostheses must be confirmed within the full range of lifetime cyclic loading. This consists of impact along with cyclic forces equal to many times the bodyweight, due to regular actions and routines (Bergman, 2001) as well as some distressing occasions including stumbles and falls (Bergman, 2004). Experts (Morlock et al., 2001 and Silva et al., 2002) have suggested that hip implants bear numerous large volume force cycles annually, showing the impact and significance of looking at fatigue study and evaluation.

For example, acetabular cup innovations attempt to reduce wall thickness to save bone, which generates large pre-stress within modular hip prostheses. Current acetabular cup implant enhancements (Dickinson et al., 2009 and Tuke 2010) have been geared to modify thickness because of this, which actually enables to maximize bearing diameter with no further bone elimination throughout operation. A big bearing diameter encourages joint stability and also lowers the chance of dislocation, enabling patients to return to an active way of life. Bone stock maintenance is helpful afterwards, when the implant might have to be revised. Nevertheless, fatigue strength confirmation can be crucial, due to the fact that decreasing the cross section of the hip implant raises the cyclic stress.

In the past 30 years, a number of different laboratory assessment and FE evaluation methods have been developed as a way to set up the working length of an implant. The earlier investigations and existing advancements are discussed in the next sections.

2.8.1 Previous developments

Among the initial options recommended by a member of the Imperial College of Science, Technology and Medicine (ICSTM) working in London (Katsutashi and Kiyoshi, 1992) planning to reduce wear, was a whole hip endoprosthesis using bearings. To accomplish this objective, the model was presented which integrated a moving bearing with conical wheels within the femoral stem neck plus femoral head that might bear considerable radial as well as axial forces. It had been realized that the rolling bearings using needles demonstrate an excellent durability against fatigue. Nonetheless there are various problems in this model. Although it is essential to guarantee an effective stability for the bearing to withstand the fatigue, a smaller diameter in the inside ring is usually necessary to provide an adjustable femoral head. As a result modifying the contact mechanism within the hip implant from one moving contact between two large surfaces, into a large number of rolling contacts, can result in many difficulties relating to performance and durability of the main implant components.

Another introduced method was a basic modification in the form of relative motion amongst different parts of the hip implant. Katsushi and Kiyoshi (1992) made another design that is an artificial hip implant having “balls train”. This generally is made up of a double joint structure. A French developer Davant (1995), proposed making a practical method called “Supertête” implant which could decrease the wear in the implant by nearly 99% (Sadeghi-mehr 1997). To be able to accomplish this outcome, a tiny round bearing of “completely unique” kind, as the creators stated, lubricated utilising synovial liquid, the normal lubricant for every prosthesis, was incorporated within the femoral head, developed and integrated in line with aeronautics industry requirements. The femoral head was reported to have minimized wear, being manufactured to take 25,000 N, while the hip joint maximum loads do not exceed 5,000 N.

2.8.2 Recent developments

Within the design procedure to obtain the optimal hip implant shape, pre-clinical scientific experiments should be performed to validate the mechanical durability to physical forces. A smart alternative technique could be the utilization of virtual finite element analysis (FEA) to get a primary view of the predicted mechanical behaviour in the prospective design. It does not

imply that the natural pre-clinical experiments might be omitted. It is merely a swift method to eliminate possibly low efficiency designs. The fact is that numerous unwanted stem fractures continue to take place these days. The necessity of hip revision is certainly harmful for the patient because it can be a more complex medical treatment with greater problems regarding rehabilitation.

In latest studies by Melvin et al. (2014), Han et al. (2013) and Griza (2013) various stem failures were reviewed. An FE-based technique for fretting wear-fatigue prediction in a total hip implant has been established by Zhang et al. (2013). Likewise because corrosion and fretting in the junctions of hip prostheses may promote implant failure, Hothi et al. (2014) have examined the reliability of a rating method for wear and fretting.

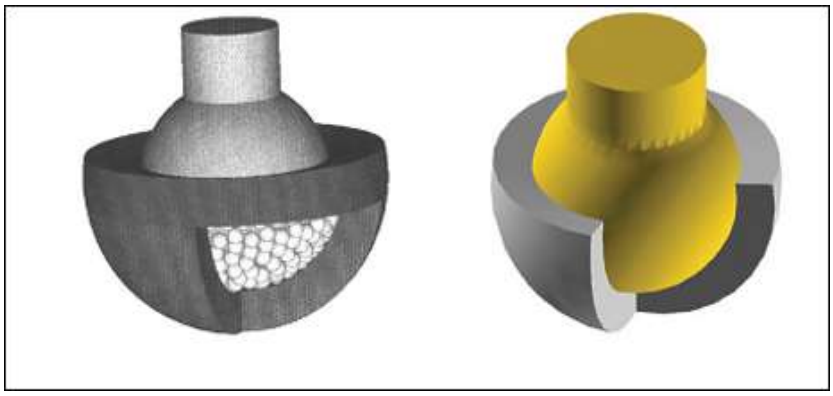

Figure. 2.9- The three-dimensional simplified models: left – model with self-directed balls, and right – classical model (Capitanu and Florescu, 2014)

Capitanu and Florescu (2014) proposed a new method minimizing friction where the “layer of balls” by “compensation space”, positioned among the acetabular cup and the femoral head. This is typically established on the principle that the rolling motion generally has a lesser friction in comparison to sliding friction.

2.8.3 Finite element method of fatigue

Failure in numerous mechanical structures comes through fatigue. Cracks might start and develop by a pre-existing macroscopic defect, for instance a notch, or through a location that has a reasonably great stress concentration. Cyclic fretting wear leads to stress concentrations in locations (e.g., stick-slip slot, contact side) on the contacting areas, resulting in early crack nucleation. This minimizes the fatigue efficiency of mechanical parts and is identified as fretting fatigue. Several real life service elements have the possibilities to encounter fretting damage, including aero-engine spline couplings and hip replacement prostheses, in which the stem and femoral head come in contact. In order to estimate fretting fatigue area and lifetime for these complicated geometries, a combination of two techniques is generally needed, including finite element method and lifetime prediction.

2.8.3.1 S-N curves and "critical plane" method

Several techniques have been implemented to estimate the fatigue safety of mechanical parts. The primary use of stress against amount of cycles to failure (S-N) curves through data about the stress area might be employed to estimate fatigue life. Conventional evaluation of fatigue strength analyzes the material's strength limit and compare it with high cyclic stress, and measures the ratio in terms of reserve factor (N_f).

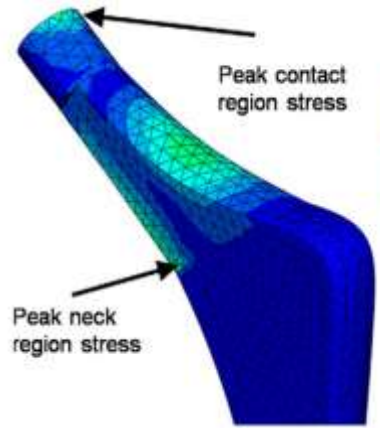

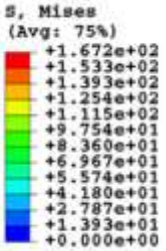

Fatigue-life estimates.

Implant region	28 mm ball diameter N_f
Neck	4.57E14
Contact	17.9E14

Figure 2.10- Von Mises stress distribution for the surface–surface separation case (FC boundary condition), 28 mm ball (Shaik et al., 2012)

A structure is regarded as secure under a supplied force regime when the reserve factor is higher than 1. A number of the recognized fatigue models which take into account the impact of mean stress are generally based on Gerber (1874), Goodman (1899), Soderberg (1939) and Morrow (1968). In an effort to calculate the fatigue life of a prosthesis, Shaik et al. (2012) have implemented the Marrow technique and utilized the effects of the von Mises stress through FE evaluation of neck along with the contact areas model. Morrow's formula or the revised Basquin's law is employed to calculate the number of cycles that will cause the hip implant to fail. N_f, is defined as:

$$(2N_f)^b = \left(\frac{\sigma_a}{\acute{\sigma}_f - \sigma_m}\right),$$

where b is the fatigue strength exponent, σ_a is the stress amplitude, σ'_f is the fatigue strength coefficient, and σ_m is the mean stress. The recognition of fatigue damage factor associated with S-N curves has been analysed by several experts to estimate the lifetime. For instance, the Smith-Watson-Topper (SWT) (1970) and Fatemi-Socie (FS) (1988) fatigue indication variables have been utilized for life evaluations in a lot of analyses. Certainly, the stress state related to fretting results in a multiaxial fatigue issue. One particular strategy employed to estimate fretting fatigue life from fretting-induced multiaxial stresses is the "critical plane" technique, e.g. Szolwinski and Farris (1996). A critical plane method that utilizes the FE analysis is established comprising the Smith Watson Topper (SWT) that utilizes multiaxial fatigue standards .This technique looks for the maximum of the fatigue damage factor (e.g. SWT) within a range of different planes and estimates lifetime using the most damaging plane.

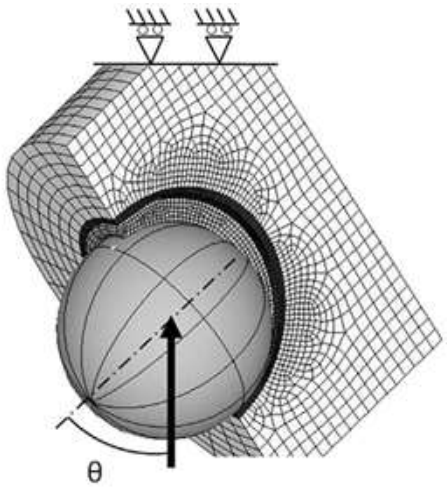

Figure 2.11- FE model of assembled cup implanted in PMMA support (Dickinson, 2014)

Table 2.2- Result of wear- fatigue FE analysis and experiments (Zhang et al. 2013)

Slip regime	**Normal load (N)**	**Half-stroke (μm)**	**Experiment**		**FE SWT life prediction**	
			Crack location($\varkappa/a_0$)	Cycles to nucleation	Crack location($\varkappa/a_0$)	Cycles to nucleation
Gross slip	500	40	N/A	$>3x10^5$	N/A	$>10^8$
Partial slip	1000	22.6	0.4 to 0.9	$<1x10^5$	0.479	$0.15x10^4$

2.8.3.2 Fretting fatigue

Fatigue lifetime of any object could be affected by fretting. Fretting fatigue is usually a mixture of two complicated phenomena that may be associated with different mechanical reactions of material, such as damage mechanics that is relevant to tribological conduct of two contacted areas (fretting damage) and at deeper stage fracture mechanics that is more linked to fatigue reaction of materials. When both of these sophisticated phenomena are matched with each other, fretting fatigue takes place. Because of fretting, fatigue life of parts reduces significantly. There are several applications that can be exposed to fretting fatigue, for instance bolted and riveted attachments, bearing shafts, blade-disk connection within gas as well as steam turbines, aero-engine splined couplings, etc.

2.8.4 Laboratory testing

One of the primary problems concerning the testing of a hip replacement implant or femur to get stress fatigue could be the simulation of everyday life conditions. There are particular criteria for examining both of these concerning the positioning of the support as well as the angle at which the hip implant is placed. Standard ISO and ASTM durability experiment approaches exist for conventional implant designs, however a difficult task for the bioengineer would be the designing of in vitro experiments that simulate medical conditions and also computational evaluation techniques as well as computational analyses for innovative designs.

2.8.4.1 Strain gauge test

The strain gauge test is used as an experimental method to calculate the strain value at a point. There are different methods of measuring the strain value and the resistance strain gauge is one of the most convenient. The strain gauge is tightly attached to the surface of the material and connected to the measuring device with wire. Then any physical strain from an applying load, is transferred to the strain gauge's resistive part and subsequently induces a proportional resistance change that can be read from the measuring device. Since there is a linear relationship between stress and strain for many materials inside the elastic limit, the stress can be calculated from the measured strain.

Figure. 2.12- Experimental rig along with strain gauges
at the time of mechanical experiment (Reikeras, 2015)

This technique of evaluating is also utilized in the ISO 7206 method and as outlined earlier, it has contributed to a substantial decrease of the failure levels from 30 years ago. The actual ISO 7206 technique is utilized as a standard for laboratory studies which identify the strength of femoral as well as hip parts. This standard adopts the application of a cement mix to fix the hip implant along with giving a range of constraints to use in the process.

2.8.4.2 Fatigue test

ASTM F 2580 is an international standard testing technique for assessment of modular connection of proximally set femoral hip implant. This experimental technique covers a process for the fatigue evaluation for metallic femoral implants employed within total hip implants. This experimental technique covers the methods for the functionality of fatigue experiments in metallic femoral hip stems utilizing a cyclic, constant-amplitude load.

The specimen holder is designed to support a testing specimen under variety of mounting angles as well as positions, while enabling variation of the holder's X-Y position within the machine base to guarantee that the direction of the force passes through the middle of the femoral head. Forces tend to be applied on the implant head by a cylindrical forcing head mounted on a low-friction bearing to avoid off-axis loading. Since biomedical prostheses will be employed in vivo, the hip replacement implant fatigue fixture is developed for biobaths to experiment in saline conditions. A special positioning fixture is also available to guarantee specific and precise fixturing of the femoral hip implant within the specimen holder. This particular fixture allows accurate measurement and realignment of the implant installation angle and height. The GF2580 hip prosthesis fatigue fixture also satisfies the needs of ASTM F1440 standard for evaluating the actual fatigue strength of metallic stemmed hip arthroplasty femoral parts without torsion, while ASTM F1612 is meant for assessing the fatigue overall performance of metallic stemmed hip arthroplasty femoral parts with torsion.

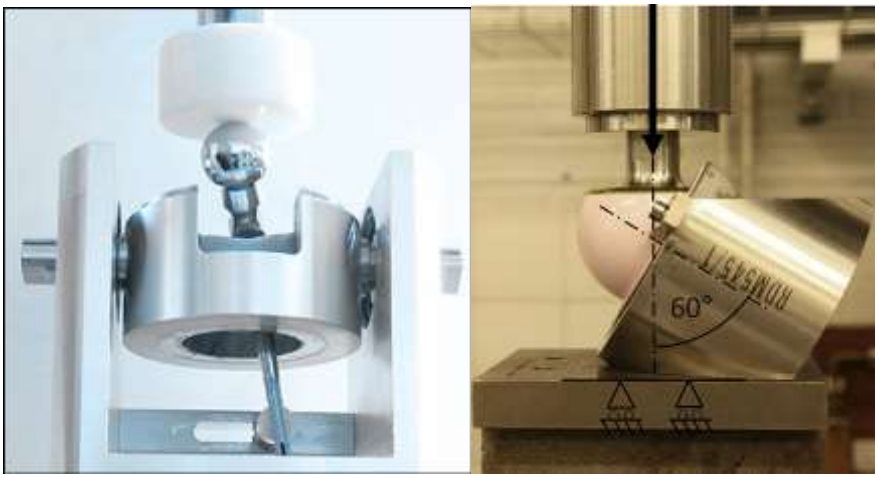

Figure 2.13- Experimental test setup of the assembled cup implanted with PMMA support. (Dickinson 2014)

In this regard, Dickinson et al. (2014) have also suggested a way for preclinical fatigue performance assessment that addresses the mean stress, stress concentration areas and materials processing. They have outlined the significance of taking the mean stress into consideration. In their proposed method, the stress distributions were estimated computationally in a complete assembly and under the in vivo forces and its cyclic residual stresses. Subsequently stress intensity was measured (Figure 2.13).

2.8.4.3 Photoelasticity test

Some of the more intriguing and major applications of PhotoStress experiment are those in the area of biomechanics. Among applications in this field, there is stress analysis of skeletal components like the femur, pelvis, knee, elbow as well as skull, and other joint replacements; dental prostheses and bridges; along with mechanical medical products including forceps and medical staplers. Specifically noteworthy is the level at which PhotoStress has been utilized in the evaluation of stresses for artificial hip implants. This work has been conducted both in orthopaedic study centres and also by companies of prosthetic products. Based on one medical study group, the application of PhotoStress on bone has a specific benefits over other strain-measurement techniques including finite element method, brittle coatings, strain gauges, as well as photoelastic modelling.

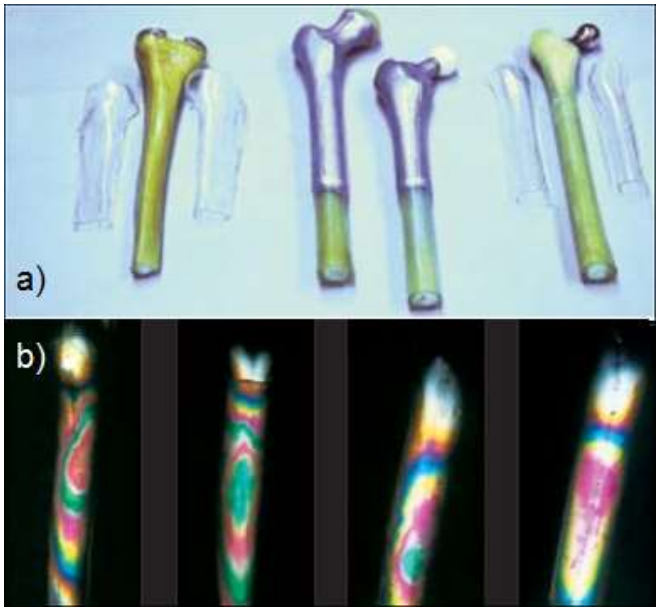

Figure 2.14- a) Setting up the experiment, b) PhotoStress results of synthetic femur

All of these kinds of techniques have restrictions in their application to the study of bone, which include directional and positional limitations, and presumptions of homogeneity. Due to its full-field capacity, PhotoStress overcomes these kinds of limitations through permitting observation as well as measuring the strain directions and magnitudes, within different complicated load modes, irrespective of material homogeneity.

Figure 2.14(a) demonstrates simulated femoral experiment specimens being set for PhotoStress evaluation of various kinds of hip implants. Figure 2.14(b) displays the resulting stress distribution of the various hip replacement prostheses used. After the modelling experiments have been finished, selected implants are then selected to be fixed in real bone for additional PhotoStress evaluation. In this regard Arno et al. (2012) have carried out a study using the PhotoStress approach to assess the femoral strains using cementless proximal-fill femoral hip prostheses of different stem size. They have analysed thirteen femurs intact, along with three different stem size prostheses: stemless, ultra-short and short.

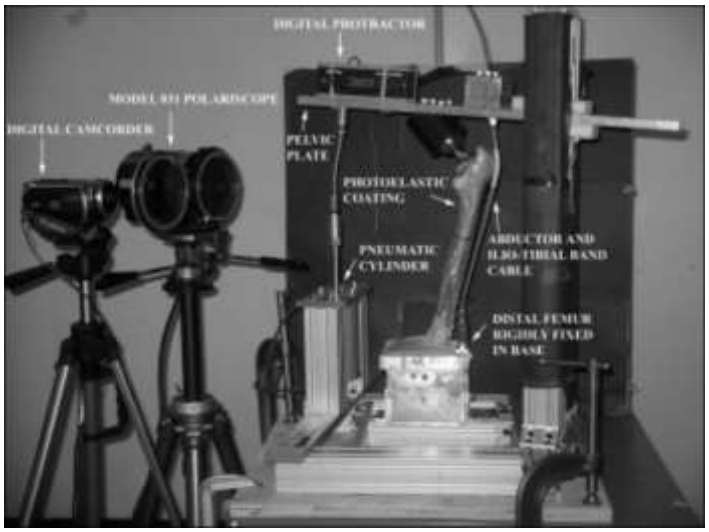

Figure 2.15- PhotoStress testing equipment (Arno et al. 2012)

2.9 Stability of hip implant

2.9.1 Implant stability

The stability between the femur bone and the prosthesis can be categorized into primary and secondary stability. Primary stability describes the stability within the bone-implant interface soon after replacement and depends completely upon mechanical factors (Viceconti et al., 2000). Secondary stability explains the biological stability of the prosthesis when bone ingrowth has taken place. Primary stability attained after surgery is a determinant issue for the long-term stability of cementless hip arthroplasty. The word primary stability is actually defined by Viceconti et al. (2006) as the level of relative micromovement within the femur and the prosthesis induced via the physiological joint forces following the surgery, before any biological process occurs.

Stability of a hip femoral stem implant is a fundamental element in its long-term clinical success. In non-cemented femoral stems, the immediate post-operative, or primary, stability is crucial since it permits the femur to develop towards the implant femoral stem to interlock it, producing secondary, long-term stability. A previous investigation created a protocol to compare the in vitro primary stability in rectangular and conical press-fit femoral stem models employing custom-designed micromotion sensors (Buhler et al., 1997).The research has identified that both femoral stems displayed similar levels of migration, however the cone-shaped femoral stem demonstrated moderately more cyclic movement than the tapered femoral stem, most of which was at the anterior-posterior area.

On the contrary, cemented fixing provides instant stability from cement-stem and cement-bone connection, but may degrade eventually (Hozack et al., 1993). Many reviews have evaluated methods to enhance the long-term clinical success in cemented prostheses by adjusting femoral stem surface features or cementing method to enhance bonding. Ahmed et al. (1984) and Stone et al. (1989) determined that cement pre-coating could boost the interface strength since the bonding takes place ex vivo and is therefore free of any involved blood or other contaminants. Cook et al. (1987) have discovered that the implant-cement interface strength of porous-coated prostheses rises with pore size, and they suggest an optimum size of 345 µm. Adjustments of the cementing method, including preheating the prostheses (Bishop et al., 1996) , distal

plugging of the medullary canal and pressurization of the cement (Bannister et al., 1988) and centrifugation of the cement (Burke et al., 1984), result in a much more homogeneous cement mantle, and subsequently a stronger cement-stem and cement-bone connection. The ultimate goal of these enhancements is to make the prosthesis more stable, and consequently prolong the fatigue life.

Even though cemented femoral stem fixation is anticipated to be much stiffer than for cementless femoral stems, detectable movements may occur under physiologic forces, and excessive movements could harm the cement mantle. Speirs et al. (2000) looked into the stability of two cemented hip prostheses under physiologic forces. The prostheses were examined in vitro, inserted in paired human femurs, and set with simulated in vivo loads on the hip joint femoral head while movements were assessed with custom-designed micromotion sensors. The different movement patterns exhibited by the two femoral stems could be used to describe the influence of model characteristics on the stability of the prosthesis.

2.9.2 Stability factors

THA includes removing neck and head of a femur and replacing them by an implant. Two forms of prosthetic products are used: cemented and cementless femoral stems. Cemented stems are set to the surrounding femur through bone cement, while cementless femoral stems are fixed to the surrounding femur through mechanical press-fit. No significant difference among cemented and cementless THR with regards to prosthesis survival as measured by revision rate has been identified (Abdulkarim et al., 2013), and controversy still exists concerning the optimal fixation techniques. Nevertheless, nowadays cementless fixations are generally favoured (Learmonth et al., 2007), particularly in young and active individuals, to remove problems related to the utilisation of cement (Jasty et al., 1991). Cementless hip femoral stems are set to the surrounding femur by means of press-fit. To guarantee an excellent press-fit, current medical method specifies an under-reaming of the femur bone cavity employing successively bigger broaches. Nevertheless, this medical technique is inaccurate. The existence of movement at the stem-bone interface results in formation of fibrous tissue that could inhibit bone ingrowth, which subsequently may result in loosening of the prosthesis (Viceconti et al., 2001). Pilliar et al. (1986) have demonstrated that an interfacial micromotion

beyond 40 μm creates partial ingrowth, while micromotion exceeding 150 μm completely inhibits femur bone ingrowth.

Primary stability relies on many factors. Many reports have targeted their interest at the femoral stem model (Callaghan et al., 1992, Ando et al., 1999; Mandell et al., 2004; Abdul Kadir et al., 2008, Reimeringer et al., 2013; Bah et al., 2015), the sensitivity to hip joint forces (Pancanti et al., 2003), the influence of physiological force formation (Abdul Kadir and Hansen, 2007), the influence of inter subject variability (Viceconti et al., 2006; Bah et al., 2015), the influence of femur bone material properties (Wang et al., 2005; Reimeringer and Nuño, 2014).

A further factor that affects the primary stability is the location of the prosthesis within the femur (Reggiani et al., 2008; Bah et al., 2011). An excellent primary stability for cementless THA is obtained by a close apposition of the prosthesis to the femur. Its location is decided over the pre-operative planning. Throughout surgery, the canal is manually broached through successively bigger broaches so that the broach contacts the hip joint femoral cortex. Furthermore, to ensure a press-fit, the recent surgical method specifies an under-reaming of the cavity. This traditional approach is inaccurate (Lattanzi et al., 2003). The contact ratio (percentage of femoral stem interface in touch with femur along the femoral stem) obtained after operation, ranged between 20% and 82% and determined by either employing a broaching technique or numerical evaluation. This can increase to 95% employing a robotic system. The absence of direct attachment among the femoral stem and the femur bone has been recognized by Viceconti et al. (2006) as the main threat for prosthesis stability. Furthermore, Tarala et al. (2013) has demonstrated that femur ingrowth close to the hip femoral stem essential for secondary stability of the prosthesis depends on femoral stem and femur bone contact region in both cortical as well as cancellous bones. Nevertheless, Park et al. (2009) suggest that when 40% of contact ratio is obtained along the femoral stem, primary stability is little influenced by a rise in this contact ratio. It has been demonstrated that full connection (100%) between femoral stem and femur is not required to attain a good primary stability. The femoral stem primary stability is affected by both the contact ratio and its position. A number of configuration settings with contact ratio less than 100% and associating either the proximal or the cortical attachment supply better primary stability compared to full contact setting.

Nevertheless, with contact ratio less than 40%, the femoral stem must be in contact with cortical femur to guarantee excellent primary stability.

2.9.3 Stability prediction techniques

The model factors, together with the primary value of the patient factors decide the prospective of a joint model to tolerate primary mechanical failure that is termed "primary stability". In case the deformations in the structure are critical (loosening), or even, the stresses in the material or on the interfaces are considerable (fracture), then failure will take place. It is difficult to measure exactly when a failure takes place since a mechanical failure, including cement fracture, does not always result in a clinical failure along with the need for a revision surgery. If the stress is not high then it feeds back to modify the control factors via biological processes. As depicted in the scheme, such biological procedures can cause the structure to deteriorate and consequently the chosen model factors are no more optimal. The level to which they are able to continue to be optimal determines the "secondary stability" of the prosthesis system, which is described as the potential to resist rapid mechanical deterioration following mechanical failure or biological adaptions that have happened.

Several approaches have been employed in estimating stresses and strain patterns in the biomechanical field such as practical methods including strain gauging to photoelastic analysis, and numerical methods including the finite element method (FEM) to attain comprehensive details on the state of stress and strain within the intact and treated femur bone. The empirical techniques of medicine has been proven as unsuitable for enhancing of biomechanical devices and mathematical packages have been created to simulate the characteristics of real systems and so provide us with the capacity to estimate how they would behave under modified circumstances (Ducheyne et al., 1984). The versatile capabilities of FEM analysis in comparison with practical techniques in cases where a structure is too complex for closed-form theories are its potential for assessing stresses/strains within the structure, in and among all materials concerned, and for parametric evaluation. Material properties, and forces and boundary conditions can readily be changed to be able to examine their effects. Because of this, the finite element technique has become a significantly useful tool in analysing the stresses in structures of complicated models, forces and material behaviour.

Faced with the task of recognizing a complex system, it is usually helpful to extract its most important characteristics and use them to produce a simplified representation, or design of the system. A model facilitates anyone to monitor more carefully the behaviour of the system as well as to make estimations regarding its overall performance under altered input conditions and distinct system factors. Finite element objects are numerical mathematical objects: numerical because they depend on computers to discover estimated solutions to huge sets of equations. Finite element method has provided many estimations relevant to orthopaedics. In most cases, these estimations have been compared to physical objects to help confirm their validity.

2.9.4 Micromotion at the femur bone prosthesis interface

Micromotions are the relative displacements that take place within the surface of an orthopaedic prosthesis and the femur bone. The magnitudes of these displacements are associated with the physiological loads that are put on the implanted joint. It is believed that once the micromotions reach a threshold value in the region of 100 μm - 200 μm, the biological fixing of the prosthesis will become compromised, and fibrous tissue will be created at the bone-implant interface, as opposed to new femur bone (Pilliar et al., 1986; Maloney et al., 1989). This fibrous tissue has inferior mechanical properties when compared to femur and therefore contributes to the premature loosening of prostheses. From the literature, it is evident that poor primary stability contributes to the failure of fixing for cementless prostheses used in THA (Maloney et al., 1989; Phillips et al., 1990). Hence, it is important to establish sound primary stability in order to achieve adequate secondary stability through full femur bone ingrowth at the bone-implant interface.

From a clinical perspective, the two main factors that contribute to the stability of an orthopaedic prosthesis are the quality and quantity of the host femur bone tissue, and the surgical fit of the prosthesis. Wirth et al. (2011) confirmed that prosthesis stability is directly affected by the microstructural quality of the periprosthetic cancellous femur bone. Bertollo et al. (2011) have studied the influence of surgical fit on prosthesis shear strength for porous

titanium and discovered that the average shear strength at cortical and cancellous femur bone sites was better in press fit and line on line fits compared to a 1mm clearance fit. This shows that creating initial contact within the interface is critical to be able to promote femur bone ingrowth and optimise secondary stability. Good primary stability would be the foundation for the long-term stability for hip implants. Later in Chapters 4, 5 and 6 both primary stability and long-term stability will be evaluated through micromotion analysis and stress distribution assessment of hip prostheses.

Chapter 3

Methodology: Experimental Testing and Numerical Modelling

This chapter explains different experiments carried out on synthetic femur models from Sawbone Company, as well as a hip implant using a strain gauge technique. Also a numerical modelling presented in the next chapter which include the review of different studies about finite element analysis to predict settlement, sometimes known as migration, of hip joints in bones. This will help to justify the best solutions for design factors.

The laboratory testing performed on the femur included the compression, torsion and Brinell hardness testing. A compression testing using strain gauge technique done on the hip implant. All compression and torsion testing was simulated in Ansys software assuming the same boundary conditions and subsequently the computational results were compared with the earlier experimental data to verify the experiments and models used.

3.1 Synthetic femur testing

3.1.1 Sawbone

Sawbone is one of the leading synthetic bone model companies that produces short fibre reinforced epoxy composite bones that are claimed to have the same mechanical properties and characteristics of real bone. These bones are largely utilised for different studies and engineering purposes as cadaveric bone substitutes in a wide variety of biomechanical tests. Having said that, it is important to validate the bone properties to make sure we are using a synthetic bone similar to a real bone. Many studies (Chong et al., 2007a; Chong et al., 2007b; Dunlap et al., 2008; Heiner 2008; Zdero et al., 2008 and Papini et al., 2007) have performed different experiments to confirm the validity of synthetic femur manufactured by Sawbone. Some of these experiments include fracture toughness, fatigue crack propagation rate and fatigue performance tests.

In this study different techniques and test methodologies were used on the 4th generation synthetic Sawbone femur to examine if properties of synthetic bone were within the range of published human bone values. The bone was made of a glass fibre polymer composite material and the properties were taken from the manufacturer's handbook (Sawbone, 2016). The

technique that is used is utilising strain gauges on mount it at specific locations on the bone and compare it with finite element analysis results.

The reliability of the FEA and also strain gauge evaluation is vital and might be doubted when going through the design optimization process of the hip implant utilizing FEA software or any other mechanical ways of testing. Researchers such as Stock et al. (2002) validated the fact that FE analysis technique as well as mechanical testing on the cemented type of hip prostheses can verify the pre-clinical experimental data along with common error that is not different more than 10%, therefore the results from FEA as well as mechanical experiments could enable the prediction and estimation of long-term failure for hip prostheses (Stolk J., 2002).

Basso et al. (2014) and other researchers have implemented strain gauge experiments upon cadaveric femur that was taken from a 64 years of age male patient just one day after his death because of a heart attack. In order to guarantee the most effective possible result from this test, bone was set and prepared before the experiment. The particular soft tissues and also condyles were taken out as a way to fix the bone into the examination rig and in addition the distal section of the bone was bonded into the cylindrical steel tube in order to ensure the balance and stability of the bone whilst force was applied. The length between the top end of the cylindrical steel stand and the tip of greater trochanter was mentioned to be 180mm (Reikeras, 2015).

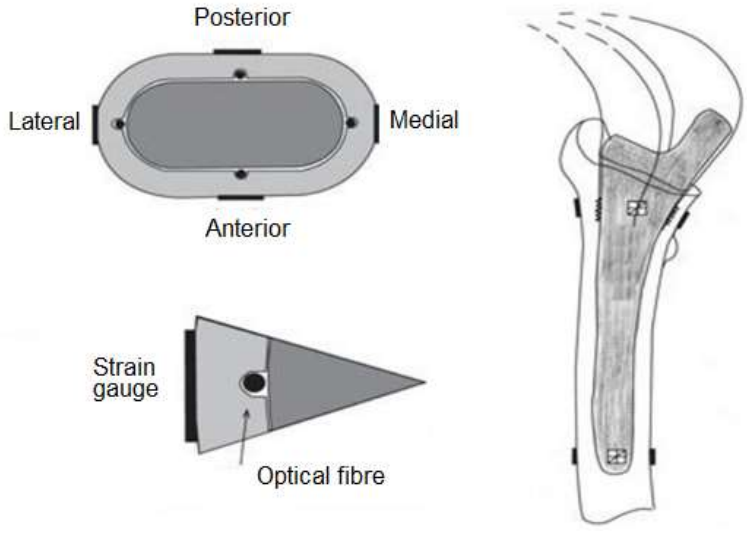

Figure 3.1- Schematic drawing of testing assembly with 4 strain gauges attached externally and also 4 internally on bone as well as on the hip implant (Reikeras, 2015)

With regard to strain gauge measuring, 8 rosette gauges were attached externally and also internally on the bone as well as the hip implant. The rosette gauges were attached anteriorly, medially, laterally and also posteriorly on each of both the bone and the hip implant (Reikeras, 2015).

The femoral canal of the bone was reamed out by the surgeons with the help of specific instruments to obtain optimal installation of the 28mm head implant having a standard neck and offset. The cemented DePuy hip implant and cementless Corail titanium prostheses were subsequently installed on the jig and a 1000N load was applied to obtain the strain reading. The femoral hip implant was later removed, reset and installed again in the jig prior to acquiring any more readings. The experiment recorded a decrease in deformation in compression particularly at the medially and proximal level. The experiment also showed 26% decrease of medial compressive strain via thin to thicker hip implant of cementless type. The development of cemented femoral stem demonstrated the relative transfer of compressive strain through medial to anterior level and on the proximal cortex. Table 3.1 below displays strain measuring in cemented and cementless hip prostheses (Reikeras, 2015).

Table. 3.1- Measured by Rosette Strain Gauges (Reikeras, 2015)

	Cementless prosthesis (με)	**Cemented prosthesis (με)**	**Change with cement (με)**
Medial			
External cortex	-570	-382	188
Internal cortex	0	-55	-55
Anterior			
External cortex	-110	-260	-150
Internal cortex	210	203	-7
Lateral			
External cortex	27	55	28
Internal cortex	-90	115	205
Posterior			
External cortex	-87	36	123
Internal cortex	-56	135	191

Authors such as Shantanu and Harsha have studied the performance of material such as cobalt chromium and titanium alloys for stems, cross-linked polyethylene for liner and Poly methyl methacrylate for bone cement. Table 3.2 below shows the material properties in FE model (Singh, 2014).

Table. 3.2- Material properties in FE model (Singh, 2014)

Material	**Elastic modulus (GPa)**	**Poisson's ratio**	**Yield strength (GPa)**	**Ultimate tensile strength (GPa)**
CoCrMo	230	0.3	0.455	0.65
Ti_6Al_4V	110	0.3	0.795	0.86
Cross linked polyethylene	1.4	0.3	0.023	0.044
Bone cement	2.5	0.38	-	0.0353
Cortical bone	17	0.29	-	-
Cancellous bone	0.52	0.29	-	-

3.2 Torsion testing

3.2.1 Experimental analysis

When the most suitable and relevant testing process had been determined, the laboratory testing could be arranged with respect to requirements of the project. The laboratory testing was basically implemented on femur. The femur initially went through torsional bending experiments, as a way to achieve the strain data. The strain gauges were precisely attached to the locations with relatively larger predicted stress values. Following identifying the exact locations on the femur bone that show maximum stress values under the twist test, the initial step was to attach the strain gauges in laboratory.

The following steps are the process of attaching strain gauges to the femur bone over a specific location:

1. The initial step involves cleaning the equipment such as the glass on which the strain gauges would be positioned and also the femur by utilising IPA (Isopropyl alcohol).

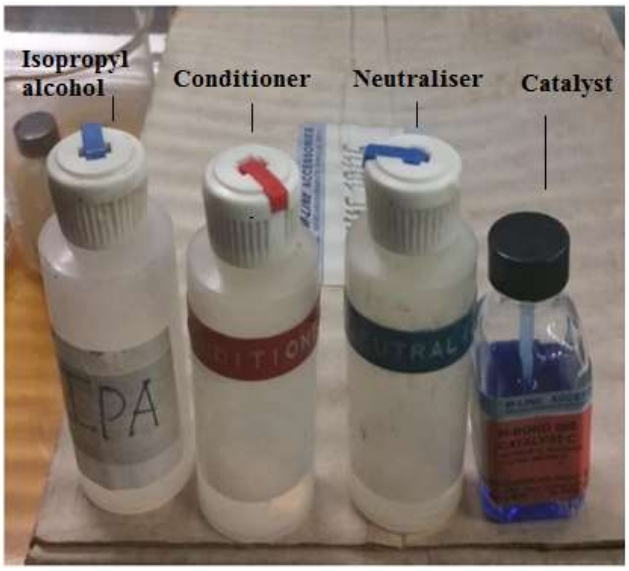

Figure. 3.2- Type of solvent employed

2. The next step includes surface area conditioning in which the conditioner was employed on the femur over the specific locations where the strain gauges would be used, this process involves applying the particular conditioner and then rubbing it by using a piece of cotton.

3. When the surface area of the femur was cleaned, neutralizer was employed on the work surface of the bone, glass and twissors in order to neutralize the surface area prior to attaching strain gauges.

4. The next step would be cleaning the glass, bone and also the tweezers by using both conditioner and neutraliser to eventually ensure the surface is thoroughly clean and prepared for implementing the strain gauges.

5. When the cleaning procedure was finished, the shiny surface area and the soldering area of the strain gauges were positioned on the glass piece and tape was placed on them when aligned correctly.

6. The catalyst was applied to the strain gauge on the tape.

7. Finally the tape was positioned on the preferred place and cyanoacrylate was used for the strain gauge to ensure that it was strongly adherent and remained in the ideal position of the femur.

8. Any excess cyanoacrylate was carefully removed by using tissue and then the strain gauge was positioned in place and hard pressed for approximately 90 seconds in order to make sure strain gauges does not detach from the surface area.

When the strain gauges was attached the next step was to solder the wire on to the strain gauges. Subsequently after wiring the strain gauge it was essential to check the following steps to make sure the wiring was done correctly and worked properly:

1. That minimal resistance is 120 ohm +/- 0. 4%.

2. That the variation in resistance surpasses 5%.

3. That the maximum resistance between the strain gauge and femur is not greater than 20 GΩ, once the femur is in position, the torsional experiment was to be performed on the particular Machine known as “testometric micro 500/50k machine”. Utilising the specific data from the literature, the test rig was assembled as shown in Figure 3.3 below.

Figure. 3.3-The rig set up for torsional bending experiment

Figures 3.3 demonstrates the way synthetic femur bone was fixed inside the vice to ensure the femur bone does not shift or rotate when a particular force was applied upon the femoral head. After the whole rig assembly was properly prepared, the load was applied to the femoral head of the synthetic bone through increments of 100N in the load range 200N up to 1000N. The strain data were obtained from the particular strain gauge meter.

There are always some restrictions and errors in the test and evaluation, where the majority of them are due to the machine, human errors and available resources. The strain gauges applied on the synthetic bone were not exclusively designed for composite material therefore the results obtained would not be as precise as expected, while still yielding acceptable and valid results.

3.2.2 Finite element analysis (FEA)

3.2.2.1 Mathematical model

The laboratory experiment, makes it possible to verify the finite element analysis of the synthetic bone and when the data were validated, further work could be continued using CAD software. When the same forces applied and real life evaluating was performed and results were properly and precisely obtained in the laboratory, it was necessary to simulate the same experiment in CAD software. Following the modelling stage it was fundamental to replicate the testing boundary condition in accordance with the experiment that was carried out in the laboratory. This was done by importing the SolidWorks 3D model as a STP file into Ansys

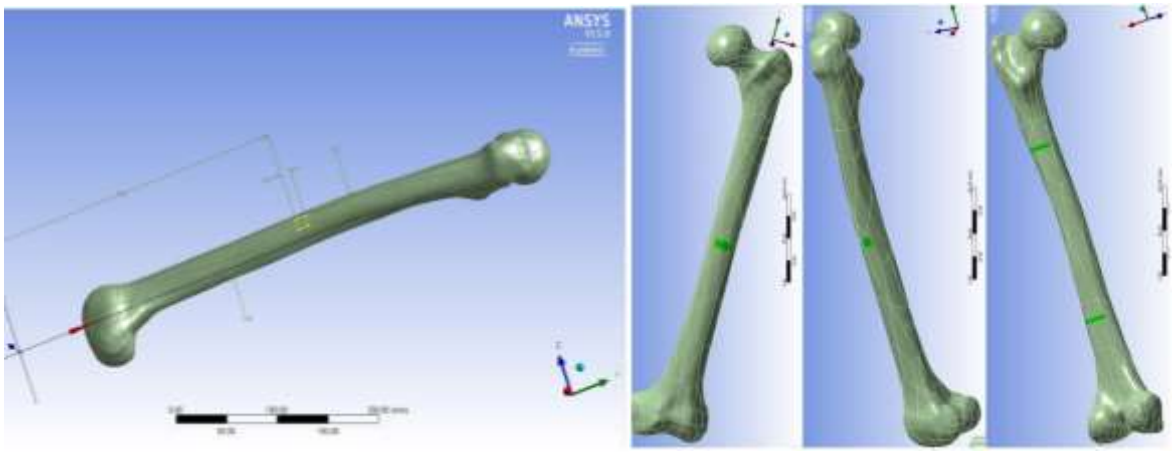

Figure. 3.4- Illustration of imprint phase

software where the specific boundary conditions were applied to the 3D model of the hip implant in order to validate the real life laboratory testing. In order to calculate the strain at a particular location, strain gauges were sketched in similar dimensions and imprinted over the femur bone model to simulate the real boundary conditions in the laboratory as demonstrated in Figure 3.4. To validate the results from the laboratory testing, the strain gauge were applied in the position as specified in Figure 3.5 below:

Figure. 3.5-Illustration of the positions of strain gauge

3.2.2.2 Boundary conditions

A real hip prosthesis model was examined in the laboratory where the loads were employed vertically over the femur head as demonstrated in Figure 3.6. The exact same boundary conditions were replicated when validating the design in the Ansys. Geometry was used to build the design imported in to Ansys. Strain gauges faces were imprinted onto the surface of the femur replicating the real life strain gauges. Following imprinting the faces on the femur, the femur could be opened up in model and boundary conditions could be employed. Since the applied force was not equally distributed, the symmetry technique along a split line could not be used to simplify the analysis. Thus the full model was used for the simulation.

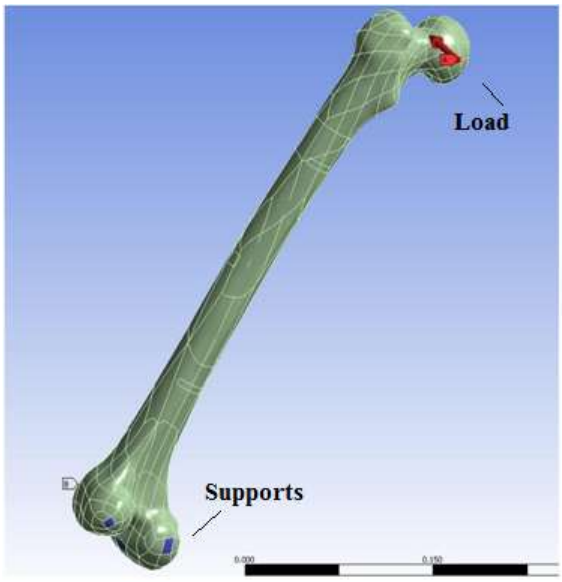

Figure. 3.6- Illustration of loads and supports

To estimate stress in one direction which simulates the real life strain gauge test, the coordinate system solution available in Ansys was implemented to resemble stress measured employing strain readings from laboratory outcomes. Figure 3.7 displays stress at imprinted faces which would be eventually compared with stress calculated employing strain from laboratory testing.

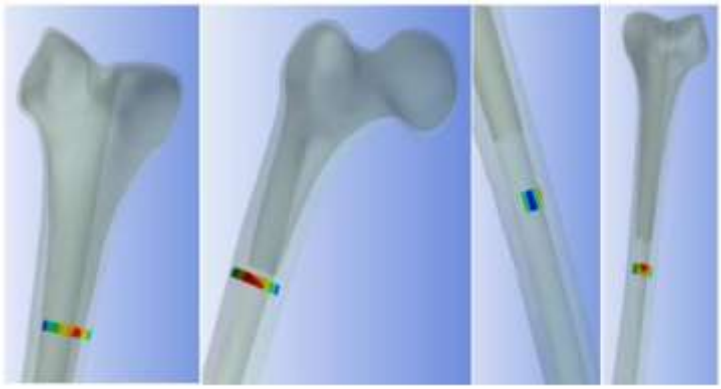

Figure. 3.7- Stress at imprinted faces

3.2.2.3 Mesh refinement

To ensure the stress values obtained from the Ansys at each imprinted face are accurate, it is vital to consider the meshing solution available in Ansys. Figures 3.8, 3.9 and 3.10 show the default, first and second meshing refinement. This meshing procedure was considered and permitted convergence and achievement of precise stress values as demonstrated in Tables 3.3, 3.4, 3.5 and 3.6 below and the next page.

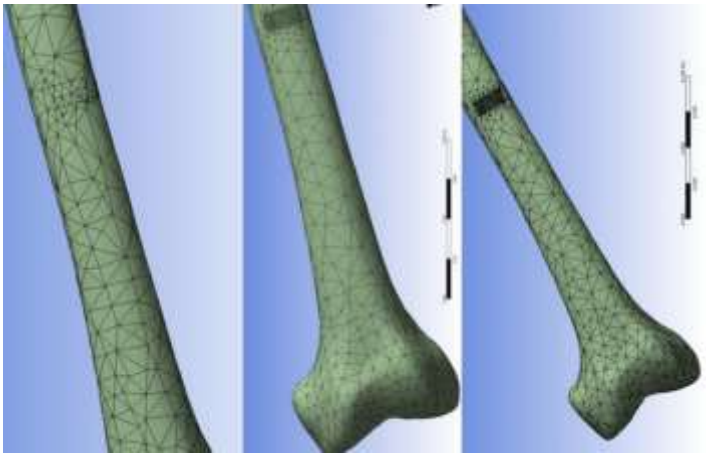

Figure. 3.8-Meshing at strain gauge number 7, 8 and 9 displaying defaults (left), first refinement (middle) and final refinement (right)

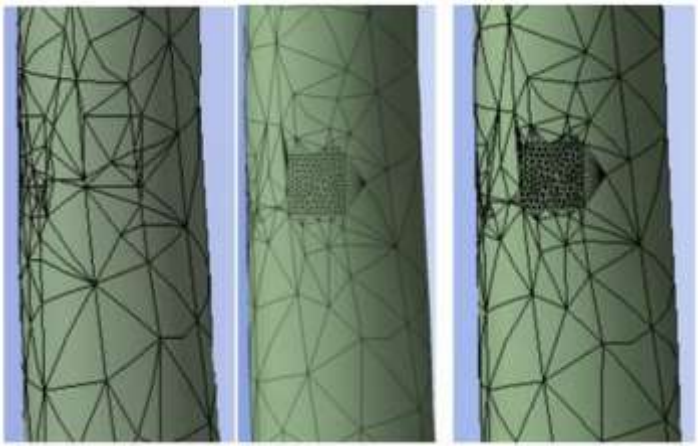

Figure. 3.9- Meshing at strain gauge number 4, 5 and 6 displaying defaults (left), first refinement (middle) and final refinement (right)

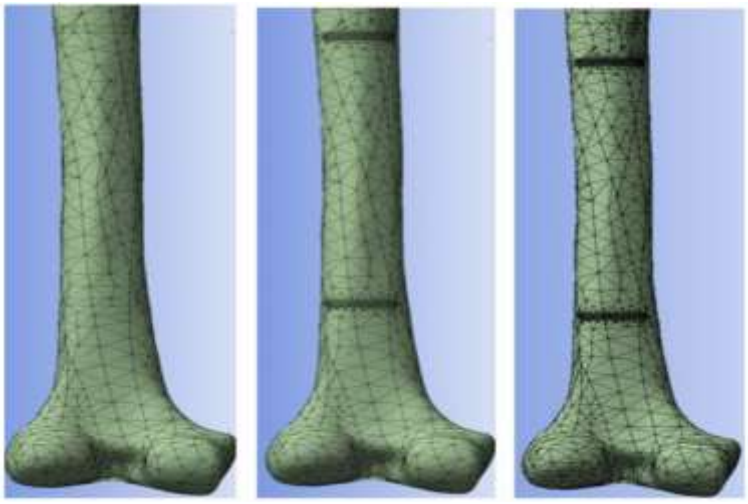

Figure. 3.10- Meshing at strain gauge number 1, 2 and 3 & 10, 11and 12 displaying defaults(left), first refinement(middle) and final refinement(right)

Table. 3.3- Position one Mesh refinement

Position 1	Method	Stress (MPa)
	Default	6.8202
1st refinement	Face sizing- Element size 1mm	10.36
2nd refinement	Face sizing- Element size 0.6mm	10.279

Table. 3.4- Position two Mesh refinement

Position 2	Method	Stress (MPa)
	Default	1.7313
1st refinement	Face sizing- Element size 1mm	2.823
2nd refinement	Face sizing- Element size 0.6mm	2.851

Table. 3.5- Position three Mesh refinement

Position 3	Method	Stress (MPa)
	Default	2.912
1st refinement	Face sizing- Element size 1mm	3.253
2nd refinement	Face sizing- Element size 0.6mm	3.365

Table. 3.6- Position 4 Mesh refinement

Position 4	Method	Stress (MPa)
	Default	8.181
1st refinement	Face sizing- Element size 1mm	8.268
2nd refinement	Face sizing- Element size 0.6mm	8.269

3.2.3 Verification and validation of simulation model

Following successful validation process between the experiment data and the Ansys final results, additional real life scenarios could be independently simulated in Ansys, without any necessary laboratory experiment for data validation. The values from laboratory testing and Ansys simulation for the femur model will be compared to evaluate the similarity and validity of data.

Figure. 3.11 -Testing rig

Figure 3.11 above displays the experimental setup for the laboratory testing. Distinct sets of loads were applied to the femoral head, where all loads were applied twice to reduce any practical errors and to achieve correct strain values at points 1, 2, 3, 4, 5,6,7,8,9,10,11 and 12.

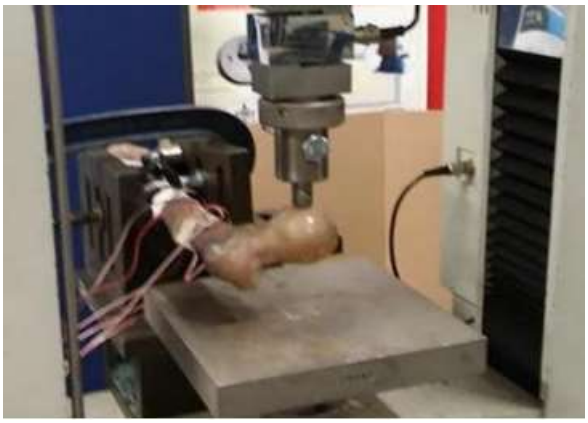

Figure. 3.12- Femur placed in the test rig

The location of distinct strain gauges 1, 2, 3, 4, 5, 6, 7, 8, 9, 10, 11 and 12 can be viewed in Figure 3.13 below, where the strain data were measured twice to insure the outcomes were accurate and the average strain values were listed and used to validate the Ansys model.

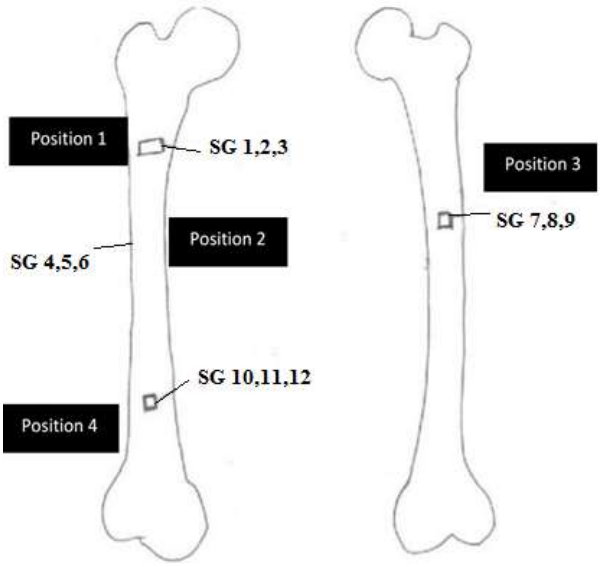

Figure. 3.13- Measurements of strain gauges distance

The laboratory testing machine that was used to, is recognized as 'Testometric micro 500/50kN'. The force was applied on the femoral head of the Sawbone femur ranging from 200N to 1000N in step of 200. Table 3.7 below is the average of first and second strain records from the laboratory testing.

Table. 3.7 - List of recorded strain values from laboratory testing

Strain gauge No.	**Strain at 200N (με)**	**Strain at 400N (με)**	**Strain at 600N (με)**	**Strain at 800N (με)**	**Strain at 1000N (με)**
1	29	57	84	131	153
2	15	31	52	69	75
3	56	113	189	217	279
4	-22	-49	-63	-91	-110
5	-39	-61	-87	-137	-179
6	43	71	137	148	193
7	-104	-213	-316	-436	-523
8	-17	-28	-43	-51	-64
9	-49	-97	-164	-217	-282
10	3	11	17	21	23
11	101	229	364	452	594
12	-6	-19	-23	-34	-38

Employing the strain values from the laboratory, the following equations were used to determine the relevant stress values at those points:

Strain values: $e_1 = 153 \times 10^{-6}$ $e_2 = 75 \times 10^{-6}$

Young's modulus: $E = 16.7 \times 10^{9}$ (N/m^2)

Poisson's ratio $\upsilon = 0.3$

Stress value: $$\sigma = \frac{E}{2}\left[\frac{e1+e3}{1-\upsilon} + \frac{1}{1+\upsilon}\sqrt{(e1+e3)^2 + (2e2 - e1 - e3)^2}\right]$$

$\sigma = 8.467 \times 10^{6}$ (N/m^2)

Table 3.8- Calculated stress from laboratory results

Strain gauge No.	**Stress calculated conversion using laboratory results**
1,2 and 3	8.467
4,5 and 6	3.872
7,8 and 9	-2.846
10,11 and 12	-7.906

Table 3.9 below displays the percentage error among 3 cases that measures up the discrepancy between Ansys simulation final results and the hand calculation of stress distribution employing laboratory testing. Formula that was used to calculate the error is as follows:

$$\frac{\text{Biggest value} - \text{smallest value}}{\text{Biggest value}} \times 100$$

Table. 3.9- Percentage errors Ansys versus calculation employing laboratory final results

Percentage error between Ansys and laboratory results	
Position	Percentage error %
1	17.63
2	26.37
3	15.42
4	4.39

The quantity r, known as the linear correlation coefficient, calculates the strength and the direction of a linear relationship among two variables. The linear correlation coefficient is often called the Pearson product moment correlation coefficient in honour of its creator Karl Pearson. The mathematical formula is:

$$r = \frac{n\sum xy - \left(\sum x\right)\left(\sum y\right)}{\sqrt{n\left(\sum x^2\right) - \left(\sum x\right)^2}\sqrt{n\left(\sum y^2\right) - \left(\sum y\right)^2}}$$

A correlation more than 0.8 is generally referred to as strong, whereas a correlation under 0.5 is typically referred to as weak. Coefficient of determination or R^2 calculated according to two sets of data obtain from laboratory testing and Ansys analysis is equal to 0.98 which shows a very strong correlation. Mathematically it indicates that 98% of the total variation in y can be described by the linear relationship among x and y. Only 2% of the total variation in y remains unexplained.

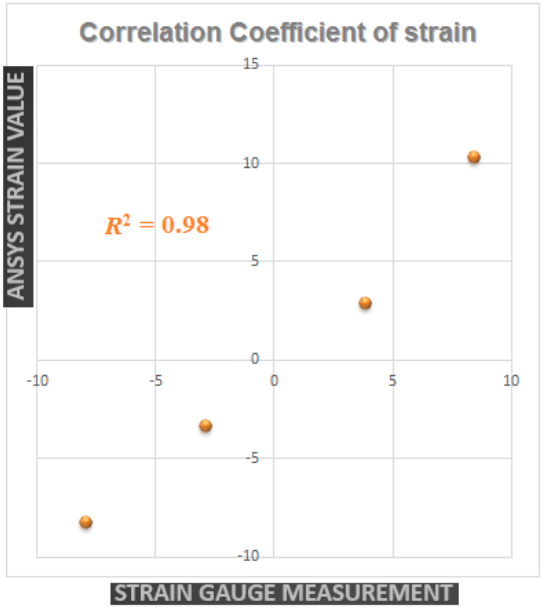

Figure 3.14- The correlation determination value of R^2=0.98 which displays a strong correlation among the laboratory testing and Ansys analysis data.

The significance level of the correlation coefficient is calculated from p-value. The p-value is calculated using a t-distribution with n-2 degrees of freedom. The formula for the test statistic is $t = \frac{r\sqrt{n-2}}{\sqrt{1-r^2}}$. In this calculation the value of t is equal to 14, and the two-tailed P value equals 0.0051. Therefore by conventional criteria, this difference is considered to be very statistically significant.

3.2.4 Discussion

The achievements of any testing is determined by the accuracy of the result. The closer the real life testing outcomes are to the final results from Ansys simulation the more accurate the measured values are. It is already understood in advance that none of the testing procedure can be 100% accurate nevertheless effort can be made to reduce the discrepancies.
The analysis of Tables 3.3, 3.4, 3.5, 3.6, 3.8 reveals that none of the outcomes exactly matches nevertheless all the stress values lie within the 30% error limit as demonstrated in Table 3.9; this could be due to several environmental and human aspects.

Considering Table 3.9 which displays the errors between Ansys vs laboratory data, differences can clearly be observed, none of the positions match up with the exact stress values. Table 3.9 clearly exhibits the percentage differences at all four locations where a strain gauge rosette was employed. The calculated stress value at position 1 employing the laboratory data is 10.279MPa whereas the estimated Ansys value is 8.467; the percentage error between the calculated and estimated is 17.63. At position 2, the calculated value is 2.851MPa while the Ansys prediction is 3.872MPa therefore the error calculated is 26.37%. At position 3 the measured percentage error is 15.42%, as the calculated stress using laboratory final results is 2.846 and the Ansys prediction is 3.365. Finally at position 4 the determined stress value is 8.269 while the calculated value using laboratory results is 7.906 and the percentage error is 4.39%. Viewing stress at position 4, the error between the laboratory and Ansys result is rather low with 4.39% difference, but the percentage difference of positions 1 and 3 are indicating 17.63% and 15.42% respectively. However the stress values at location 2 are furthest apart with an error of 26.37%.

The inaccuracy of the measured result might be a result of improper application of the strain gauge. Failing to clean the area where strain gauge would be employed, improper wiring or existence of air bubbles following applying on the femur bone would restrict the accuracy of the measured result. The strain gauges were applied manually. It is not possible for a human to put the strain gauge in the exact locations which were assumed in Ansys and hand calculation due to parallax error or imprecise measurement would again contribute to error in strain values at position 1, 2, 3 and 4 hence the stress values calculated would be imprecise. The difference between the model that was developed in Catia software and the femur bone that was examined in laboratory could also be a reason for difference between laboratory testing, Ansys and hand

calculated results. Slight difference in femur dimensions among the created and examined component could also cause differences obtained by Ansys and hand calculated data. The loads were assumed to be applied to the centre of the femoral head of Sawbone. However as the test rig was set manually there is a chance that the force could have not been employed exactly in the centre which would lead to differences in the strain values from the laboratory testing leading to inaccurate calculated stress values compared to Ansys outputs. Various loads were applied on the femur component, from 200N-1000kN in the steps 200N. The loads quantity used in this experiment were applied with the intervals of 200N ±20. The slight difference among the actual forces applied and simulated forces creates an error. The femur model was set in the vice to guarantee femur bone does not move nevertheless reliable fixation was obtained. These are some errors that may have caused the difference among the strain values resulting in inaccurate calculated stress values.

There are other errors may have played a role in differences of the final results. Overall the discrepancies among the laboratory, Ansys and hand calculation are reasonably small. Coefficient of regression (R^2) calculated in Figure 3.14 based on two set of data obtained from laboratory testing and Ansys analysis is equal to 0.98 which displays a very strong correlation. The error should remain in 20% range for the test to be valid and therefore the final results would be regarded as valid. This investigation validated the Sawbone femur and increased our general understanding of its resemblance of the real cadaveric femur bone. It has also show the capacity of this synthetic mechanical analogue femur model for further reliable exploration of implant performance.

3.3 Compression testing

3.3.1 Experimental analysis

The first testing carried out was the application of a vertical load onto the artificial femur. In accordance with the appropriate examples identified from research, the femoral neck stresses as well as femoral shaft stresses were identified by placing two strain gauges on the appropriate locations (Figure 3.15). Two rectangular strain gauge rosettes were utilised on the prosthetic bone. Setting up the gauges required the degreasing and cleaning of the femoral surface to ensure a proper installation, the gauges were attached to the femoral surface employing an M-bond adhesive. After the gauges were correctly positioned onto the surface the strain gauges were wired and ready to be examined. Table 3.10 below displays the information from the installation check of each strain gauge.

To apply a force on the artificial femur it was necessary to create a support that could restore the femur in place temporarily for the purpose of compression testing. To replicate a realistic representation of a loaded femur the supports are placed on the lower end of the femur (Figure 3.16).

Strain Gauge		1	2	3	4	5	6
Nominal Resistance (Ω)		**120**	**120**	**120**	**120**	**120**	**120**
Variation (Ω)	5%	**0.2**	**0.15**	**0.22**	**0.2**	**0.1**	**0.15**
	1%	**0.18**	**0.12**	**0.2**	**0.22**	**0.08**	**0.15**
Maximum resistance flowing capacity (KΩ)		**20**	**20**	**20**	**20**	**20**	**20**

Table 3.10- Installation check values

Figure 3.15 - Strain gauge applied to the composite femur

The vertical downward load was put on the prosthetic femur employing a Testometric - micro 500 machine. The set of 6 strain gauges were wired to an amplifier to record data from each gauge. The gauge factor was set on the amplifier in according with the strain gauge information provided by the manufacturer. Each strain gauge value was balanced to zero; this was essential because of the fact that the femur material is non-metal, causing small fluctuations. The Testometric machine worked at a speed of 10mm/min. The strain data were obtained from each gauge at intervals of 300N until the applied force was 1500N. The recorded values are provided below in Table 3.11.

Figure 3.16 - Support system applied to the composite femur

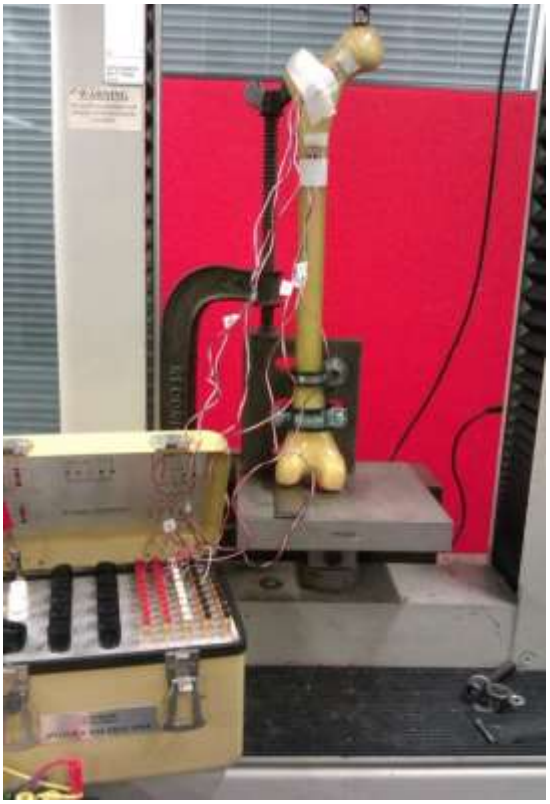

Figure 3.17 - composite femur under load applied along with relative supports

Table 1.11 - Strain values as obtained from the practical experiment

		Strain Gauge Measurement (εμ)					
		1	2	3	4	5	6
Force (N)	305	**112**	**25**	**-165**	**-12**	**12**	**10**
	594	**209**	**40**	**-329**	**30**	**10**	**6**
	905	**322**	**70**	**-488**	**-32**	**14**	**18**
	1210	**440**	**90**	**-655**	**-24**	**28**	**35**
	1505	**565**	**123**	**-814**	**-19**	**-39**	**50**

3.3.2 Finite element analysis (FEA)

Reddy (2004) explained why numerical methods are extremely powerful tools for engineering analysis. With the advent of computers, there has been a tremendous explosion in the development and use of numerical methods. Of these, the finite difference methods and the finite element method and their variants are the most commonly used methods in the analysis of practical engineering problems. In finite difference methods, derivatives of various order are approximated using Taylor's series. On the other hand, the finite element method is based on the idea that every system is physically composed of different parts and hence its solution may be represented in parts. In addition, the solution over each part is represented as a linear combination of undetermined parameters and known functions of position and possibly time. The parts can differ from each other in shape, material properties, and physical behaviour.

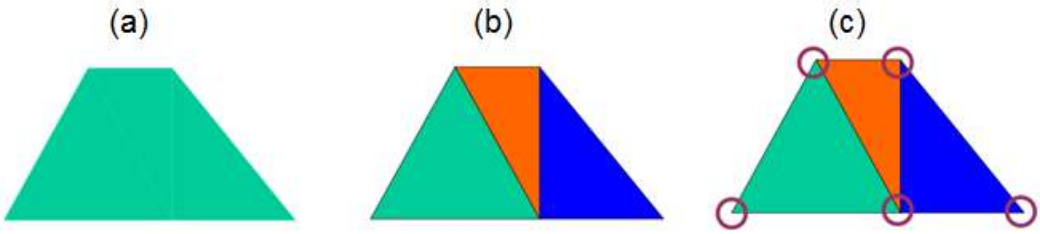

Figure 3.18- (a) Basic geometry (b) Example of elements (c) Example of nodes

In engineering analyses, bodies of complex geometry subjected to multiple boundary conditions and loading are often encountered. The various analyses include stress, thermal, fluid flow, electromagnetic, steady state, unsteady state, dynamic, etc. Under such complex conditions it may not be possible to derive a theoretical solution for continuum. FEA is the process of discretizing a complex continuum into a finite number of regions called elements which are connected at the nodes, or grids. The solution is obtained at the discrete nodes, which approximates the solution for continuum at those points in space and time (Shivaswamy, 2010).

FEA procedure can be broadly divided into three important steps. Pre-processing, Analysis, and Post-processing. The pre-processing stage involves discretization of the continuum into elements (mesh generation), getting the geometry data (x, y and z coordinates, and element nodal connectivity data) of the elements, obtaining details of the boundary conditions and the force applied.

$$[\mathbf{K}]\{\mathbf{u}\} = \{\mathbf{F}\} \quad \Rightarrow \quad \{\mathbf{u}\} = [\mathbf{K}]^{-1}\{\mathbf{F}\}$$

Property Behavior Action

Unknown

	Property [K]	Behavior {u}	Action {F}
Elastic	stiffness	displacement	force
Thermal	conductivity	temperature	heat source
Fluid	viscosity	velocity	body force
Electrostatic	dialectric permittivity	electric potential	charge

Figure 3.19- Stiffness matrix [k], boundary condition {F} and unknown behaviour {u}

In the analysis stage, the data generated in the pre-processor step is read and analysed. Based on the geometry and material properties, the stiffness matrix **K** for each element is formed. The individual elemental stiffness matrices are then assembled into the global stiffness matrix $\mathbf{K_G}$.

The post-processing stage involves processing and visualization of the results from the analysis in a suitable form. This includes plotting of parameters of interest, animation of the system's response, etc.

The stiffness matrix relates force in a degree of freedom (DOF) due to a unit displacement at the same, or another DOF. An element K_{ij} of a stiffness matrix represents the force in the DOF *i* due to a unit displacement at the DOF *j*. For example, for a 4 noded quadrilateral membrane element with 2 DOF (*u, v*) at each node, an 8x8 stiffness matrix will be formed (Figure 3.20). Then all element stiffness matrixes will form the global stiffness matrix which can later be used to solve the unknowns of the equation.

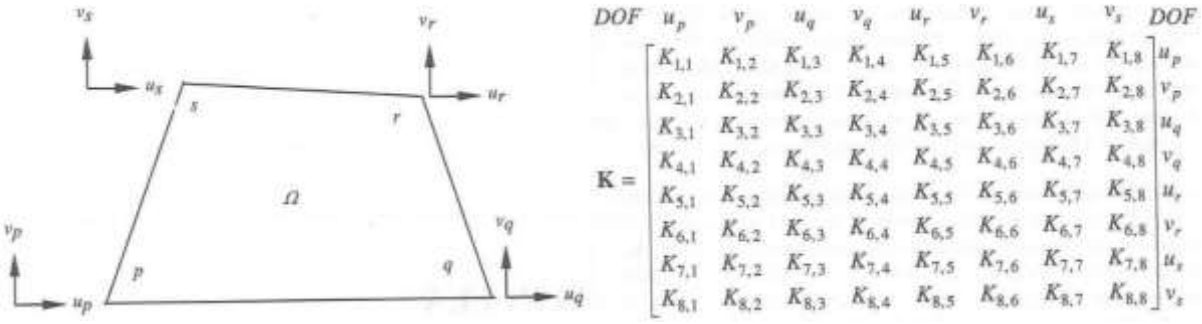

Figure 3.20- (left) 4 noded quadrilateral element with 2 DOF, (right) 8x8 stiffness matrix formed for the same individual element (Shivaswamy, 2010)

3.3.2.1 Mathematical model

The comparison of the final results extracted from simulation with those found practically can verify the use of finite element analysis for being a precise tool. The fourth generation femur product utilised in the simulation is an exact model of the artificial femur used in the practical test (Figure 3.21).

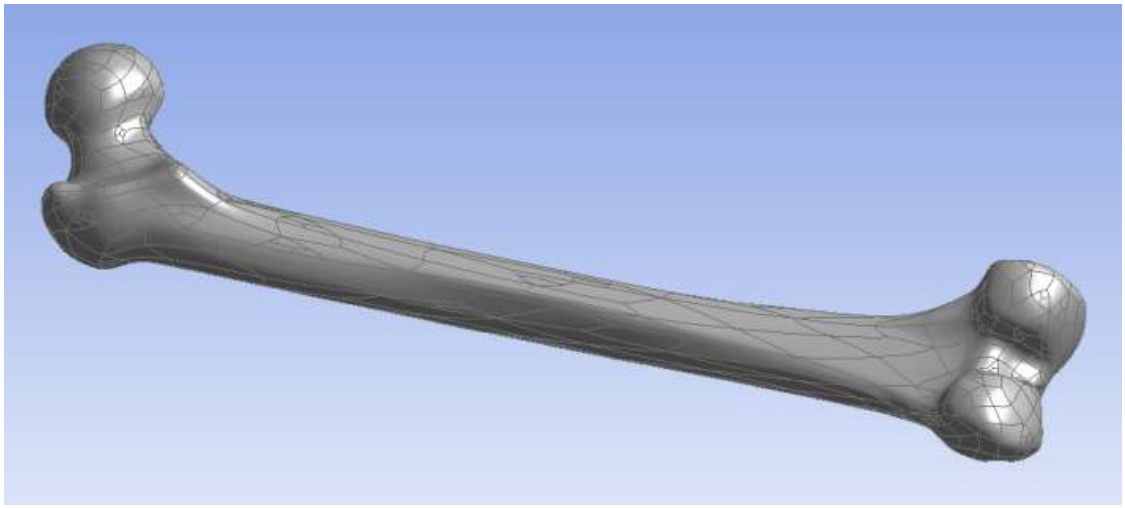

Figure 3.21- Fourth generation femur model

To determine the strain values in Ansys in the same position of those existing in the practical experiment we have to make sure the gauge locations are clean over the actual model. A sketch of the strain gauge with the same dimensions was produced at the same place (Figure 3.22).

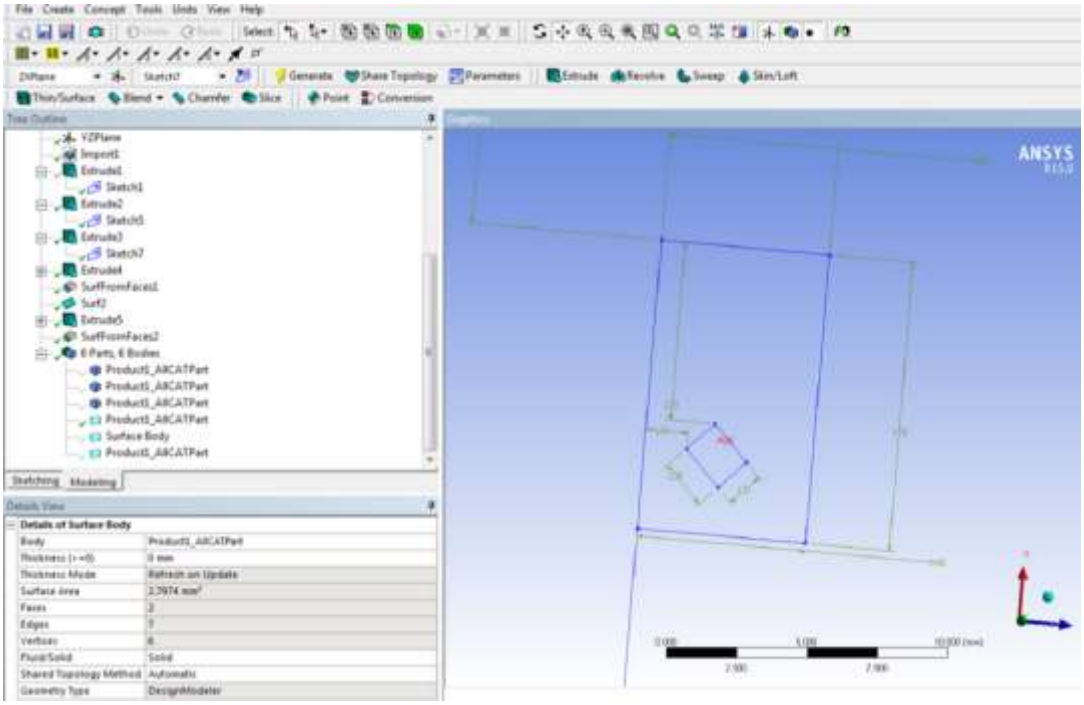

Figure 3.22- Sketch of a single strain gauge

As shown in figure 3.23, the sketch could subsequently be imprinted upon the surface of the composite femur. This facilitated the location of each strain gauge to be easily highlighted. This step was carried out for each specific gauge that was used on this femur model.

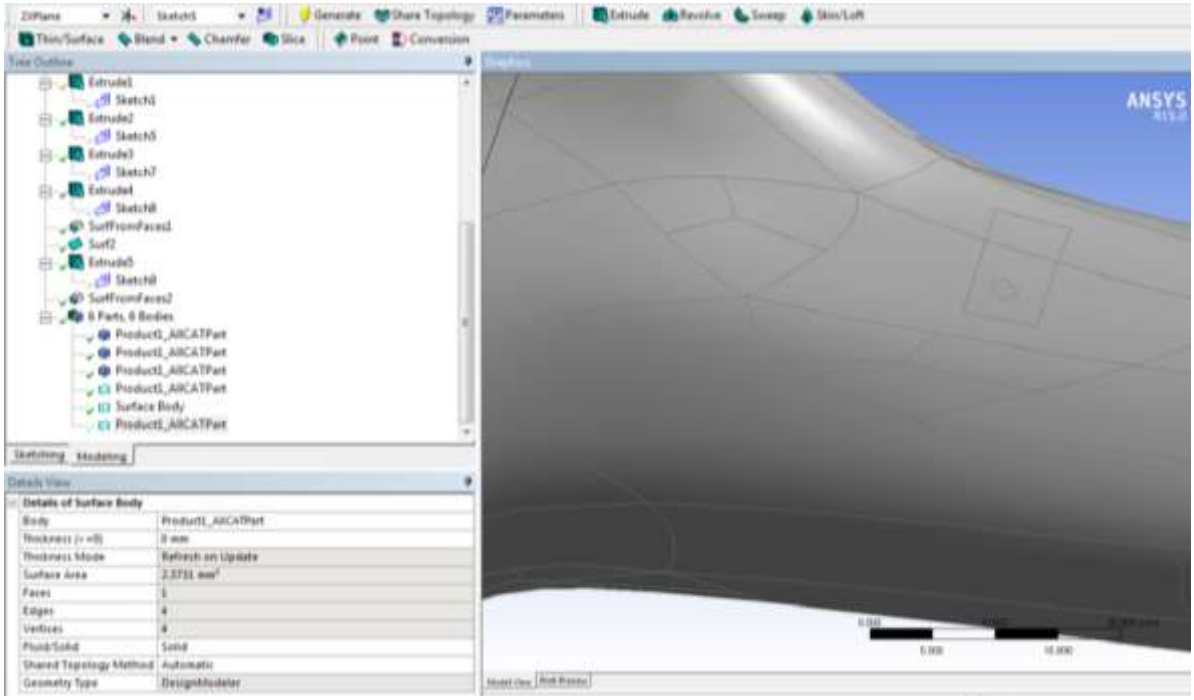

Figure 3.23- Strain gauge sketch imprinted onto the femur surface

Once the surface of the strain gauge was imprinted onto the femur surface it was possible to establish a surface body for each gauge imprinted. The surface body was produced by choosing the imprinted face and setting the thickness of it to a small value of 0.1mm (Figure 3.24).

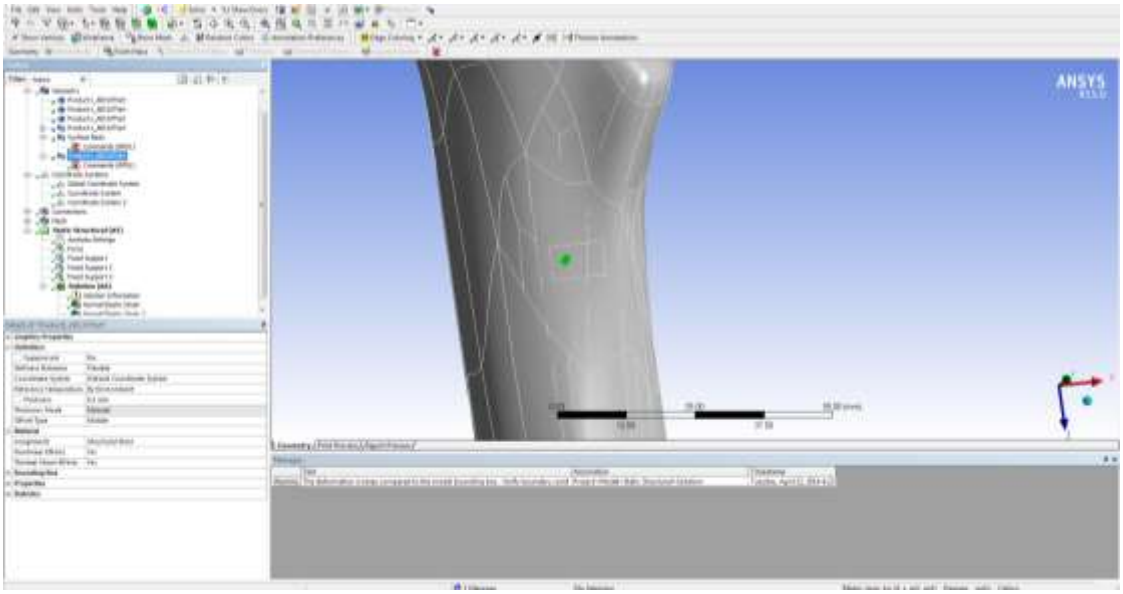

Figure 3.24- Surface body generated from imprinted sketch

After the surface body was given a particular thickness value, a command function was written for the surface body geometry. The following code was keyed in:

et,matid,181

Keyopt,matid,1,2

The initial line of this code enables the surface body to utilise elements of type 181 when a mesh is generated. The second line, commands that element type 181 to possess a stiffness value equal to zero.

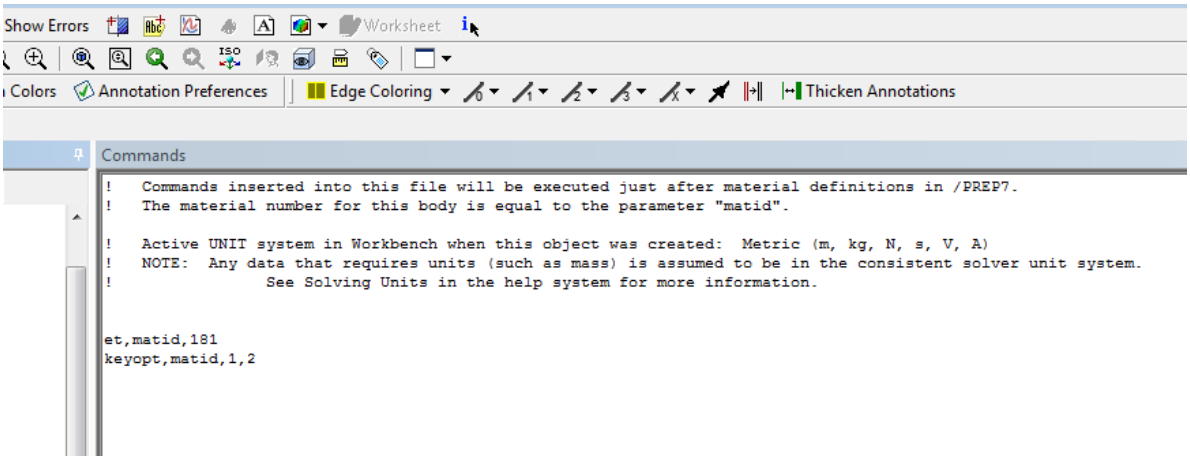

Figure 3.25- Command function inserted to the surface body geometry

After the commands were applied to every surface body representing a strain gauge, the connection configurations required to be changed. The formulation of every contact was modified from "program controlled" to pure penalty.

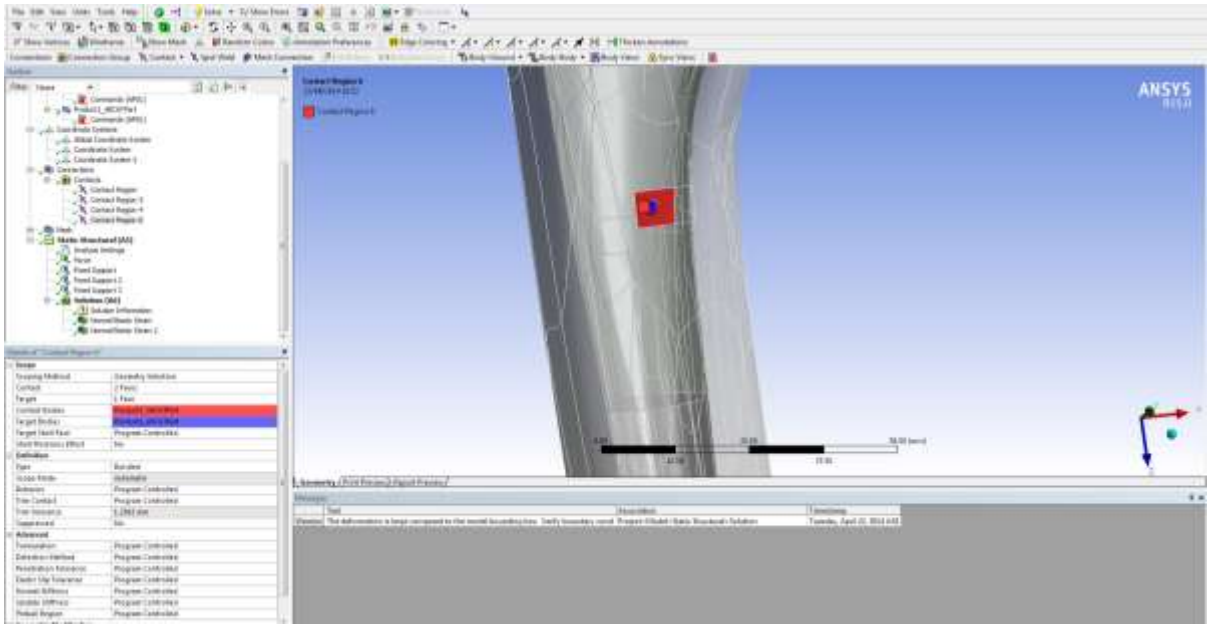

Figure 3.26- Contact type selection

To estimate the strain value in the similar way as that of the experiment, the correct components must be applied. For this purpose, several coordinate systems can be produced to ensure that the strain values are being evaluated in the correct directions (Figure 3.27).

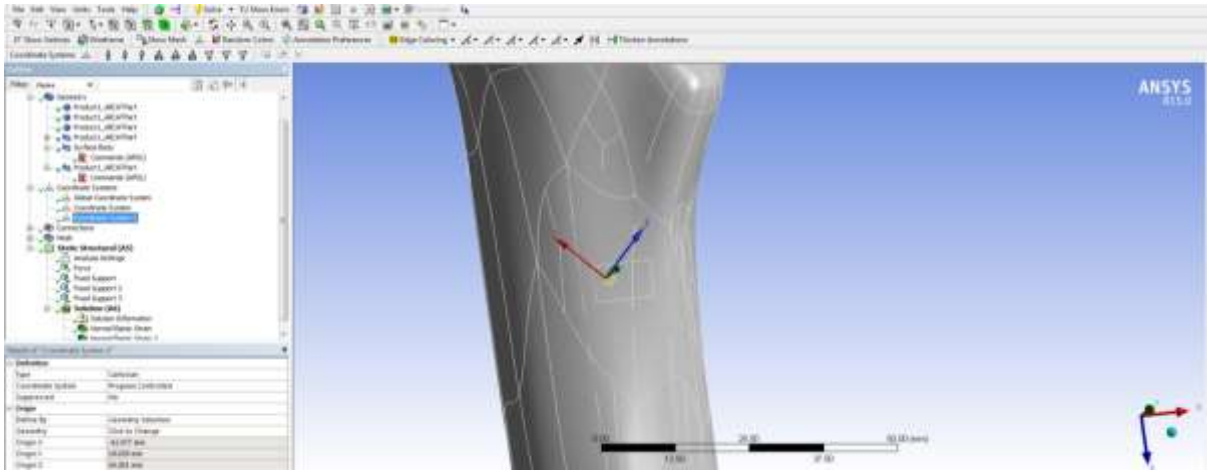

Figure 3.27- Creating a new coordinate system

The normal elastic strain values could be obtained for each gauge by deciding on the face of the surface body as the appropriate geometry. This technique provides a large variety of strain values over the whole surface of each strain gauge.

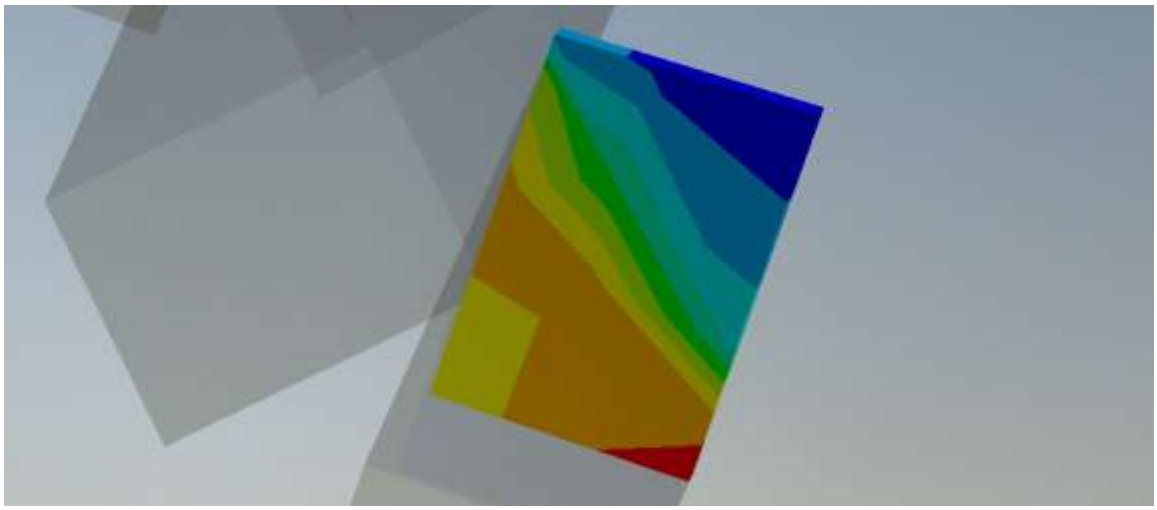

Figure 3.28- Normal strain over the whole strain gauge region

To be able to obtain a single strain measuring for each gauge, the mesh must be customized. A “sizing tool” can be employed to customize the mesh so as to achieve the correct result. Once the sizing tool has been chosen, each edge of the strain gauge is picked as the appropriate geometry. The type of edge sizing to be employed is "number of divisions", the value that was assigned is one (Figure 3.29).

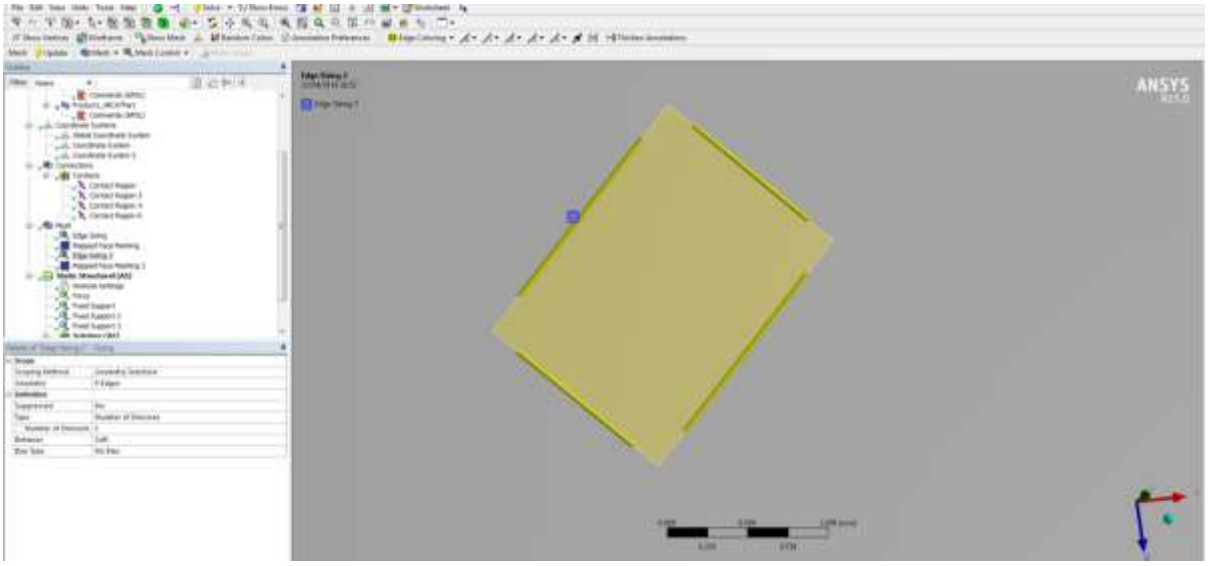

Figure 3.29- Edge sizing applied to the strain gauge body

Once the edge sizing has been finalized the mapped face meshing tool can be used. The area of the surface body was picked as the appropriate geometry for meshing.

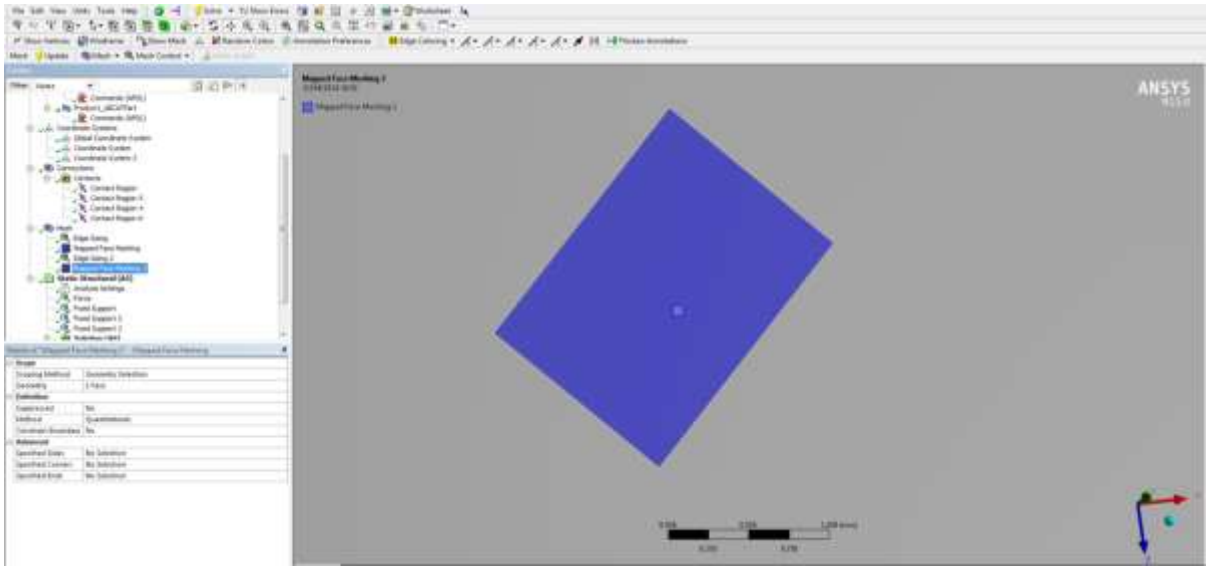

Figure 3.30- mapped face meshing applied to the strain gauge body

As displayed below, when the mesh sizing has been completed it is possible to achieve a single value over the whole area of each strain gauge.

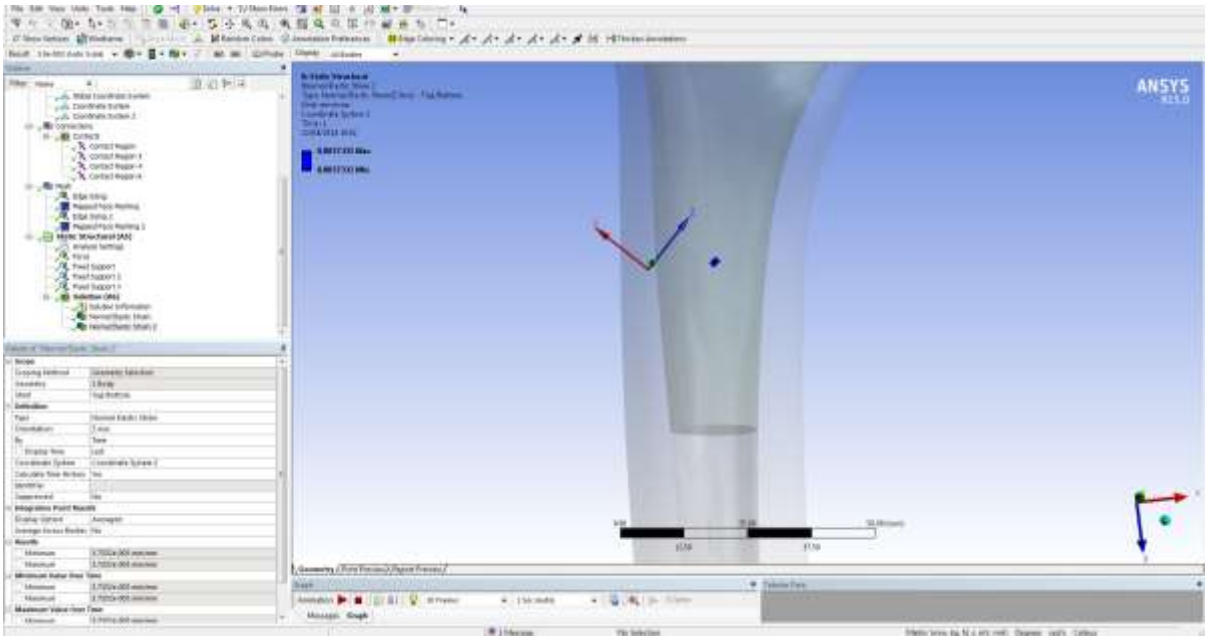

Figure 3.31- Single strain reading given for the strain gauge face

3.3.2.2 Boundary conditions

The Figures 3.32 and 3.33 display the simulated supports used on the femur model together with the supports included in the practical experiment. Supports were also included at the distal end of the subject (Figure 3.34).

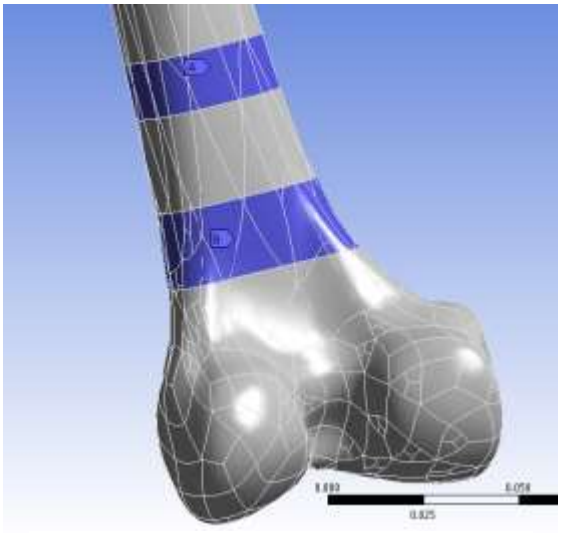

Figure 3.32- Location of supports simulated using Ansys

Figure 3.33- Support system used in the practical experiment

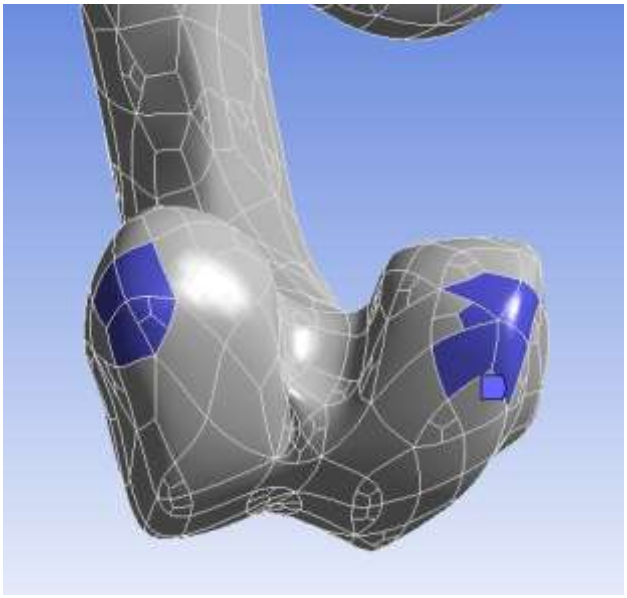

Figure 3.34- Location of supports added to the Ansys

The simulated force is demonstrated together with the actual force applied during the experiment in figure 3.35 and 3.36 respectively. The starting point for determining the strain values in the same position of those existing in the practical experiment is to make sure the gauge locations are clean over the actual model. After reading the experimental results we can compare them with the Ansys results for verification and validation process.

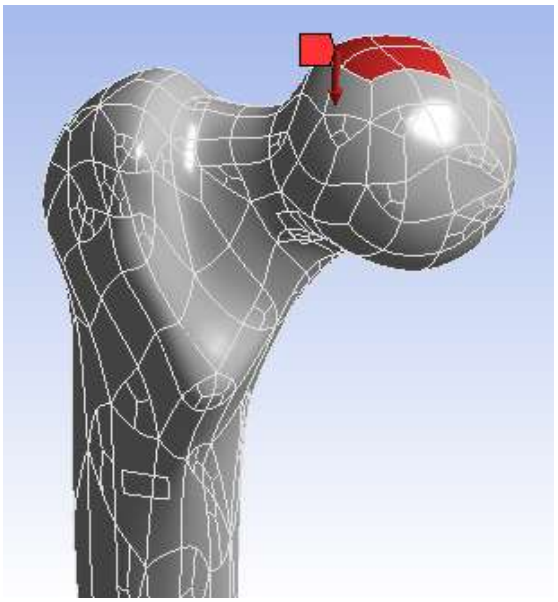

Figure 3.35- Location of applying load to the 3D femur model using Ansys

Figure 3.36- Load applied to the composite femur bone model in the practical experiment

3.3.3 Verification and validation of simulation model

Employing the Ansys software it was possible to evaluate the stress value in the same places as those in which the strain gauges were used in the practical test. The stress distributions are demonstrated later in Figure 3.41 for the neck and shaft of the synthetic femur. Strain values were obtained for each single strain gauge for each load that was applied in the practical testing. Tables 3.12 and 3.13 below show the experimental data and Ansys results respectively.

Table 3.12 - Strain values as recorded in practical testing

		Strain Gauge Measurement (με)					
		1	2	3	4	5	6
Force (N)	305	**112**	**25**	**-165**	**-12**	**12**	**10**
	594	**209**	**40**	**-329**	**30**	**10**	**6**
	905	**322**	**70**	**-488**	**-32**	**14**	**18**
	1210	**440**	**90**	**-655**	**-24**	**28**	**35**
	1505	**565**	**123**	**-814**	**-19**	**-39**	**50**

Table 3.13 - Strain values listed from Ansys simulation

		Ansys Strain value (με)					
		1	2	3	4	5	6
Force (N)	305	**108.6**	**23.9**	**-146.9**	**-10.7**	**11.3**	**7.2**
	594	**200.6**	**38.5**	**-306.8**	**-28.3**	**9.4**	**4.9**
	905	**309.1**	**63.1**	**-453.4**	**-30.1**	**13.3**	**15.3**
	1210	**422.4**	**86.2**	**-563.6**	**-21.6**	**25.8**	**29.6**
	1505	**536.8**	**116.9**	**-740.7**	**-17.8**	**-36.3**	**42.8**

The comparison of these outcomes (Table 3.14) reveals minor differences among the simulation and the laboratory experiment. The use of finite element analysis cannot entirely recreate testing conditions to perfection. Employing Ansys software it was possible to identify the stress value in the same areas as those in which the strain gauges were used in the laboratory experiment. The strain distributions are displayed in Figure 3.38 for the neck and shaft of the synthetic femur. Strain values were obtained for each individual strain gauge and for every force that was placed in the laboratory experiment.

3.3.4 Discussion

Table 3.14- The strain values of synthetic femur, exposed to various axial loading conditions, derived from FEA method and recorded by strain gauges at 6 femur points as displayed in Figure 3.38.

Applied Force (N)	Measuring method	Strain (με) values at 6 different points					
		1	**2**	**3**	**4**	**5**	**6**
305	Strain gauge	112	25	-165	-12	12	10
	FEA	108.6	23.9	-146.9	-10.7	11.3	7.2
594	Strain gauge	209	40	-329	30	10	6
	FEA	200.6	38.5	-306.8	-28.3	9.4	4.9
905	Strain gauge	322	70	-488	-32	14	18
	FEA	309.1	63.1	-453.4	-30.1	13.3	15.3
1210	Strain gauge	440	90	-655	-24	28	35
	FEA	422.4	86.2	-563.6	-21.6	25.8	29.6
1505	Strain gauge	565	123	-814	-19	-39	50
	FEA	536.8	116.9	-740.7	-17.8	-36.3	42.8

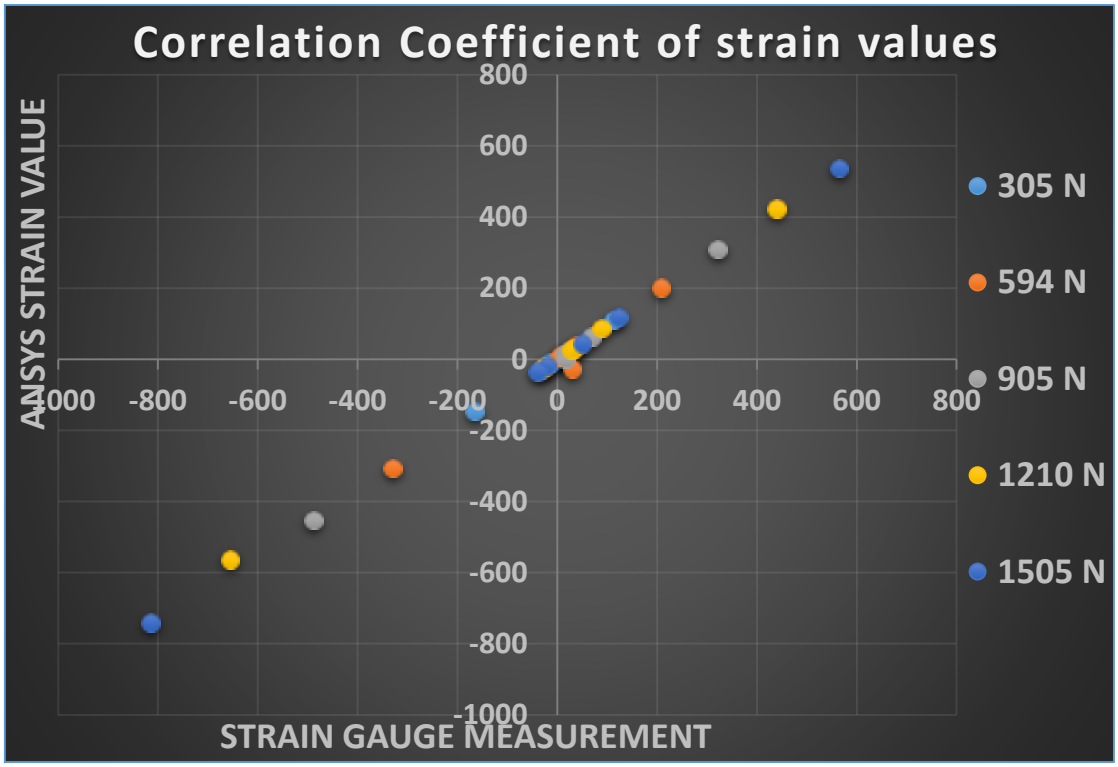

Figure 3.37- The correlation coefficient between the Ansys simulation and the laboratory results that shows a close value of R^2=0.99

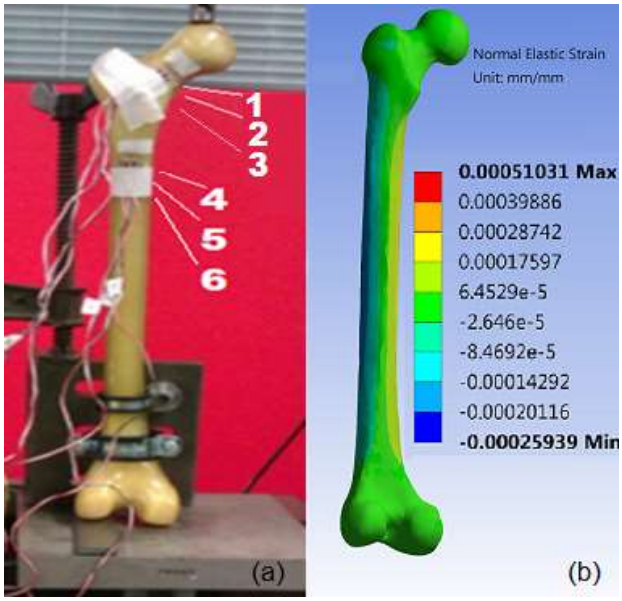

Figure 3.38. (a) Mechanical testing of synthetic femur, displaying the areas of strain gauges employed to measure strain values. (b) Strain distributions within the synthetic femur

The comparison of FEA and strain gauge final results are displayed in Figure 3.37. This suggests that an excellent correlation between the FEA and the practical measurement of strain exists. Therefore it can be assumed that FEA is an accurate representation of how a body functions when it undergoes an applied force. The application of FEA to enhance a hip replacement has been found to be a viable technique.

3.4 Brinell hardness testing

To correctly evaluate the synthetic Sawbone it was essential to be aware of mechanical properties of the material. A hardness test provided an overall knowledge of the material. Due to the softness of the material, the experiment used on the synthetic Sawbone was a Brinell hardness test. The Brinell hardness experiment is an ideal option in this case as it is less affected by indentations and scratches on the surface area than other hardness testing techniques. The value extracted from the experiment was 43 HB, a realistic value for this glass composite material.

The Young's Modulus of a glass-fibre femur composite was obtained from the manufacturers handbook (Sawbone, 2016) and also verified with past reports (Chong et al., 2007a; Chong et al., 2007b; Dunlap et al., 2008; Heiner 2008; Zdero et al., 2008 and Papini et al., 2007) which was mentioned earlier in the beginning of this chapter. Using this value it was possible to enter data into the Ansys software for the simulation to be as accurate as possible. The maximum principal stress distribution for the loaded synthetic femur bone is displayed below when a force of 1505N is applied (Figure 3.39).

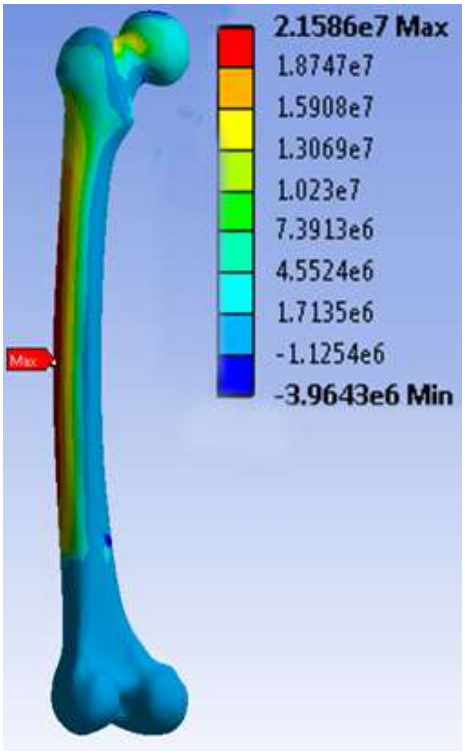

Figure 3.39- Maximum principal stress (Pa) distribution for a composite femur model with a load of 1505N applied

Figure 3.40- Brinell hardness testing

Another important measure of stress is the von-Mises stress method. This represents an equivalent stress in a body subjected to a multi-axial state of stress. The von-Mises stress is used for checking yielding in ductile materials (Shivaswamy, 2010). It is also more accurate in dynamic loadings.

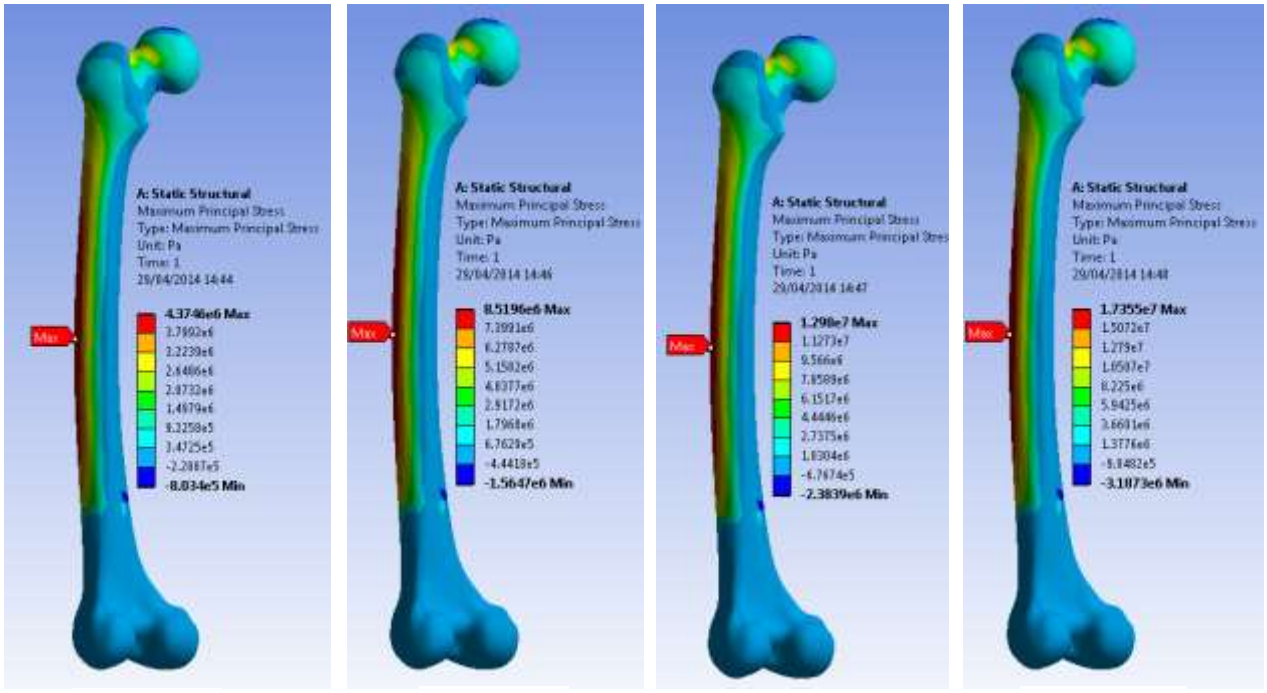

F = 305N F = 594N F = 905N F = 1210N

Figure 3.41- Maximum principal stress distribution for a composite femur bone at different applying loads

Table 3.15 below shows how the maximum principal stress values in the glass-fibre synthetic femur model vary in comparison to the applied force. Maximum principal stresses and applied forces are proportional to each other and stress over femur increases by raising the applied force.

Table 3.15 – Comparison of the maximum principal stress values variation in a glass-fibre composite bone model with respect to the applied forces

Load (N)	Maximum Principal Stress (MPa)
305	**4.4**
594	**8.5**
905	**13.0**
1210	**17.4**
1505	**21.6**

3.5 Hip stem testing

3.5.1 Experimental analysis

To set up the experiment in real life, many important items and equipment are required including a mould or block to hold the hip stem, strain gauges, the strain gauge reading meter and the hip stem.

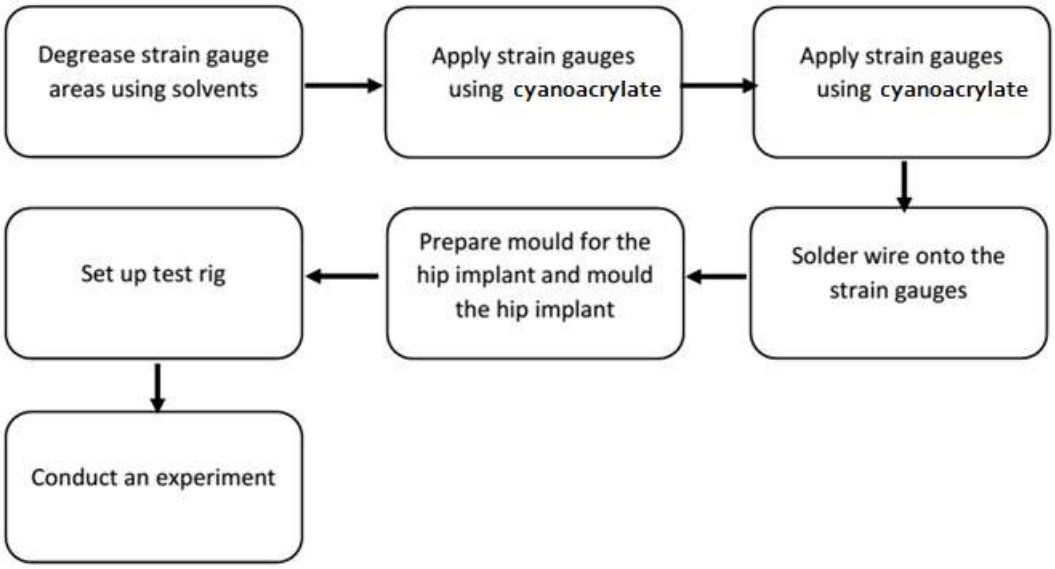

Figure 3.42- Different steps to perform a strain gauge experiment

The main reason for the surface development is to provide a chemically cleaned surface that has roughness suitable to the strain gauge installation. Cleanliness is essential throughout the cleaning procedure and it is also essential to preserve the surface that is cleaned therefore the following must be avoided:

- Touching the cleaned surface area of strain gauges with hands without gloves
- Leaving the cleaned surface area for long before applying the strain gauges
- Taking the product out of the clean surface area

Furthermore, it is best practice to commence the task with washed hands as well as wearing gloves in the course of the process. These steps are essential as they play a big role in the accuracy and precision of the strain values recorded from the strain gauges. Four steps were undertaken as a way to clean the hip stem.

Solvent degreasing- This is the initial step of cleaning the prostheses and it is carried out to eliminate any greases, oils and other chemical residues.

Surface abrading- when planning to employ strain gauges onto the surface area it is essential that the surface is flat and clear of any sort of loose bonds e.g. oxides, galvanised coating, scale rust etc. Abrading is employed to establish a suitable surface for applying the strain gauge. There are a number of distinct techniques for performing the abrading including sander, file or grinder but in this example a sand paper was utilised to abrade the target surface.

Surface conditioning- conditioner is used regularly following the surface abrading (Figure. 3.43). Throughout this procedure the surface has to remain wet while cleaning. At the end, by using cotton or tissue the surface needs to be wiped.

Neutralizing- This is the final phase of the cleaning process that brings the surface condition back to the point in which the strain gauges can be employed while it is totally free of any kinds of loose bonds or greases. Following this stage the strain gauges were applied on the hip prosthesis.

Figure. 3.43- Different kind of solvents that were utilised to clean up the implant

The strain gauges that were applied to the hip prosthesis were connected to two electrical wires, and were soldered on by means of a soldering iron. The wire attachments provide the facility

to read the strain values that would be obtained from each strain gauge by connecting the opposite end of the wire to a strain gauge meter.

The hip prosthesis must be set into a place to get it completely stationary such that no movement occurs after fixation. A metal block was used in the role of a mould in order to fix the hip implant. To get the best fixation, a substance known as "fantastic plastic" was used to minimize the size of the holes mounted on the metal block.

Plastic pellets (Figure. 3.44) have many distinct functions however in this case were employed to push the hole of the mould in order to modify it into the suitable size and shape. Plastic pellets were employed pursuing the following steps:

1. Heating up some water
2. Adding some amount of plastic pellets as required into the hot water
3. Waiting for the pellets to remodel into a transparent moulding liquid
4. Pouring moulding liquid from container into the mould to get a desired shape

Figure. 3.44- Plastic pellets applied to acquire a firm fixation inside the mould

Nevertheless, in this specific example the transparent moulding liquid was pressed into the hole of the metal block whilst it was hot and mouldable. Subsequently the hip stem was pushed into the mould. It was left still to get solidified and fully fixed. This gave a very strong outcome to the fixation of the hip stem. It took two attempts to get the mould in the correct position into the hole of metal block.

As stated previously in the literature review there are several techniques of conducting an experiment in real life that can be followed by simulating with FEA software. Abhijit and Sandip (2011) and Singh (2014) have conducted the experiment employing FEA software nevertheless both tests that were carried out had a different approach. Abhijit and Sandip

utilised a femur bone model which includes a hip implant whereas in Singh's approach, the hip implant was used inside a metal block for fixation. This experiment followed the procedure and approach used by Singh (2014).

Figure. 3.45- Metal block and plastic when solidified

After the hip stem was set into the metal block as demonstrated in Figure. 3.45, the block needed to be fixed. Some necessary fixation devices was used to fix the metal block, including a table, small clamp along with a larger clamp. The metal was positioned onto the table that was fixed by a bolt onto the testing machine, subsequently the metal block was fixed using the small clamp while the larger clamp tightened the assembly in vertical direction. The smaller clamp was utilised to fix the table onto the machine while the larger clamp was utilised to fix the metal block onto the table as it is demonstrated in Figure 3.46.

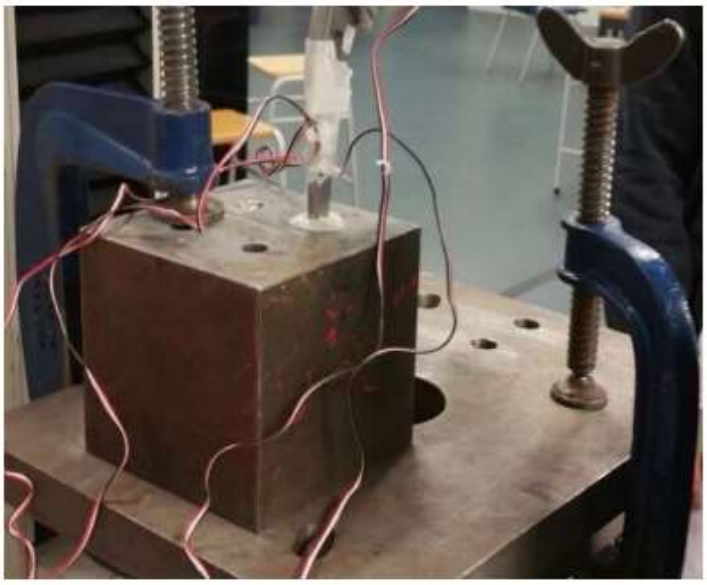

Figure. 3.46- Using a small and large clamps to for fixation

The experiment on the hip implant was performed with the help of a ‘testometric micro 500/50kN machine’. The force was applied upon the hip implant in increments of 100N up to 1000N via a load head that was pushing down onto the hip implant head. The experiment is demonstrated in Figure 3.47.

Figure. 3.47- Load head being pushed onto the head of the hip implant

3.5.2 Finite element analysis (FEA)

The primary reason for testing the hip prosthesis in real life is to validate the final results with a further type of testing. Validating a hip model ensures that it is authentic and outcomes that are obtained from the test do match up. In order to achieve a correct validation process, it is essential that the hip model that will be used for simulation is similar to the design that is used in real life. This could be done in various different approaches including employing the CMM machine which places a point on the model which can then be observed in the software in Catia or Delcam. An alternative way which can be applied is to observe the model and take dimensions employing appropriate tools and equipment including compass, ruler, Vernier calliper and micrometre. Laboratory testing assembly shows that the hip model is setup to be able to obtain the strain value at each point where strain gauges are placed. Similar boundary conditions might be replicated by means of Ansys software.

3.5.2.1 Mathematical model

The strain gauges that were employed in the testing by means of cyanoacrylate, would be simulated in similar positions in Ansys using the 'imprint faces' method. The initial step was to recognize a common file extension between Catia and Ansys so that the 3D file could be saved and imported to Ansys where it was possible to open and carry out the analysis. Saving the file in STP format is shown in Figure. 3.48. Another common file extension could be IGS but this is less accurate for a more complex models.

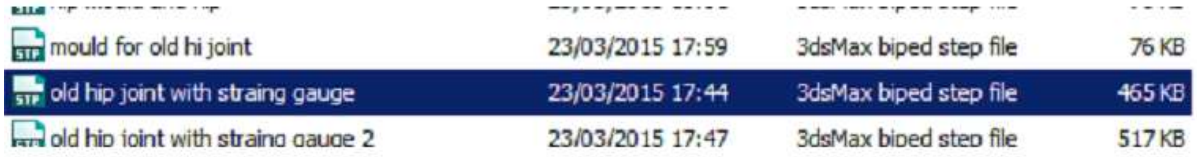

Figure. 3.48- Representation of files saved as STP file

Subsequent to saving the file in STP format, it was possible to open and carry out the analysis in Ansys, this is demonstrated in Figure 3.49.

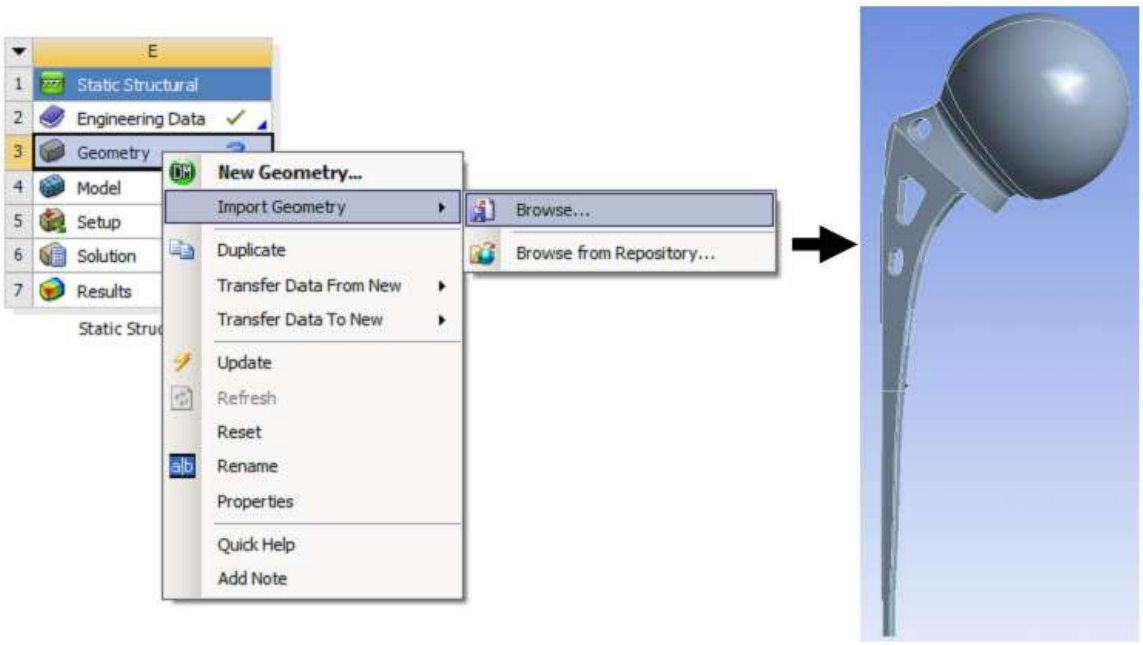

Figure. 3.49- 3D model file imported to Ansys

Strain gauges were subsequently replicated over the surface area of 3D model by means of the sketching and then imprinting options. The dimensions of the strain gauges and the exact locations were also considered as this can be seen in Figure 3.50.

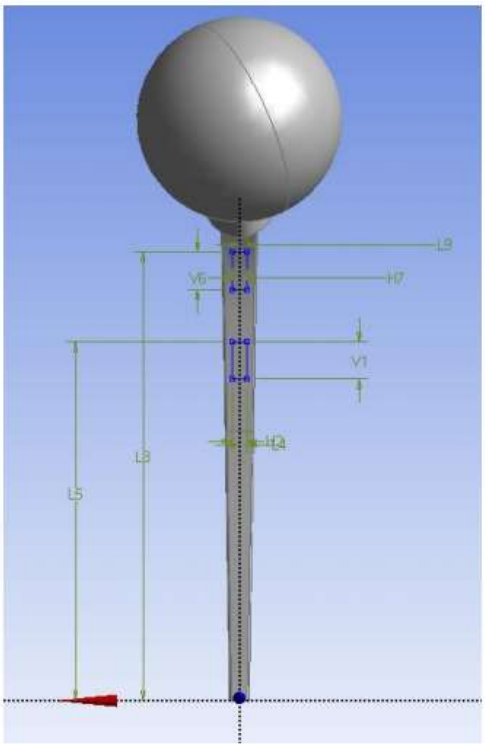

Figure. 3.50- Imprinting of strain gauges over the surface area of 3D model

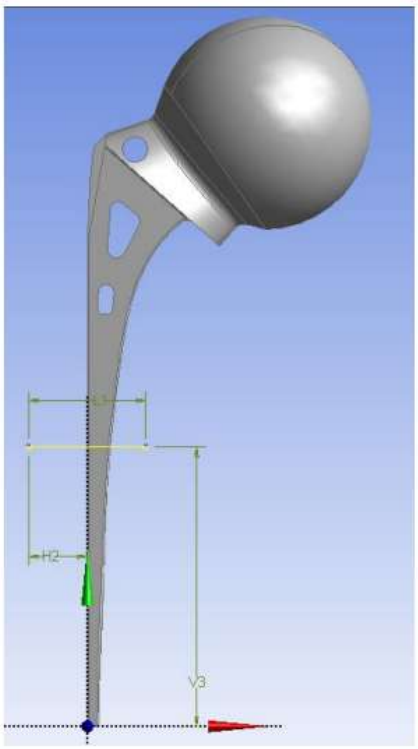

Figure. 3.51- Imprinting faces of fixed support

The hip model during the laboratory experiment was fixed in a metal block and the femoral stem of the hip joint design was 73mm deep inside the metal block. This could be represented in two different ways in Ansys employing the metal block and fixing the hip joint design inside the metal block or just the same length of the femoral stem that is inside the mould could be fixed. The replication of fixation of the hip implant is shown in Figure. 3.51.

3.5.2.2 Boundary conditions

Assuming that the 3D model which is used in Ansys is identical to the experimental one in the laboratory, the next step is applying the similar boundary conditions of experimental conditions to that 3D model.

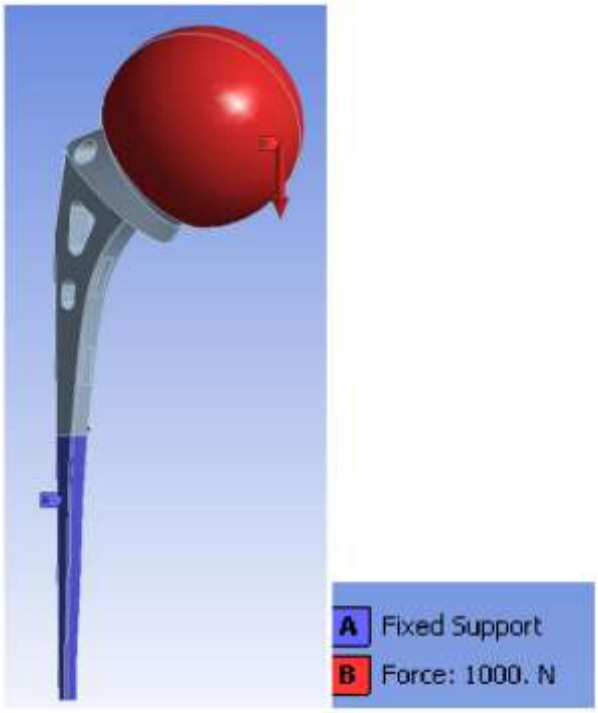

Figure. 3.52- Applied load and fixed support

The fixed support on the hip prosthesis which was applied through fixation inside the metal block in experimental testing is demonstrated in the figure above, blue region highlighted and force is simulated downwards acting over the femoral head as displayed in Figure. 3.52.

The selected methodology does have limitations. Human and experimental errors might affect the final result. Moreover, the complexity of the hip prosthesis model and conversion to another file format might possibly cause a little inaccuracy in the 3D model.

3.5.2.3 Mesh refinements

Mesh refinement was carried out to be able to attain more accurate results. Various diverse methods and software options could be used as a way to mesh the hip implant 3D model including “edge sizing”, “face sizing” as well as adding in the “sphere of influence”. Meshing is a procedure that breaks down the model into numerous elements which can be meshed. The mesh refinement must be performed on certain area of the model where the intention is to achieve better stress or strain values. Mesh refinement is essential because it gives considerably more accurate answer which is made possible through repeating the process of increasing number of meshing in a particular area until the data and values become relatively identical after every time refinement carried out. This is typically known as "convergence" where the answers converge to a certain number. As the mesh becomes finer, a more accurate data is produced. Initial mesh of the hip implant 3D model is demonstrated below on each of the strain gauges. The fine mesh might not visible owing to the large number of elements.

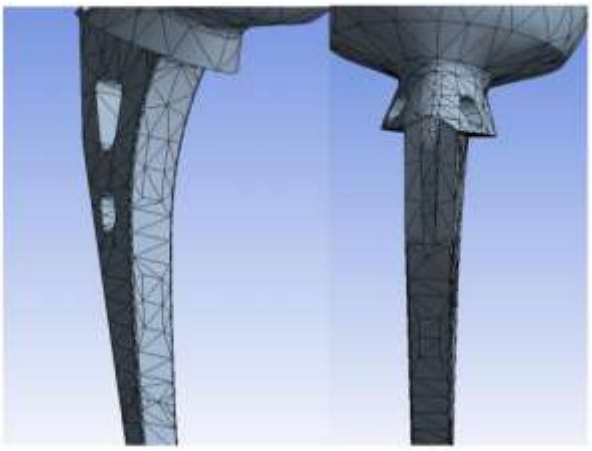

Figure. 3.53- Initial mesh

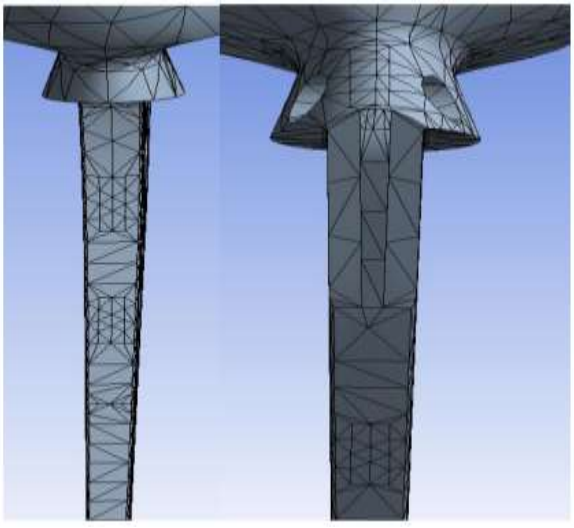

Figure. 3.54- First refinement

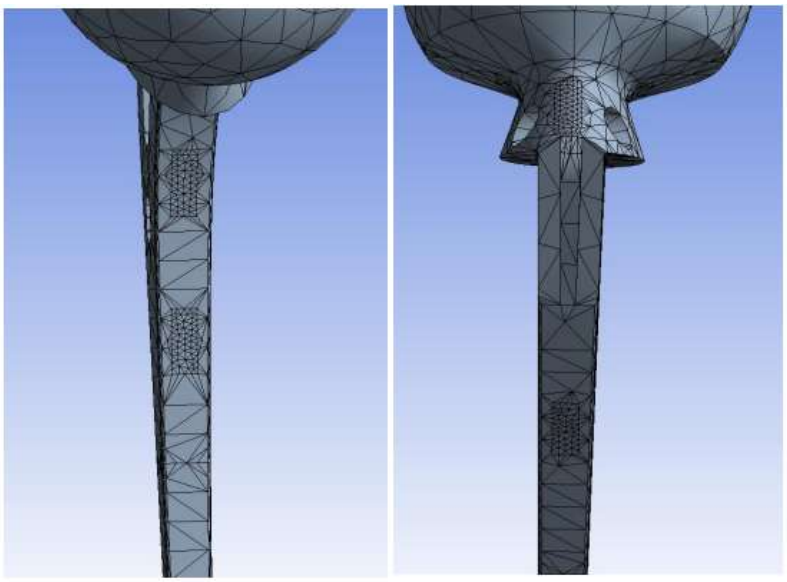

Figure. 3.55- Second refinement

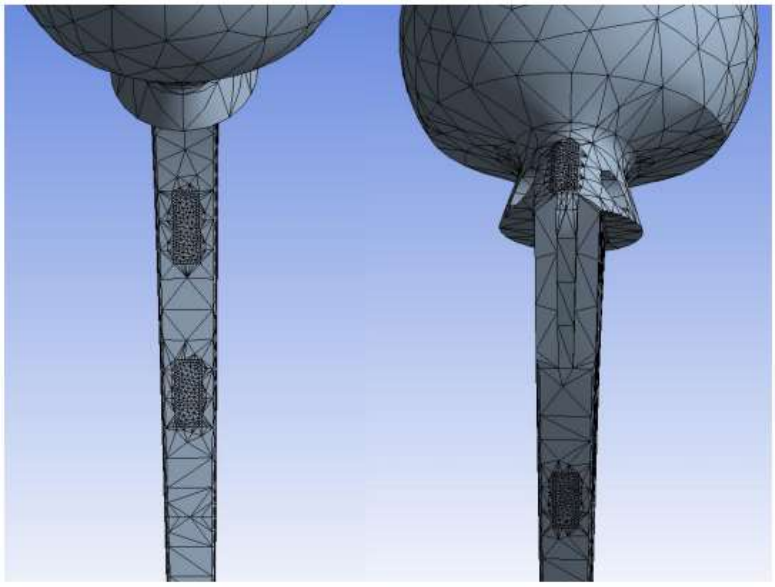

Figure. 3.56- Third and final refinement

The number of the elements was increased particularly over the strain gauge areas. The element size was reduced to 3mm enabling a more accurate answer to be obtained.

The second refinement included further reducing the element size to 1mm while in the final refinement the element size was lowered even further to 0.5mm giving a much more precise answer with refined mesh. Figures 3.53 to 3.56 show the mesh refinement over the strain gauges until reaching the convergence.

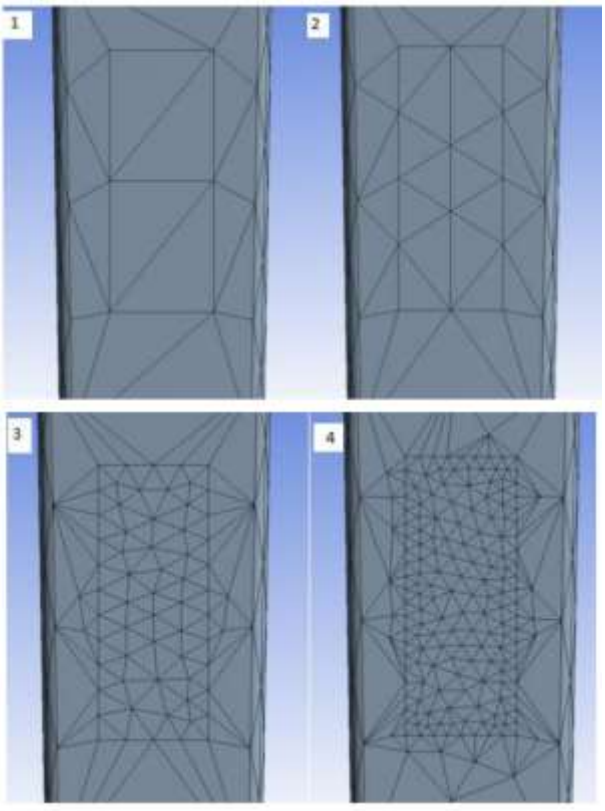

Figure. 3.57- Four steps of refinement

It can be seen in Figure 3.57 the order in which the meshing refinement was done. The first meshing on the strain gauge has a small number of elements and therefore the size of each element is large. A sample of final result at strain gauge 4 under 1000N is shown in Figure 3.58 which obtain after reaching convergence.

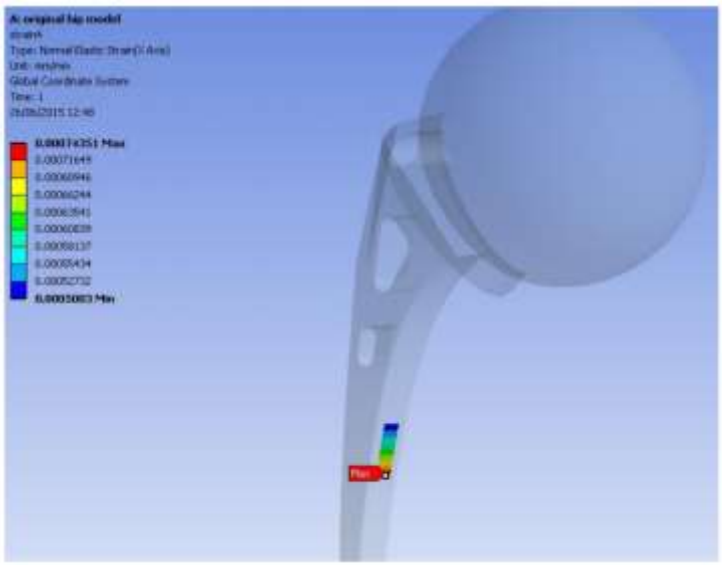

Figure. 3.58- Sample print screen to show validation

Table 3.16- Strain results after refinement at strain gauge 1

Position 1	Method	No. of elements	Strain (με)
	Default	4267	199
1st refinement	Face sizing- Element size 3mm	4344	210.2
2nd refinement	Face sizing- Element size 1mm	5729	216
3rd refinement	Face sizing- Element size 0.5mm	6231	218.98

Table 3.17- Strain results after refinement at strain gauge 2

Position 2	Method	No. of elements	Strain (με)
	Default	4267	297
1st refinement	Face sizing- Element size 3mm	4344	320
2nd refinement	Face sizing- Element size 1mm	5729	329
3rd refinement	Face sizing- Element size 0.5mm	6231	334.23

Table 3.18- Strain results after refinement at strain gauge 3

Position 3	Method	No. of elements	Strain (με)
	Default	4267	406
1st refinement	Face sizing- Element size 3mm	4344	423
2nd refinement	Face sizing- Element size 1mm	5729	428.5
3rd refinement	Face sizing- Element size 0.5mm	6231	428.4

Table 3.19- Strain results after refinement at strain gauge 4

Position 4	Method	No. of elements	Strain (με)
	Default	4267	727
1st refinement	Face sizing- Element size 3mm	4344	736
2nd refinement	Face sizing- Element size 1mm	5729	743
3rd refinement	Face sizing- Element size 0.5mm	6231	743.51

3.5.3 Verification and validation of simulation model

Boundary conditions used for Ansys software in the same way as they were applied for the laboratory experiment. The hip implant was examined using a metal block. The same boundary conditions has been simulated in Ansys software as shown in Figures 3.59 and 3.60. In the laboratory experiment the strain was recorded in one direction, to replicate that a co-ordinate system was established.

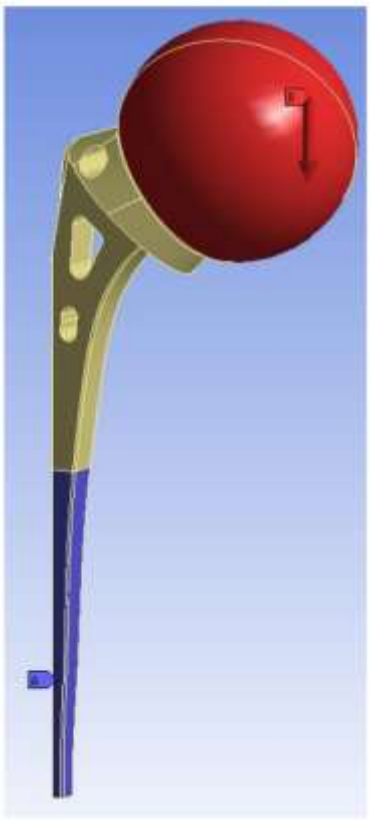

Figure. 3.59- Boundary conditions of 3D hip implant

The strain gauges were labelled on the hip for the laboratory experiment and the same labels were simulated on the 3D model that had been designed using Catia in order to match and relate every strain value to the correct strain gauge. This is displayed in Figure. 3.61.

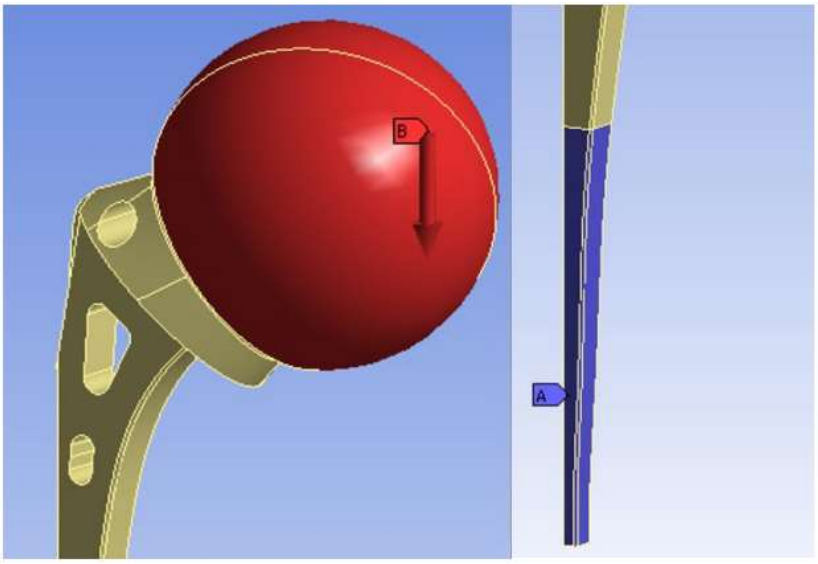

Figure. 3.60- Displaying boundary condition with a closer view

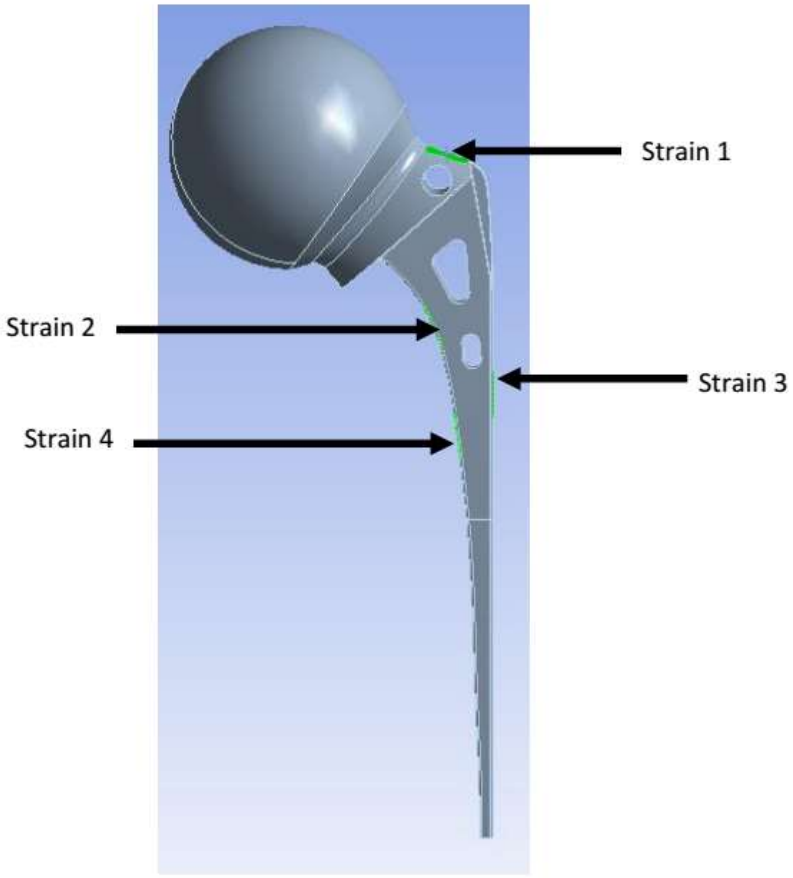

Figure. 3.61- Strain gauges labelled

Table 3.20- Strain values from laboratory experiment

Experimental results					
Number of strain gauge	**Strain at 200N (μ)**	**Strain at 400N (μ)**	**Strain at 600N (μ)**	**Strain at 800N (μ)**	**Strain at 1000N (μ)**
1	173	193	210	233	283
2	212	245	289	316	371
3	342	395	425	445	466
4	454	598	685	721	784

Table 3.21- Strain values from Ansys simulation

Ansys results					
Number of strain gauge	**Strain at 200N (μ)**	**Strain at 400N (μ)**	**Strain at 600N (μ)**	**Strain at 800N (μ)**	**Strain at 1000N (μ)**
1	99	131	146	185	192
2	185	201	243	269	297
3	201	305	361	386	406
4	397	511	623	695	727

There are 20 unique final results provided by laboratory results and Ansys data (Tables 3.20 and 3.21). Meshing could be conducted over all strain gauges under every loading applied. The data here shown just one of the applied forces with respect to the meshing at all four strain gauges. Mesh refinement has been shown at 1000N on all four strain gauges.

3.5.4 Discussion

Most experiments include human and machine error and there is always a particular discrepancy due to different type of reasons depending on testing conditions and environmental situation. The testing of the hip prosthesis was done in the laboratory where the strain gauges were applied on to the hip prosthesis by means of super glue and the wires were connected employing a soldering iron. Laboratory and Ansys strain values are presented in Tables 3.20 and 3.21 showing that there are small differences between experimental and Ansys data. A particular force i.e. 1000N was used to compare the strain data of the strain gauges 1, 2, 3 and 4 with the experimental and the Ansys outcomes.

Strain values of the strain gauge number one, under 1000N load are 283με for the laboratory experiment and 192με for the Ansys evaluation. The percentage difference among the final results is 32.16%. Viewing strain gauge 2, the practical result for the strain value under a force of 1000N is 371με while the value obtained from the Ansys is 297 με. The percentage difference among final results at position 2 is 19.95%. The laboratory strain value obtained for the strain 3 and 4 are 466με and 784με respectively and the value obtained for these positions from Ansys evaluation is 406με and 727με respectively. The percentage difference for the strain value at position 3 is 12.86% and for strain values at position 4 is 7.27%. The biggest percentage difference viewed on the strain gauge 1 equal to 32.16% and the minimum percentage difference was found on the strain gauge 4 equal to 7.27%. There can be various reasons for the discrepancies of the outcomes.

Error could be caused for a variety of diverse reasons that leads to percentage differences within the final results obtained from several experiments. The machine setup for the hip prosthesis might affect the results. The application of the strain gauges and surface attachment might influence the outcomes. The optimal way of employing a strain gauge to thoroughly clean surface using various solvents and solutions is very sensible and might affect the outcomes. If any strain gauge were not put on the hip joint in the correct manner this will provide an inaccurate reading of strain values. Moreover, any small difference in CAD 3D model of hip joint compare to laboratory model might possibly cause the difference of strain values compared to the experimental data.

Other human errors at the same time have possible role in the difference of the strain outcomes. The hip model was examined on a machine and several loads were applied including 200kN, 400kN, 600kN, 800kN and 1000kN. Applying of loads was paused manually whenever reaching a specific value which in turn might have a slight influence on the outcome. The Pearson coefficient of correlation that was explained earlier in other experiments above, shows a strong correlation between the experimental and Ansys data which indicate the Ansys data are appropriate and valid.

Chapter 4

The Influence of Hip Prosthesis Design on Stability

This chapter evaluated the influence of hip prosthesis design on primary stability. Three distinct groups were created from a range of cementless femoral stem models including straight cylindrical, taper and anatomical. A representative of every group was evaluated where the same stress distributions and magnitudes were calculated with the simulated physiological forces. The three most frequent materials employed for implant, metal base alloys like titanium alloys, chromium alloys and isoelastic composite, were also evaluated. The isoelastic stem, however touted since mechano-compatible because of its similarity with femur properties, developed a tenfold increase in general micromotion. In view of the particular usage of a short stem in the conventional method, the finite element method demonstrated that an extremely short stem which protects the proximal area sacrificed the primary stability. An evaluation has also been performed between the proximal and distal fixation stem in which the proximal model was discovered to become unstable in the gait and stair-climbing exercises.

4.1 The global geometry cementless

Femoral stems are available in different sizes and shapes. To be able to evaluate effectively the influence of these distinct geometries and shapes on primary stability, all the stems were classified into various groups according to their attributes. There is not really a consensus right now with regards to grouping cementless femoral stems based on their geometry and shapes, mainly because of the huge number of cementless femoral stems presented in the market nowadays. Healy (2002) has classified cementless hip components into 5 general categories presenting samples for each of these categories : the cylindrical distal filling (the AML, the Solution), the anatomic, proximal fit and fill (the PCA, the Anatomic), combination (the S-ROM, the Bridge), dual, tapered wedge (the Omninfit, the Osteolock, the Mallory-Head, the Synergy, the Summit), and flat, tapered wedge (the Tri-Lock, the Taperloc, the Accolade). Mallory et al. (2001) have classified them into three unique model geometries and concepts - the extensive porous coating with distal fixation (the AML), the anatomic proximal fixation (the PCA, the Anatomic) and gradual proximal to distal off-loading tapered geometry (the Mallory-Head). Two other papers suggested similar categories (Bourne 1998, Reitman 2003).They classified the total geometry into three major groups: cylindrical, tapered and

anatomic. A further study by Parvizi et al. (2004) has presented a comparison among the tapered Taperloc femoral stem to the anatomic PCA and cylindrical femoral stems including the Harris-Galante, the APR-1 and the AML, even though it failed to categorically classify the distinct types of cementless femoral stems, but it did point out a comparison among the tapered Taperloc femoral stem to the anatomic PCA and cylindrical femoral stems including the Harris-Galante, the APR-1 and the AML.

A literature review was carried out in the literature for those follow-up research projects and in vitro practical attempt to obtain as much data as possible on the different models of cementless femoral stems. Aside from the papers and articles, nine cementless primary femoral stems producers were included within the investigation as well: 1. Aesculap, Tuttlingen, Germany. 2. Biomet, Warsaw, IN. 3. Corin Medical, Gloucestershire, UK. 4. DePuy, Warsaw, IN. 5. Smith and Nephew, Memphis, TN. 6. Stryker Howmedica Osteonics, Rutherford, NJ. 7. S and G Prostheses, Lübeck, Germany. 8. Wright Medical Technology, Arlington, TN. 9. Zimmer, Warsaw, IN.

From this investigation, three categories based on the general geometry of the femoral stem were selected similar to the work suggested by some other researchers stated above; the tapered model, the anatomic and the straight cylindrical. Femoral stems that were not tapered in any plane within the distal half were classified with one another. Since most femoral stems in this category were also cylindrical, the category was classified as straight cylindrical (Figure. 4.1). The top of the femoral stem might or might not be tapered. Tapered femoral stems were described as stems that possess a proximal to distal taper in both or either of the sagittal or longitudinal directions (single-planar/biplanar tapered) (Figure. 4.2). Several tapered models including the Mallory-Head have a posterior to anterior taper within the coronal plane as well (tri-planar tapered).

Anatomic femoral stems were defined as stems developed with an anterior-posterior shape that imitates the natural curve of the real human femur (Figure. 4.3). The femoral stems should consequently come in a left and right component. All cementless hip stems have a press-fit physical interface in which contact stress among two components of different young's modulus, the femur and the hip prosthesis, generate deformation. The femur displays viscoelastic behaviour, which in turn restricts the efficiency of the press-fit by relaxing the contact stress at the interface (Howard et al., 2004). The cylindrical distal fixation femoral stems rely on cortical bone contact in the distal part of the femoral stem for stability, whilst

tapered femoral stems rely on proximal, cancellous femur support and a 3-point fixation pattern. The Anatomic femoral stems implement curved models within both

Figure. 4.1- Hip femoral components having straight cylindrical design, obtained from manufacturers' websites

Figure. 4.2-Hip joint femoral components with tapered design, obtained from manufacturers' websites

A-P and M-L planes, and also have a large proximal part to attain a better fit towards the natural endosteal cavity in the proximal side of the femur bone. Kim et al. (2003) have reported that this model feature enhances the potential to accommodate axial, bending and twisting loads. The categories were created in line with the general geometry of the femoral stem. The concepts

might or might not be classified together. The straight cylindrical model, for instance, may possess two forms of fixation that are distal and proximal. The Prodigy is a distally fixed model, whereas the AML model, though designed for distal fixation, can potentially function as proximal fixation model as well. Likewise with regard to the tapered category, the Alloclassic is distally constrained, while the CLS is proven to be a proximal fixation model. For the anatomical category, the ABG as well as the IPS use a distal femur bone over-reaming method for proximal fixation, however the Profile implant, that employs a similar fixation approach, does not utilize the over-reaming technique. The challenges of proximal and distal fixation techniques will be covered later in chapter 5.

Figure. 4.3- Hip joint femoral components with anatomic design, obtained from manufacturers' websites

To be able to evaluate the stability of these femoral stems, a typical model from each category was selected and evaluated. The selected model was simply based on the availability of the particular 3D CAD design acquired from the specific company. They include the AML for category 1, the Alloclassic for category 2, and the ABG for category 3.

The Anatomic Medullary Locking (AML) femoral stem (Depuy, Warsaw, Indiana) is a nontapered collared model having a comparatively long femoral stem. The design of the stem is cylindrical to match the medullary canal while tapered at the tip to decrease the possibility of thigh pain. Since the femoral stem is not tapered, the hip prosthesis does not wedge in position. Rather than that, fixation depends upon a so-called 'scratch fit' among the particular rough exterior area of the hip prosthesis and a similarly formed femur bone canal (Richards et al., 2010). The femoral stem is porous coated for approximately 80 % of its size from the proximal end and is polished at the distal end. It is developed from cobalt chromium (CoCr) together with the porous coating developed from sintered CoCr beads with an average pore size of 200 microns. The actual pores over the surface have been proven to supply an appropriate surface to stimulate tissue ingrowth and enhance the stability of hip femoral stems.

The Alloclassic (Zimmer, Warsaw, IN) is typically a cementless, collarless flat and tapered femoral stem employing distal fixation press-fit method. The surface is entirely grit blasted (4 to 6 microns) using corundum particles, for long-term femoral ongrowth. An improved proximal fit is possible by the lateral side engaging the greater trochanter, reported to enhance axial stability. It is produced from Protasul-100 titanium alloy (Ti Al Nb) in which niobium is utilized rather than the typical vanadium employed in titanium alloy. The straight taper is actually flat in transverse area and wedged shaped mediolaterally. It is particularly developed to fit the hip joint femoral canal on the frontal plane though does not fill in the lateral plane. It attains self-locking to the endosteal femur bone as a result of 4 corners of the particular rectangular design that are elongated through the whole stem.

The Anatomique Benoist Giraud (ABG) hip joint femoral stem (Stryker Howmedica Osteonics, Rutherford, NJ) is known as a cementless anatomic hip femoral component made out of titanium alloy along with a 50 micron coating of hydroxyapatite applied to its proximal 1/3. A proximal press-fit method is implemented with distal hip joint femoral over-reaming as a standard surgical procedure to prevent femur bone contact in this region. This model of

proximal metaphyseal fixation in the ABG was an effort to transmit stresses much more proximally to preserve femur bone density.

4.1.1 Finite element modelling

Whilst all three selected hip prostheses (ABG, Alloclassic and AML) have been classified into unique groups of femoral stem models, these prostheses had some other unique features or special characteristics of their own (Figure. 4.4 and Table 4.1). This created difficulties in the evaluation and analysis since the particular features of the prostheses could possibly have interacted when using the global geometry and influenced the general primary stability. As a result, these prostheses were adjusted, in order that an effective assessment according to the categories above could be done. For the AML, the collar was eliminated, the femoral stem was shortened to the average size of the Alloclassic and also the ABG, while at the same time the distinction among the porous coated and the smooth area was neglected. The implant was considered having a homogeneous surface area design across the femoral stem. This was equally employed on the ABG, where the unique surface area finish among the proximal and distal section was neglected. The indentation elements in the proximal section of the ABG were eliminated. The surgical method of the ABG demands that the distal section is over-reamed to prevent cortical bone contact within this region. In the interests of evaluating the distinct categories in this section, femur bone over-reaming was not modelled. For all of designs and models, the surface area within the femur and hip stems were considered to be in complete contact. The coefficient of friction was defined as 0.4 in addition to an interference fit to be equal to 0.1 mm all through. The adapted models would therefore be mentioned as the ‘cylindrical’ (category 1), the ‘tapered’ (category 2) and the ‘anatomical’ (category 3) designs respectively. The models were entered according to both Fisher’s gait analysis and Duda’s stair-climbing forces and the final results were subsequently compared among each other.

Figure. 4.4-Pictures of the AML, the Alloclassic and the ABG, obtained from manufacturers' websites

Table 4.1- Three kinds of femoral stem models evaluated and their features

Stem	Fixation type	Material	Stem length	Stem shape	Symmetry	Surface finish
ABG	Proximal	Ti Al	Medium	Cylindrical	No	Macrofeature
AML	Distal	Co Cr	Long	Cylindrical	Yes	Porous-coated
Alloclassic	Distal	Ti Al Nb	Medium	Rectangular	Yes	Grit- blasted

From the 1st set of final results, femur elements with a surface region of higher than 50 µm of interface micromotion were aligned to ensure that contact among these elements and the hip prosthesis was no longer available. This process was carried out to simulate the influence of interfacial femur bone loss. The 3D models were then reloaded with physiological walking and stair-climbing forces to examine the instability.

4.1.2 Biomechanical evaluation of different femoral stem designs

Figure 4.5 shows that the magnitudes and distribution of micromotion were matching in all three kinds of prostheses, within both physiological walking and stair-climbing. Significant micromotions were identified in the proximal regions and around the distal femoral stem tip.

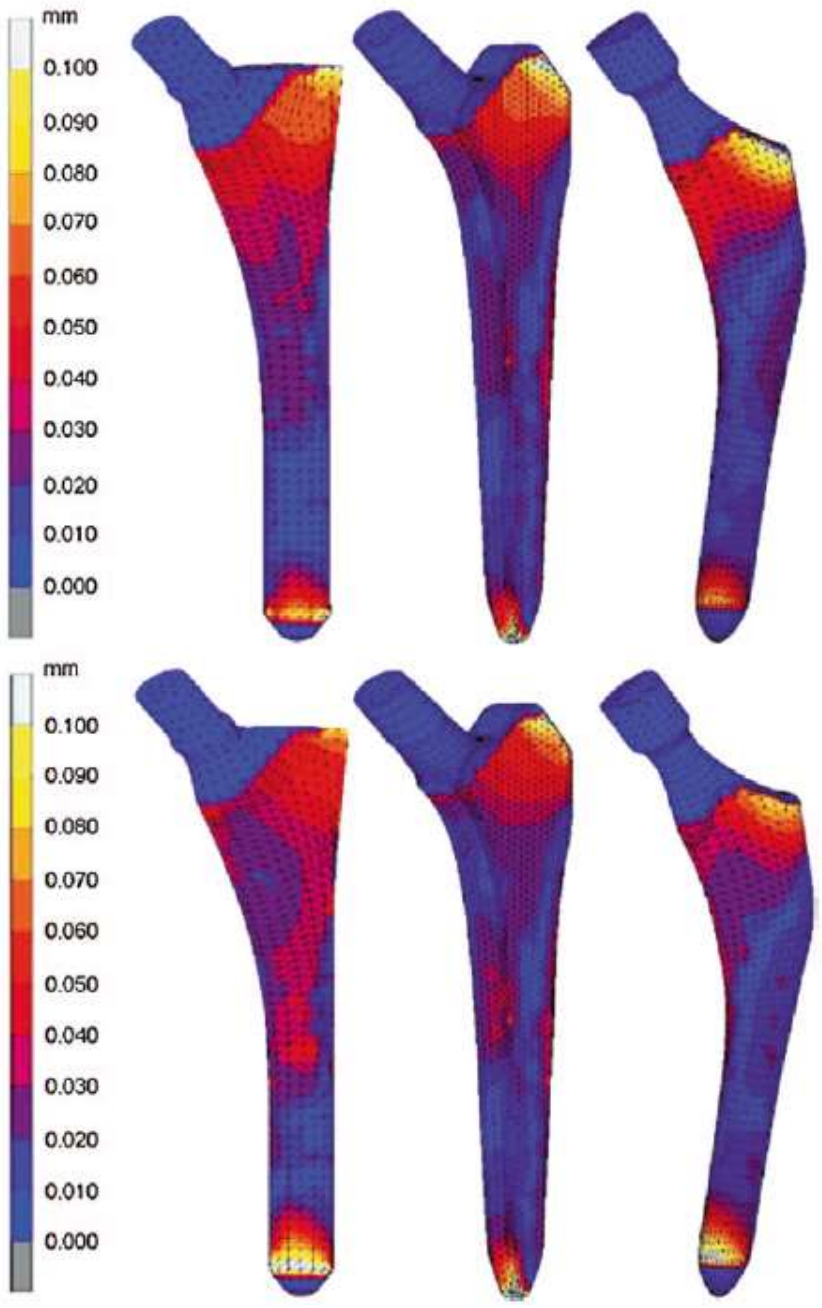

Figure. 4.5- Contour plots of micromotion with regard to the cylindrical (left), the tapered (middle) and the anatomical (right) employing Fisher's gait forces (top) and Duda's stair-climbing forces (bottom) after initial iteration (Abdul Kadir and Kamsah 2009)

With regards to the amount of surface region with higher than 50 μm of interface micromotion, it was ranging between 8 and 10 % for all models. It demonstrated that no particular global model feature was superior compared to the others. Following eliminating the bones with micromotion greater than the selected threshold limit to simulate interfacial femoral bone loss, outcomes were then evaluated once more (Figures. 4.6, 4.7 and Table 4.2). Overall, all models were identified to be stable with femoral bone loss only increased slightly (up to 13 %). The

anatomical model was discovered to be the most stable having a minimal increase in surface region beyond 50 μm. The cylindrical model was the least beneficial in stair-climbing with a rise in impractical surface region from 9 to 13 %. The tapered model was the worst in physiological walking in which there was a rise from 8 to 10 %.

The three groups of hip femoral stems evaluated in this section, the cylindrical, the anatomical and tapered models had identical distribution of micromotion and all appeared to be stable when femoral bone loss was simulated. The results were in agreement with published outcomes of actual hip femoral stems that belong to these categories. The ABG, the Alloclassic and the AML are all prostheses with good survival rates in short and long term.

The AML is an efficient femoral stem and performed effectively in hip arthroplasty. The outcomes are well published and the reports included patients over a large range of age groups. In one of the early investigations in this subject, Engh et al. (1994) have presented 15 years of clinical experience that includes the AML model. Out of 393 AML femoral stems replacements merely six revised; 3 of those were because of the loosening. A further research by Nercessian et al. (2001) has mentioned a survival rate of 92 % in more than ten years when using the AML design. 88 % of the patients experienced good as well as excellent medical outcomes, but calcar resorption was identified in 40 %. One particular medical study included 433 patients that had the hip operation in 1991 and 1992 (Schwerter et al., 2013). 145 (33.5 %) of them were followed up fully both radiologically and clinically. The AML prostheses were observed for a minimum of 15 years, where the authors reported excellent durable outcomes in the young patients. The claimed survival rate was in fact 97.5 percent of that includes femur bone ingrown, 3 percent consistent fibrous tissue as well as just one percent was identified unstable.

The finite element outcomes shown in this section appeared to be also in agreement with some other follow-up reports with regards to predicting femur bone ingrowth. Researchers Woolson and Adler (2002) have claimed that when stable primary fixation is achieved intraoperatively and radiographically employing the AML femoral stem, femoral bone ingrowth reliably takes place regardless of whether a part or even full weight bearing postoperative process is followed. It has been also suggested that femur bone ingrowth had taken place in 93 % of the instances in which highest stability was obtained. One of the beginning retrieval investigations about an AML prosthesis before gross failure exhibited dense cortical bone and cancellous femur bone ingrowth. Strength of connection of the metal hip prosthesis to femur bone was effective

without any slipping discovered at the interface when examined under torsional and also axial force. Engh et al. (1994) have employed backscattered scanning electron microscopy (SEM) in order to evaluate femur bone growth of the AML femoral stem. They suggested that average femur bone ingrowth has been identified with 57 % of the porous surfaced region of the hip femoral parts.

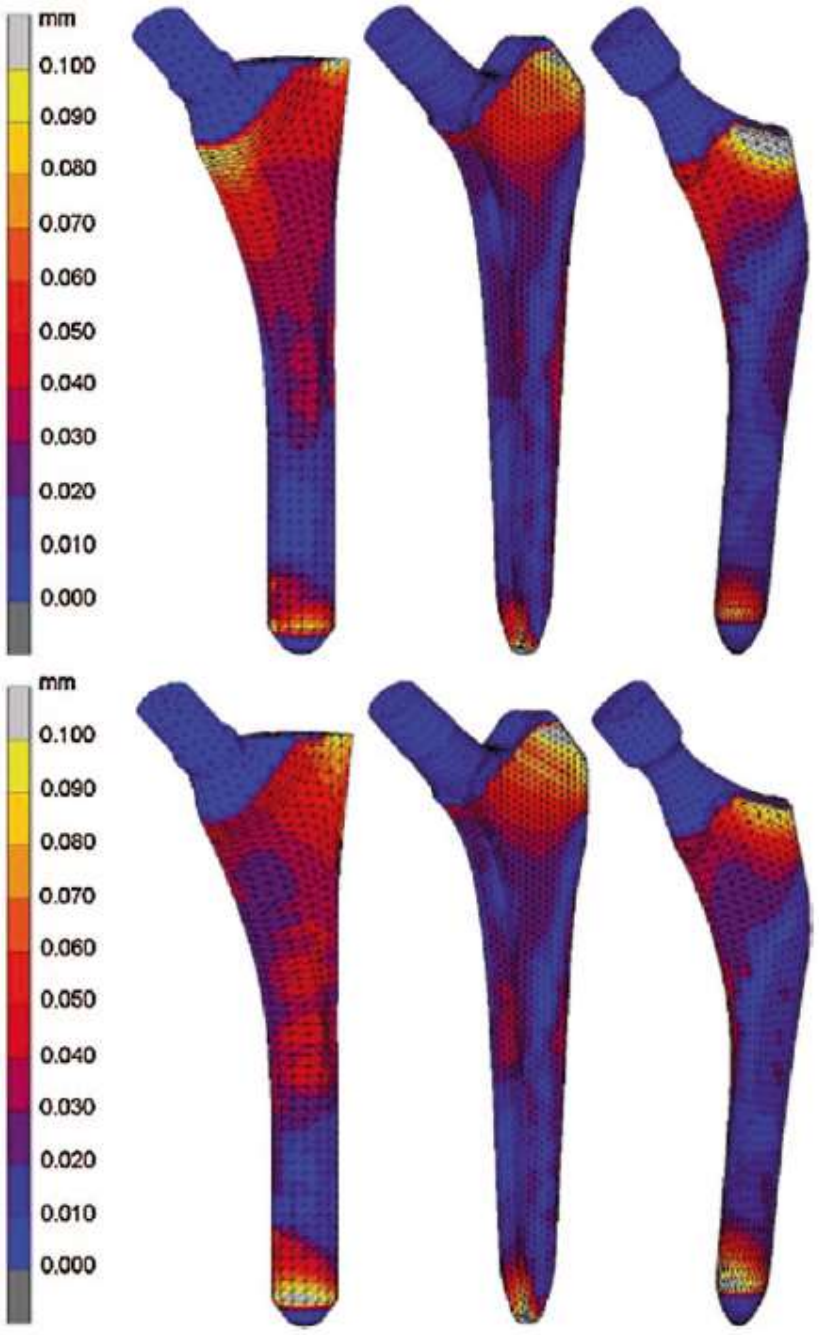

Figure. 4.6- Contour plots of micromotion for the cylindrical (left), the tapered (middle) and the anatomical (right) employing Fisher's gait loading (top) and Duda's stair-climbing loads (bottom) after simulated interfacial femoral bone loss (Abdul Kadir and Kamsah, 2009)

Research has been carried out comparing a newly inserted AML femoral stem and a sample removed from a deceased individual (Sugiyama et al., 1994). They discovered that micromotion appeared to be higher proximally with the newly replaced femoral stem in comparison with the femur bone ingrown restored sample. In addition they discovered that the slick and clear distal femoral stem of the restored sample induced greater micromotion compared to new prosthesis that was implanted. The authors suggested that the flexibility in the femur leads to higher micromotion in the femur surrounding the slick and clear distal femoral stem in spite of the primarily firm distal fixation.

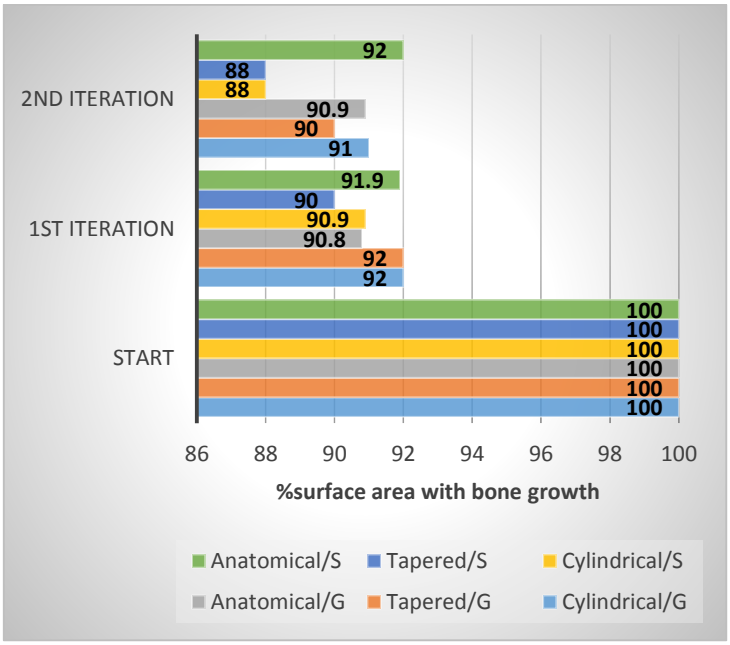

Figure. 4.7- Percentage area of predicted femur bone ingrowth for the cylindrical, the tapered and the anatomical femoral stem designs employing Fisher's gait (G) and Duda's stair-climbing (S) loads (Abdul Kadir and Kamsah, 2009)

Table 4.2- Surface region > 50 μm of micromotion for the cylindrical (7,345 mm^2), the tapered (7,690 mm^2) and the anatomical (7,222 mm^2) after each iterations (Abdul Kadir and Kamsah, 2009)

Loadcase	Stem	First iteration		Second iteration		Third iteration	
		Area> 50μm(mm2)	%	Area> 50μm(mm2)	%	Area> 50μm(mm2)	%
Fisher's gait	Cylindrical	604	8	674	9	695	9
	Tapered	642	8	740	10	771	10
	Anatomic	633	9	653	9	-	-
Duda's stair climbing	Cylindrical	647	9	875	12	951	13
	Tapered	757	10	893	12	925	12
	Anatomic	562	8	584	8	-	-

For the anatomical model, some other follow-up reviews are verifying the finite element simulations. The ABG hip femoral stem has been claimed to have good medical and radiographic outcomes in the short term and within 5 years follow-up study (Giannikas et al., 2002), although the rate of survival decreased as a result of wear within the polyethylene acetabular cup. Herrera et al. (2004) have reported a rate of survival of 97 % during seven to ten years, nevertheless yet again considerable polyethylene wear was noticed in a large number of the acetabular cups. In order to compare these finite element outcomes with the follow-up reports about the ABG implants the over-reaming of the distal section was not modelled. Some other anatomical models, that do not employ an over-reaming method, are the Profile and also the APR-II. A follow-up research by Kim et al. (2003), which was mentioned earlier, about the Profile over nearly a decade has demonstrated outstanding medical and radiographic outcomes, without any femoral stems revised due to aseptic loosening thigh pain was discovered in just 10 % of cases. The APR-II femoral stem has also been identified to be particularly efficient by Kang et al. (2000). From 99 overall hip arthroplasties observed during up to 4 years, all had proximal femoral bone ingrowth fixation without any patient having thigh pain following 3 years. Distal cortical hypertrophy related to tip fixation occurred in 49 % of cases while proximal stress-shielding seemed to be present in 43 % of cases.

An in vitro practical companion between a curved anatomical femoral stem and a straight femoral stem discovered the fact that during low angles in flexion, the curved hip stem and straight hip stem exhibited identical patterns of movement. Nevertheless, at higher torsional scenarios including the movement that occurring the course of stair-climbing, the curved femoral stem was discovered to be much more stable compared to straight femoral stem. In a further test comparing straight and asymmetrical hip femoral stems using 1,000 N of force employed on the prosthetic head, in terms of the axial micromotions they were discovered to be minimal for both femoral stems, with the symmetrical femoral stem experiencing the minimum axial micromotion (an average about 6 μm) when compared to the asymmetrical femoral stem, which shows the average micromotions of about 19 μm. Nevertheless, a torsional loading experiment demonstrated that the straight femoral stem experienced approximately ten times higher relative rotational movement than two other hip prostheses. Chen et al. (2014) have done a further investigation and demonstrated that straight and curved femoral stems worked similarly with regards to micromotion in the course of single leg stance as well as at small loads within the stair-climbing. When great torsional moments (22 Nm) were employed, the straight femoral stem generated 2-4 times higher micromotion compared to the curved

femoral stems. Each of these three articles suggested that straight femoral stems generated higher micromotion compared to curved anatomic femoral stems in the course of stair-climbing. The finite element outcomes, however did not demonstrate a large difference between the two models with this physiological forces. The explanation might be that within the finite element models, a perfect fixation was made with an interference of 0.1 mm throughout the surface area of the femoral stem. The finite element outcomes demonstrated that the straight femoral stem had 9 % surface region over the threshold limit of 50 μm micromotions in the interface as opposed to anatomic model with 8 %. Nevertheless, after the femoral elements were modified to simulate femoral loss, the region for the straight femoral stem rose to 12 %, however the anatomic model remained at 8 %. This demonstrated that straight femoral stems were a lot more vulnerable to micromotion throughout stair-climbing where a perfect and complete fixation within the interface was not obtained.

The Alloclassic femoral stem, that represented the tapered category, is another successful model with a rate of survival of 99.3 to 100 % over 5 and 11 years (Pieringer et al., 2003). In one of the follow-up studies of the Alloclassic model, 98 % of the hip joints were graded good or excellent clinically within a median of four years. No femoral stem was categorized as definitely loose and no hip joints needed revision. There was also no occurrence of hip joint femoral osteolysis. Delaunay et al. (2001) have suggested that only 3 out of 133 femoral stems subsided 2-5 mm in addition to one that subsided 5-10 mm during the 1st year, however no progressive subsidence could be recognized after this period. Effenberger et al. (2002) have reported excellent outcomes at 8 years for the Alloclassic model with 83 % exhibiting no radiolucency and 17 % displaying radiolucency merely proximally. The retrieval research on the Alloclassic model discovered that considerable bone to implant apposition took place around the interface across the femoral stem between 6 weeks and 5 years. The mean appositional femur index was in fact 48 %. Other tapered models have also been demonstrated to have excellent outcomes during by Keisu et al. (2001) at 5 years and Eingartner et al. (2000) and Park et al. (2003) at 10 years.

The hip models representing the three categories have been customized whenever possible so that an appropriate comparison could be made between them. Nevertheless, the lateral flare feature of the Alloclassic model was not eliminated due to the problems in redesigning the implant in three dimensions. The lateral flare is actually a proximal lateral extension that is created to accommodate the lateral cortex of the femur in the metaphysis, enabling a much

wider base of support within this region. This enables higher concentric forces within the proximal femur and reduces distal stress transfer. Leali et al. (2002) have discussed that this element supplies extra primary stability in cementless hip femoral stems. In further research, Effenberger et al. (2001) have claimed that prostheses having a lateral flare, including the Alloclassic model, have greater rotational stability in comparison to the Schenker implant, a femoral stem with no lateral flare. The micromotion algorithm could only demonstrate resultant interface relative movement and could not divide this into axial and rotational factors. For that reason the rotational micromotion of the Alloclassic model could not be calculated. The influence of a lateral flare element will be evaluated in chapter 5 when proximal and distal replacement models are reviewed.

Rotational stability to torsional forces has been mentioned by Gortz et al. (2002). Four hip femoral stems were assessed practically, two belonging to the tapered category (the Alloclassic model and the CLS), one to the anatomical category (the ABG), and one related to the straight cylindrical category (the S-ROM). They discovered that the relative rotational movement for the anatomical ABG model as well as the tapered CLS was greater distally than proximally, whilst the Alloclassic model, which is in the similar category as the CLS, demonstrated the opposite; that is larger proximally compared to distal. Although their investigations could not be linked to the finite element final results here, because of the restriction of the micromotion algorithm, it demonstrated that the general geometry solely could not entirely be the reason for the stability of cementless hip femoral stems. Different methods of fixation, particularly proximal and distal fixation, equally play a part in the stability of hip joint femoral parts.

In summary, this section demonstrated the outcomes of a finite element micromotion study that verified the stability of three groups of hip stems 1) Anatomical, 2) Tapered and 3) Cylindrical models. Certain features of these prostheses were eliminated whenever possible to ensure that an effective comparison among the three groups could be made. One of the restrictions of this research was the inability to divide the resulting micromotion data into axial and rotational components. Therefore it is unknown, for instance, which kind of femoral stem was superior with regard to sustaining torsional forces. Regardless of these restrictions, this research verified the stability of these types of femoral stem models.

4.2 The material stiffness

Among the many design factors that needs to be taken into account is the type of material employed, in which a trade-off between force transfer and hip prosthesis stability is the crucial matter. The previous generation of cementless femoral stems were stiff in comparison with the femur bone, about 10 times stiffer. A stiff material is going to make force transfer ineffective, and ultimately result in 'stress-shielding', an undesirable femoral remodelling phenomenon in which bone tissue is resorbed in regions where it is not exposed to loading to physiological levels. The stiffness mismatch between the femoral stem and the femur leads to loss in proximal cancellous femur along with thickening of distal cortical femur bone. It was, and still is, one of the leading issues in hip arthroplasties, for both cemented hip replacement and cementless.

The issue of force transfer from stiff prostheses to the femur resulted in the creation of low stiffness femoral stems, also known as 'isoelastic' femoral stems. The purpose of isoelasticity was to deform the hip prosthesis and the femur bone as a single unit, hence preserving the bone structure more effectively. With regard to preserving femoral bone stock, compliant femoral stems have been proven to be a lot better than stiff femoral stems. Sumner et al. (1998) have carried out an in vivo investigation on canine designs and demonstrated that decreased femoral stem stiffness improved proximal force transfer, thus reducing proximal femoral bone loss. Ang et al. (1997) have studied 14 patients in which 6 patients acquired isoelastic prostheses, and showed their total Bone Mineral Density (BMD), a parameter that calculates femoral quality, increased by a mean of 12.6 %. For those having a fairly stiff titanium hip, BMD reduced by a mean of 27 % following 12 months. Caouette et al. (2011) have carried out a finite element femoral remodelling research comparing the influence of the modulus of elasticity of different femoral stems and showed that low stiffness material including a CFRP composite decreased stress-shielding in the proximal femur as compared to the titanium alloy.

Although there appears to be a benefit of employing isoelastic femoral stems, many authors suggested that utilizing these femoral stems induced high rate of aseptic loosening. The RM implant and the Morscher implant were two of the first isoelastic cementless femoral stems. There seemed to be a high rate of aseptic loosening during a follow-up study of 9 years. The later generation of isoelastic femoral stems including the prototype carbon fibre-reinforced composite experienced a similar fate (Adam et al., 2002). The authors mentioned tiny aseptic loosening and fibrous interface fixation for 92 % of carbon fibre hip implants during 6 years.

In this section, a 3D finite element method was carried out on three unique material properties including composite material, titanium alloy (TiAl) and cobalt chromium (CoCr), to evaluate the micromotion among them within physiological forces.

4.2.1 Finite element modelling

The femoral stems were evaluated by (Tarala et al. 2011) assigning different distinct elastic moduli addressing composite material, titanium alloy and cobalt chromium. The reconstructions were subjected to an alternating loading history of normal walking and stair climbing. The normal walking consisted of two peak hip joint forces occurring during the walking cycle (the beginning and end of single support phase). The stair climbing load consisted of the peak force occurring during a stair climbing cycle.

4.2.2 Biomechanical influence of distinct mechanical properties

As potential implant compositions, we chose porous tantalum (Ta) in three constitutions: Ta60, Ta80 and Ta80-solid core (Table 4.3). A layered composite construct consisting of a CoCrMo core, a PEEK inner layer and an outer Ti fiber metal layer. In order to analyze the various material combinations, the same layers used with different material properties (Figure 4.8). Bone osseointegration was assumed to occur when micromotions at the implant–bone interface remained below 40 μm and the interfacial gap remained smaller than 500 μm for 5 subsequent increments (Figure 4.9).

The remodeling simulations showed that the composite stems performed better than the stem made of solid Ti alloy. The flexible femoral stems induced higher micromotion compared to the stiff models. This is in agreement with the practical results of Gortchacow et al. (2012). They carried out micromotion tests on cementless femoral stems with three distinct material properties; carbon stainless steel (200 GPa), titanium alloy (100 GPa) and composite (E = 18.6 GPa). They noted that the carbon composite femoral stem generated considerably larger micromotion proximally and noticeably smaller micromotion distally compared to the two metals. They suggested that proximal stress transfer could very well be enhanced by a flexible femoral stem, however they mentioned the potential of increasing micromotion in the proximal region. They also have proposed that enhanced proximal fixation might be essential to obtain medical success with flexible composite hip femoral components.

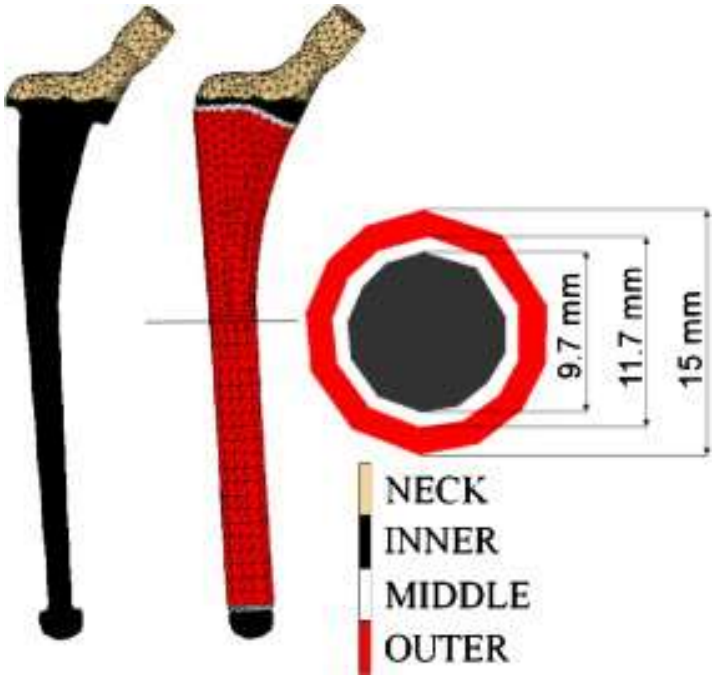

Figure. 4.8- The proposed stem which is a layered composite (Tarala et al. 2011)

Table 4.3- Proposed stem compositions and their bending stiffness (Tarala et al. 2011)

Name	**Neck**	**Inner**	**Middle**	**Outer**	**Bending stiffness (10^3 Nm^2)**
Epoch	CoCrMo	CoCrMo	PEEK	Fiber metal	116.7
Ti alloy	TiAlV	TiAlV	TiAlV	TiAlV	260.8
Ta60	CoCrMo	60% porosity Ta	60% porosity Ta	60% porosity Ta	14.4
Ta80	CoCrMo	80% porosity Ta	80% porosity Ta	80% porosity Ta	4.5
Ta80-solid core	CoCrMo	CoCrMo	80% porosity Ta	80% porosity Ta	107.9

There are extensive other reports including Elliott et al. (2011), Yildiz et al. (1998a) and Yildiz et al. (1998b) comparing prostheses with various stiffnesses that demonstrated substantial improvement in proximal micromotion for a flexible hip prosthesis compared to titanium alloy or steel prostheses. A pilot investigation on the goat (McCarthy et al., 2010), also showed that stiff prostheses exhibited favourable primary interface micromotion for femoral bone ingrowth.

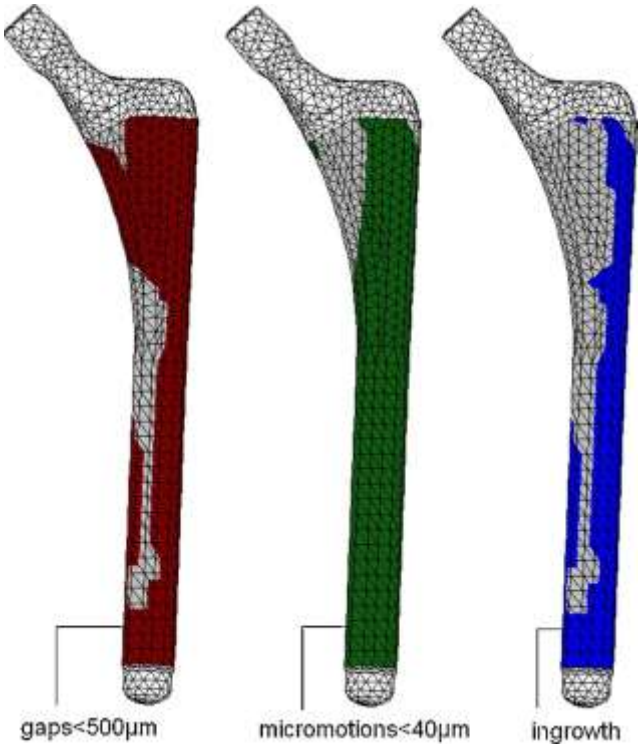

Figure. 4.9- Distribution of factors (gaps and micromotions) that govern the ingrowth process (Ta80) (Tarala et al. 2011)

These practical findings were furthermore established by numerical studies. Employing a simplified cylindrical design, the authors noticed that the interface micromotion decreased by about half for Co-Cr-Mo alloy in comparison with a hip prosthesis having a stiffness ten times lower. A further finite element study on the influence of material stiffness used 2D design of a replaced implant. The authors identified that a flexible femoral stem produced movements around three to four times greater proximally than those of a stiff femoral stem. These published outcomes along with our results demonstrated that even if flexible prostheses could enhance force transfer, their flexibility could remove the environment that is required for osseointegration.

While stiff femoral stems prompted femoral bone loss because of stiffness mismatch, Jauch et al. (2014) showed that compliant femoral stems created difficulties in stability because the hip prosthesis is easier to displace and rotate than its stiffer counterpart. To be the compromise amongst the influence of ‘stress-shielding’ of a stiff femoral stem and the influence of ‘excessive micromotion’ associated with flexible femoral stems, most hip femoral stems these days are produced out of titanium alloy. Apart from having great structural strength as well as being relatively bio-inert, it offers a stiffness value of approximately 100 GPa still greater than

the stiffness of femoral bone, but much less stiff compared to prostheses manufactured from steel or cobalt chromium.

Early samples of flexible femoral stems were the RM implant and the Morscher implant. Both prostheses demonstrated promising first outcomes however with a high rate associated with aseptic loosening in long-term follow-up. Hip femoral components were noticed to be very loose and easily removable, having a thick, polished fibrous membrane in the interface, with no signs of any femoral bone ingrowth. Very high flexibility in the proximal section of the implant was held responsible for femoral bone resorption and hip prosthesis loosening. Adam et al. (2002) have suggested macroscopic aseptic loosening along with fibrous interface fixation within 92% of carbon fibre-reinforced composite hip implants during 6 years. A further research comparing isoelastic Butel femoral stems and stiffer PCA femoral stems revealed that isoelastic femoral stems showed an extremely high rate of loosening (43%) compared to stiff femoral stems at 4 years post-operatively. The Butel femoral stems, nevertheless, gave less evidence of stress-shielding radiologically.

In spite of the above studies of hip femoral stems loosening by using compliant material, a recent short-term (24 months) follow-up study by Karrholm et al. (2002) has reported an encouraging outcome of the isoelastic Epoch femoral stems. The migration of the Epoch was not seen to be statistically considerable as opposed to relatively stiffer Anatomic femoral stems. Both femoral stems stabilised with migration under 100 μm during 2 years using the Anatomic design displaying less migration than the Epoch. None of the femoral stems were changed during the time of follow-up study and the Epoch demonstrated considerably decreased femur bone loss in Gruen zones 1, 2, 6 and 7 at 2 years in comparison to the Anatomic design. The Epoch isoelastic femoral stem appeared to demonstrate better short-term stability compared to early generations of isoelastic femoral stems for example the Butel, the Morscher and the RM. This might be associated with other model aspects of the hip prosthesis such as the general geometry of the femoral stem as well as the type of surface finish. The RM implant, for instance, was not created to fill the canal while the Butel implant had a polished surface. The Epoch however is actually a ‘fit and fill’ model that has porous coating all over the length of the femoral stem. The results by numerical simulation also demonstrated that despite the fact that a compliant material created greater micromotion compared to stiffer prostheses, using a ‘fit and fill’ model, the distal half of the femoral stem was indeed as stable as its stiffer counterpart.

This section evaluated the influence of material stiffness upon interface micromotion. Our assessment demonstrated that micromotion increased as the stiffness was decreased. Our outcomes were in agreement with some other published reviews regarding the material stiffness, whether finite element, practical or follow-up reports. In this study, not only comparative micromotion outcomes were displayed, but stability was also estimated for the three unique hip stems' elastic moduli by simulating interfacial femoral bone loss. The final results demonstrated that despite the fact that flexible femoral stem generated greater micromotion and considerable proximal interface femoral bone loss, it will still be stable in case which tight fixation was accomplished distally.

4.3 The influence of femoral stem length

The investigation of femoral stem length is especially relevant for prostheses that are to be employed in revision surgery. As a result of loss of femoral bone stock mainly in the proximal femur, after a failed primary arthroplasty, surgeons need to depend on the cortical femoral bone distally. For that reason, revision hip stems are usually longer compared to their primary counterparts to be able to obtain proper stability via distal fixation. The ideal femoral stem length is nevertheless a subject of debate and controversy in revision surgery.

There are relatively few scientific studies about the optimum length of hip stems intended for primary arthroplasty. These investigated the influence of femoral stem length for a certain type of hip implant in which the distal section of the femoral stem was thinner compared to the medullary canal. Considering that the distal section of the femoral stem did not fit and fill the medullary canal, it might be hypothesized that the distal section of the femoral stem had no mechanical purpose, consequently the study of femoral stem length. One of these reports by Tanner et al. (1995) has compared three femoral stem lengths of the Freeman femoral stem, including the full length of 172 mm, a medium length of 132 mm as well as a short femoral stem of 92 mm. A finite element object of each of these was developed and evaluated, and the actual implants with various femoral stem lengths were examined experimentally. They discovered that enhancing the length of the femoral stem led to a sudden rise in the amount of compressive stresses laterally around the tip. With the short femoral stem, there was a rise in the proximal stresses medially whilst experiencing some lateral stresses distally. All femora with short femoral stem parts also failed under forces between 800 to 1200 N, while no femora

with longer femoral stems failed. They suggested that an appropriate length of femoral stem was that of the medium stems. On the other hand a further finite element investigation by van Rietbergen and Huiskes (2001), demonstrated that decreasing femoral stem length in order to efficiently eliminate it did not raise failure possibility, and it did not decrease stress-shielding either. They suggested that decreasing the femoral stem length to the metaphyseal region was not beneficial. Both of these investigations, nevertheless, failed to discuss if stability was affected by using a short femoral stem.

Although the analysis of femoral stem length is especially popular in revision operation, it is also essential for primary hip arthroplasty. If we could possibly use as short a femoral stem as possible in the beginning, subsequently if the need for revision operation occurred, the loss of femoral bone stock would be significantly less than when a longer femoral stem was employed. Since the two articles discussed above have already considered the stresses at different femoral stem lengths, the purpose of this investigation is to discover, by using FE method, the influence of femoral stem lengths over interface micromotion.

Before starting to evaluate the influence of femoral stem length, it is essential to notice that this investigation could also be linked to the investigation concerning proximal and distal fixation methods, which will be highlighted in the following section. In the approach for proximal fixation, if the hip prosthesis is fixed proximally, then there might be no need for a long femoral stem. Nevertheless, design factors of a proximally-fixed model are more than simply using a short femoral stem, and therefore an independent investigation of proximal compared to distal fixation femoral of stems is described in a different chapter.

4.3.1 Finite element modelling

A comparative analysis was carried out by Gabarre et al. (2016) about two stems.They used 3D scanner to make the model of two stems called Linea stem and Minihip stem. The model for the Linea stem consisted of 395909 elements for bone and 31162 elements for stem, while the model for the Minihip stem consisted of 393744 elements for bone and 22773 elements for stem. The material of both stems was titanium alloy (Young’s modulus: 110316 MPa; Poisson ratio: 0.3).

4.3.2 Biomechanical evaluation of various femoral stem lengths

Differences between press-fit levels are fairly similar, showing a very uniform behaviour along the stem. Gabarre et al. (2016) showed that the general motion pattern exhibited higher amplitude of micromotion for the Minihip stem compared to the Linea stem. Conversely to it, micromotion increased towards the bottom of the stem. They explained the increased load level of gait cycle led to similar results in the Linea stem: it augmented the amplitude. Press-fit levels decreased micromotion as the contact pressure generated grew. A similar effect was also observed here: micromotion levels tended to be more uniform between each other whenever press-fit was applied, the stem has a less solid rigid motion.

According to their investigation press-fit is believed to stabilize cementless stems, limiting the relative motion at bone interface. Figure 4.10 clearly shows this trend: average amplitude of cyclic motion diminishes as press-fit level increases. Another conclusion to point out is that the relative difference of amplitude along each plane is smaller when introducing press-fit. This effect can be related to the fact that press-fit introduces a compression state on the stem that makes it work less as a solid rigid, prevailing the complete elastic subsidence. Figures also show the increasing effect of amplitude as the load scenario becomes greater: a "vigorous" gait cycle increases micromotion amplitude.

They explained that once migration occurs, a repeated reversible cyclic micromotion is developed and stabilized as gait cycle times are simulated. Micromotions were evaluated for each stem at six different levels along repeated gait cycles. The general motion pattern exhibited higher amplitude of micromotion for Minihip compared to Linea stem.

The results of the investigation on the femoral stem length demonstrated the significance of cortical attachment in obtaining stability. The length of the very short femoral stem was selected so that attachment between the femoral stem and cortical femoral bone was minimal. The finite element outcomes demonstrated that this femoral stem had the biggest micromotion of all.

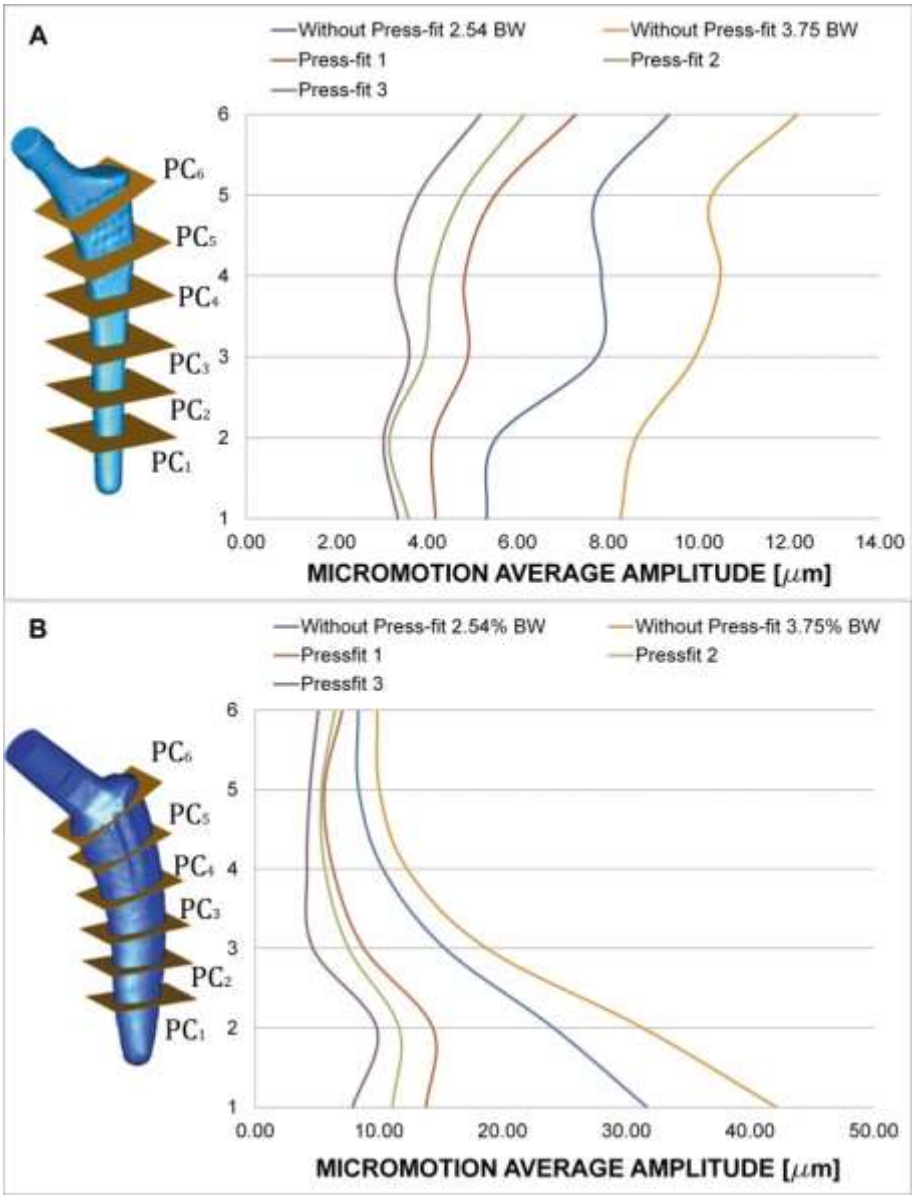

Figure. 4.10 - Average amplitude of micromotions for different press-fit levels and gait load cycle (friction coefficient μ = 0.5, Titanium alloy), (A) Linea stem. (B) Minihip stem (Gabarre et al. 2016)

Between different femoral stem lengths, the short femoral stem experienced greater and a lot more broadly spread micromotion. Nevertheless, the ultimate outcomes after the final iteration of simulated femoral bone loss demonstrated that this did not have an impact on its stability. The only available research with which to compare these outcomes appeared to be the report of Molt et al. (2015), in which 60 patients experienced hip replacement having custom-made hip joint femoral components of two unique lengths. At the time of follow-up study, there had been simply no statistical differences medically and radiographically between the 125 mm long

femoral stem and the 100 mm long femoral stem. The short-stem Mayo implant had a double-wedged contour and was set in place employing 3-point proximal femur fixation. The follow-up timeframe was 12 months and from about 20 patients, just one was revised due to loosening while the rest were considered reasonable. It is questionable that longer-term assessment has not been released, and it is definitely discouraging to find out that a femoral stem had loosened after just 12 months. Since there are not many studies on short-stemmed implants, it is challenging to come up with a solid conclusion over their stability. Nevertheless, the two studies above demonstrated that provided that there was stiff cortical bone attachment on the femoral stem, primary stability was not jeopardized. This is verified by this finite element research, that despite the fact that shorter femoral stems have higher and bigger micromotion than longer length femoral stems, they should nevertheless be stable.

The key benefit of using a short-stemmed implant over long-stemmed is the convenience of changing to a further hip prosthesis, if failure occur. Since less femoral bone is eliminated, it offers a chance of long-term compatibility. With regards to interface micromotion of the implant, a short-stemmed hip stem could be developed to a more stable implant through some other design factors, including a pronounced lateral flare which sets on the inferolateral side of the greater trochanter as well as by using macro-features. This research demonstrated that shorter femoral stems could have the prospect of turning into the next generation of cementless hip femoral stems provided that their stability is enhanced.

Chapter 5

Proximal and Distal Fixation

As explained in the previous chapter, there are two major model concepts of fixation regarding cementless hip stems: proximal fixation and distal fixation. Distal fixation is generally attained via the press-fit method in which the distal section of the femoral stem is fixed to the cortex of the diaphysis, one example of which is the AML model. Proximal fixation, alternatively, relies for the stability on the cancellous femoral bone around the proximal section, which includes the ABG femoral stem. Design factors for both methods of fixation may differ, for instance using a straight or curved femoral stem, rectangle-shaped or cylindrical shape, collared as well as non-collared, types of materials utilised, length of femoral stem in addition to types and scale of coating.

Proximal or distal fixing are both model methods for decreasing femoral bone loss, particularly in the proximal region by enhancing the force transfer. Which model concept is superior remains a debatable matter. Supporters of the distal fixation approach argue that solid primary stability is essential and it is possible through solid and reliable cortical attachment distally. Once the hip prosthesis is stably fixed, femoral bone ingrowth can then develop throughout the femoral stem. Supporters of the proximal fixation approach believe that femoral bone resorption in the proximal region can be decreased if the loads from the hip are transferred to the majority of proximal section of the femur. An additional explanation for employing a metaphyseal filling, proximal fixation model is to keep the endosteum of the diaphysis for later operation, if a revision be required at some point.

The design associated with the distal or proximal fixation varies. The proximal fixation model was attributed to anatomical femoral stems such as the APR-II femoral stem where the proximal hip prosthesis geometry must fit and fill as much as possible the proximal femur. As such, the proximal section is widened in the antero-posterior along with medio-lateral directions to enable a larger region of femoral bone attachment proximally. Nevertheless, the operative method of the APR-II femoral stems uses a tight circumferential diaphyseal fixation. It is therefore unclear if full proximal force transfer is practical. Recent generations of proximally fixed models, like the ABG and the IPS models, applied distal over-reaming method as a standard surgical process. In theory this will enable higher proximal forces than the

diaphyseally fit method utilised for the APR-II design. A further benefit of distal over-reaming is that it considerably decreased thigh pain (Giannikas et al., 2002). This over-reaming method has also been examined on the distal fixation AML femoral stem. The researchers suggested that fractures were possible to take place employing the under-reaming method, and hence turned to over-reaming the distal endosteal femoral bone. Both approaches were observed to give successful results.

A tapered model may be either distally or proximally set since the stability can be attained by wedging the hip prosthesis into the femur. The Alloclassic, for instance, gets a wedge-fit in the diaphysis and for that reason is classified as a distal fixation model. The CLS model, on the contrary, has a tri-tapered model with a square cross section and a slim femoral stem tip. A wedge-fit is attained in the metaphyseal region and as such it is regarded as a proximal fixation model.
In this section the finite element method will be carried out to evaluate interface micromotion, and consequently the stability of two model methods for cementless fixation, the proximal fixation model and also the distal fixation model.

5.1 Finite element modelling

To ensure an appropriate and standard comparison amongst proximal and distal fixation femoral stems, a model was selected to represent both methods to make certain that the minimal modifications possible can be created while keeping the key factors of the model concept. The AML model was selected as the distal fixation model. To produce a proximal model from the AML model, the femoral stem was shortened to about a half, and the proximal component was enlarged within the medio-lateral and antero-posterior sides to allow it to interact with the proximal cortical shell. The medio-lateral measurements was enlarged through having a lateral expansion that filled the infero-lateral section of the greater trochanter. The distal section of the femoral stem was shortened by 80 mm, and the endosteal cavity over-reamed by 28 mm distally, making the effective length for the femoral stem equal to 74 mm. This was carried out for the reason that femoral stems designed for proximal force transfer most often have the distal cavity over-reamed, consequently the distal femoral stem (if perfectly fixed) represents no role in force transfer. Both models were linked with walking and stair-climbing configurations.

5.2 Biomechanical influence of different femoral stem fixations

The average micromotion, corresponding standard deviation, its range, the global distribution and the distribution per area of the stem presented in Figure 5.1, in the range of bone growth expected when only one contact area is achieved with a gap present on the three other interfaces. Four cases were evaluated by Reimeringer and Nuño, (2016) for this configuration: proximal, middle, distal and cortical contacts. The average micromotion predicted is always higher than 40 µm and the maxima always higher than 150 µm. For the four cases, maxima are located in a gap area. However, for the proximal and cortical cases, more than 50% of the interface is in the range of bone growth expected. Conversely, for the middle or distal contact, more than 50% of the stem surface is in the range of partial osteointegration expected.

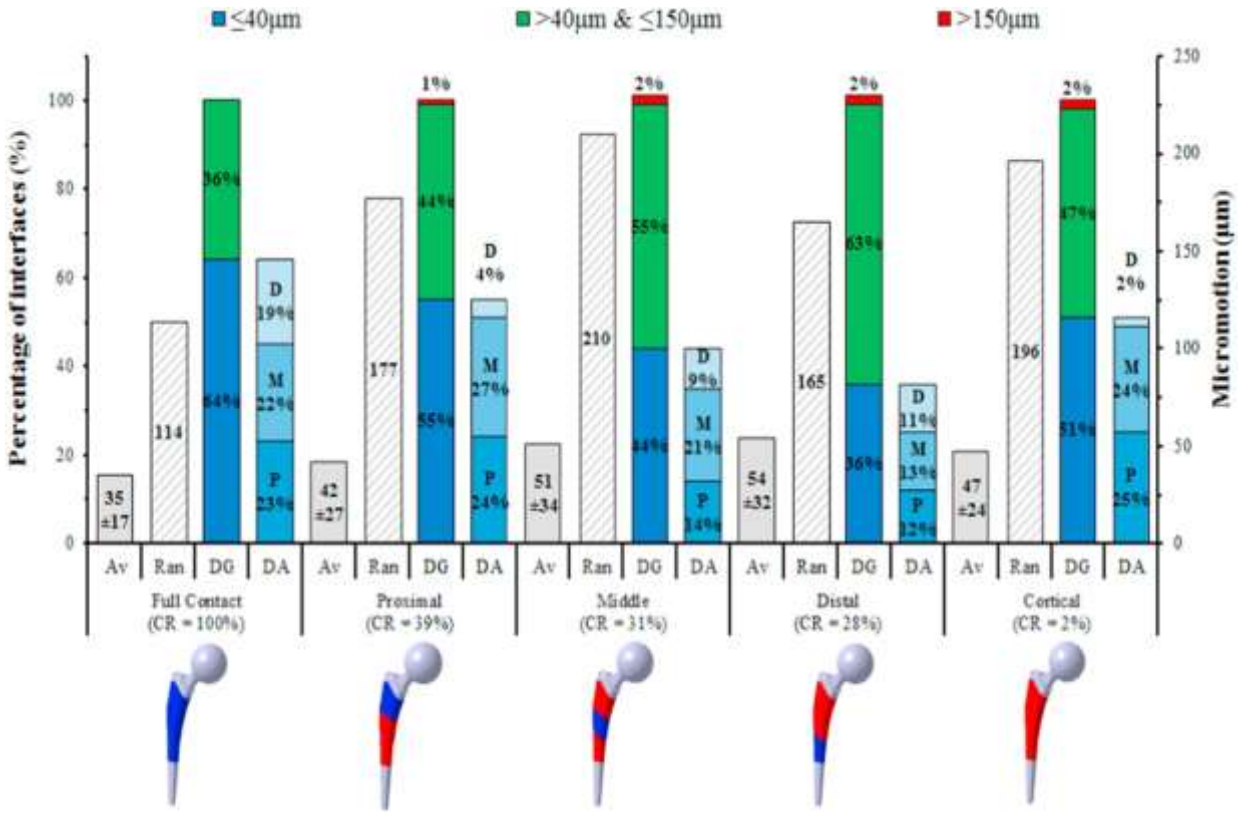

Figure. 5.1-Average value (Av) and standard deviation (±SD), range (Ran) of micromotion (µm), global distribution of interfaces (DG (%)) where the micromotion is: ≤40 µm in blue, >40 µm & ≤150 µm in green and >150 µm in red when full contact is achieved (all press-fit) and four configurations when one contact area is achieved (one press-fit) with a gap of 50 µm present on the three other interface areas and DA (%) the distribution per area (proximal (P), middle (M), distal (D)) in the bone growth expected (Reimeringer and Nuño, 2016)

The distal fixation design had micromotion mostly in the lateral region of the proximal side and around the anterior tip in the femoral stem. The proximal model, however, received micromotion distributed more about the medial section of the femoral stem. Table 5.1 shows that unfeasible regions for femoral bone ingrowth were larger in the proximal model by 2-6 times in comparison with the distal model. For the proximal fixation model, the femoral stem appeared to be more unstable during walking, with surface regions surpassing the threshold limit about two times when compared with surface regions at the time of stair-climbing. Nevertheless, as soon as interfacial bone loss was simulated, the proximal fixation model failed within both physiological forcing scenarios (Figure 5.2).

Table 5.1- Surface region higher than 50 μm of micromotion for the distal fixation model (8,976 mm^2) and the proximal fixation model (5,370 mm^2) (Abdul Kadir and Kamsah 2009)

Fixation type	Loadcase	First iteration		Second iteration	
		Area> 50μm(mm2)	%	Area> 50μm(mm2)	%
Proximal	Fisher's gait	2899	54	5105	95
	Duda's stair climbing	1257	23	4274	80
Distal	Fisher's gait	769	9	890	10
	Duda's stair climbing	999	11	1113	12

The distal fixation model was much more stable than the proximal fixation model by as much as six times, when applying a 50 μm threshold limit for femur bone ingrowth. This might be credited to the greater surface region in attachment with the cortical femoral bone for the distal model. Laine et al. (2000) have demonstrated that there was considerably higher cortical attachment in the diaphyseal region for the distal fixation model evident, and that subsidence of over 2 mm was a lot more common in the proximal fixation ABG, even though the stability was not affected. This has been done by comparing the straight femoral stem distal fixation Bi-Metric femoral stem with the distally over-reamed proximal fixation of ABG femoral stem. Both hip femoral stem models, nevertheless, were identified to be clinically successful during 5 years. There was a tight diaphyseal fixation that developed outstanding stability for the distal fixation model, but this resulted in stress to be transmitted in this area and consequently raised stress shielding within the proximal metaphyseal region in comparison to the proximal fixation ABG.

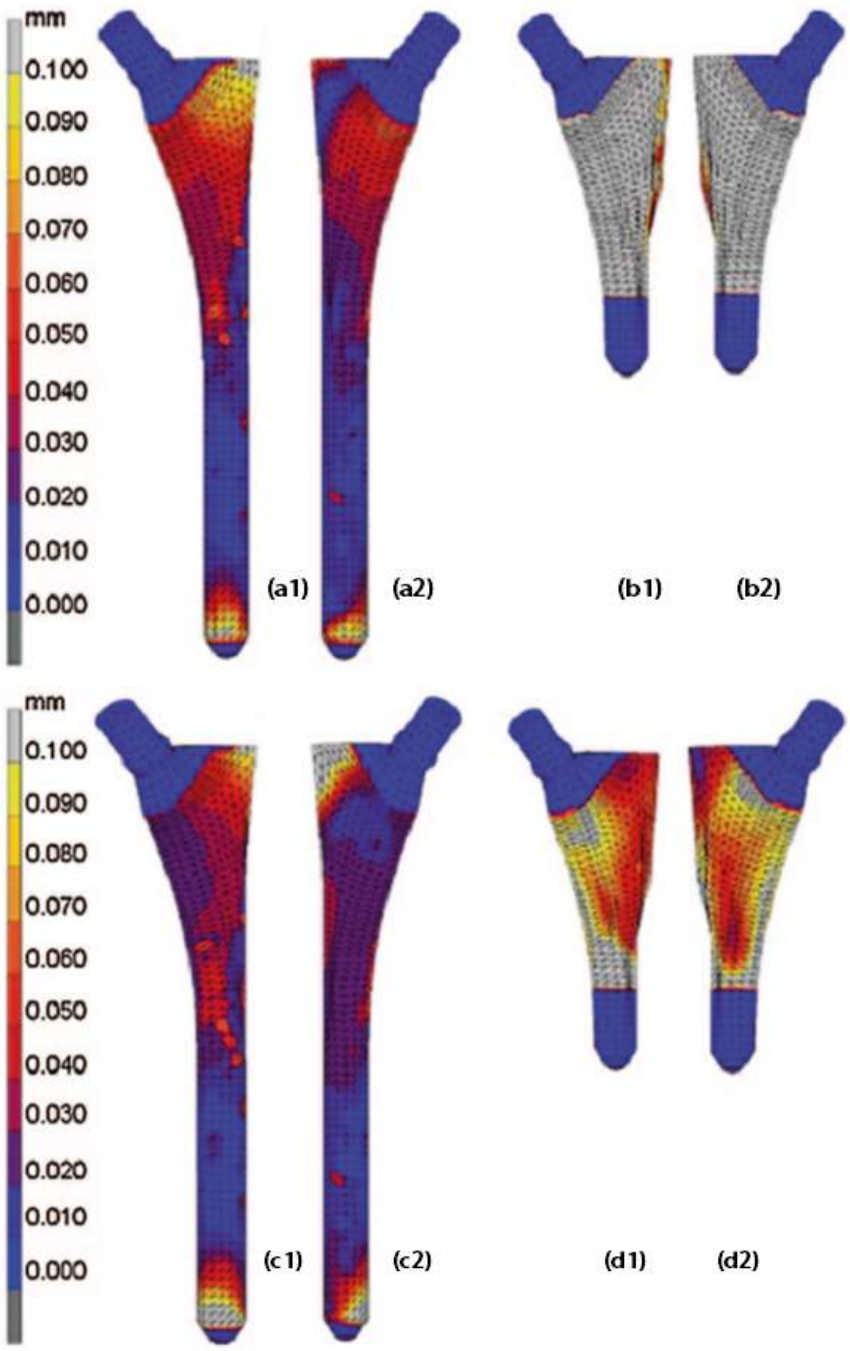

Figure. 5.2- Contour plots of micromotion for a distally fixed design (a, c) and a proximally fixed model (b, d) employing Fisher's gait cycle (a, b) and Duda's stair-climbing (c, d) following the final iteration. Posterior section on the left (a1, b1, c1, d1) and anterior section on the right (a2, b2, c2, d2) - modified picture (Abdul Kadir and Kamsah 2009)

Regarding the stability of the proximal model in stair-climbing, this has additionally been verified by others, as stated in the last section. Hips femoral stems with a lateral flare element in its model, has been verified to produce extra initial stability, specially the rotational stability in comparison to a femoral stem without lateral flare (Effenberger et al., 2001). Iguchi et al. (2013) have also verified that a lateral flare has been beneficial to a cementless femoral stem

model and that the femoral stems could possibly be made shorter than models with no lateral flare. Within their finite element review, migration was identified to be reduced for the lateral flare when compared to a simple straight femoral stem design. A follow-up study of the lateral flare element from the same authors also demonstrated that trabecular femur bone connected to the lateral flare covered with HA. Leali et al. (2002) have suggested that cementless femoral stems with a lateral flare supplied primary stability and generated a small subsidence, an average of 0.32 mm over 2 years.

Gortz et al. (2002) have carried out a practical study exploring the rotational stability of the two fixation models. Two proximally fixed femoral stems, the CLS model and the ABG design, were observed to display higher rotational micromotion distally compared to proximally. The distally fixed Alloclassic model, nevertheless, was noted to generate higher rotational micromotion at the proximal than at the distal end. The rotational micromotion inside the proximal region was greater for the Alloclassic model by about two times in comparison to the CLS model and nearly three times in comparison to the ABG. More effective rotational stability for the two proximal fixation models could possibly be as a result of macro-features around the anterior and posterior edges of both hip femoral stems. The CLS model possessed the tapered fins macrofeature while the ABG model possessed the semi-circular indentations macrofeature.

Possible reduction of stress shielding in the case of proximal fixation of the stem is detected by Levadnyi et al. (2017). In the case of diaphyseal fixation (A, AB, ABC), the stress–strain state of the stem was determined by combining the bending moment acting in the frontal plane and compression forces acting in the axial direction. Calculation results show that diaphyseal–metaphyseal (ABCD) and metaphyseal–diaphyseal (ABCDE) fixations of the hip joint stem endoprosthesis are most appropriate. The metaphyseal–diaphyseal (BCDE) and metaphyseal (CDE) types of endoprosthesis fixation give similar values of stress in the implant when compared to the full fixation (ABCDE) (Figure 5.3).

The maximum micromotion under loads during gait cycle depending on the fixation of the stem are shown in Figure 5.4. The maximum values of micromotion were calculated in each finite element n in terms of micro-displacement.

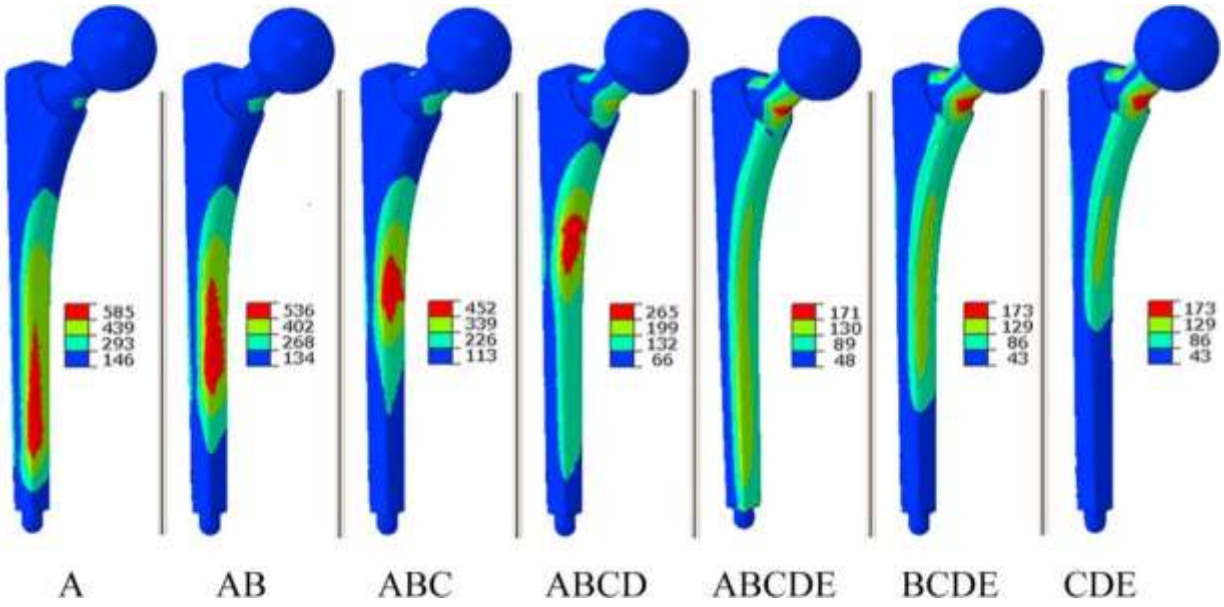

Figure. 5.3- Distribution of von Mises stresses on the medial side of the tapered stem, depending on the type of fixation. Applied loading conditions correspond to the peak hip contact forces during normal walking (Levadnyi et al. 2017)

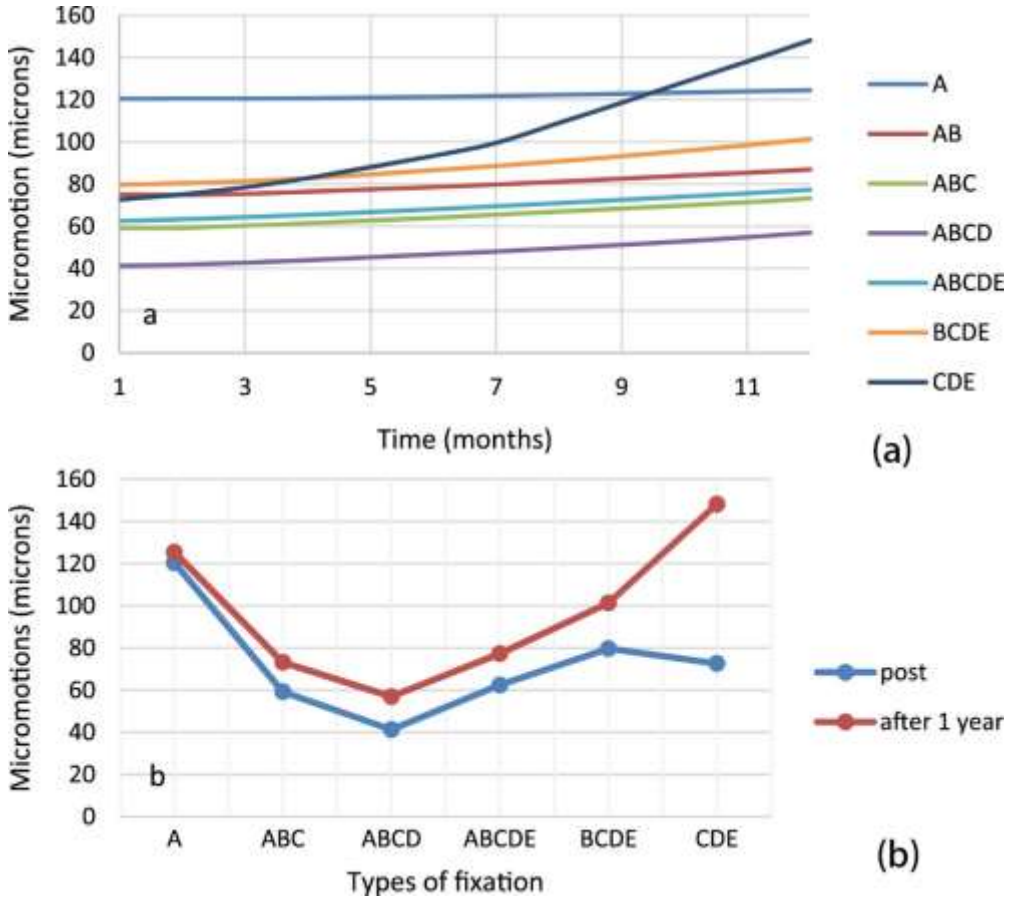

Figure. 5.4- a) Changes in the maximum micromotion of the implant surface during 1 year for different variants of implant fixation. b) Comparison between the maximum micromotion of the implant surface in the post-operative period and 1 year after the implantation (Levadnyi et al. 2017)

A further in vitro experiment investigated four unique cementless femoral stems (Sadoghi et al., 2013). One of the examined femoral stems was the CLS model and a second one was the Zweymuller that includes a tapered model similar to the distally mounted Alloclassic model. The other designs were the Muller 85 and also the anatomical PCA. They identified that the CLS model had the greatest mean interface micromotion under a force simulating single leg stance up to about 10 times higher motion compared to the most stable femoral stem (the anatomical PCA). It has been suggested the migration of the proximally replaced CLS femoral stems. The mean hip joint femoral stem migration was 2 mm during 2 years and 3.66 mm during 7 years. Even though these studies demonstrated higher migration and micromotion in a proximally fixed model, follow-up reports of the ABG model and the CLS model by Rogers et al. (2003) and Schreiner et al. (2001) have confirmed that these implants were successful.

The final results from finite element evaluation demonstrated that the proximal fixation model, even though it shows relatively less stability compared to the distally fixed model, overall represents better potential. As highlighted in the earlier section, the benefit of using a short-stemmed implant is its long-term compatibility. In case a revision is needed, much less difficulty will be experienced with a short stem implant since the cortical femoral bone will be available distally for fixation. Nevertheless, the outcomes from the earlier section demonstrated that full proximal force transmitted by using a very short femoral stem induced great interface micromotion and consequently instability. In this section, the micromotion of short-stemmed implants was decreased by using a proximal enlargement in the antero-posterior and also medio-lateral direction. The femoral stem was unsuccessful under both physiological loadings once femur bone loss was simulated since the majority of the excessive micromotion was distributed on the medial region, so stability was compromised due to the fact that the connection in the medial region was lost. The relative loss of stability within the proximal fixation model in this section could be considerably improved more by using an anatomic model and adding macro-features in the proximal part.

Chapter 6

Dynamic Loadings and Long-term Stability Analysis

One of the restrictions of micromotion analysis that was presented in chapter 4, was the inability to divide the final results of micromotion data, into axial and rotational components. Therefore it would have been inappropriate to eventually conclude the best femoral stem, without considering the sustaining torsional loadings. Another limitation is that the micromotion analysis would not reflect the stress distribution on the hip prosthesis and consequently would ignore the potential high stress concentration that is associated with post operative pain as well as low durability and long-term stability. For these reasons, a separate stress analysis was carried out to examine the von Mises stress, shear stress and principal stress distribution of cementless hip implants, under dynamic loadings of nine different activities.

Total hip replacement implants are fixed to the femur in two ways, namely cemented or cementless. The latter method was more commonly used until a few years ago, the implant is fixed to the bone with PMMA bone cement (polymethyl methacrylate). However due to the issues in using the cemented hip prosthesis, the preferred method is now cementless (National Joint Registry, 2015). The cemented hip replacement has decreased considerably from 54% in 2004 to 32% in 2014. While during the same period cementless procedure has increased from almost 21% to 42%. The main disadvantage in using the cement substance is that the exothermic heat resulting during the processing chemical reaction can potentially harm the bone tissues. However, in the cementless design the parts are press fitted in the prepared bone, where the bone is expected to grow in crevices of the implant. This type of hip replacement is expected to last longer and eliminates pain.

In this section a cementless hip prosthesis design was used to investigate the stress distribution on the implant and femur assembly under nine different loading conditions using Ansys software, as a finite element analysis (FEA) package, which simulates the frequent activities of daily living.

6.1. Loading and boundary conditions

Many researchers including Bergmann et al. (2001), Heller et al. (2001), Lengsfeld et al. (2000), Costigan et al. (2002), Stansfield and Nicol (2002) have presented and employed different loading conditions on the hip prosthesis. They have used experimentally measured forces during gait and stair climbing in extensive musculoskeletal studies. Bergmann et al. (2001) have presented a brief calculation of the mechanical loadings and the function of hip and proximal femur. Their results indicate that the average person loaded their hip with a maximum of 238% BW (percent of body weight) when walking at about 4 km/h and with slightly less when standing on one leg. When climbing upstairs the joint contact force recorded 251% BW which is less than the 260% BW when going downstairs. Inward torsion of the implant is probably critical for the stem fixation. On average it was 23% larger when going upstairs than during normal level walking. The inter- and intra-individual variations during stair climbing were large and the highest torque values are 83% larger than during normal walking.

A typical coordinate system for measured hip contact forces is shown in Figure 6.1. The hip contact force vector $-F$ and its components $-F_x$, $-F_y$, $-F_z$ acts from the pelvis to the implant head and is measured in the femur coordinate system x, y, z. The magnitude of contact force is denoted as F. The axis z is taken as parallel to the idealized midline of the femur; x is parallel to the dorsal contour of the femoral condyles in the transverse plane. The contact force causes a moment M with the components M_x, $M_{y'}$ and $M_z = -M_t$ at the point NS of the implant. A positive torsional moment M_t rotates the implant head inwards. M is calculated in the implant system x, y', z'. Both systems deviate by the angle S. AV is the anteversion angle of the implant (Bergmann et al., 2001). One of the major factors to be considered is the loading condition. Some type of loads may have a more significant effect on the design. Biegler et al. (1995) have developed a brief FE analysis and calculation of two designs of hip prostheses in one-legged stance and stair climbing configurations. They showed that the torsional loads during stair climbing contribute to larger amounts of implant micro motion than stance loading does.

The relative motion between the bone-prosthesis interfaces is more dependent on load type than on implant geometry or surface coating type. In addition, the resultant force of each activity is applied at a specific angle with respect to XY and XZ plane, as considered in Figure 6.2. There are various loading conditions tested on different patients. These real life activities

are shown in different diagrams that include slow, normal and fast walking, upstairs, down stairs, standing up, sitting down, standing on 2-1-2 legs and also knee bending condition (Figure 6.3). Similar diagrams are introduced for moment M. Sets of all data are presented in appendix B.

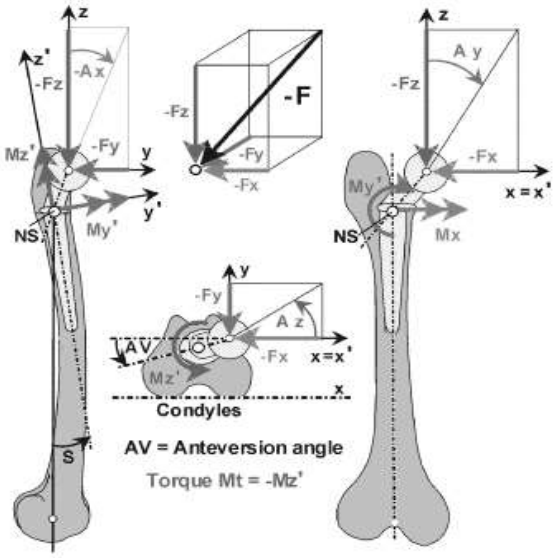

Figure 6.1- Coordinate System at Left Femur (Bergmann et al., 2001)

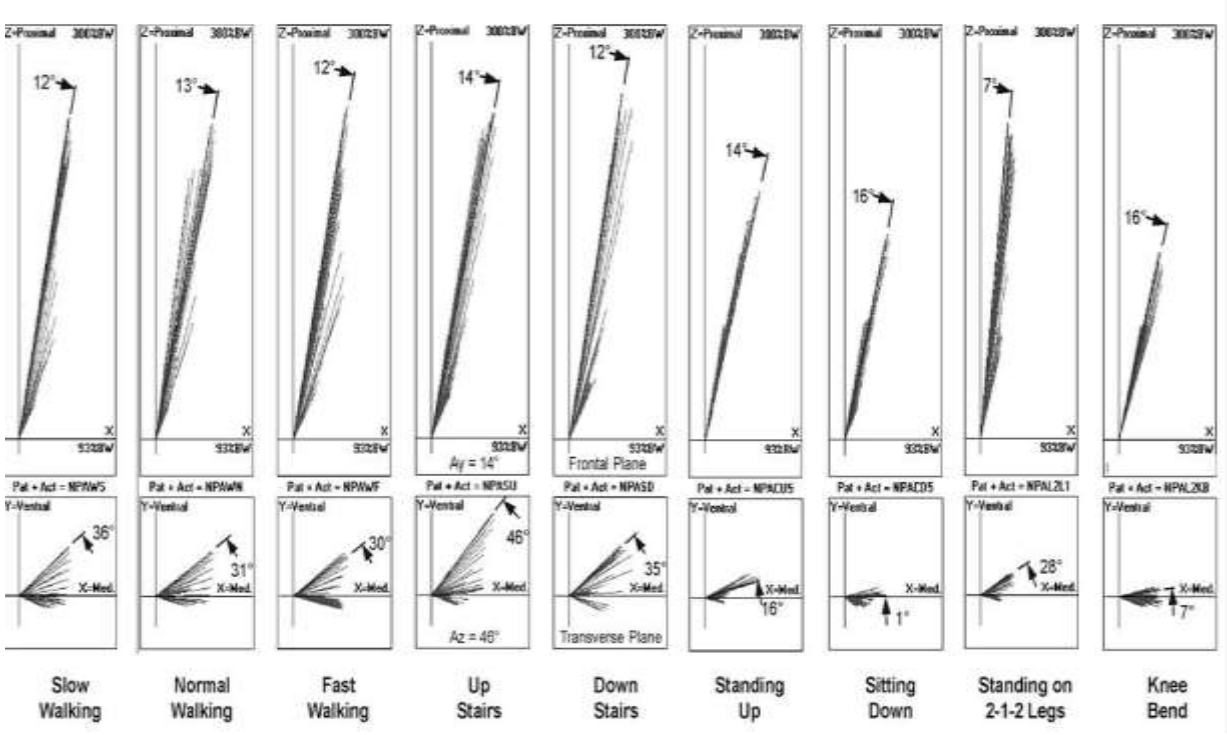

Figure 6.2- Upper diagrams: Force vector F and direction A of F in the frontal plane. Lower diagrams: Force vector F and direction A of F in the transverse plane. y_z (Bergmann et al., 2001)

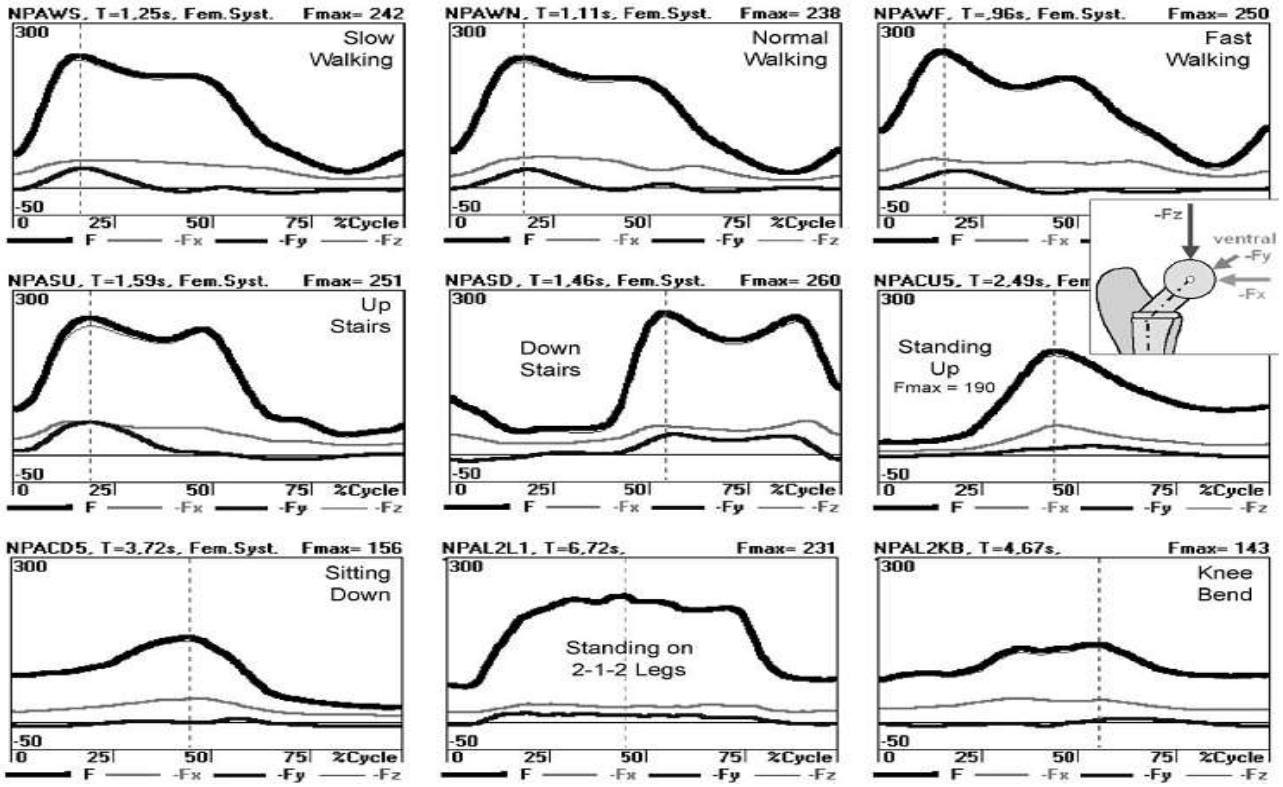

Figure 6.3- Contact force F of a typical patient from averaged data during nine activities. Contact force F and its components $-F_x$, $-F_y$, $-F_z$. F and $-F_z$ are nearly identical. The scale range is 50–300% BW (body weight). Cycle duration and peak force $F_p = F_{max}$ is indicated in diagrams (Bergmann et al., 2001)

Apart from the resultant force applied on the prosthesis, there are few muscles attached to femur that induce extra tension on bone. As shown in Figure 6.4, at 85% of the gait cycle, a simplified set of active muscles are the abductor muscles, located on the greater trochanter (Gluteus medius and Gluteus minimus), and the ilio-tibial band (Gluteus maximus and tensor fascia latae) (El'Sheikh et al., 2003).

Furthermore Sowmianarayanan (2006) has worked on finite element analysis of proximal femur nail, and assumed the distal end of the femur model to be fully fixed. According to Simoes et al. (2000) the various loads including body weight and different muscles at the proximal femur were considered for this analysis. The applied loads consist of joint reaction force, abductor force, Iliopsoas force and vastas lateral and are close to data from El'Sheikh et al. (2003). In this study the relative forces and their location are shown in Table 6.1 and Figure 6.5.

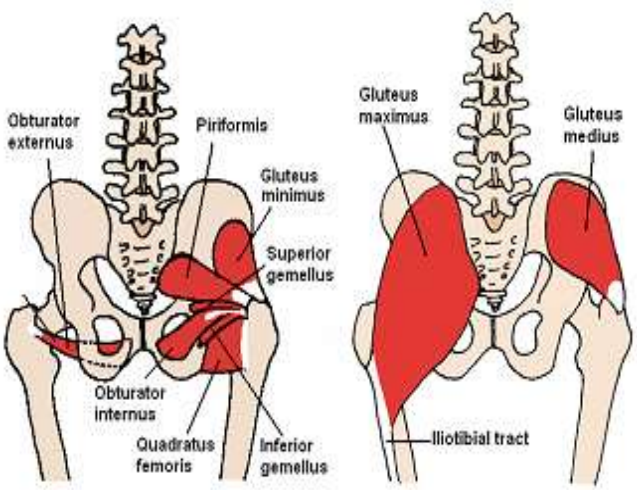

Figure 6.4- The involved muscles with femur: Gluteus medius & Gluteus minimus, ilio-tibial band (Gluteus maximus & tensor fascia latae) (El'Sheikh et al., 2003)

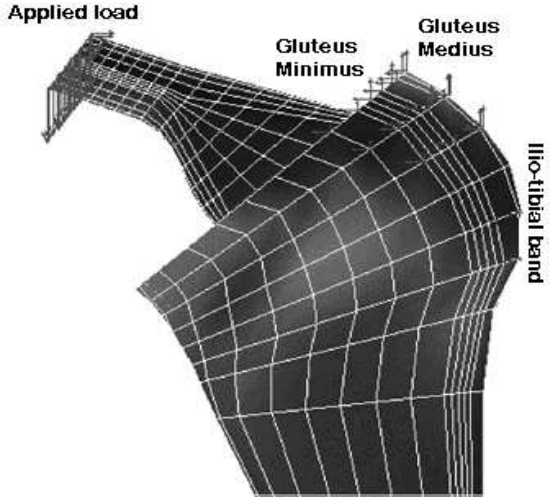

Figure 6.5- Position of applied forces (El'Sheikh et al., 2003)

Table 6.1- Muscles-forces applied on the femur (El'Sheikh et al., 2003)

		Muscles		
		Gluteus Medius	**Gluteus Minimus**	**Ilio-tibial band**
Average Force (N)	F_x	-259	-279	-59
	F_y	160	269	-74
	F_z	319	134	-58

6.2 Numerical methods and analysis

In this study a series of 3D CAD models were produced in SolidWorks using a hip prosthesis manufactured by Johnson & Johnson. The resultant model was fitted into a 3D model of a femoral bone that is similar in shape and size to the standard femur. The 3D model of femur bone was created by 3D laser scanning by Redding Industries, Inc.

The SolidWorks models of the prosthesis and femur assembly were subsequently imported to Ansys for finite element analysis under 9 frequent activities of daily life including: slow walking, normal walking, fast walking, upstairs, down stairs, standing up, sitting down, and standing on 2-1-2 legs and knee bending. The relevant materials were assigned to different parts of the 3D model and then the whole assembly was meshed to achieve an overall 30341 nodes and 16095 elements. At each stage of the modelling process, different boundary conditions were applied for each of 9 activities during various periods of action. This included all the relevant forces and moments.

The hip endoprosthesis examined was a cementless implant from J&J Company which consists of a femoral component and an acetabular component. The material assigned to the femoral stem was titanium. The material for acetabular cup and femoral head was Co-Cr and the plastic liner was ultra-high-molecular-weight polyethylene (UHMWPE). The femur bone has been assumed to be isotropic and linearly elastic. The relevant material properties have been taken from the findings of Bougherara et al. (2010), since the practical and theoretical results were found to be similar. Hence the bone properties assumed in this study include cortical ($E = 10$ GPa, $\upsilon = 0.3$) and cancellous ($E = 206$ MPa, $\upsilon = 0.3$).

6.3 Discussion

In this study three different stress distribution data including von Mises stress, maximum principal stress and shear stress have been assessed. It should be noted that each of these nine activities was performed during different time intervals and ultimately the peak stress during each activity was evaluated to compare the performance of the prosthesis.

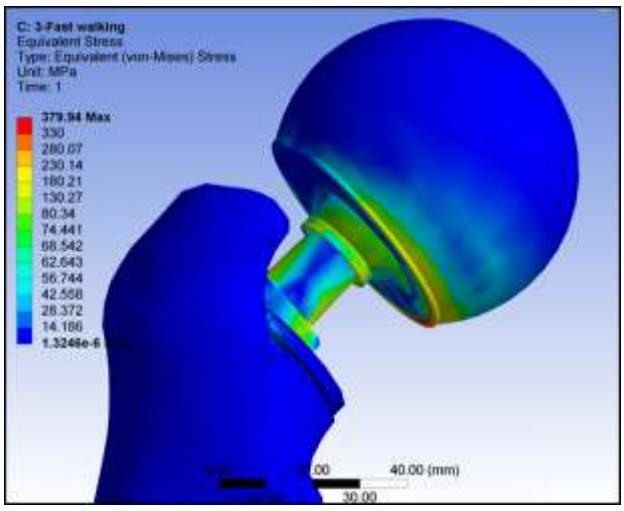

Figure 6.6- von Mises stress distribution of prosthesis- femur assembly during fast walking at the time of peak load, showing the critical stresses around the femoral neck and sharp edges of acetabular cup.

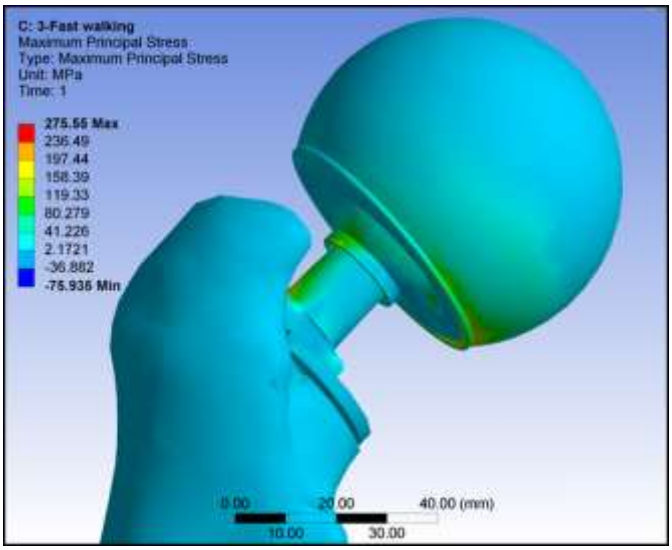

Figure 6.7- Principal stress distribution of prosthesis- femur assembly during fast walking at the time of peak load, showing high tensile stresses on the upper side of the femoral neck

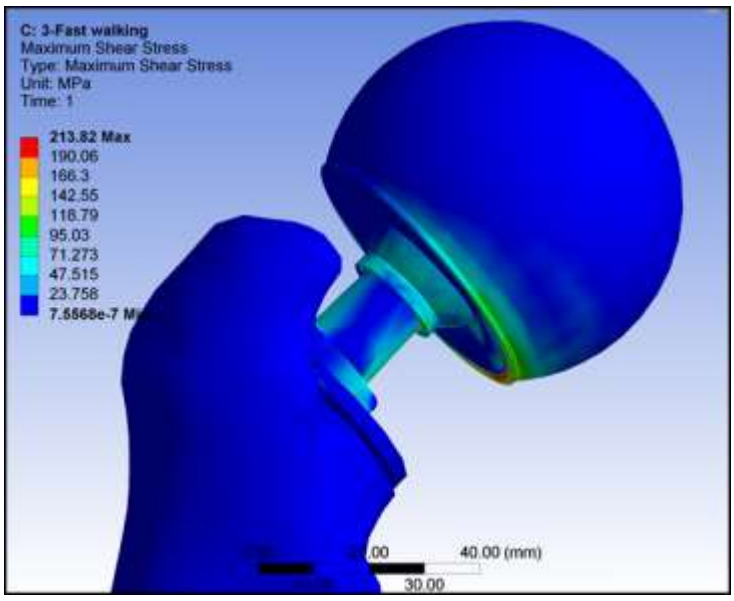

Figure 6.8- Shear stress distribution of prosthesis- femur assembly during fast walking at the time of peak load, showing stress concentration on the femoral cup and the edges of acetabular cup

The results for fast walking indicate that von Mises stresses at the peak load shows the critical areas around the femoral neck and sharp edges of acetabular cup (Figure 6.6). Whilst the maximum principal stress distribution displays high tensile stresses on the upper side and lower side of the femoral neck respectively. This is because the loads applied on the acetabular cup are eccentric and follows the angles given in Figure 6.2. At the same time the shear stress distribution indicates the critical areas on the femoral cup (Figure 6.8).

The maximum von Mises stress during slow, normal and fast walking were calculated as 342MPa, 352 MPa and 380MPa respectively. This shows throughout walking activity, stress increases gradually as speed of action rises. It indicates that going "upstairs" imposes more stress of about 23MPa on the joint than going "down stairs". This is similar to the situation with "standing up" and "sitting down". Although the last two actions apply considerably lower stress on the hip joint that going up or down stairs. The highest pressure would be in the "standing on 2-1-2 legs" activity by nearly 400MP in contrast with "bending knee" that enforces the lowest and only half of that stress on the joint at 200MPa (Figure 6.14). Maximum principal and shear stresses show lower values but follow almost the same curves (Figures 6.12 and 6.13). Also force patterns shows that the component F_y which causes much of the implant torque, is larger when going upstairs than all walking activities.

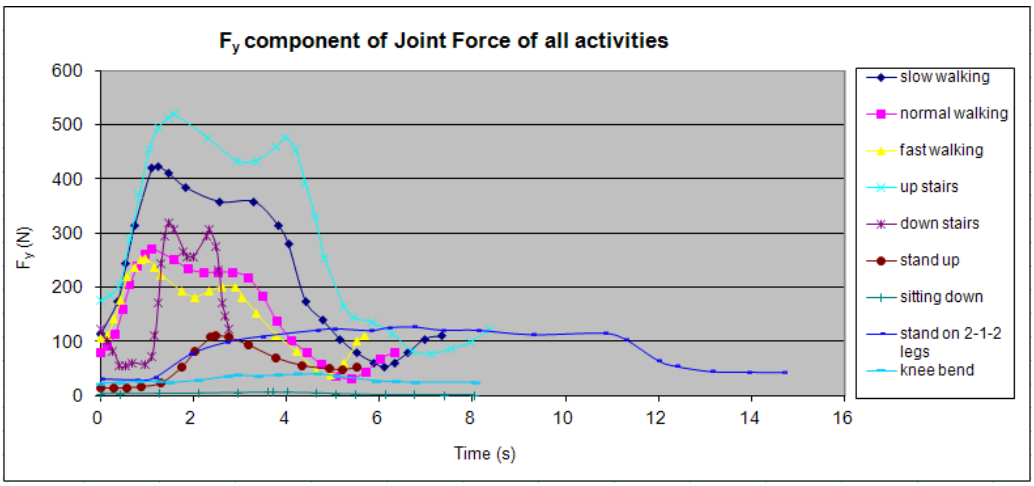

Figure 6.9- F_y component of joint force of all activities

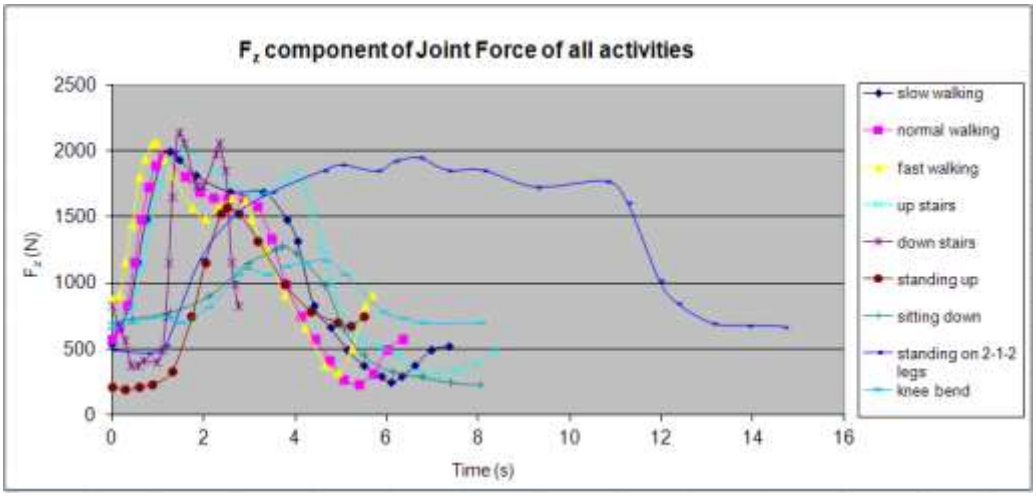

Figure 6.10- F_z component of joint force of all activities

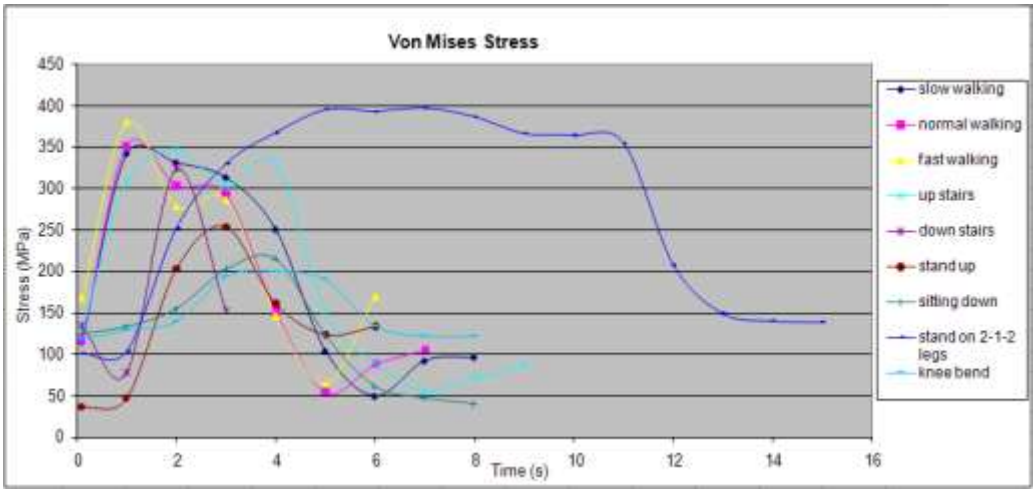

Figure 6.11- von Mises stress of nine activities during different time intervals

Down stairs the peak force F_z slightly exceeds that from going upstairs. Standing up from a chair loads the hip more than sitting down but much less than walking. The rotating component F_y is very small when sitting down (Figures 6.9 and 6.10). Bergmann et al. (1993) have also calculated the higher body weight percentage of about 409% of a patient with disrupted pattern which supports the opinion that dysfunction of one muscle increases the joint contact force, because a part of the required joint moment is taken over by other muscles with unfavourably short lever arms and therefore higher forces.

Although proper inter-study comparison is difficult because of the variety of implant materials, implant geometries, and conditions used in the literature, resulting in a broad range of stress levels achieved on implant surfaces, there are other studies presented on stress distribution of hip prosthesis. For example Mathias et al. (1998) have calculated the stress levels in the femoral component of a total hip prostheses. In that study they used a static point load of 2.5 KN that is applied vertically through the centre of the head of the femoral component. This load is approximately three times body weight, which is of the order of the load applied to the prosthesis in the living body. This study showed the status of a hip prosthesis under nine different loading conditions which can be effective to predict critical areas and important times of those activities so that we can optimise a design accordingly.

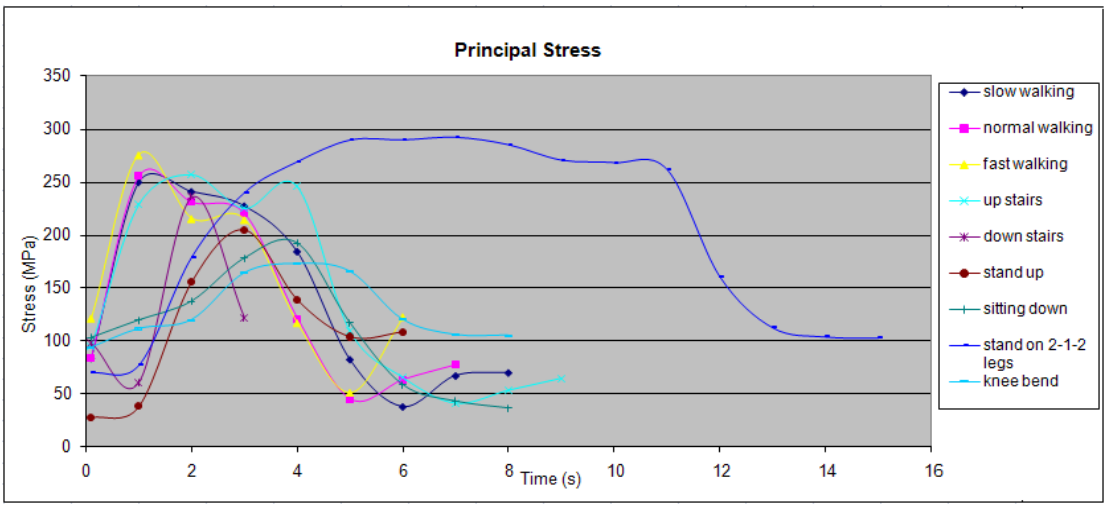

Figure 6.12- Principal stress of nine activities during different time intervals

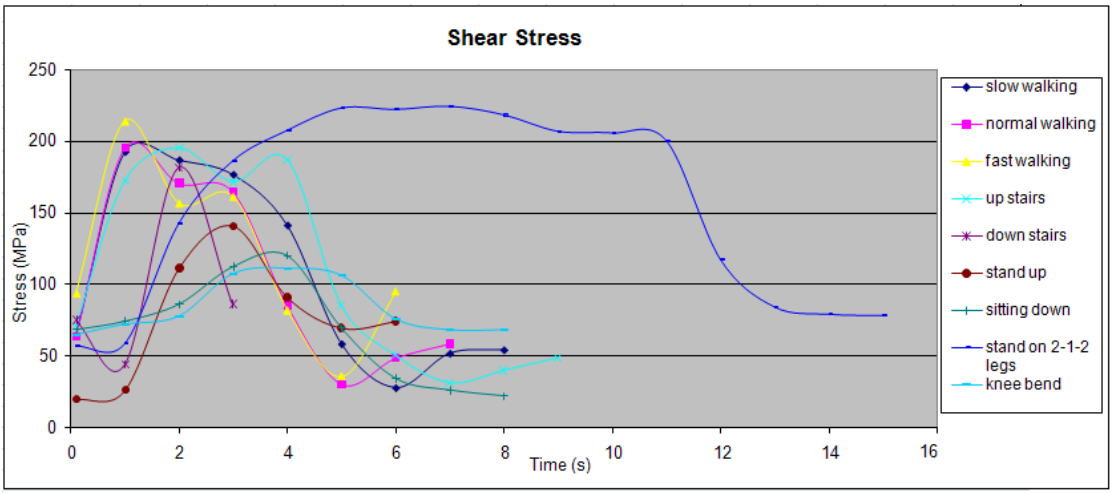

Figure 6.13- Shear stress of nine activities during different time intervals

The purpose of this chapter was to investigate the biomechanical influence of different load types on the stress distribution through a hip implant. The critical areas were shown and discussed. The influence of speed and contribution of torsional load in different activities of daily living was explained. These loading conditions had more influence than implant geometry or surface coating type. In this study the FEA was chosen, since it is a greatly validated technique (Herrera et al., 2007). The research data can be related to the application of Frost's law in bone remodelling in order to predict the bone growth in different areas.

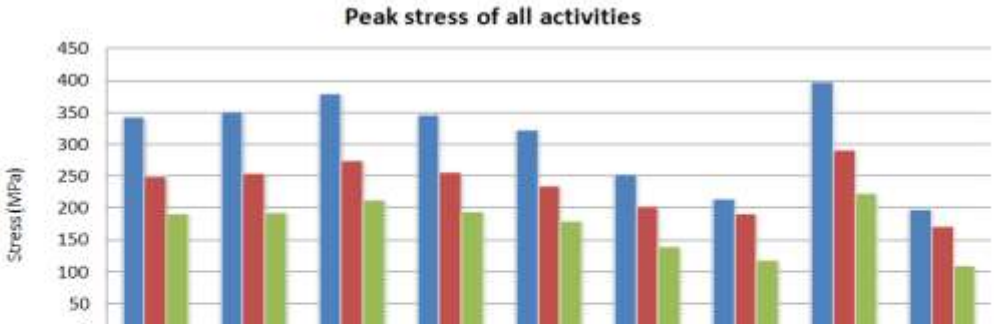

	Slow walking	Normal walking	Fast walking	Up stairs	Down stairs	Standing up	Sitting down	Standing on 2-1-2 legs	Knee bending
Max.Von Mises	342.45	351.93	379.94	345.95	323.48	253.67	215.97	398.05	199.97
Max.Principal	249.83	255.49	275.55	256.3	235.6	204.73	192.56	292.44	172.78
Max.Shear	192.48	195.01	213.82	195.36	181.42	140.99	119.95	224.05	111.44

Figure 6.14- Comparative study of peak stress of all activities

The stress distribution of a complete assembly of femur and hip prosthesis was investigated with realistic boundary conditions under nine routine activities using finite element analysis. In each activity, different forces of varying magnitude and orientation were applied on the prosthesis over a period of time to examine the critical points developed in the entire 3D model. This includes a full description of the geometry, material properties, all boundary conditions, forces and moments. The activities comprised slow walking, normal walking, fast walking, upstairs, down stairs, standing up, sitting down, and standing on 2-1-2 legs and knee bending. The simulation can help to develop a more optimized hip prosthesis by altering the design to achieve more balanced stresses.

Chapter 7

Optimal Design

This chapter presents the primary design concepts that led to the final optimal design. The hip implants were redesigned by focusing on the main areas of stress concentration. The identical load was applied to the femoral head vertically downwards and the support was applied to the lower end of the stem. These boundary conditions were recreated for each redesigned model. Also a technique that was used to choose the best potential design for further optimisation to get the final optimal design was described and discussed. Subsequently at the end of the chapter the optimal design was demonstrated and the features and details of it were explained.

The models that will be shown are the initial hip implant designs that were created in SolidWorks and simulated in Ansys. The optimal design is presented at the end of the chapter. For the first design maximum stress appears around the screws. Upper and lower parts of the neck are not stable enough and can cause a considerable stress. Empty space around the screws could be a disadvantage. In second design maximum stress appears around the screws. Upper and lower parts of design are not stable enough and can cause a considerable stress. However compare to design 1, the fixed holes of lower part, improved the stability. Empty spaces around the screws could be a disadvantage. In third design maximum stress appears around the screws. Upper and lower parts of design are not stable enough and can cause a considerable stress. Adding extra screws does not seem to reduce the stress. Like design 2, the groove in the lower part could be a disadvantage. For the fourth design maximum stress appears around a hole. However it is considerably smaller than in design 1, 2 and 3. Upper and lower parts of the design are fixed well together than previous designs. Removing the groove in the design has eliminated the disadvantage of empty spaces. In design 5, Maximum stress appears around the hole as shown. However it is considerably smaller than in previous designs. Upper and lower parts of the design are fixed together better and compare to design 1, 2, 3 and 4 the stress values reduced noticeably. Removing the groove in the design has eliminated the disadvantage of empty spaces. In the last design maximum stress appears around the neck and femoral head.

However it is considerably smaller than in other designs. Upper and lower parts of design are fixed together better. Removing the groove and screws in the design has eliminated the disadvantage of empty spaces and high stress concentrations. Figure 7.1 to Figure 7.20 show different design concepts, which will be discussed and optimised later.

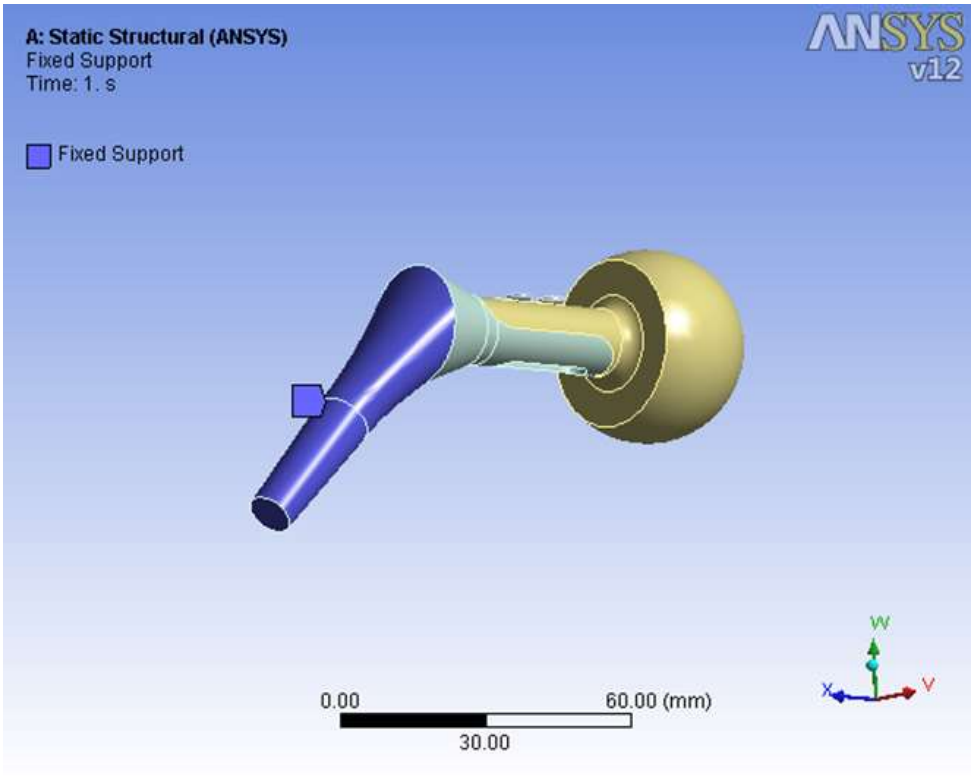

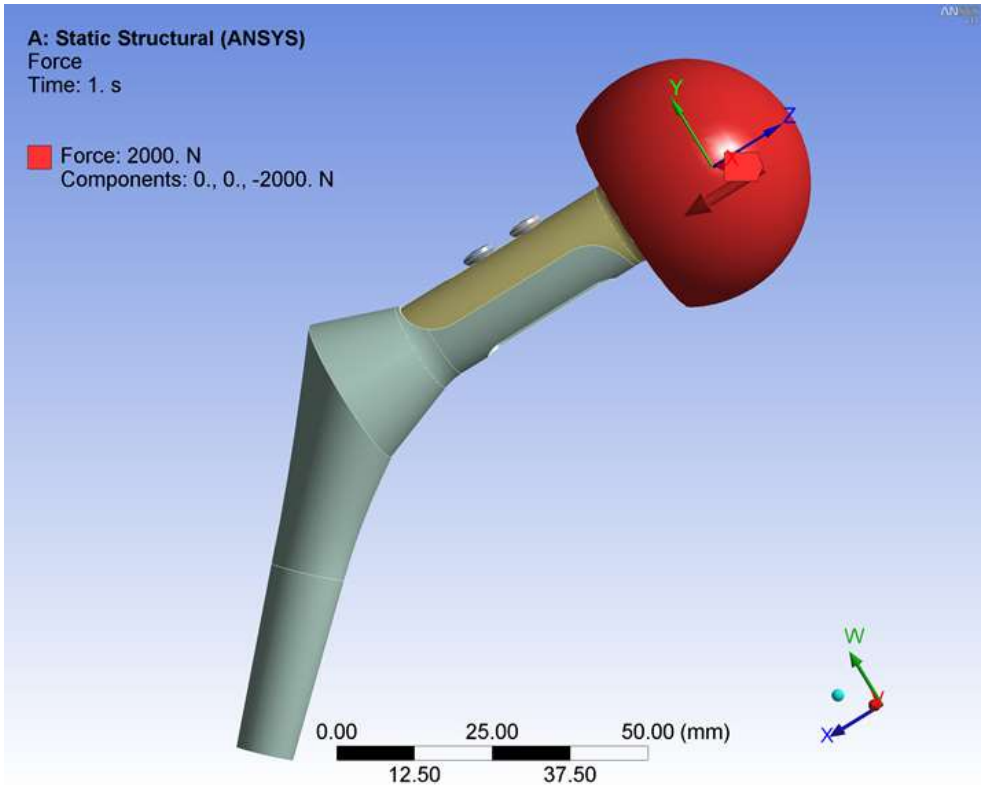

Figure 7.1- Boundary condition of design concept 1

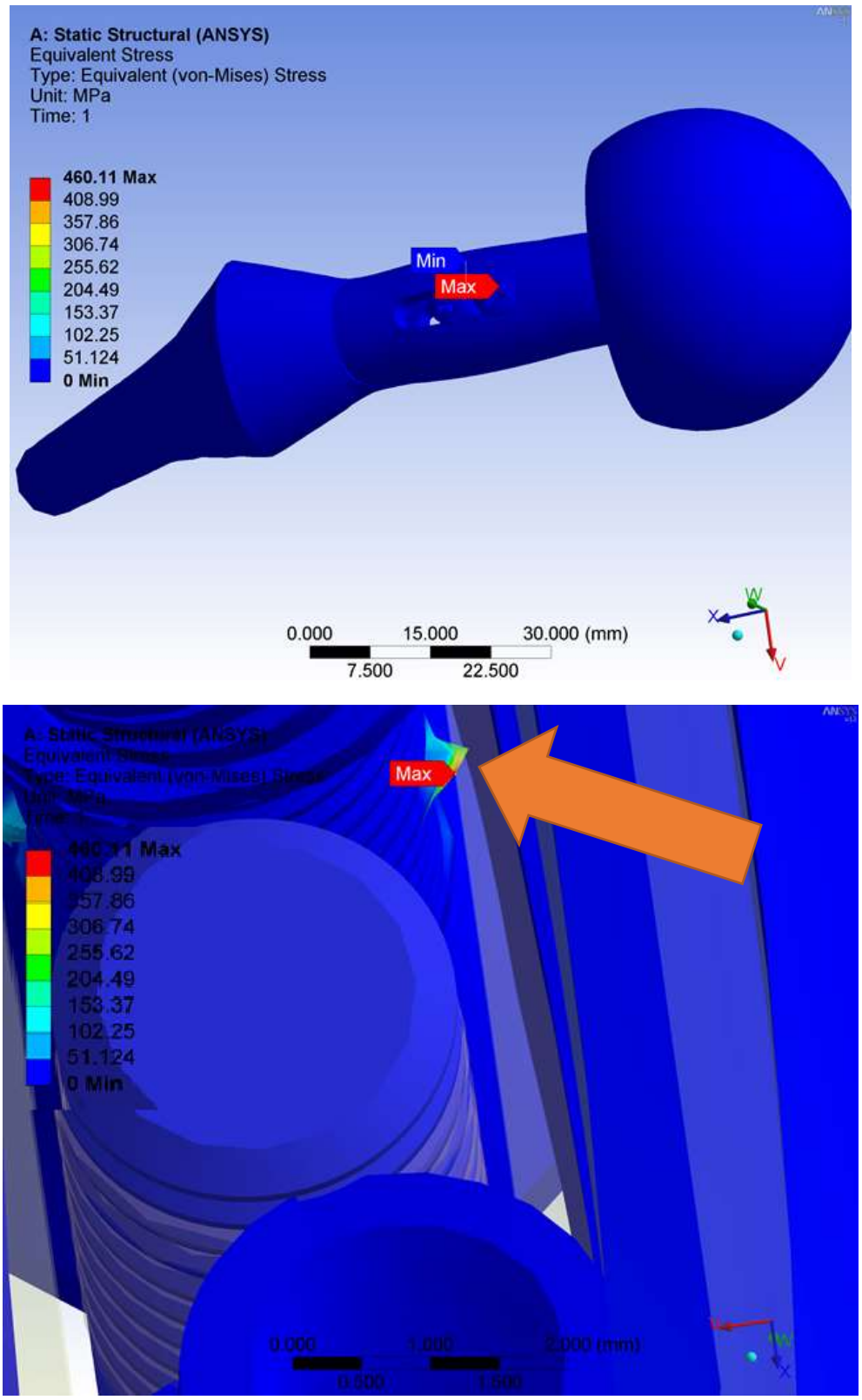

Figure 7.2- Stress distribution of design concept 1

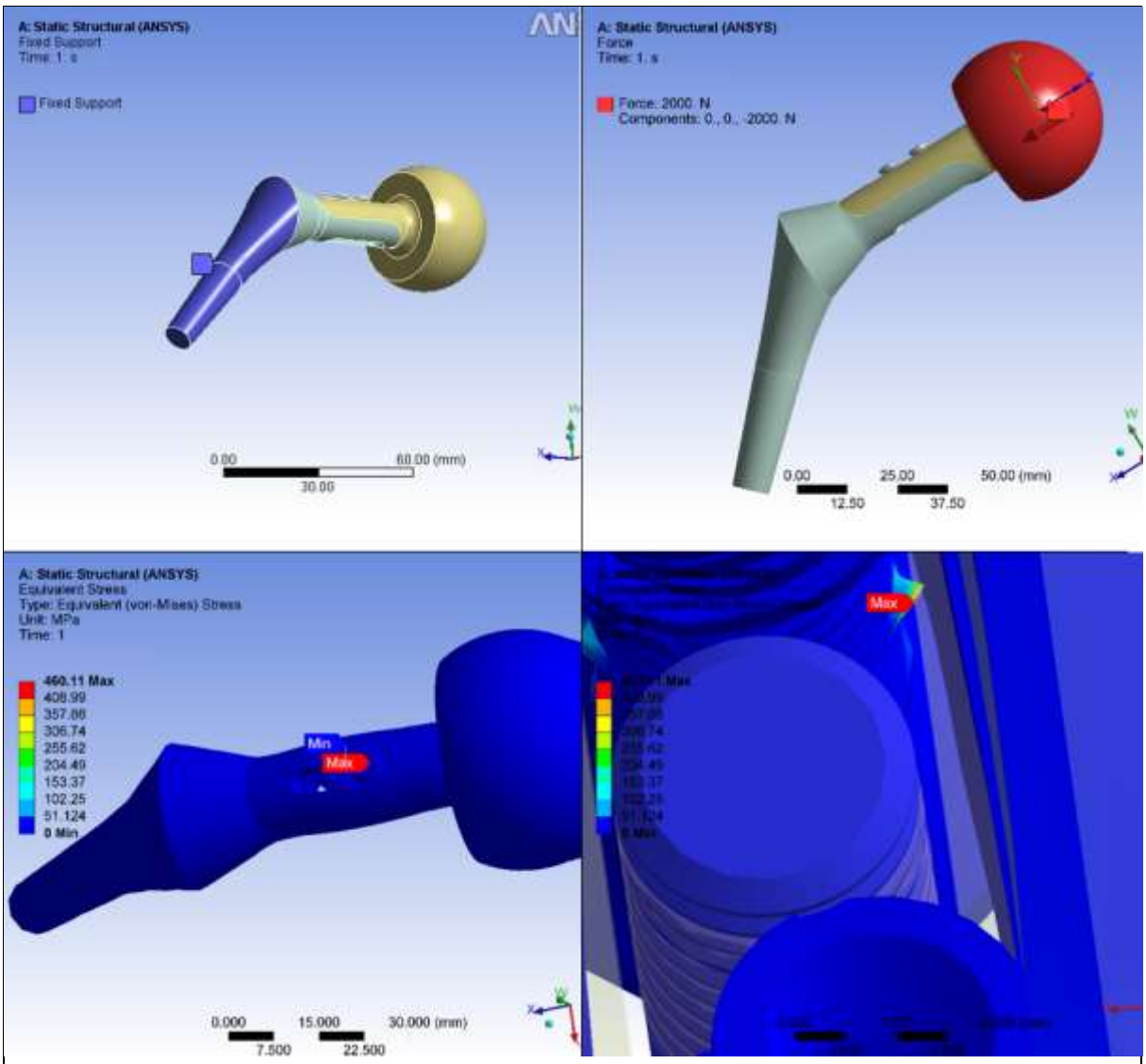

Figure 7.3- Boundary condition and stress distribution of design concept 1

Design 1

Maximum von-Mises Stress: 460.11 MPa

Comment:

Max stress appears around the screws. Upper and lower parts of the neck are not stable enough and can cause a considerable stress. Empty space around the screws could be a disadvantage.

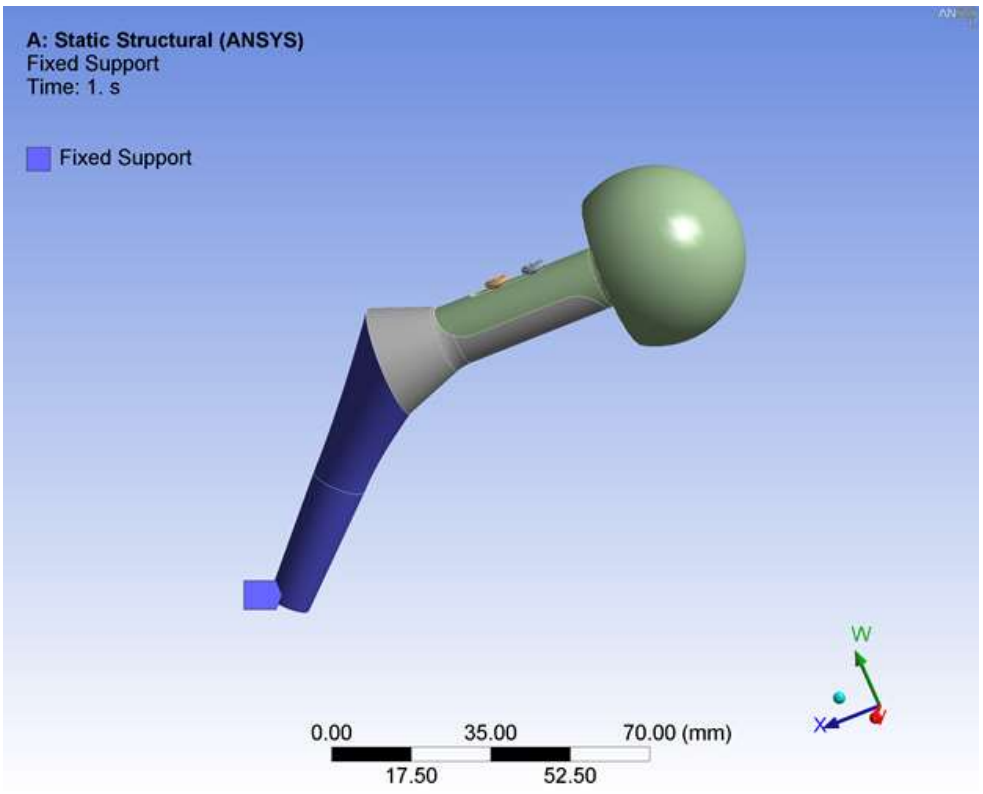

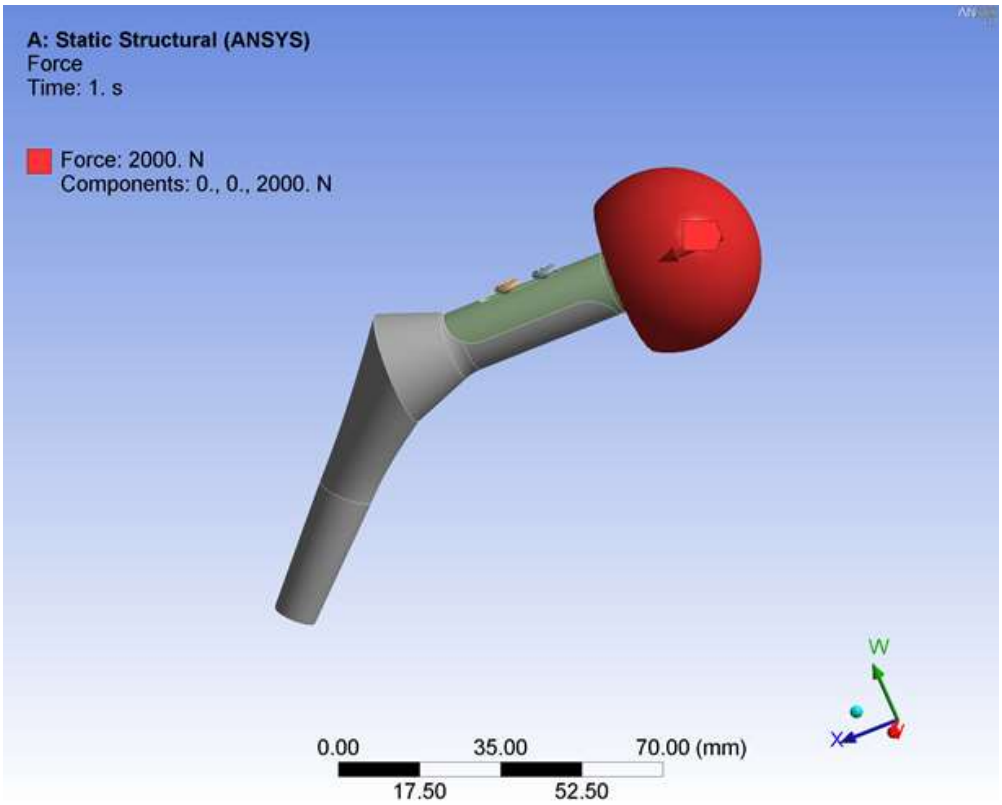

Figure 7.4- Boundary condition of design concept 2

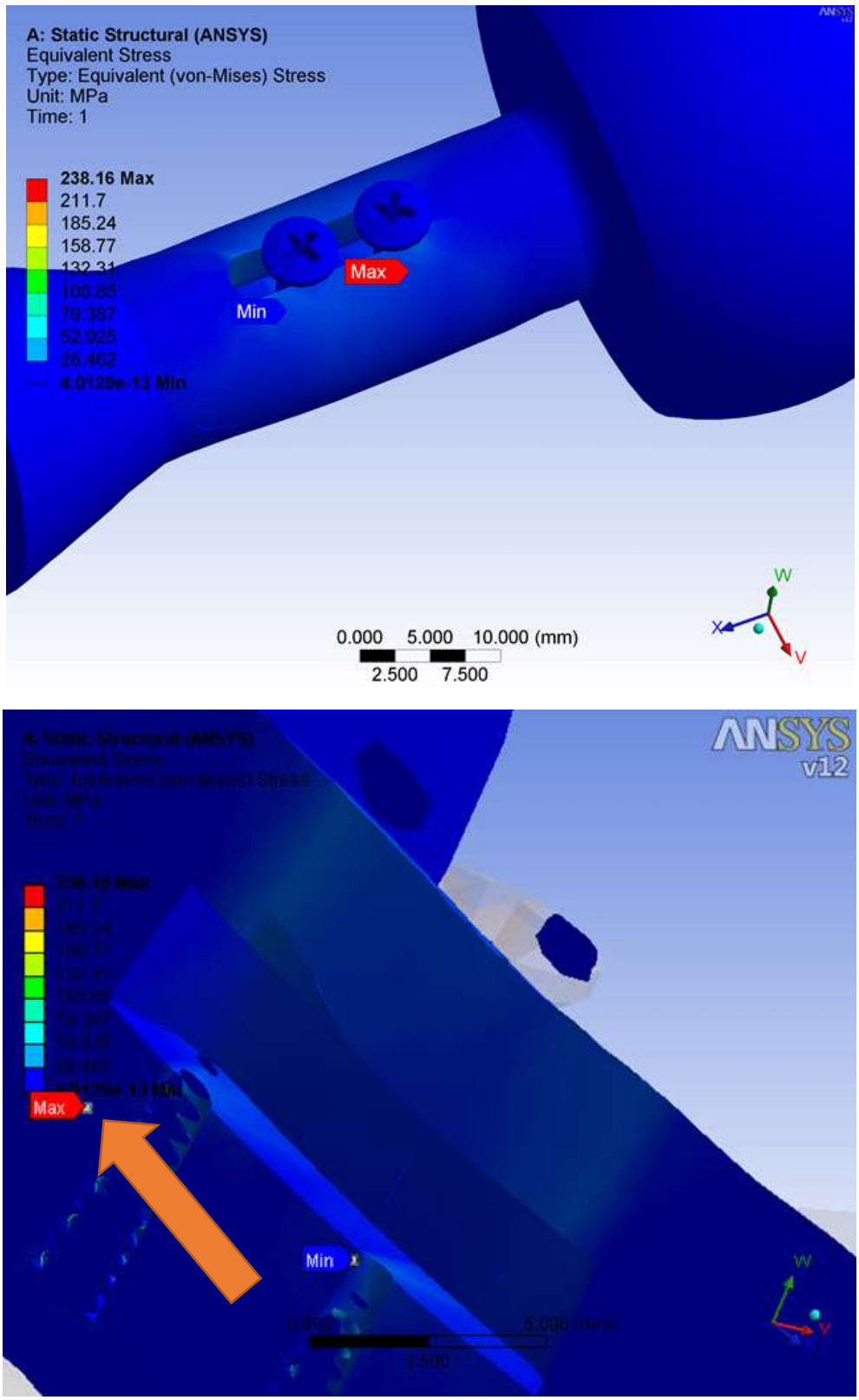

Figure 7.5- Stress distribution of design concept 2

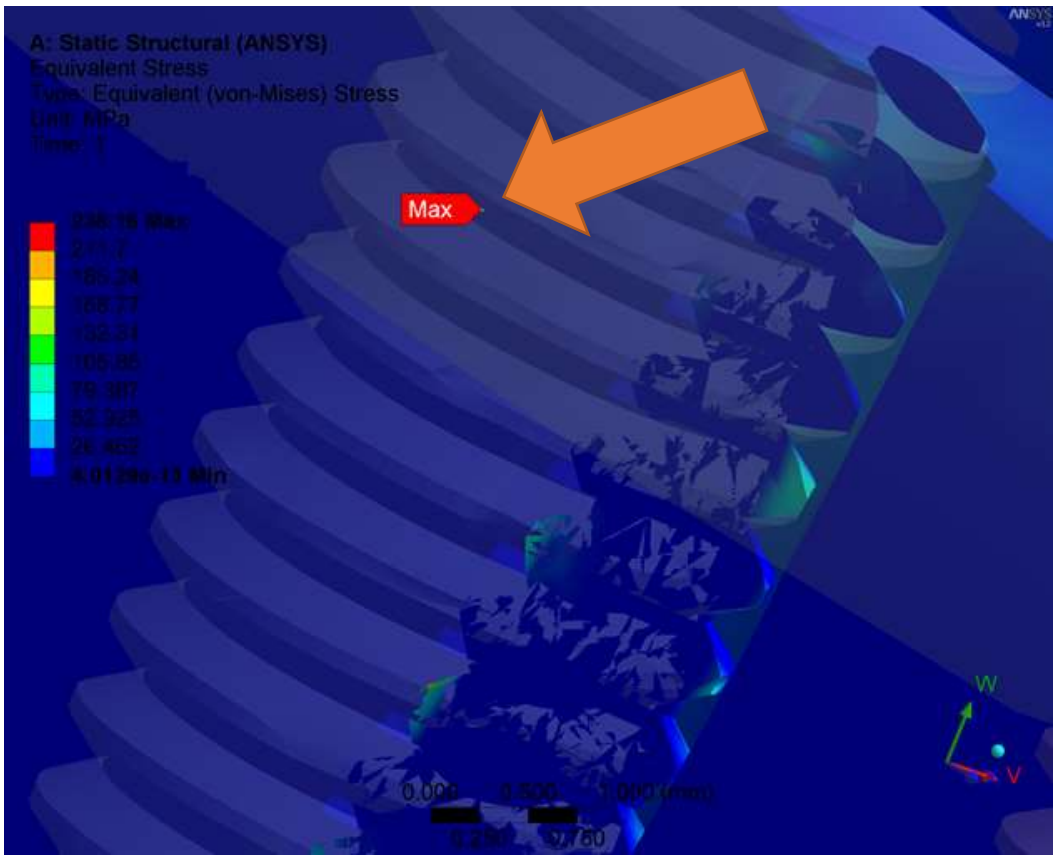

Figure 7.6- Stress distribution of design concept 2

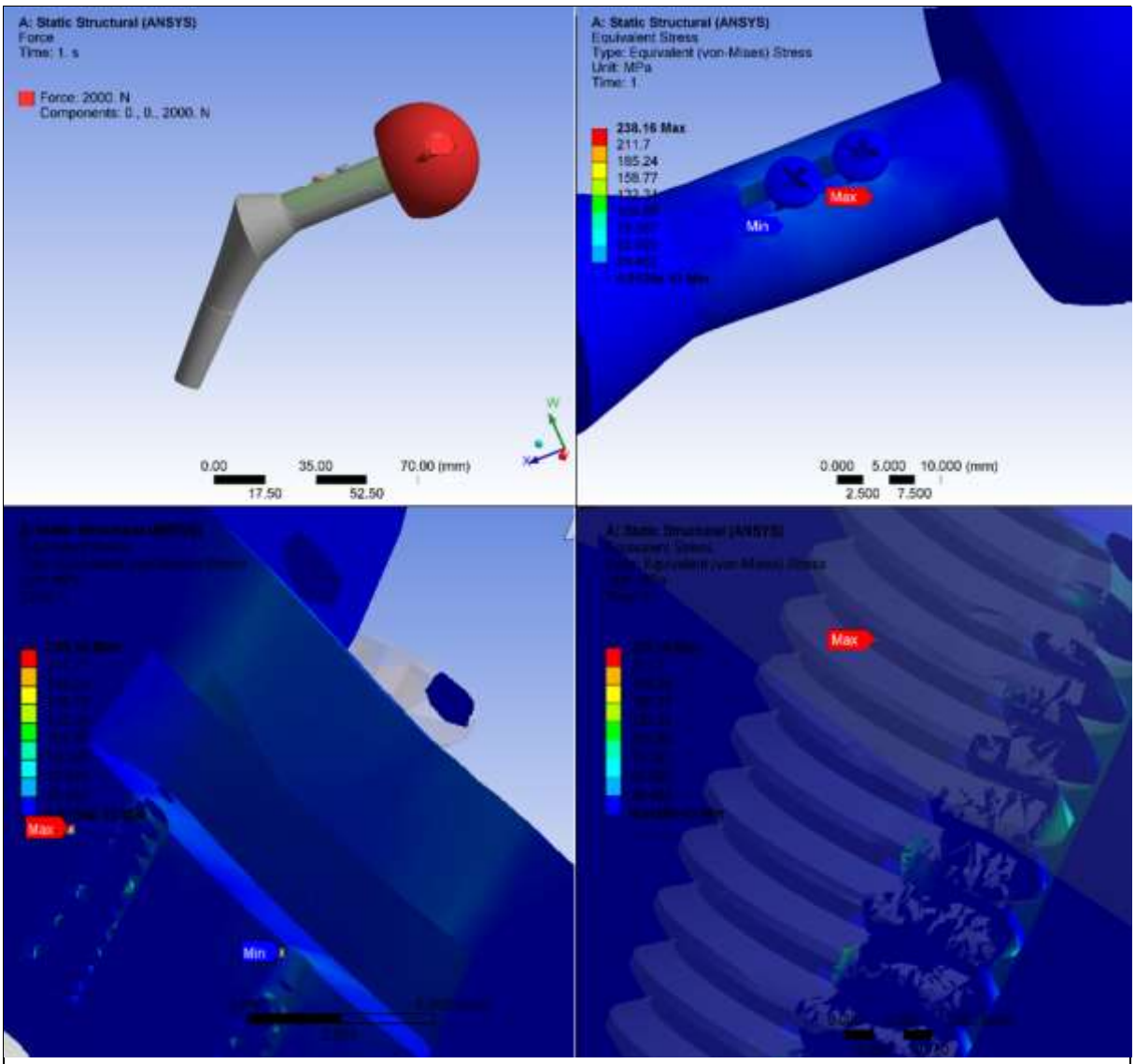

Figure 7.7- Boundary condition and stress distribution of design concept 2

Design 2

Maximum von-Mises Stress: 238.16 MPa

Comment:

Max stress appears around the screws. Upper and lower parts of design are not stable enough and can cause a considerable stress. However compare to design 1, the fixed holes of lower part, improved the stability. Empty spaces around the screws could be a disadvantage.

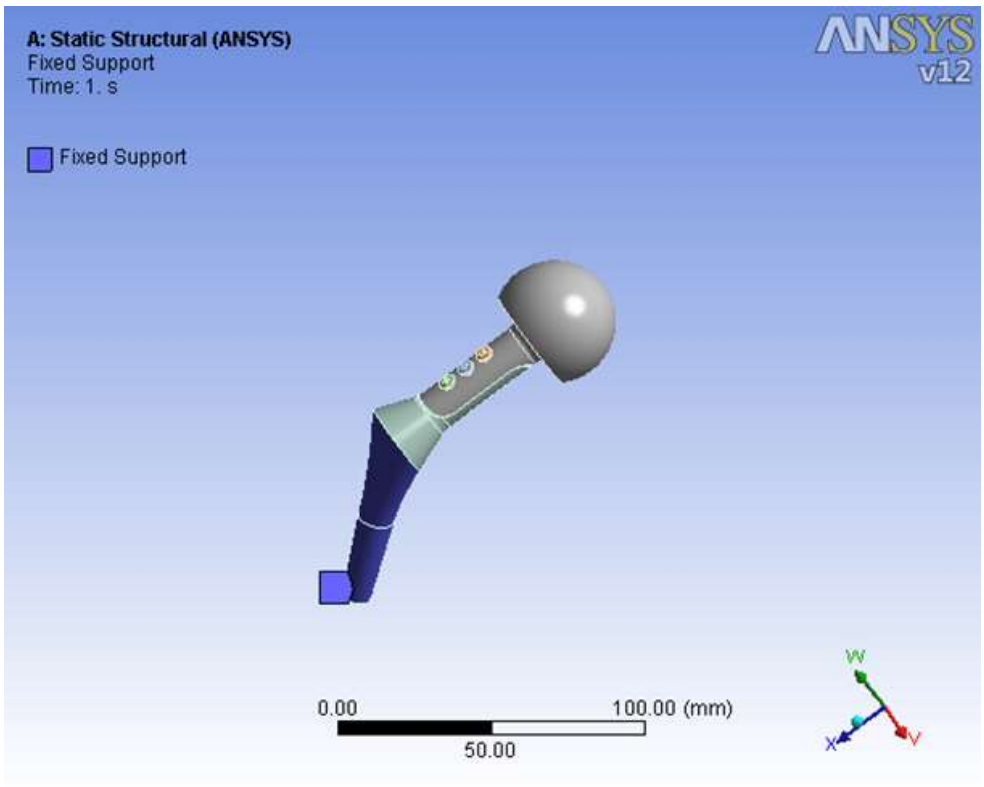

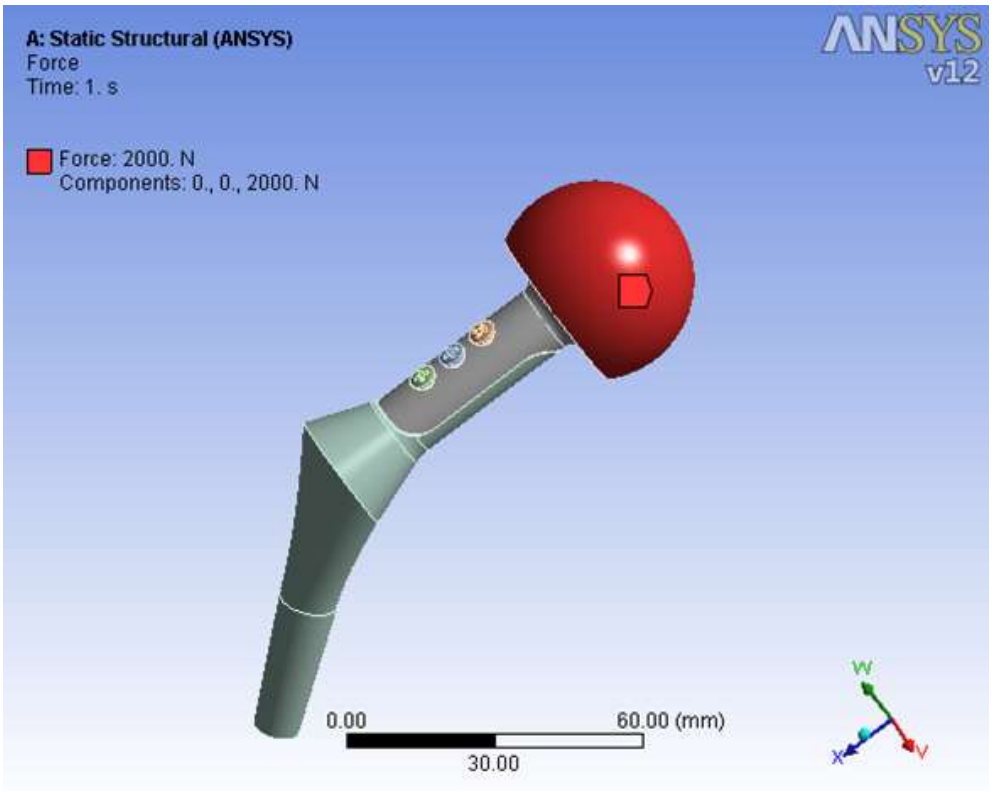

Figure 7.8- Boundary condition of design concept 3

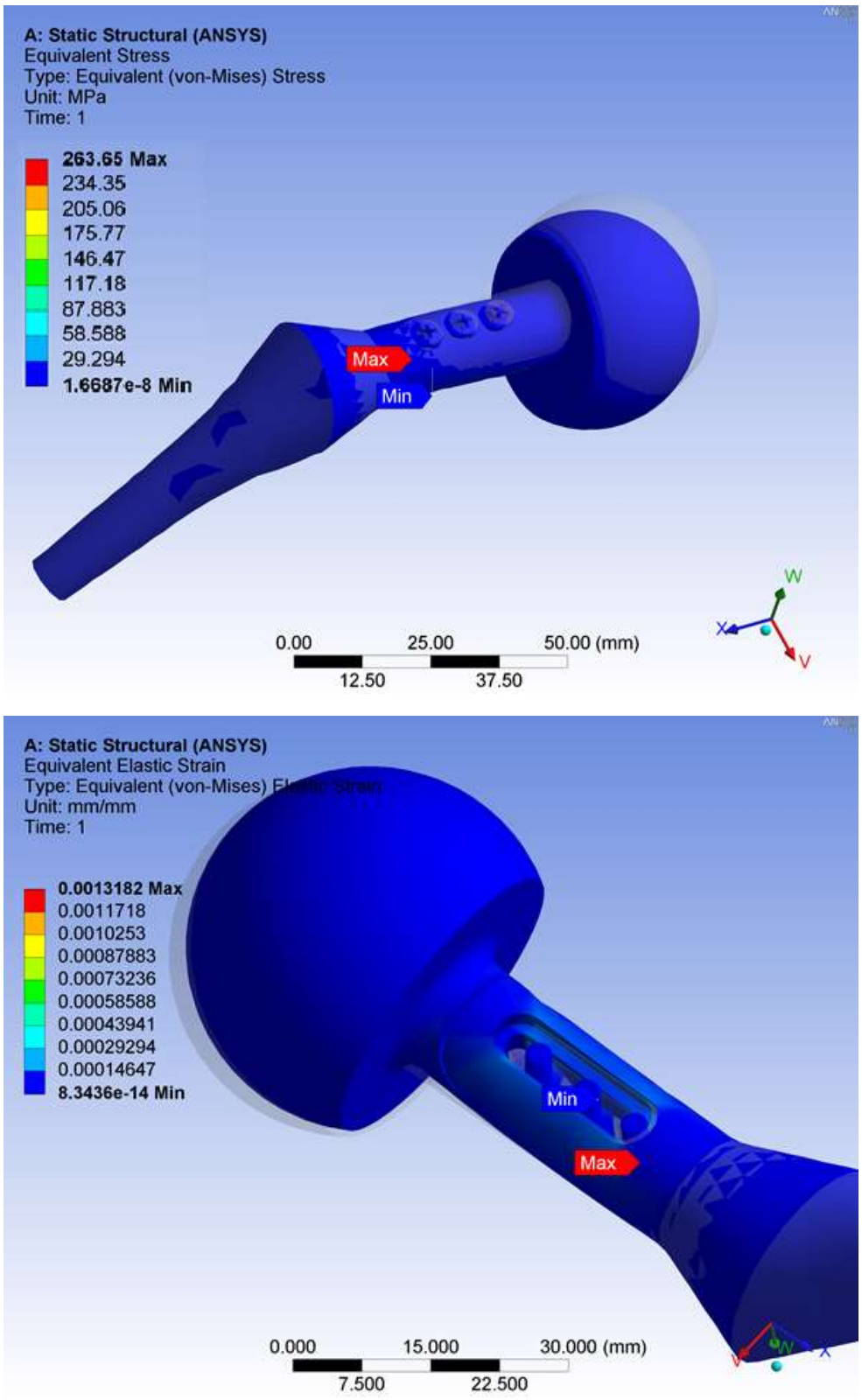

Figure 7.9- Stress distribution of design concept 3

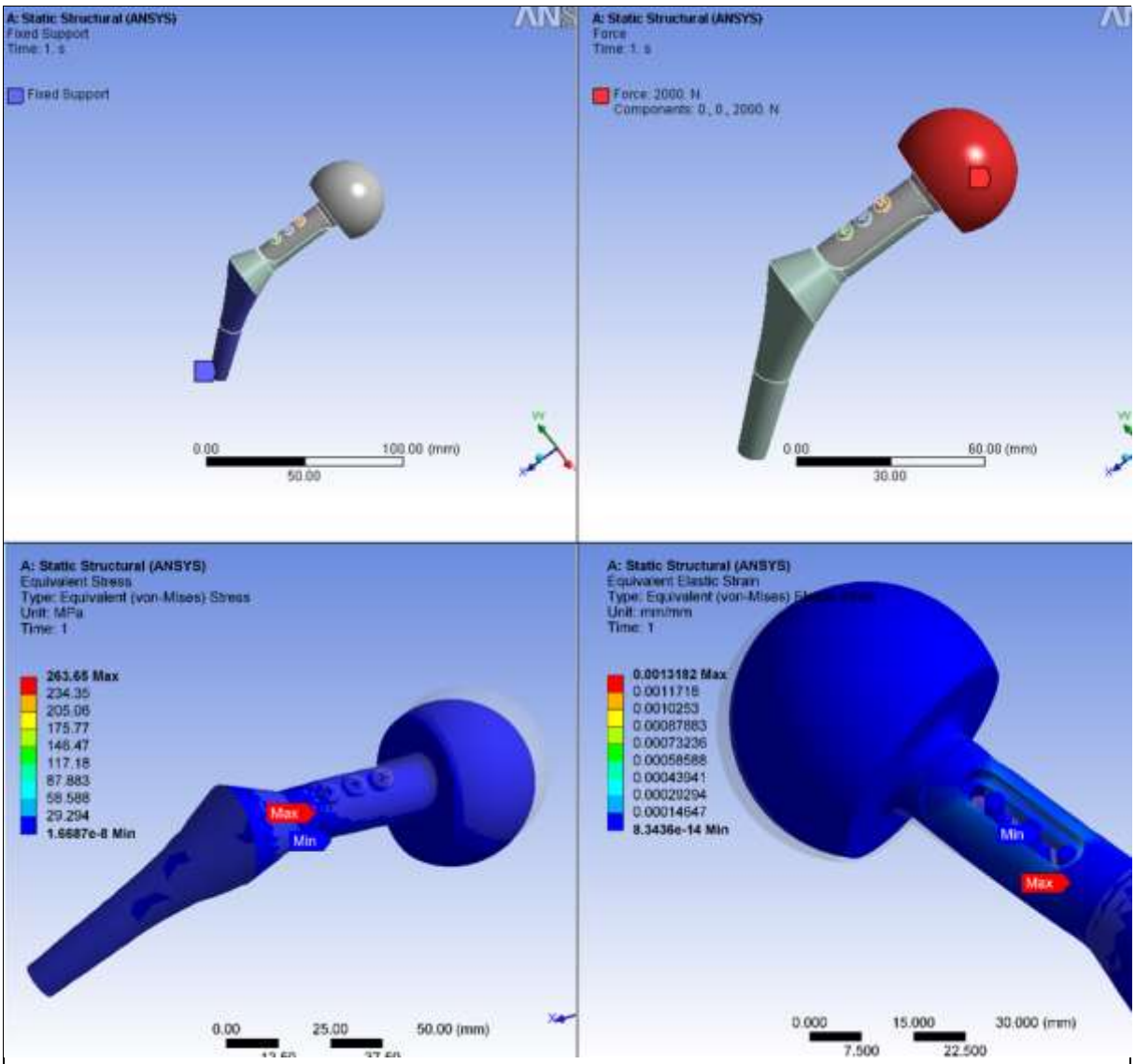

Figure 7.10- Boundary condition and stress distribution of design concept 3

Design 3
Maximum von-Mises Stress: 263.65 MPa

Comment:

Max stress appears around the screws. Upper and lower parts of design are not stable enough and can cause a considerable stress. Adding extra screws does not seem to reduce the stress. Like design 2, the groove in the lower part could be a disadvantage.

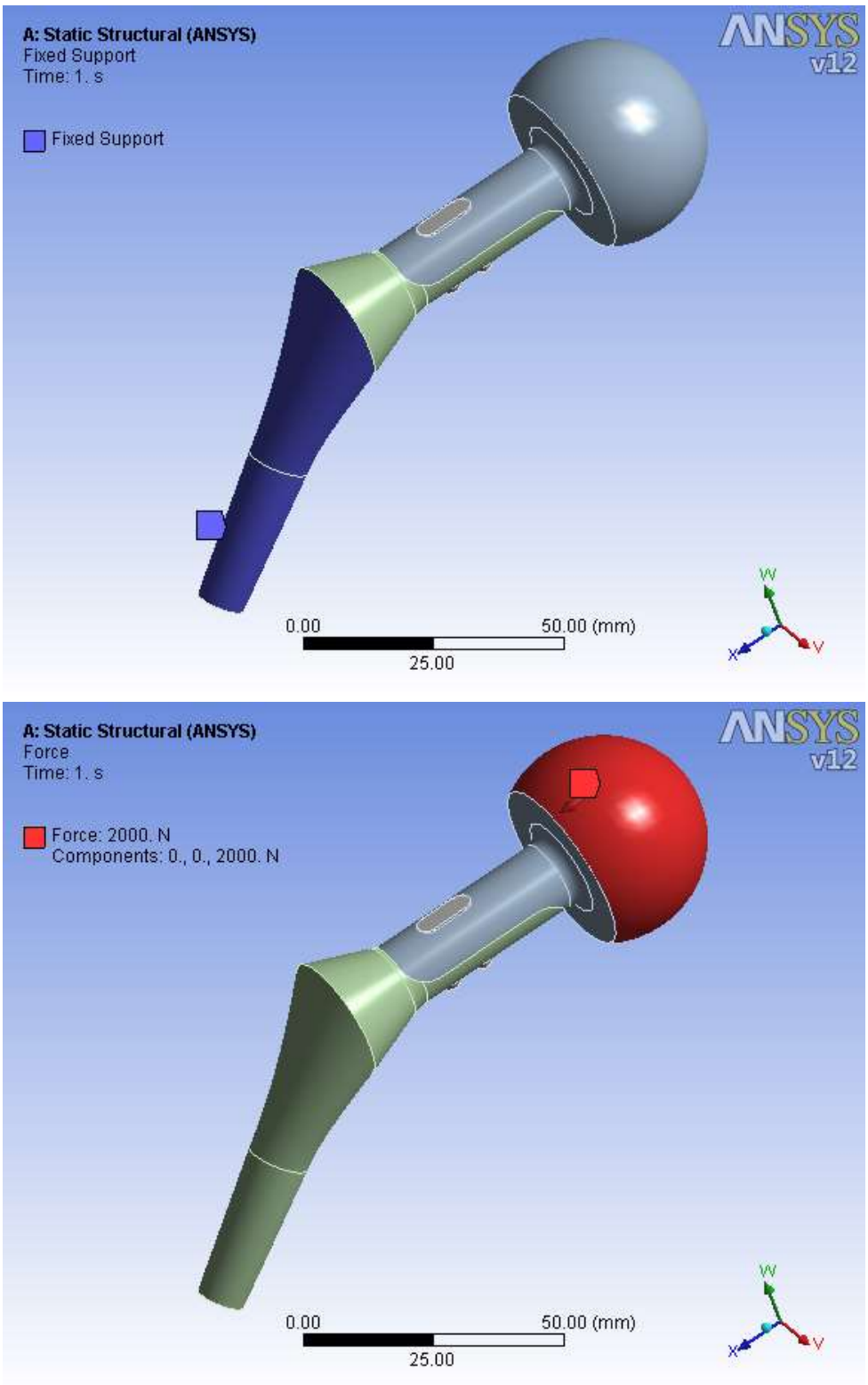

Figure 7.11- Boundary condition of design concept 4

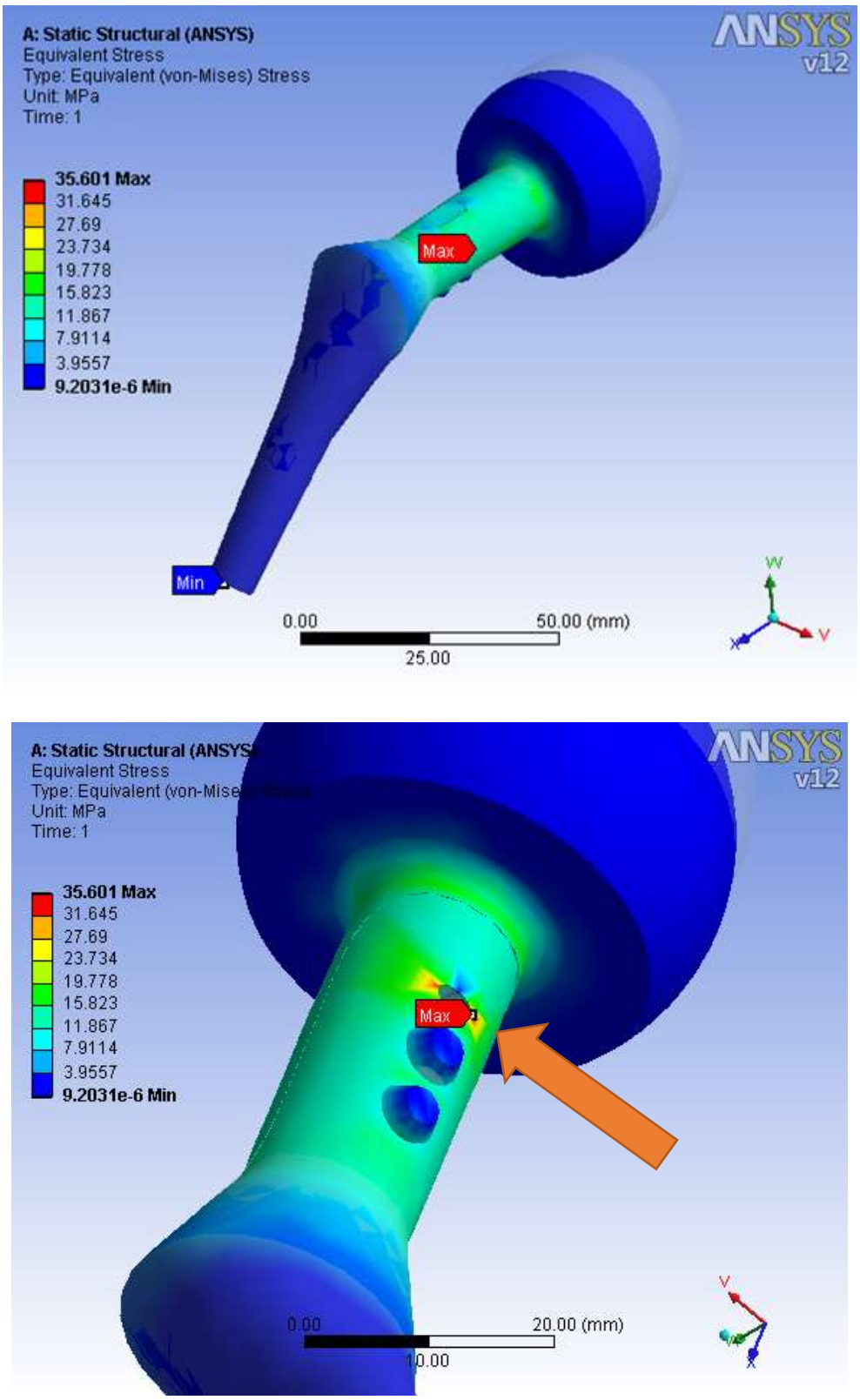

Figure 7.12- Stress distribution of design concept 4

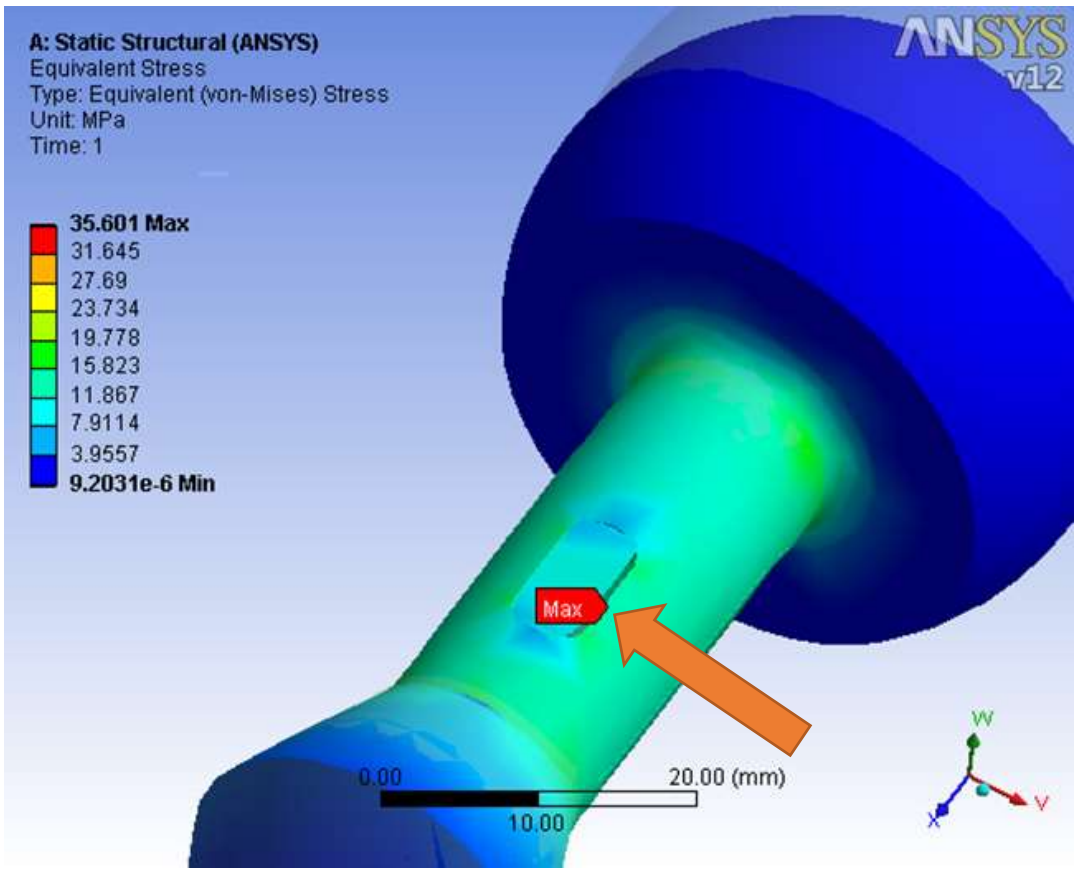

Figure 7.13- Stress distribution of design concept 4

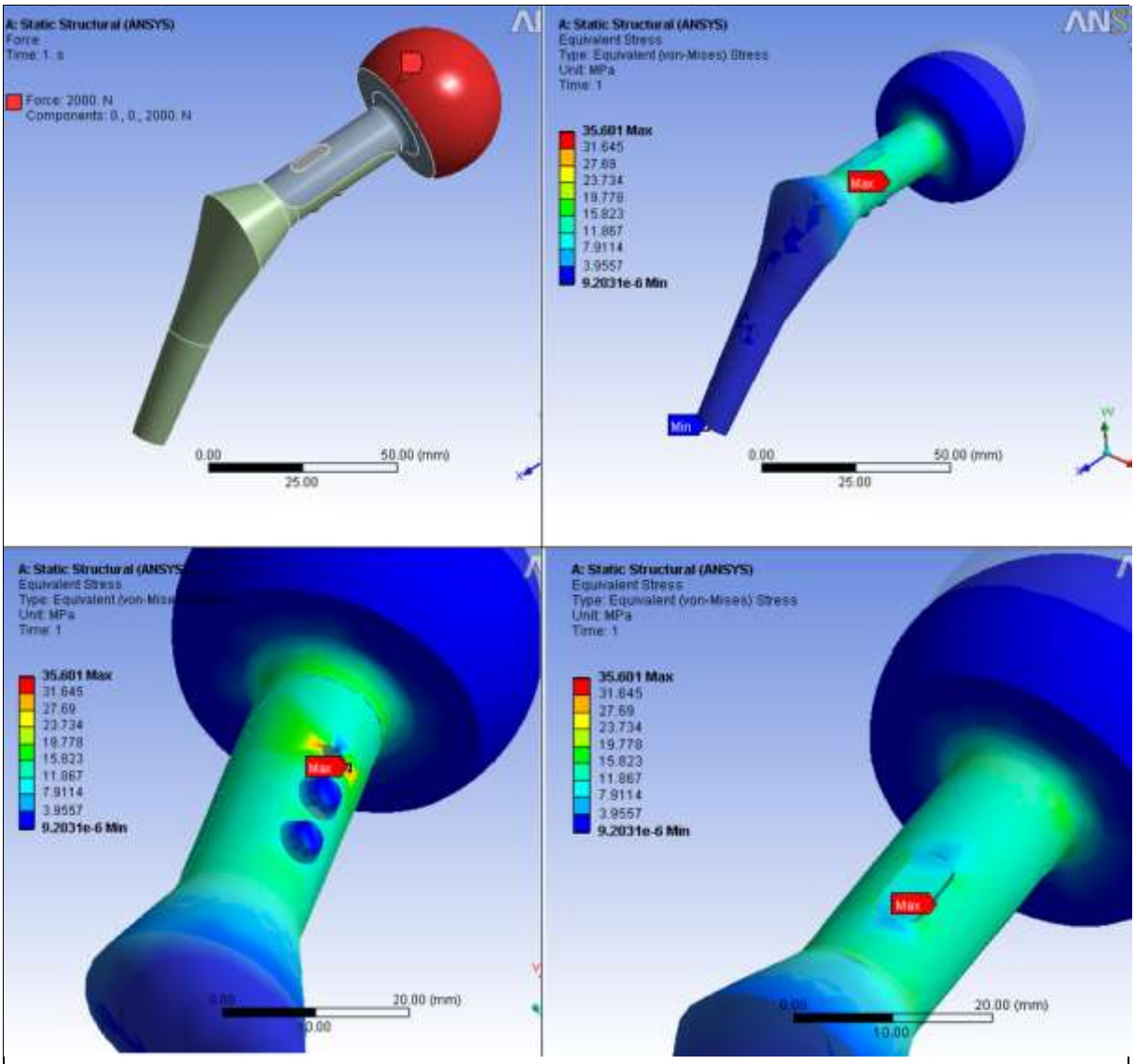

Figure 7.14- Boundary condition and stress distribution of design concept 4

Design 4
Maximum von-Mises Stress:35.601 MPa

Comment:

Max stress appears around a hole. However it is considerably smaller than in design 1, 2 and 3. Upper and lower parts of the design are fixed well together than previous designs. Removing the groove in the design has eliminated the disadvantage of empty spaces.

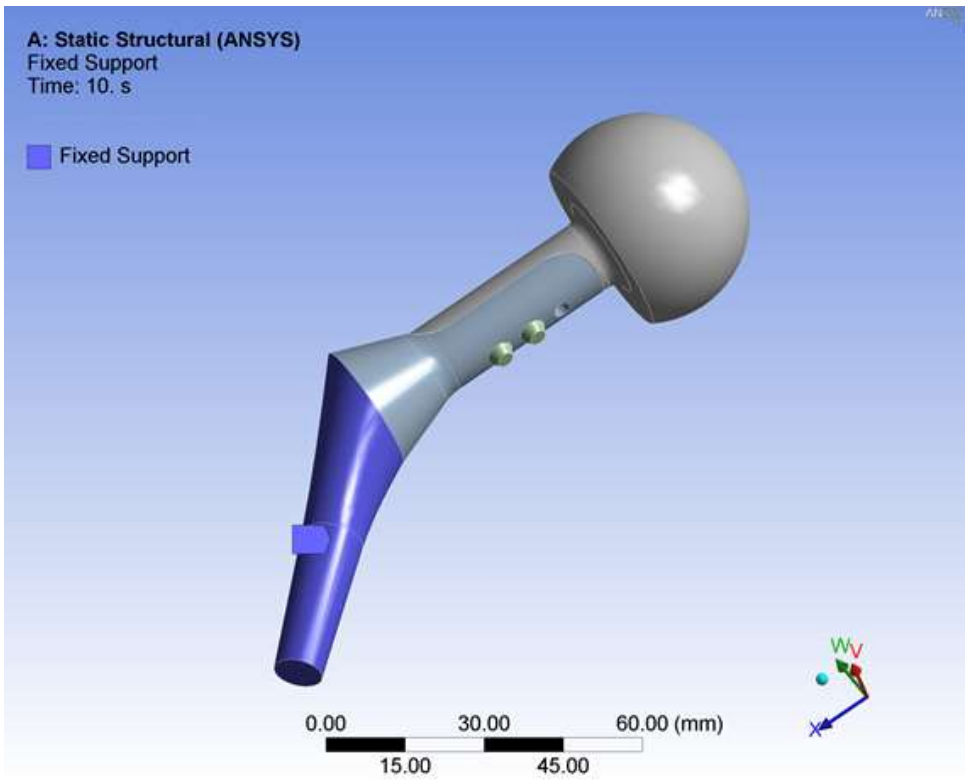

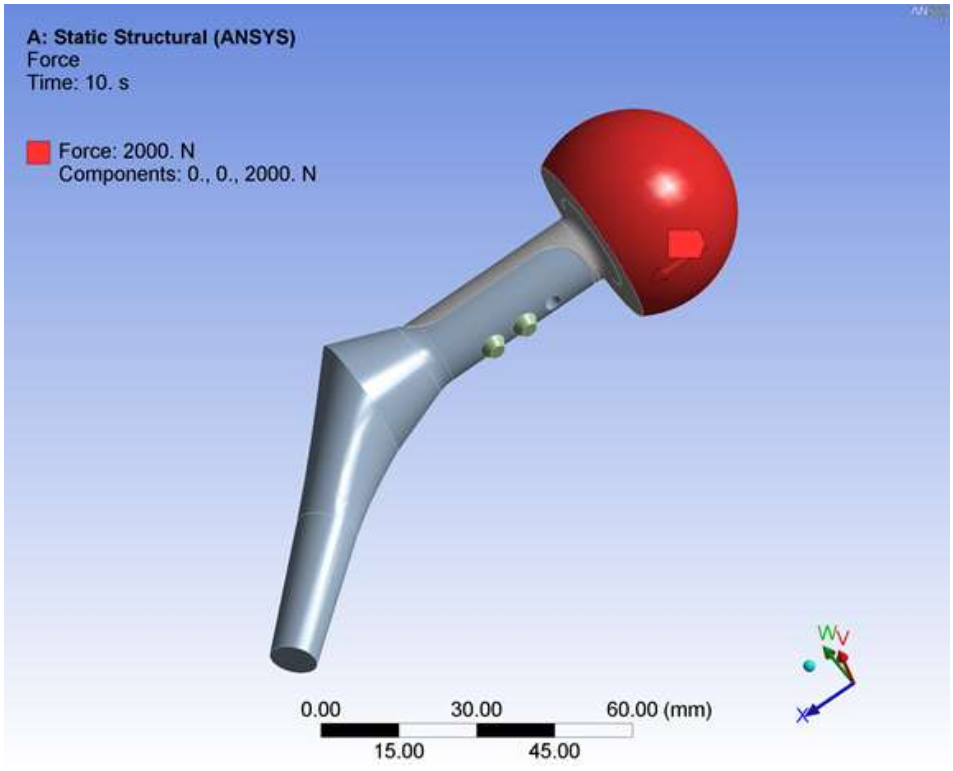

Figure 7.15- Boundary condition of design concept 5

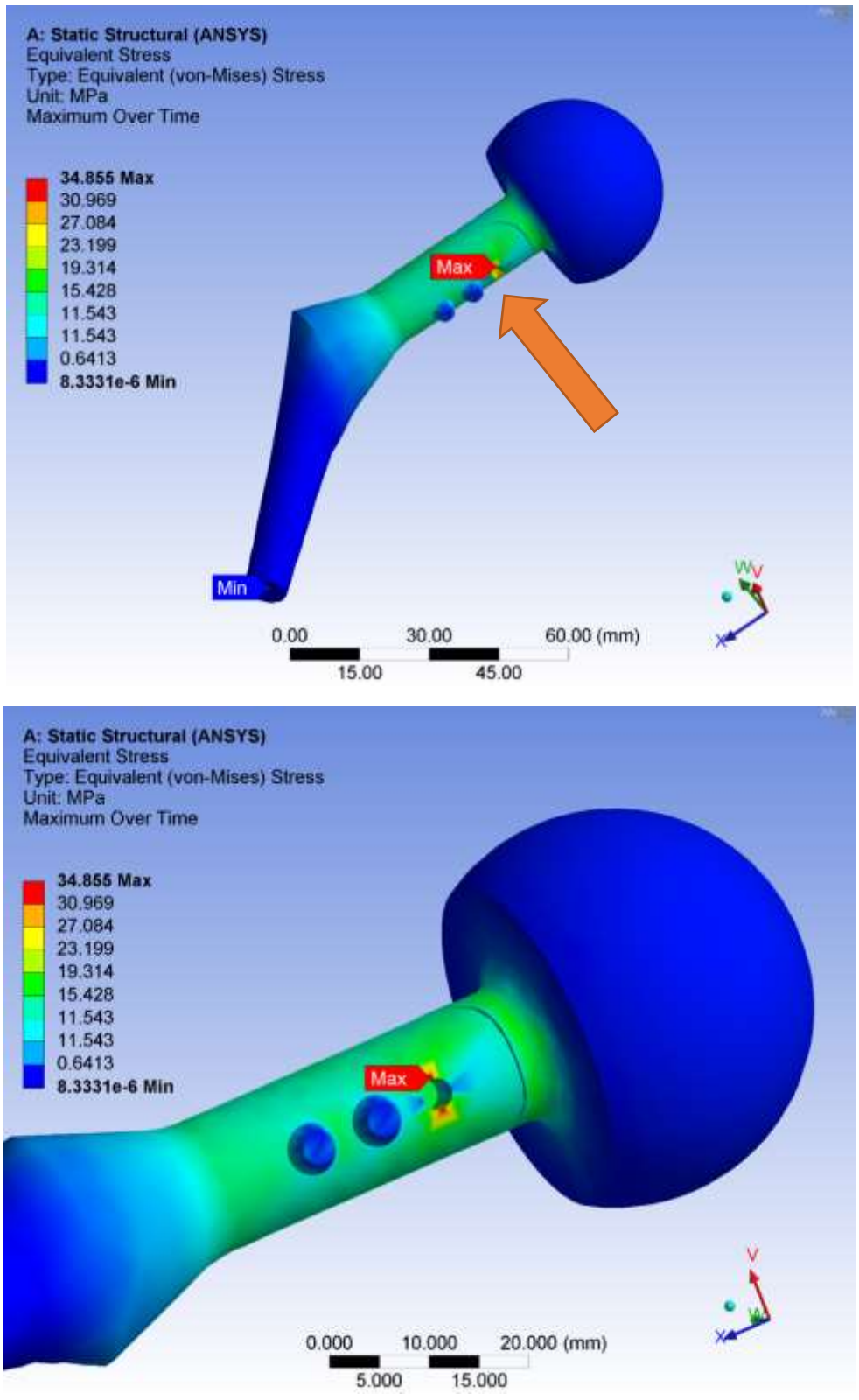

Figure 7.16- Stress distribution of design concept 5

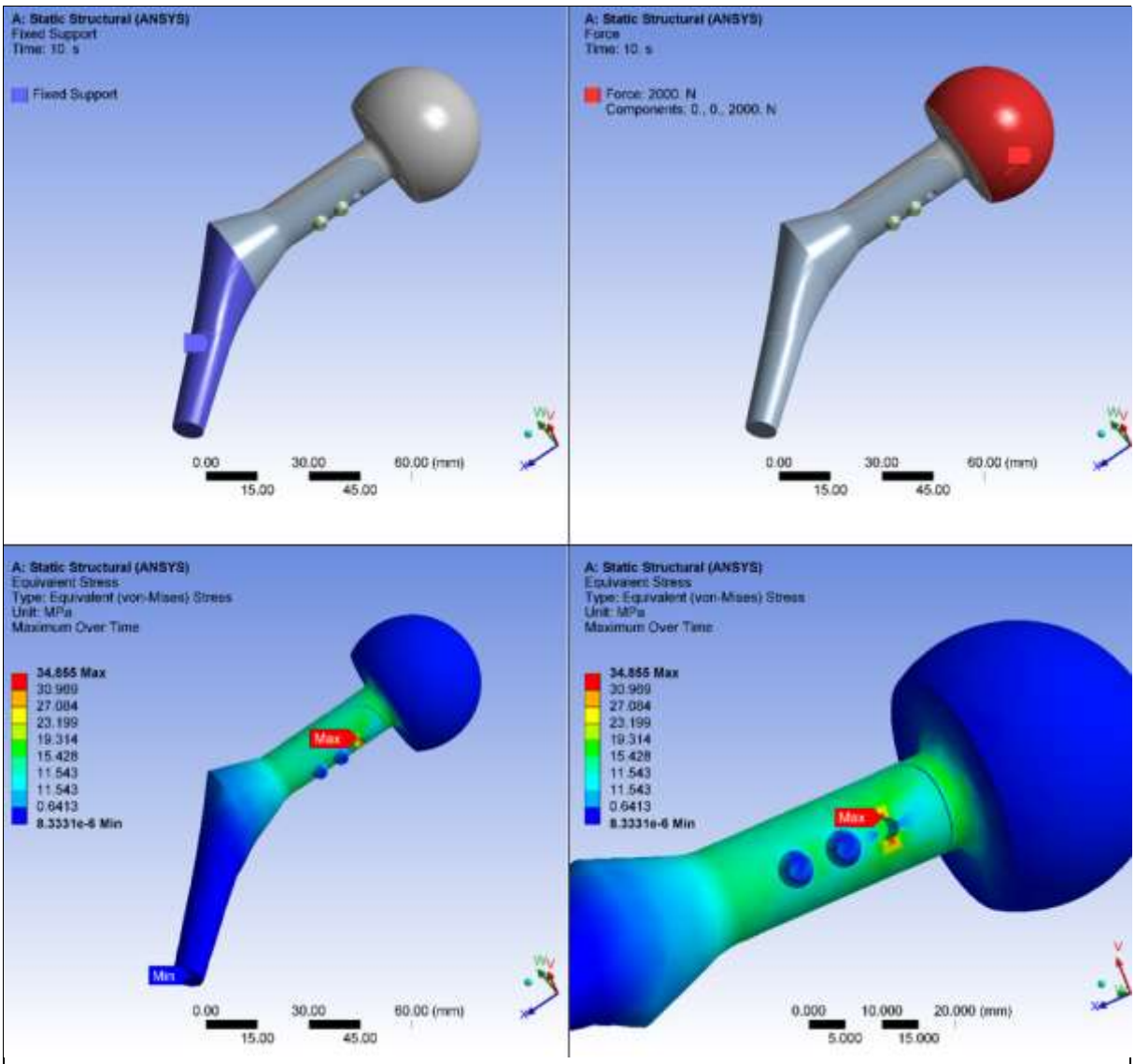

Figure 7.17- Boundary condition and stress distribution of design concept 5

Design 5

Max von-Mises Stress: 34.855 MPa

Comment:

Maximum stress appears around the hole as shown. However it is considerably smaller than in previous designs. Upper and lower parts of the design are fixed together better and compare to design 1, 2, 3 and 4 the stress values reduced noticeably. Removing the groove in the design has eliminated the disadvantage of empty spaces.

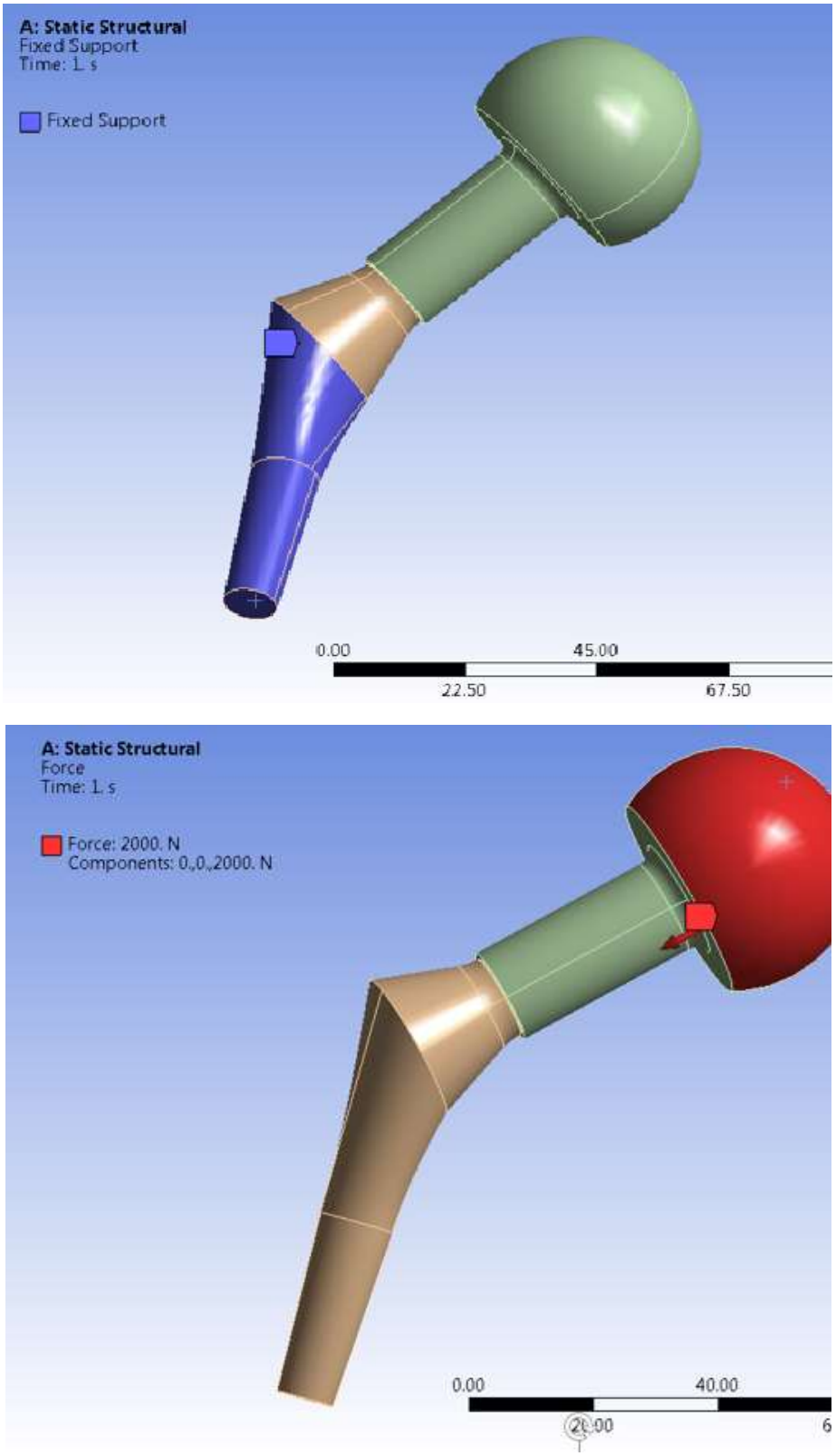

Figure 7.18- Boundary condition of design concept 6

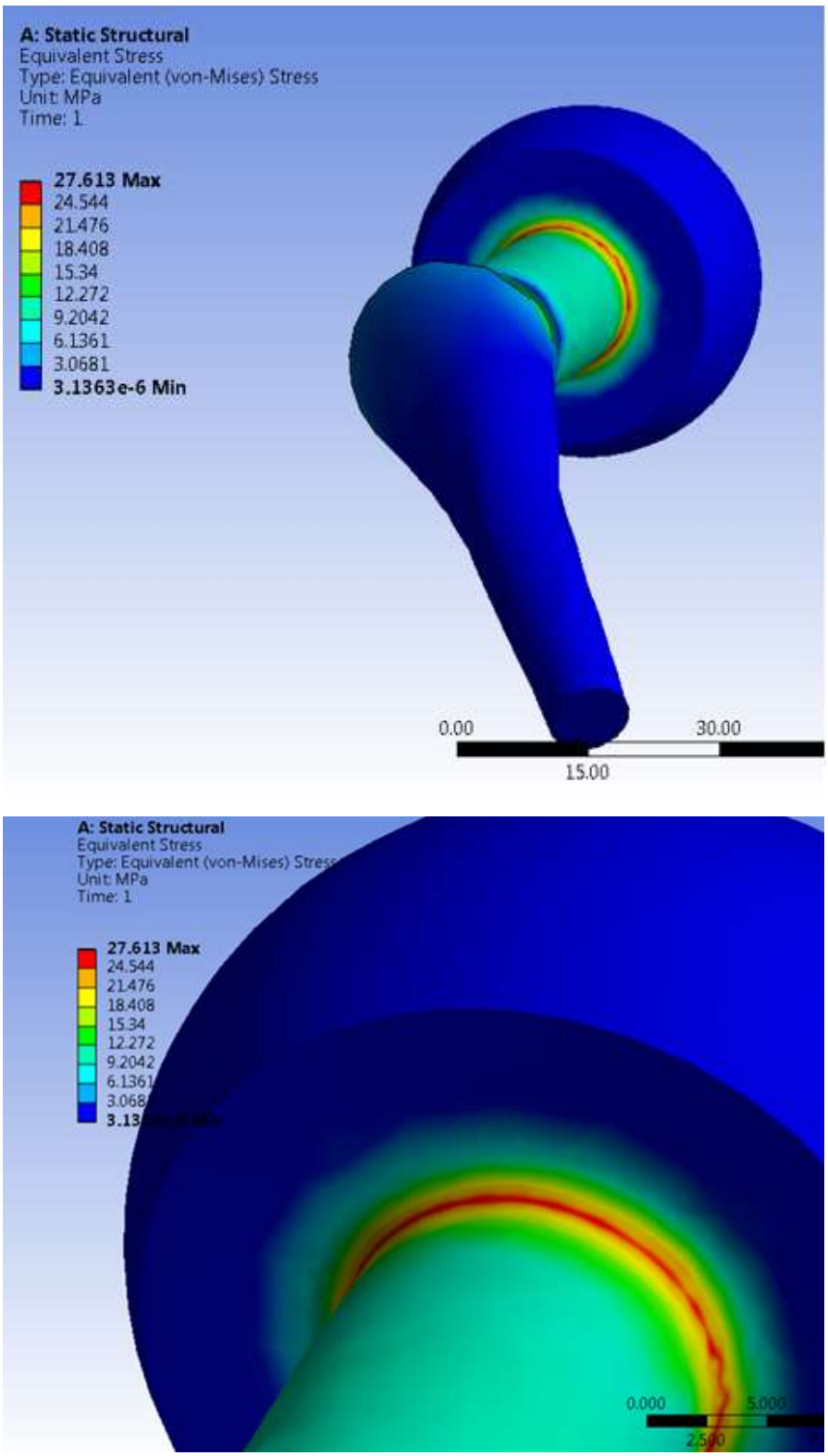

Figure 7.19- Stress distribution of design concept 6

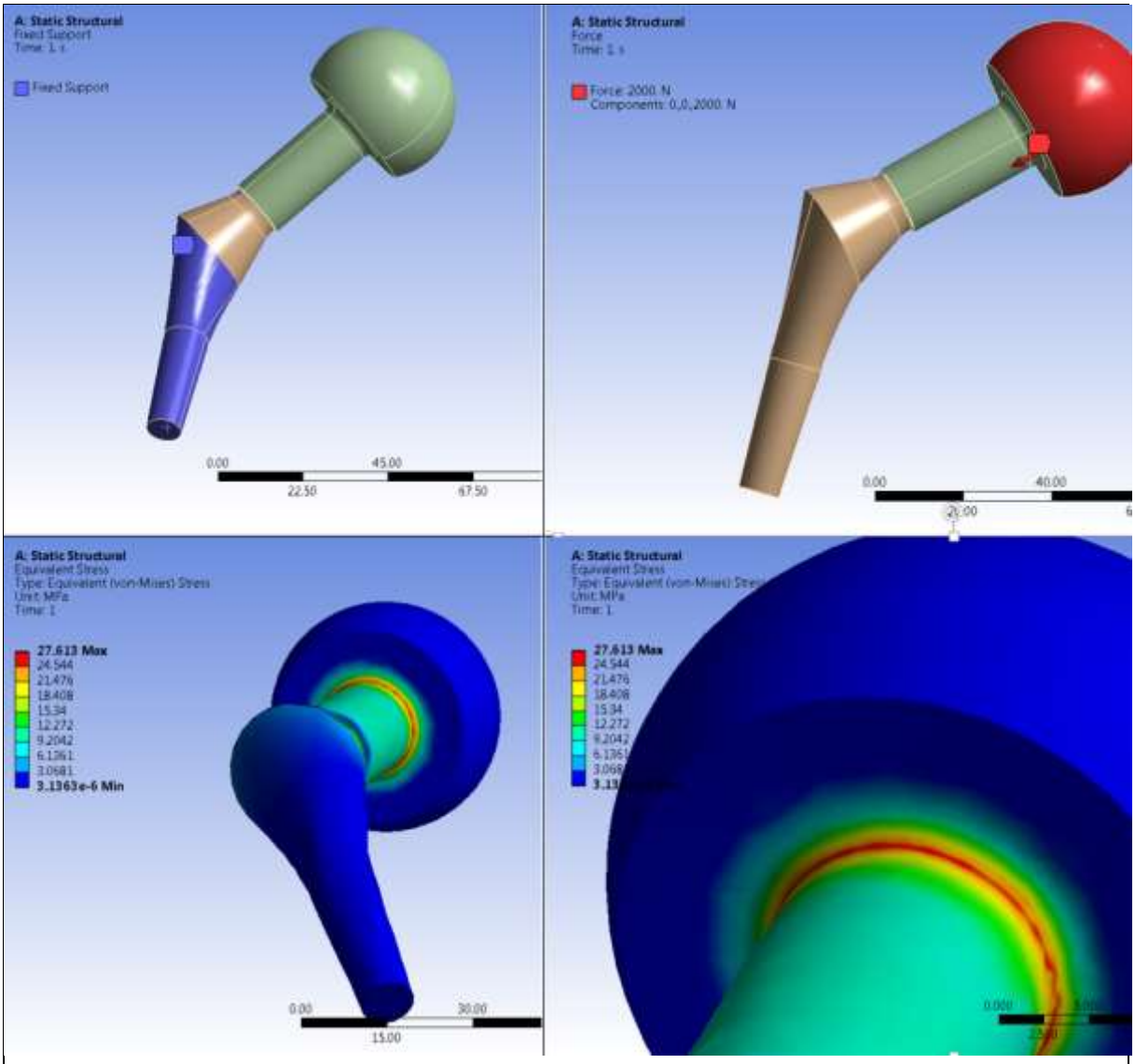

Figure 7.20- Boundary condition and stress distribution in design concept 6

Design 6

Maximum von-Mises Stress : 27.61 MPa

Comment:

Maximum stress appears around the neck and femoral head. However it is considerably smaller than in other designs. Upper and lower parts of design are fixed together better. Removing the groove and screws in the design has eliminated the disadvantage of empty spaces and high stress concentrations.

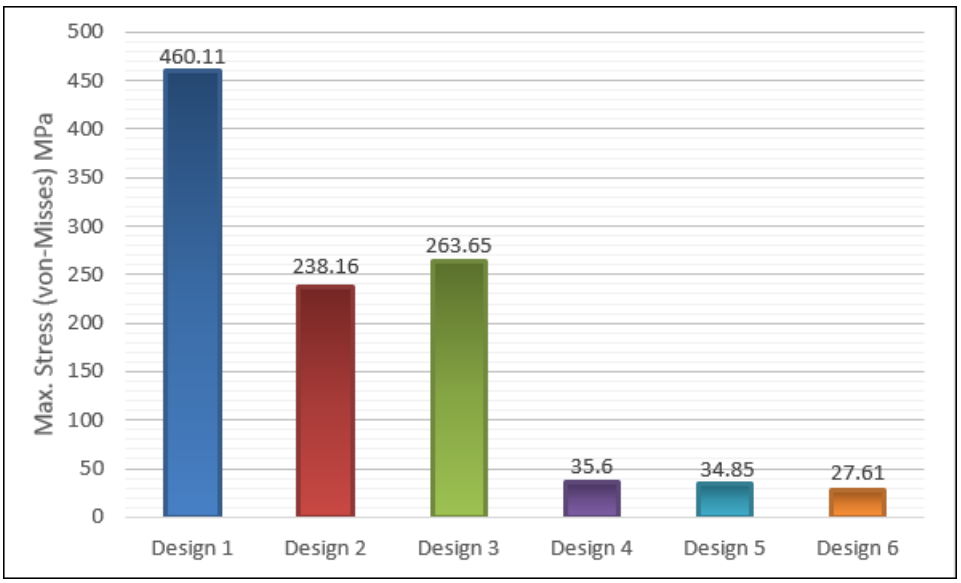

Figure 7.21- Maximum stress (von-Mises) in MPa in of all designs.

The Figure 7.21 shows the maximum stress in MPa of each design. Designs 5 and 6 have the lowest stress concentration compared to other designs. However to choose the best design we need to consider other factors too. We are required to examine many features like strength and stiffness, biocompatibility, cost, user friendly design, ease of manufacturing and stability. The finest design is the one that is top in most of these criteria.

Table 7.1- Comparing all of solutions against given criteria.

Pugh Chart						
Criteria	Design 1	Design 2	Design 3	Design 4	Design 5	Design 6
Strength/stiffness	-	-	+	+	+	+
Biocompatibility	+	+	+	+	+	+
Cost	+	+	+	+	+	+
User friendly	-	-	-	+	+	+
Ease of manufacturing	-	-	+	+	-	+
Stability	-	-	-	-	+	+
Total	**-2**	**-2**	**+3**	**+4**	**+4**	**+5**

To choose the best solution to start with from all available designs, the well-known "Pugh chart" is a good option (Table 7.1). Developed by Professor Stuart Pugh in university of Strathclyde, the Pugh chart is great for organizing complicated lists of pros and cons, as well as comparing your possible solutions against a set of criteria. (Pugh, 1990).

As discussed in chapter 4, the ideal stem length was chosen to be small for many benefits that were explained, and enhanced by macro-features in the shape of horizontal and vertical grooves intended to distribute loading forces and reduce micromotions. In chapter 6 the influence of moments and rotational components in daily activities and specifically going up stairs were highlighted. A rectangular cross section was designed for a better rotational stability contrary to the initial round cross section. In terms of femoral head, a relatively big head diameter was chosen as it prevents dislocation and results in a larger range of motion (Cross et al., 2012). Also a tapered neck feature was added which prevents impingement of cup and neck and enhances range of motion of the implant. As discussed in chapter 2 for a better biological fixation, titanium plasma spray coating was used for the distal part of the stem (Aebli et al. 2003). This feature can be enhanced as currently there are many researchers working to propose better bioactive coatings to replace the conventional materials and techniques. High offset stem option is a unique feature that helps tightening the abductor and boosts the hip implant stability with the ability to adjust neck and offset. It gives a surgeon more options to fix the most accurate offset and do the operation more effectively. The findings from micromotion analysis and stress distribution simulations, were used to decide the best optimal hip stem design and were accompanied and improved with future stress analysis of different design factors to get the final optimal model.

The related data is attached in the appendix. Some of the main advantages of the optimal design are as follows:

- Slim body that benefits bone preservation.
- Smaller stem length that preserves more bone and reduces the patient pain.
- Rectangular cross section provides rotational stability.

- Big head diameter that reduces the risk of dislocation.
- Tapered neck which preserves impingement of the cup and neck while enhancing ROM at the same time.
- Titanium plasma spray coating that helps enhancing biological fixation.
- A unique mechanism that lateralizes femur to help tighten abductor and enhance joint stability, through ability to change neck length and offset.

Fatigue life analyses were carried out which shows about 15% improvement compared to average standard life of hip prostheses. This optimal hip joint design was the outcome of a scientific approach and based on a lot of data analysis including micromotion analysis, various stress analysis under both static and dynamic loadings and different activities and also the fatigue life analysis considering von Mises stresses, and is shown in Figure 7.22.

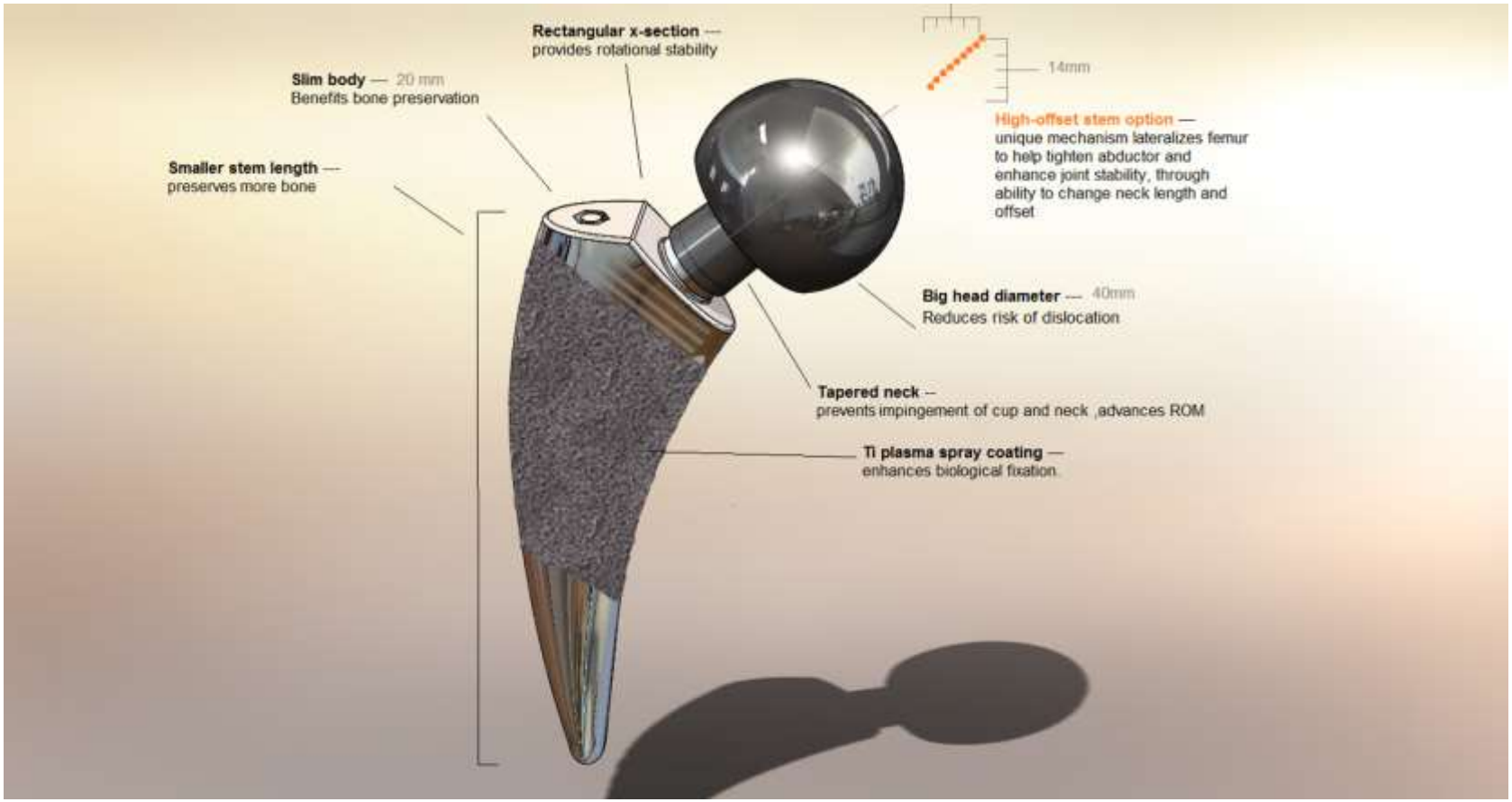

Figure 7.22- Optimal hip implant

Chapter 8

Conclusions and Recommendations for Future Work

This chapter explains the outcome and different findings of this research. In other words, the contribution to knowledge and also potential research that can be carried out in future based on this study is elaborated. The description backed by the past studies where it was needed.

8.1 Analysis of primary stability and micromotions

In this research the aseptic loosening which is the main problem associated with total hip replacement has been studied. Although multiple patient, surgical and prosthesis-related factors are involved, the final pathway to the development of aseptic loosening is a process of mechanical failure of the construct driven by the bone loss. Improving the stability of the implant can significantly reduce the risk of loosening. The stability between the bone and the implant can be classified into primary and secondary stability. Primary stability refers to the stability at the bone-implant interface immediately after implantation and depends entirely upon mechanical factors (Viceconti et al., 2000). Secondary stability describes the biological stability of the implant when bone ingrowth as occurred. Primary stability achieved after surgery is a determinant factor for the long-term stability of cementless hip arthroplasty. The term primary stability has been defined by Viceconti et al. (2006) as the amount of relative micromovement between the bone and the implant induced by the physiological joint loading early after the operation, before any biological process takes place.

Therefore the focus of this research is on primary stability and the long-term stability of cementless hip implants. The influence of implant design on stability and micromotions between the bone and implant were evaluated using finite element analysis method by considering different types of designs. The factors that were particularly investigated include: Biomechanical assessment of different hip stem designs, biomechanical effect of different materials and mechanical properties, biomechanical assessment of stem lengths and biomechanical effect of different stem fixations.

8.2 Analysis of long-term stability, stress distribution and dynamic loadings

One of the restrictions of micromotion analysis that was presented in chapter 4, was the inability to divide the final results of micromotion data, into axial and rotational components. Therefore it would have been inappropriate to eventually conclude the best femoral stem, without considering the sustained torsional loadings. Another limitation is that the micromotion analysis would not reflect the stress distribution on the hip prosthesis and consequently would ignore the potential high stress concentration that is associated with post-operative pain as well as low durability and long-term stability. For these reasons, a separate stress analysis was carried out to examine the von Mises stress, shear stress and principal stress distribution of cementless hip implants, under dynamic loadings of nine different activities. The axial and rotational forces were also evaluated in that simulation. The factors that were particularly investigated include: Effect of nine different activities of daily life on stress distribution, assessment of different body weight force components, relative moment components, muscle loadings, angle of line of action of forces, axial and torsional forces that are all associated with each of nine different activities, effect of improved von Mises stresses on fatigue life analysis.

8.3 Optimal hip joint design

Laboratory experiments were carried out to verify the FE results and also the equipment that was used including the standard composite femur bone known as Sawbone. Lastly all data from micromotion analysis and stress distribution simulations, were used to decide the best optimal hip stem design and was accompanied and improved with future stress analysis of different design factors to get the final optimal model. The outcome was an optimal hip prosthesis design, through a scientific approach and based on much of data analysis including micromotion analysis, various stress analyses under both static and dynamic loadings and different activities and also the fatigue life analysis considering von Mises stresses.

8.4 Findings

8.4.1 Contact ratio and location

It has been shown that full connection between femoral stem and femur is not required to attain a good primary stability. The femoral stem primary stability is affected by both the contact ratio and its position. A number of configuration settings with contact ratio less than 100% and associating either the proximal or the cortical bonding supply better primary stability compared to full contact setting. Nevertheless, with contact ratio less than 40%, the femoral stem must be in contact with cortical bone to guarantee an excellent primary stability.

8.4.2 Curved or straight shape

Regarding the shape of femoral stem it was shown that at higher torsional scenarios including the movement that viewed in the course of stair-climbing, the curved femoral stem are very much more stable compared to straight femoral stem. However the evaluations comparing a curved anatomical femoral stem and a straight femoral stem, revealed the fact that during low angles in flexion, the curved hip stem and straight hip stem exhibited identical patterns of movement.

8.4.3 Femur bone preservation and revision surgery/ Stress shielding

It was recommended that a short hip femoral stem could supply vertical stability through the wedge shape of the femoral stem along with adding a lateral flare and maintaining the femoral neck. The preservation of the femoral neck offers greater torsional stability and decreases distal migration of the hip joint femoral stem. The lack of any diaphyseal fixation attempts to obtain proximal force transfer in order to minimize stress shielding and thigh pain.

In particular the extremely proximal place of these femoral stems, keeps the possibility of an implantation of a non-revision femoral stem in the course of revision operation. Short-stem implants with a close anatomical fit to the proximal cortex increase primary stability. While the evaluation of hip joint femoral stem length is particularly popular in revision surgery, it is

also crucial for primary hip replacement. If we presumably use a short hip femoral stem is used in the beginning, subsequently if the need for a revision operation raised, the loss of femoral bone stock would be significantly less compared to when a longer hip joint femoral stem is employed.

The shorter shaft leads to more physiological loading of the femur, thereby limiting potential bone resorption due to stress shielding. It also helps to preserve the femoral canal and femoral elasticity, and ease the revision.

8.5 Future work

Bone-saving hip replacement employing metaphyseal femoral stems is gaining importance considering the growing number of young patients, and the fact that hip resurfacing is not often indicated. In the last decade, the practice of hip replacement has changed; a younger age-group a lot more frequently experience surgery due to their need for a better quality of life. The achievement of cementless total hip replacement relies on osteo-integration of the prostheses.

Clinical reports looking at the migrational behaviour of hip femoral components have demonstrated that the failure rate of cementless stems correlates with migration or interfacial micromotions between femur and implant (Krismer et al., 1999). Sychterz has identified that in vivo bone loss was most extensive within the proximal-medial area (Sychterz et al., 2002). Following traditional arthroplasty operations, femoral bone density measurement has demonstrated a femur bone loss of 16 to 30% (Kim et al., 2003; Schmidt et al., 2002; Sychterz et al., 2002). Engh's post mortem study has discovered 7 to 52% femoral bone loss around cementless hip femoral components with osteo-integration (Engh et al., 1992). DXA measurements by Kishida et al. (2004) proved that two years after resurfacing procedures 12% rise in bonedensity developed in the Gruen 7 zone (Kishida et al., 2004). The advantages and disadvantages of short-stem arthroplasty are suggested through the author’s experiences with the metaphyseal stems (Toth et al., 2010).

In general the key benefit of using a short-stemmed implant over long-stemmed is the convenience of changing to a further hip prosthesis should failure take place. Since less femur is eliminated, it offers a chance of long-term compatibility. With regards to interface micromotion of the implant, a short-stemmed hip joint could be developed to a more stable implant through some other design factors, including a pronounced lateral flare which sets on the inferolateral side of the greater trochanter as well as by using macro-features. This investigation demonstrated that shorter femoral stems could have the prospect of becoming the next generation of cementless hip femoral stems provided that their stability can be enhanced. Future work could focus on a universal modular short stem implant design that is surgeon friendly and provides them all options to modify different design factors while performing the operation, instead of the conventional modular designs that cover all different angles and sizes through more than 50 different femoral necks and items. Overall, this research was a success. The main reason of aseptic loosening was studied in depth by considering both primary stability and long-term stability. Through comparing results obtained from both experimental records and computer finite element analysis data, it was possible to validate the use of finite element analysis as a method of prediction and fulfilling the objectives of this project.

References

Abdul karim, A., Ellanti, P., Motterlini, N., Fahey, T. and O'Byrne, J.M. (2013) 'Cemented versus uncemented fixation in total hip replacement: a systematic review and meta-analysis of randomized controlled trials.', *Orthopedic reviews*, 5(1), pp 34–44. doi: 10.4081/or.2013.e8.

Abdul Kadir M and Kamsah N. (2009) 'Interface micromotion of cementless hip stems in simulated hip arthroplasty.', *American journal of applied sciences.* 6 (9): pp 1682-1689.

Abhijit, R., Shinge, Sandip, S. and Anasane (2011) 'Finite element analysis of modified hip prosthesis.', *International Journal of Advanced Biotechnology and Research pp*, 2(2), pp. 278–285.

Adam, F., Hammer, D.S., Pfautsch, S. and Westermann, K. (2002) 'Early failure of a press-fit carbon fiber hip prosthesis with a smooth surface.', *The Journal of arthroplasty*, 17(2), pp. 217–23.

Aebli, N., Krebs, J., Schwenke, D., Stich, H., Schawalder, P. and Theis, J.C. (2003) 'Degradation of hydroxyapatite coating on a well-functioning femoral component.', *The Journal of bone and joint surgery. British volume*, 85(4), pp. 499–503.

Ahmed, A.M., Raab, S. and Miller, J.E. (1984) 'Metal/cement interface strength in cemented stem fixation.', *Journal of orthopaedic research : official publication of the Orthopaedic Research Society*, 2(2), pp. 105–18. doi: 10.1002/jor.1100020201.

Ando, M., Imura, S., Omori, H., Okumura, Y., Bo, A. and Baba, H. (1999) 'Nonlinear three-dimensional finite element analysis of newly designed cementless total hip stems.', *Artificial organs*, 23(4), pp. 339–46.

Arabnejad Khanoki, S. and Pasini, D. (2013) 'Fatigue design of a mechanically biocompatible lattice for a proof-of-concept femoral stem.', *Journal of the mechanical behavior of biomedical materials*, 22, pp. 65–83. doi: 10.1016/j.jmbbm.2013.03.002.

Arno, S., Fetto, J., Nguyen, N.Q., Kinariwala, N., Takemoto, R., Oh, C. and Walker, P.S. (2012) 'Evaluation of femoral strains with cementless proximal-fill femoral implants of

varied stem length.', *Clinical biomechanics (Bristol, Avon)*, 27(7), pp. 680–5. doi: 10.1016/j.clinbiomech.2012.03.006.

Aubault, M., Druon, J., Le Nail, L. and Rosset, P. (2013) 'Outcomes at least 10 years after cemented PF® (Zimmer) total hip arthroplasty: 83 cases.', *Orthopaedics & traumatology, surgery & research : OTSR*, 99(4 Suppl), pp. S235–9. doi: 10.1016/j.otsr.2013.03.006.

Bah, M.T., Nair, P.B., Taylor, M. and Browne, M. (2011) 'Efficient computational method for assessing the effects of implant positioning in cementless total hip replacements.', *Journal of biomechanics*, 44(7), pp. 1417–22. doi: 10.1016/j.jbiomech.2010.12.027.

Bah, M.T., Shi, J., Heller, M.O., Suchier, Y., Lefebvre, F., Young, P., King, L., Dunlop, D.G., Boettcher, M., Draper, E. and Browne, M. (2015) 'Inter-subject variability effects on the primary stability of a short cementless femoral stem.', *Journal of biomechanics*, 48(6), pp. 1032–42. doi: 10.1016/j.jbiomech.2015.01.037.

Bannister, G.C. and Miles, A.W. (1988) 'The influence of cementing technique and blood on the strength of the bone-cement interface.', *Engineering in medicine*, 17(3), pp. 131–3.

Barnett, A.J., Burston, B.J., Atwal, N., Gillespie, G., Omari, A.M. and Squires, B. (2009) 'Large diameter femoral head uncemented total hip replacement to treat fractured neck of femur.', *Injury*, 40(7), pp. 752–5. doi: 10.1016/j.injury.2009.01.009.

Basso, T., Klaksvik, J., Syversen, U. and Foss, O.A. (2014) 'A biomechanical comparison of composite femurs and cadaver femurs used in experiments on operated hip fractures.', *Journal of biomechanics*, 47(16), pp. 3898–902. doi: 10.1016/j.jbiomech.2014.10.025.

Bennett, D. and Goswami, T. (2007) 'Finite element analysis of hip stem designs.', *Mater Des*, 29(1), pp. 45–60.

Bergmann, G., Deuretzbacher, G., Heller, M., Graichen, F., Rohlmann, A., Strauss, J. and Duda, G.N. (2001) 'Hip contact forces and gait patterns from routine activities.', *Journal of biomechanics*, 34(7), pp. 859–71.

Bergmann, G., Graichen, F. and Rohlmann, A. (1993) ‘Hip joint loading during walking and running, measured in two patients.’, *Journal of biomechanics*, 26(8), pp. 969–90.

Bergmann, G., Graichen, F. and Rohlmann, A. (2004) ‘Hip joint contact forces during stumbling.’, *Langenbeck’s archives of surgery / Deutsche Gesellschaft fur Chirurgie*, 389(1), pp. 53–9. doi: 10.1007/s00423-003-0434-y.

Bertollo, N., Matsubara, M., Shinoda, T., Chen, D., Kumar, M. and Walsh, W.R. (2011) ‘Effect of surgical fit on integration of cancellous bone and implant cortical bone shear strength for a porous titanium.’, *The Journal of arthroplasty*, 26(7), pp. 1000–7. doi: 10.1016/j.arth.2010.12.007.

Bever, M. and Duwez, P. (1972) ‘Gradients in composite materials.’, *Materials Science and Engineering pp*, 10, pp. 1–8.

Bhatt, H. and Goswami, T. (2012) ‘Effect of Geometrical Parameter in Hip Implant Penetration.’, *Contact Stress and Wear 309*, 1.

Biegler, F.B., Reuben, J.D., Harrigan, T.P., Hou, F.J. and Akin, J.E. (1995) ‘Effect of porous coating and loading conditions on total hip femoral stem stability.’, *The Journal of arthroplasty*, 10(6), pp. 839–47.

Biihler, D., Berlemann, U., Lippuner, K., Jaeger, P. and Nolte, L. (1997) ‘P. “Threedimensional primary stability of cementless femoral stems”, Clin Biomech, 12(2), pp. 75–86.

Bishop, N.E., Ferguson, S. and Tepic, S. (1996) ‘Porosity reduction in bone cement at the cement-stem interface.’, *The Journal of bone and joint surgery. British volume*, 78(3), pp. 349–56.

Boudeau, N., Liksonov, D., Barriere, T., Maslov, L. and Gelin, J. (2012) ‘Composite based on polyetheretherketone reinforced with carbon fibres, an alternative to conventional materials for femoral implant: Manufacturing process and resulting structural behaviour.’, *Materials Design*, 40, pp. 148–156.

Bougherara, H., Zdero, R., Shah, S., Miric, M., Papini, M., Zalzal, P. and Schemitsch, E.H. (2010) 'A biomechanical assessment of modular and monoblock revision hip implants using FE analysis and strain gage measurements.', *Journal of orthopaedic surgery and research*, 5, p. 34. doi: 10.1186/1749-799X-5-34.

Bourne, R.B. and Rorabeck, C.H. (1998) 'A critical look at cementless stems. Taper designs and when to use alternatives', *Clinical orthopaedics and related research*, (355), pp. 212–23.

Brown, B., Smallwood, R., Barber, D., Lawford, P., Hose, D., Buma, P., van Loon, P., Versleyen, H., Weinans, H., Slooff, T., de Groot, K. and R (1998) *Medical Physics and Biomedical Engineering.* (18 Vols).

Burke, D.W., Gates, E.I. and Harris, W.H. (1984) 'Centrifugation as a method of improving tensile and fatigue properties of acrylic bone cement.', *The Journal of bone and joint surgery. American volume*, 66(8), pp. 1265–73.

Callaghan, J.J., Fulghum, C.S., Glisson, R.R. and Stranne, S.K. (1992) 'The effect of femoral stem geometry on interface motion in uncemented porous-coated total hip prostheses. Comparison of straight-stem and curved-stem designs.', *The Journal of bone and joint surgery. American volume*, 74(6), pp. 839–48.

Caouette, C., Yahia, L. and Bureau, M.N. (2011) 'Reduced stress shielding with limited micromotions using a carbon fibre composite biomimetic hip stem: A finite element model', *Proceedings of the Institution of Mechanical Engineers, Part H: Journal of Engineering in Medicine*, 225(9), pp. 907–919. doi: 10.1177/0954411911412465.

Capitanu, L., Florescu, V. and Badita, L.-L. (2014) 'New concept in durability improvement of hip total joint endoprostheses.', *Acta of bioengineering and biomechanics / Wroclaw University of Technology*, 16(1), pp. 75–82.

Chen, W.-C., Lai, Y.-S., Cheng, C.-K. and Chang, T.-K. (2014) 'A cementless, proximally fixed anatomic femoral stem induces high micromotion with nontraumatic femoral avascular necrosis: A finite element study', *Journal of Orthopaedic Translation*, 2(3), pp. 149–156.

Chong, A.C.M., Friis, E.A., Ballard, G.P., Czuwala, P.J. and Cooke, F.W. (2007) 'Fatigue performance of composite analogue femur constructs under high activity loading.', *Annals of biomedical engineering*, 35(7), pp. 1196–205. doi: 10.1007/s10439-007-9284-z.

Chong, A.C.M., Miller, F., Buxton, M. and Friis, E.A. (2007) 'Fracture toughness and fatigue crack propagation rate of short fiber reinforced epoxy composites for analogue cortical bone.', *Journal of biomechanical engineering*, 129(4), pp. 487–93. doi: 10.1115/1.2746369.

CJRR. (2014), Annual report of Canadian Joint Replacement Registry, [Online] Available at: https://secure.cihi.ca/free_products/CJRR%14%20Annual%20Report_EN-web.pdf. (Accessed Dec 2014).

Cook, S.D., Thongpreda, N., Anderson, R.C., Thomas, K.A., Haddad, R.J. and Griffin, C.D. (1987) 'Optimum pore size for bone cement fixation.', *Clinical orthopaedics and related research*, (223), pp. 296–302.

Costigan, P.A., Deluzio, K.J. and Wyss, U.P. (2002) 'Knee and hip kinetics during normal stair climbing.', *Gait & posture*, 16(1), pp. 31–7.

Cowin, S., Hegedus, D., Bone, A. and Remodelling, I. (1976) 'Theory of adaptive elasticity.', *Journal of Elasticity pp*, 6(3), pp. 313–326.

Cross, M.B., Nam, D. and Mayman, D.J. (2012) 'Ideal femoral head size in total hip arthroplasty balances stability and volumetric wear.', *HSS journal : the musculoskeletal journal of Hospital for Special Surgery*, 8(3), pp. 270–4. doi: 10.1007/s11420-012-9287-7.

Davant, J. (no date) 'Chirurgie de la hance. Mieux vivre avec une prosthesis.', *Fonder l'Avenir*, 23, pp. 53–56.

Delaunay, C., Bonnomet, F., North, J., Jobard, D., Cazeau, C. and Kempf, J.F. (2001) 'Grit-blasted titanium femoral stem in cementless primary total hip arthroplasty: a 5- to 10-year multicenter study.', *The Journal of arthroplasty*, 16(1), pp. 47–54. doi: 10.1054/arth.2001.17940.

Dickinson, A., Browne, M., Jeffers, J. and Taylor, A. (2009) 'Analysis of a thin walled, large bore ceramic Acetabular cup with improved in-vivo stability and integrity.', *Trans Ortho Res Soc p2399*, 55.

Dickinson, A.S., Browne, M., Roques, A.C. and Taylor, A.C. (2014) 'A fatigue assessment technique for modular and pre-stressed orthopaedic implants.', *Medical engineering & physics*, 36(1), pp. 72–80. doi: 10.1016/j.medengphy.2013.09.009.

Dorr, L.D., Absatz, M., Gruen, T.A., Saberi, M.T. and Doerzbacher, J.F. (1990) 'Anatomic Porous Replacement hip arthroplasty: first 100 consecutive cases.', *Seminars in arthroplasty*, 1(1), pp. 77–86.

Ducheyne, P. and Hasting, G. (1984) 'Functional behavior of orthopaedic biomaterials, Volume I: Fundamentals.', *CRC Series in Structure-Property Relationships of Biomaterials*.

Dunlap, J.T., Chong, A.C.M., Lucas, G.L. and Cooke, F.W. (2008) 'Structural properties of a novel design of composite analogue humeri models.', *Annals of biomedical engineering*, 36(11), pp. 1922–6. doi: 10.1007/s10439-008-9568-y.

Ebrahimi, H., Rabinovich, M., Vuleta, V., Zalcman, D., Shah, S., Dubov, A., Roy, K., Siddiqui, F.S., H Schemitsch, E., Bougherara, H. and Zdero, R. (2012) 'Biomechanical properties of an intact, injured, repaired, and healed femur: an experimental and computational study.', *Journal of the mechanical behavior of biomedical materials*, 16, pp. 121–35. doi: 10.1016/j.jmbbm.2012.09.005.

Effenberger, H., Heiland, A., Ramsauer, T., Plitz, W. and Dorn, U. (2001) 'A model for assessing the rotational stability of uncemented femoral implants.', *Archives of orthopaedic and trauma surgery*, 121(1-2), pp. 60–4.

Effenberger, H., Ramsauer, T., Böhm, G., Hilzensauer, G., Dorn, U. and Lintner, F. (2002) 'Successful hip arthroplasty using cementless titanium implants in rheumatoid arthritis.', *Archives of orthopaedic and trauma surgery*, 122(2), pp. 80–7. doi: 10.1007/s004020100320.

Eingartner, C., Volkmann, R., Winter, E., Maurer, F., Sauer, G., Weller, S. and Weise, K. (2000) 'Results of an uncemented straight femoral shaft prosthesis after 9 years of follow-up.', *The Journal of arthroplasty*, 15(4), pp. 440–7. doi: 10.1054/arth.2000.5265.

El' Sheikh, H., MacDonald, B. and Hashmi, M. (2003) 'Finite element simulation of the hip joint during stumbling: a comparison between static and dynamic loading.', *Journal of Materials Processing Technology 143FEA 144 pp, ,* pp. 249–255.

Elliott, B. and Goswami, T. (2011) 'Implant material properties and their role in micromotion and failure in total hip arthroplasty', *International Journal of Mechanics and Materials in Design*, 8(1), pp. 1–7.

Engh, C.A., Hooten, J.P., Zettl-Schaffer, K.F., Ghaffarpour, M., McGovern, T.F., Macalino, G.E. and Zicat, B.A. (1994) 'Porous-coated total hip replacement.', *Clinical orthopaedics and related research*, (298), pp. 89–96.

Engh, C.A., McGovern, T.F., Bobyn, J.D. and Harris, W.H. (1992) 'A quantitative evaluation of periprosthetic bone-remodeling after cementless total hip arthroplasty.', *The Journal of bone and joint surgery. American volume*, 74(7), pp. 1009–20.

Faizan, A., Wuestemann, T., Nevelos, J., Bastian, A.C. and Collopy, D. (2015) 'Development and verification of a cementless novel tapered wedge stem for total hip arthroplasty.', *The Journal of arthroplasty*, 30(2), pp. 235–40. doi: 10.1016/j.arth.2014.09.023.

Fatemi, A. and Socie, D. (1988) 'A critical plane approach to multiaxial fatigue damage including out-of-phase loading.', *Fatigue Fracture of Engineering Materials Structures*, 11, pp. 149–65.

Finite Element Analysis. (2014), FEA and Simulation Software-Autodesk, Available at: http://usa.autodesk.com/adsk/servlet/item?siteID=123112&id=17670721 (Accessed 26 April 2014).

Gabarre, S., Herrera, A., Ibarz, E., Mateo, J., Gil-Albarova, J., & Gracia, L. (2016) 'Comparative Analysis of the Biomechanical Behaviour of Two Cementless Short Stems for Hip Replacement: Linea Anatomic and Minihip.', *PLoS ONE*, 11(7), e0158411.

Geesink, R.G., de Groot, K. and Klein, C.P. (1988) 'Bonding of bone to apatite-coated implants.', *The Journal of bone and joint surgery. British volume*, 70(1), pp. 17–22.

Gepreel, M. and Niinomi, M. (2013) ‘Biocompatibility of Ti-Alloys for Long-Term Implantation.’, *Journal of the Mechanical Behavior of Biomedical Materials*, 20, pp. 407–415.

Gerber, H. (1874) ‘Bestimmung der zulassigen Spannungen in Eisen-konstructionen.’, *Zeitschrift des Bayerischen Architeckten und ingenieurVereins*, 6, pp. 101–10.

Giannikas, K.A., Din, R., Sadiq, S. and Dunningham, T.H. (2002) ‘Medium-term results of the ABG total hip arthroplasty in young patients.’, *The Journal of arthroplasty*, 17(2), pp. 184–8.

Gil, L., Bruhl, S., Jimenez, L., Leon, O., Guevara, R. and Staia, M. (2006) ‘Corrosion performance of the plasma nitrided 316L stainless steel.’, *Surface and Coatings Technology pp*, 201(7), pp. 4424–4429.

Gomez, P.F. and Morcuende, J.A. (2005) ‘Early attempts at hip arthroplasty--1700s to 1950s.’, *The Iowa orthopaedic journal*, 25, pp. 25–9.

Gong, H., Wu, W., Fang, J., Dong, X., Zhao, M. and Guo, T. (2012) ‘Effects of materials of cementless femoral Stem on the functional adaptation of bone.’, *Journal of Bionic Engineering pp*, 9(1), pp. 66–74.

Goodman, J. (1899) ‘Mechanics applied to engineering.’, *London Longmans Green and Co*.

Gortchacow, M., Wettstein, M., Pioletti, D.P., Müller-Gerbl, M. and Terrier, A. (2012) ‘Simultaneous and multisite measure of micromotion, subsidence and gap to evaluate femoral stem stability’, *Journal of Biomechanics*, 45(7), pp. 1232–1238

Gortz, W., Nagerl, U., Nagerl, H., M and J (2002) ‘Thomsen micromovements of uncemented femoral components after torsional loads.’, *Eng*, 124(6), pp. 706–713.

Graver, R., Deppo, L.Da., Harris, E. and Feinglass, S. (2010) ‘The total “economic cost” of primary total joint replacement surgery in the United States.’, *American Academy of Orthopaedic Surgeons Annual Meeting Proceedings*.

Grivas, T.B., Savvidou, O.D., Psarakis, S.A., Bernard, P.-F., Triantafyllopoulos, G., Kovanis, I. and Alexandropoulos, P. (2007) 'Neck fracture of a cementless forged titanium alloy femoral stem following total hip arthroplasty: a case report and review of the literature.', *Journal of medical case reports*, 1, p. 174. doi: 10.1186/1752-1947-1-174.

Griza, S., Ueki, M.M., Souza, D.H.G., Cervieri, A. and Strohaecker, T.R. (2013) 'Thermally induced strains and total shrinkage of the polymethyl-methacrylate cement in simplified models of total hip arthroplasty.', *Journal of the mechanical behavior of biomedical materials*, 18, pp. 29–36. doi: 10.1016/j.jmbbm.2012.09.018.

Gruber, F.W., Böck, A., Trattnig, S., Lintner, F. and Ritschl, P. (2007) 'Cystic lesion of the groin due to metallosis: a rare long-term complication of metal-on-metal total hip arthroplasty.', *The Journal of arthroplasty*, 22(6), pp. 923–7. doi: 10.1016/j.arth.2006.10.002.

Gruen, T.A., McNeice, G.M. and Amstutz, H.C. (1979) '"Modes of failure" of cemented stem-type femoral components: a radiographic analysis of loosening.', *Clinical orthopaedics and related research*, (141), pp. 17–27.

Han, S.-I., Lee, J.-H., Kim, J.W., Oh, C.W. and Kim, S.-Y. (2013) 'Long-term durability of the CLS femoral prosthesis in patients with osteonecrosis of the femoral head.', *The Journal of arthroplasty*, 28(5), pp. 828–31. doi: 10.1016/j.arth.2012.09.017.

Healy, W. (2002) 'Implant selection for total hip arthroplasty in elderly patients.', *Clin Orthop Relat Res*, 405, pp. 54–64.

Hearn, S.L., Bicalho, P.S., Eng, K., Booth, R.E., Hozack, W.J. and Rothman, R.H. (1995) 'Comparison of cemented and cementless total hip arthroplasty in patients with bilateral hip arthroplasties.', *The Journal of arthroplasty*, 10(5), pp. 603–8.

Heiner, A.D. (2008) 'Structural properties of fourth-generation composite femurs and tibias.', *Journal of biomechanics*, 41(15), pp. 3282–4. doi: 10.1016/j.jbiomech.2008.08.013.

Heller, M.O., Bergmann, G., Deuretzbacher, G., Dürselen, L., Pohl, M., Claes, L., Haas, N.P. and Duda, G.N. (2001) 'Musculo-skeletal loading conditions at the hip during walking and stair climbing.', *Journal of biomechanics*, 34(7), pp. 883–93.

Herrera, A., Canales, V., Anderson, J., García-Araujo, C., Murcia-Mazón, A. and Tonino, A.J. (2004) 'Seven to 10 years followup of an anatomic hip prosthesis: an international study.', *Clinical orthopaedics and related research*, (423), pp. 129–37.

Herrera, A., Panisello, J.J., Ibarz, E., Cegoñino, J., Puértolas, J.A. and Gracia, L. (2007) 'Long-term study of bone remodelling after femoral stem: a comparison between dexa and finite element simulation.', *Journal of biomechanics*, 40(16), pp. 3615–25. doi: 10.1016/j.jbiomech.2007.06.008.

Hothi, H.S., Matthies, A.K., Berber, R., Whittaker, R.K., Skinner, J.A. and Hart, A.J. (2014) 'The reliability of a scoring system for corrosion and fretting, and its relationship to material loss of tapered, modular junctions of retrieved hip implants.', *The Journal of arthroplasty*, 29(6), pp. 1313–7. doi: 10.1016/j.arth.2013.12.003.

Howard, J.L., Hui, A.J., Bourne, R.B., McCalden, R.W., MacDonald, S.J. and Rorabeck, C.H. (2004) 'A quantitative analysis of bone support comparing cementless tapered and distal fixation total hip replacements.', *The Journal of arthroplasty*, 19(3), pp. 266–73.

Hozack, W.J., Rothman, R.H., Booth, R.E. and Balderston, R.A. (1993) 'Cemented versus cementless total hip arthroplasty. A comparative study of equivalent patient populations.', *Clinical orthopaedics and related research*, (289), pp. 161–5.

Huiskes, R., Ruimerman, R., van Lenthe, G.H. and Janssen, J.D. (2000) 'Effects of mechanical forces on maintenance and adaptation of form in trabecular bone.', *Nature*, 405(6787), pp. 704–6. doi: 10.1038/35015116.

Huiskes, R., Weinans, H., Grootenboer, H.J., Dalstra, M., Fudala, B. and Slooff, T.J. (1987) 'Adaptive bone-remodeling theory applied to prosthetic-design analysis.', *Journal of biomechanics*, 20(11-12), pp. 1135–50.

Huiskes, R., Weinans, H. and van Rietbergen, B. (1992) 'The relationship between stress shielding and bone resorption around total hip stems and the effects of flexible materials.', *Clinical orthopaedics and related research*, (274), pp. 124–34.

Hwang, K.-T., Kim, Y.-H., Kim, Y.-S. and Choi, I.-Y. (2012) 'Total hip arthroplasty using cementless grit-blasted femoral component: a minimum 10-year follow-up study.', *The Journal of arthroplasty*, 27(8), pp. 1554–61. doi: 10.1016/j.arth.2012.02.005.

Iguchi, H., Mitsui, H., Murakami, S., Watanabe, N., Tawada, K., Nozaki, M., Goto, H., Kobayashi, M. and Otsuka, T. (2013) 'Has the Lateral Flare Short Stem Improved Proximal Fit Than the Standard Lateral Flare Stem', *Bone & Joint Journal Orthopaedic Proceedings*, 95-B(SUPP 34), p. 81.

Jasty, M., Maloney, W.J., Bragdon, C.R., O'Connor, D.O., Haire, T. and Harris, W.H. (1991) 'The initiation of failure in cemented femoral components of hip arthroplasties.', *The Journal of bone and joint surgery. British volume*, 73(4), pp. 551–8.

Jauch, S.Y., Huber, G., Haschke, H., Sellenschloh, K. and Morlock, M.M. (2014) 'Design parameters and the material coupling are decisive for the micromotion magnitude at the stem–neck interface of bi-modular hip implants', *Medical Engineering & Physics*, 36(3), pp. 300–307.

Kadir, A.M. and Hansen, U. (2007) 'The effect of physiological load configuration on interface micromotion in cementless femoral stems.', *Jurnal Mekanikal*, 23, pp. 50–61.

Kadir, A.M., Hansen, U., Hansen, U., Klabunde, R., Lucas, D. and Amis, A. (2008) 'Finite element modeling of primary hip step stability: the effect of interference fit.', *J Biomech*, 41, pp. 587–594.

Kai, C., Dekun, Z., Gaofeng, Z., Tianqing, H. and Shirong, G. (2014) 'Research on the torsional fretting behavior of the head-neck interface of artificial hip joint, Materials & Design; .', 56, pp. 914–922.

Kang, J.S., Dorr, L.D. and Wan, Z. (2000) 'The effect of diaphyseal biologic fixation on clinical results and fixation of the APR-II stem.', *The Journal of arthroplasty*, 15(6), pp. 730–5. doi: 10.1054/arth.2000.9057.

Karachalios, T., Tsatsaronis, C., Efraimis, G., Papadelis, P., Lyritis, G. and Diakoumopoulos, G. (2004) 'The long-term clinical relevance of calcar atrophy caused by stress shielding in

total hip arthroplasty: a 10-year, prospective, randomized study.', *The Journal of arthroplasty*, 19(4), pp. 469–75.

Karrholm, J., Anderberg, C., Snorrason, F., Thanner, J., Langeland, N., Malchau, H., Herberts (2002) 'Evaluation of a femoral stem with reduced stiffness. A randomized study with use of radiostereometry and bone densitometry.', *Journal of Bone Joint Surg Am 84A9*, , pp. 1651–1658.

Katoozian, H. and Davy, D.T. (2000) 'Effects of loading conditions and objective function on three-dimensional shape optimization of femoral components of hip endoprostheses.', *Medical engineering & physics*, 22(4), pp. 243–51.

Katsuthashi, B., Kiyoshi, S. (1992) 'Artificial Joint.', *US Patent 5092898/ 0303*.

Kavanaugh, B., Wallrichs, S., Dewitz, M., Berry, D., Currier, B., Ilstrup, D. and Coventry, M. (1994) 'Charnley low-friction arthroplasty of the hip: Twenty-year results with cement.', *The Journal of Arthroplasty pp*, 9(3), pp. 229–234.

Keisu, K.S., Orozco, F., McCallum, J.D., Bissett, G., Hozack, W.J., Sharkey, P.F. and Rothman, R.H. (2001) 'Cementless femoral fixation in the rheumatoid patient undergoing total hip arthroplasty: minimum 5-year results.', *The Journal of arthroplasty*, 16(4), pp. 415–21. doi: 10.1054/arth.2001.23506.

Kharmanda, G. (2016) 'Integration of multi-objective structural optimization into cementless hip prosthesis design: Improved Austin-Moore model.', *Computer methods in biomechanics and biomedical engineering*, 19(14), pp. 1557–66. doi: 10.1080/10255842.2016.1170121.

Kim, Y.-H., Oh, S.-H. and Kim, J.-S. (2003) 'Primary total hip arthroplasty with a second-generation cementless total hip prosthesis in patients younger than fifty years of age.', *The Journal of bone and joint surgery. American volume*, 85-A(1), pp. 109–14.

Kishida, Y., Sugano, N., Nishii, T., Miki, H., Yamaguchi, K. and Yoshikawa, H. (2004) 'Preservation of the bone mineral density of the femur after surface replacement of the hip.', *The Journal of bone and joint surgery. British volume*, 86(2), pp. 185–9.

Krismer, M., Biedermann, R., Stöckl, B., Fischer, M., Bauer, R. and Haid, C. (1999) 'The prediction of failure of the stem in THR by measurement of early migration using EBRA-FCA. Einzel-Bild-Roentgen-Analyse-femoral component analysis.', *The Journal of bone and joint surgery. British volume*, 81(2), pp. 273–80.

Kröger, H., Venesmaa, P., Jurvelin, J., Miettinen, H., Suomalainen, O. and Alhava, E. (1998) 'Bone density at the proximal femur after total hip arthroplasty.', *Clinical orthopaedics and related research*, (352), pp. 66–74.

Kuiper, J.H. and Huiskes, R. (1997) 'Mathematical optimization of elastic properties: application to cementless hip stem design.', *Journal of biomechanical engineering*, 119(2), pp. 166–74.

Kurtz, S., Ong, K., Lau, E., Mowat, F. and Halpern, M. (2007) 'Projections of primary and revision hip and knee arthroplasty in the United States from 2005 to 2030.', *The Journal of bone and joint surgery. American volume*, 89(4), pp. 780–5. doi: 10.2106/JBJS.F.00222.

Laine, H.J., Puolakka, T.J., Moilanen, T., Pajamäki, K.J., Wirta, J. and Lehto, M.U. (2000) 'The effects of cementless femoral stem shape and proximal surface texture on "fit-and-fill" characteristics and on bone remodeling.', *International orthopaedics*, 24(4), pp. 184–90.

Langton, D.J., Sidaginamale, R., Lord, J.K., Nargol, A.V.F. and Joyce, T.J. (2012) 'Taper junction failure in large-diameter metal-on-metal bearings.', *Bone & joint research*, 1(4), pp. 56–63. doi: 10.1302/2046-3758.14.2000047.

Latham, B. and Goswami, T. (2004) 'Effect of geometric parameters in the design of hip implants paper IV.', *Mater Des*, 25(8), pp. 715–22.

Lattanzi, R., Grazi, E., Testi, D., Viceconti, M., Cappello, A. and Toni, A. (2003) 'Accuracy and repeatability of cementless total hip replacement surgery in patients with deformed anatomies.', *Medical informatics and the Internet in medicine*, 28(1), pp. 59–71. doi: 10.1080/1463923031000124128.

Leali, A., Fetto, J., Insler, H. and Elfenbein, D. (2002) 'The effect of a lateral flare feature on implant stability.', *International orthopaedics*, 26(3), pp. 166–9. doi: 10.1007/s00264-002-0355-3.

Learmonth, I.D., Young, C. and Rorabeck, C. (2007) 'The operation of the century: total hip replacement.', *Lancet (London, England)*, 370(9597), pp. 1508–19. doi: 10.1016/S0140-6736(07)60457-7.

Lengsfeld, M., Bassaly, A., Boudriot, U., Pressel, T. and Griss, P. (2000) 'Size and direction of hip joint forces associated with various positions of the acetabulum.', *The Journal of arthroplasty*, 15(3), pp. 314–20.

Levadnyi, I., Awrejcewicz, J., Goethel, M., and Loskutov, A. (2017) 'Influence of the fixation region of a press–fit hip endoprosthesis on the stress–strain state of the "bone–implant" system.', *Computers in biology and medicine*, 84, pp 195-204.

Lewis, C.L. and Sahrmann, S.A. (2015) 'Effect of posture on hip angles and moments during gait.', *Manual therapy*, 20(1), pp. 176–82. doi: 10.1016/j.math.2014.08.007.

Mai, K.T., Verioti, C.A., Casey, K., Slesarenko, Y., Romeo, L. and Colwell, C.W. (2010) 'Cementless femoral fixation in total hip arthroplasty.', *American journal of orthopedics (Belle Mead, N.J.)*, 39(3), pp. 126–30.

Mallory, T.H., Lombardi, A.V., Leith, J.R., Fujita, H., Hartman, J.F., Capps, S.G., Kefauver, C.A., Adams, J.B. and Vorys, G.C. (2001) 'Minimal 10-year results of a tapered cementless femoral component in total hip arthroplasty.', *The Journal of arthroplasty*, 16(8 Suppl 1), pp. 49–54.

Maloney, W.J., Jasty, M., Burke, D.W., O'Connor, D.O., Zalenski, E.B., Bragdon, C. and Harris, W.H. (1989) 'Biomechanical and histologic investigation of cemented total hip arthroplasties. A study of autopsy-retrieved femurs after in vivo cycling.', *Clinical orthopaedics and related research*, (249), pp. 129–40.

Mandell, J.A., Carter, D.R., Goodman, S.B., Schurman, D.J. and Beaupré, G.S. (2004) 'A conical-collared intramedullary stem can improve stress transfer and limit micromotion.', *Clinical biomechanics (Bristol, Avon)*, 19(7), pp. 695–703. doi: 10.1016/j.clinbiomech.2004.04.004.

Manley, M.T., Capello, W.N., D'Antonio, J.A., Edidin, A.A. and Geesink, R.G. (1998) 'Fixation of acetabular cups without cement in total hip arthroplasty. A comparison of three different implant surfaces at a minimum duration of follow-up of five years.', *The Journal of bone and joint surgery. American volume*, 80(8), pp. 1175–85.

Martelli, S., Calvetti, D., Somersalo, E., Viceconti, M. and Taddei, F. (2013) 'Computational tools for calculating alternative muscle force patterns during motion: a comparison of possible solutions.', *Journal of biomechanics*, 46(12), pp. 2097–100. doi: 10.1016/j.jbiomech.2013.05.023.

Marti, A. (2000) 'Cobalt-base alloys used in bone surgery.', *Injury*, 31 Suppl 4, pp. 18–21.

Mathias, K.J., Leahy, J.C., Heaton, A., Deans, W.F. and Hukins, D.W. (1998) 'Hip joint prosthesis design: effect of stem introducers.', *Medical engineering & physics*, 20(8), pp. 620–4.

McCarthy, J.J., Noonan, K.J., Nemke, B. and Markel, M. (2010) 'Guided growth of the proximal Femur: A Pilot Study in the Lamb Model.', *Journal of Pediatric Orthopaedics*, 30(7), pp. 690–694.

McKee, G.K. and Watson-Farrar, J. (1966) 'Replacement of arthritic hips by the McKee-Farrar prosthesis.', *The Journal of bone and joint surgery. British volume*, 48(2), pp. 245–59.

Meftah, M., John, M., Lendhey, M., Khaimov, A., Ranawat, A.S. and Ranawat, C.S. (2013) 'Safety and efficacy of non-cemented femoral fixation in patients 75 years of age and older.', *The Journal of arthroplasty*, 28(8), pp. 1378–80. doi: 10.1016/j.arth.2012.11.007.

Melvin, J.S., Karthikeyan, T., Cope, R. and Fehring, T.K. (2014) 'Early failures in total hip arthroplasty -- a changing paradigm.', *The Journal of arthroplasty*, 29(6), pp. 1285–8. doi: 10.1016/j.arth.2013.12.024.

Molt, M. and Toksvig-Larsen, S. (2015) '2-year follow-up report on micromotion of a short tibia stem', *Acta Orthopaedica*, 86(5), pp. 594–598.

Mont, M.A., Yoon, T.R., Krackow, K.A. and Hungerford, D.S. (1999) 'Clinical experience with a proximally porous-coated second-generation cementless total hip prosthesis: minimum 5-year follow-up.', *The Journal of arthroplasty*, 14(8), pp. 930–9.

Morlock, M., Schneider, E., Bluhm, A., Vollmer, M., Bergmann, G., Müller, V. and Honl, M. (2001) 'Duration and frequency of every day activities in total hip patients.', *Journal of biomechanics*, 34(7), pp. 873–81.

Morrow, J. (1968) 'Fatigue design handbook-Advances in Engineering.', *Warrendale PA Society of Automotive Engineers pp*, , pp. 21–9.

Morscher, E.W., Widmer, K.H., Bereiter, H., Elke, R. and Schenk, R. (2002) 'Cementless socket fixation based on the "press-fit" concept in total hip joint arthroplasty.', *Acta chirurgiae orthopaedicae et traumatologiae Cechoslovaca*, 69(1), pp. 8–15.

Nakahara, I., Takao, M., Bandoh, S., Bertollo, N., Walsh, W.R. and Sugano, N. (2013) 'In vivo implant fixation of carbon fiber-reinforced PEEK hip prostheses in an ovine model.', *Journal of orthopaedic research : official publication of the Orthopaedic Research Society*, 31(3), pp. 485–92. doi: 10.1002/jor.22251.

Nercessian, O.A., Wu, W.H. and Sarkissian, H. (2001) 'Clinical and radiographic results of cementless AML total hip arthroplasty in young patients.', *The Journal of arthroplasty*, 16(3), pp. 312–6. doi: 10.1054/arth.2001.21503.

Niinomi, M. (2008) 'Mechanical biocompatibilities of titanium alloys for biomedical applications.', *Journal of the mechanical behavior of biomedical materials*, 1(1), pp. 30–42. doi: 10.1016/j.jmbbm.2007.07.001.

Niinomi, M. and ls Transactions, A. (2002) 'Recent metallic materials for biomedical applications.', *Metallurgical and Materia pp*, 33(3), pp. 477–486.

National Joint Registry. (2015), 12th Annual Registry for England, Wales and Northern Ireland, [Online] Available at: http://www.njrcentre.org.uk (Accessed 21 Sep 2015).

Oshkour, A., Osman, A.A., Bayat, M., Afshar, R. and Berto, F. (2014) 'Three-dimensional finite element analyses of functionally graded femoral prostheses with different geometrical configurations.', *Materials Design*, 56, pp. 998–1008.

Pancanti, A., Bernakiewicz, M. and Viceconti, M. (2003) 'The primary stability of a cementless stem varies between subjects as much as between activities.', *Journal of biomechanics*, 36(6), pp. 777–85.

Papini, M., Zdero, R., Schemitsch, E.H. and Zalzal, P. (2007) 'The biomechanics of human femurs in axial and torsional loading: comparison of finite element analysis, human cadaveric femurs, and synthetic femurs.', *Journal of biomechanical engineering*, 129(1), pp. 12–9. doi: 10.1115/1.2401178.

Park, M.-S., Choi, B.-W., Kim, S.-J. and Park, J.-H. (2003) 'Plasma spray-coated Ti femoral component for cementless total hip arthroplasty.', *The Journal of arthroplasty*, 18(5), pp. 626–30.

Park, Y., Choi, D., Hwang, D. and Yoon, Y. (2009) 'Statistical analysis of interfacial gap in cementless stem FE model.', *J Biomed Eng*, 131, pp. 1–8.

Parvizi, J., Keisu, K.S., Hozack, W.J., Sharkey, P.F. and Rothman, R.H. (2004) 'Primary total hip arthroplasty with an uncemented femoral component: a long-term study of the Taperloc stem.', *The Journal of arthroplasty*, 19(2), pp. 151–6.

Patton, K.T. (2015) *Anatomy and physiology*. 9th edn. Philadelphia, PA, United States: Mosby.

Phillips, T.W., Messieh, S.S. and McDonald, P.D. (1990) 'Femoral stem fixation in hip replacement. A biomechanical comparison of cementless and cemented prostheses.', *The Journal of bone and joint surgery. British volume*, 72(3), pp. 431–4.

Pieringer, H., Auersperg, V., Griessler, W. and Böhler, N. (2003) 'Long-term results with the cementless Alloclassic brand hip arthroplasty system.', *The Journal of arthroplasty*, 18(3), pp. 321–8. doi: 10.1054/arth.2003.50045.

Pilliar, R.M., Lee, J.M. and Maniatopoulos, C. (1986) 'Observations on the effect of movement on bone ingrowth into porous-surfaced implants.', *Clinical orthopaedics and related research*, (208), pp. 108–13.

Ploeg, H., Bürgi, M. and Wyss, U. (2009) 'Hip stem fatigue test prediction.', *International Journal of Fatigue*, 31(5), pp.894-905.

Pompe, W., Worch, H., Epple, M., Friess, W., Gelinsky, M., Greil, P., Hempel, U., Scharnweber, D. and Schulte, K. (2003) 'Functionally graded materials for biomedical applications.', *Materials Science and Engineering A 362 pp4060*, pp. 1–2.

Pugh, S. (1990) 'Total design: Integrated methods for successful product engineering.', *1st ed., Essex: Pearson Education Limited*.

Pyburn, E. and Goswami, T. (2004) 'Finite element analysis of femoral components paper III hip joints.', *Mater Des*, 25(8), pp. 705–13.

Reddy, J. (2004). *An introduction to the finite element method*. 1st ed. Boston: McGraw-Hill.

Reese, N. and Bandy, W. (2016) 'Joint range of motion and muscle length testing.', *3rd edn United States Saunders*.

Reggiani, B., Cristofolini, L., Taddei, F. and Viceconti, M. (2008) 'Sensitivity of the primary stability of a cementless hip stem to its position and orientation.', *Artificial organs*, 32(7), pp. 555–60. doi: 10.1111/j.1525-1594.2008.00577.x.

Reilly, D.T. and Burstein, A.H. (1975) 'The elastic and ultimate properties of compact bone tissue.', *Journal of biomechanics*, 8(6), pp. 393–405.

Reimeringer, M., Nuño, N. (2014) 'Effect of femoral mechanical properties on primary stability of cementless total hip arthroplasty: a finite element analysis.', *Adv Biomech Appl*, 1(3), pp. 187–210.

Reimeringer, M., Nuño, N. (2016) ‘The influence of contact ratio and its location on the primary stability of cementless total hip arthroplasty: A finite element analysis.’,*Journal of Biomechanics*, 49(7), pp. 1064–70.

Reimeringer, M., Nuño, N., Desmarais-Trépanier, C., Lavigne, M. and Vendittoli, P.A. (2013) ‘The influence of uncemented femoral stem length and design on its primary stability: a finite element analysis.’, *Computer methods in biomechanics and biomedical engineering*, 16(11), pp. 1221–31. doi: 10.1080/10255842.2012.662677.

Renkawitz, T., Santori, F.S., Grifka, J., Valverde, C., Morlock, M.M. and Learmonth, I.D. (2008) ‘A new short uncemented, proximally fixed anatomic femoral implant with a prominent lateral flare: design rationals and study design of an international clinical trial.’, *BMC musculoskeletal disorders*, 9, p. 147. doi: 10.1186/1471-2474-9-147.

Richards, C.J., Duncan, C.P., Masri, B.A. and Garbuz, D.S. (2010) ‘Femoral revision hip Arthroplasty: A comparison of Two stem designs’, *Clinical Orthopaedics and Related Research®*, 468(2), pp. 491–496.

Rietbergen, B. and Huiskes, R. (2001) ‘Load transfer and stress shielding of the hydroxyapatite ABG hip: a study of stem length and proximal fixation.’, 16(8, Suppl 1), pp. 55–63.

Ring, P.A. (1968) ‘Complete replacement arthroplasty of the hip by the ring prosthesis.’, *The Journal of bone and joint surgery. British volume*, 50(4), pp. 720–31.

Rogers, A., Kulkarni, R. and Downes, E.M. (2003) ‘The ABG hydroxyapatite-coated hip prosthesis: one hundred consecutive operations with average 6-year follow-up.’, *The Journal of arthroplasty*, 18(5), pp. 619–25.

Rohlmann, A., Cheal, E.J., Hayes, W.C. and Bergmann, G. (1988) ‘A nonlinear finite element analysis of interface conditions in porous coated hip endoprostheses.’, *Journal of biomechanics*, 21(7), pp. 605–11.

Sadeghi-Mehr, M. (1997) ‘Investigations of Rolling Element Bearing for Hip Joint Prosthesis.’, *Phd Imperial College of Science, Technology and Medicine University, London.*

Sadoghi, P., Janda, W., Agreiter, M., Rauf, R., Leithner, A. and Labek, G. (2013) 'Pooled outcome of total hip arthroplasty with the CementLess Spotorno (CLS) system: A comparative analysis of clinical studies and worldwide arthroplasty register data', *International Orthopaedics*, 37(6), pp. 995–999.

Sawbone. (2016), [Online] Available at: http://bit.ly/1GhCwwJ (Accessed on Jan 2016).

Schmidt, R., Muller, L., Kress, A., Hirschfelder, H., Aplas, A. and Pitto, R.P. (2002) 'A computed tomography assessment of femoral and acetabular bone changes after total hip arthroplasty.', *International orthopaedics*, 26(5), pp. 299–302. doi: 10.1007/s00264-002-0377-x.

Schneider, E., Kinast, C., Eulenberger, J., Wyder, D., Eskilsson, G. and Perren, S.M. (1989) 'A comparative study of the initial stability of cementless hip prostheses.', *Clinical orthopaedics and related research*, (248), pp. 200–9.

Schreiner, U., Scheller, G., Herbig, J. and Jani, L. (2001) 'Mid-term results of the cementless CLS stem. A 7- to 11-year follow-up study.', *Archives of orthopaedic and trauma surgery*, 121(6), pp. 321–4.

Schwerter, K., Meyenberg, A., Sander, K., Layher, F. and Roth, A. (2013) '[15-year results following implantation of a stem type AML hip prosthesis]', 151(3), pp. 231–238. doi: 10.1055/s-0032-1328495.

Senalp, A., Kayabasi, O. and Kurtaran, H. (2007) 'Static, dynamic and fatigue behavior of newly designed stem shapes for hip prosthesis using finite element analysis.', *Mater Des*, 28(5), pp. 1577–83.

Shah, S.J., Bougherara, H., Schemitsch, E.H., & Zdero, R. (2012) 'Biomechanical stress maps of an artificial femur obtained using a new infrared thermography technique validated by strain gages.' *Medical engineering & physics*, 34 10, 1496-502.

Shaik, S., Bose, K. and Cherukuri, H. (2012) 'A study of durability of hip implants.', *Materials Design*, 42, pp. 230–237.

Shivaswamy, S. (2010). *Finite element analysis and programming*. 1st ed. Oxford: Alpha Science.

Silva, M., Shepherd, E.F., Jackson, W.O., Dorey, F.J. and Schmalzried, T.P. (2002) 'Average patient walking activity approaches 2 million cycles per year: pedometers under-record walking activity.', *The Journal of arthroplasty*, 17(6), pp. 693–7.

Simões, J.A. and Marques, A.T. (2005) 'Design of a composite hip femoral prosthesis', *Materials & Design*, 26(5), pp. 391–401. doi: 10.1016/j.matdes.2004.07.024.

Simões, J., Vaz, M., Blatcher, S. and Taylor, M. (2000) 'Influence of head constraint and muscle forces on the strain distribution within the intact femur', *Medical Engineering and Physics*, 22, pp. 453–459.

Singh, S. (2014) 'Analysis of Femoral Components of Cemented Total Hip-Arthroplasty.', *Indian Institute of Technology p 3*.

Skedros, J. and Baucom, S. (2007) 'Mathematical analysis of trabecular 'trajectories' in apparent trajectorial structures: The unfortunate historical emphasis on the human proximal femur.', *Journal of Theoretical Biology, 244(1), pp.15-45.*

Smith, K.N., Watson, P. and Topper, T.H. (1970) 'A stress-strain function for the fatigue of metals.', *Journal of materials*, 15, pp. 767–78.

Smith, S.W., Estok, D.M. and Harris, W.H. (1998) 'Total hip arthroplasty with use of second-generation cementing techniques. An eighteen-year-average follow-up study.', *The Journal of bone and joint surgery. American volume*, 80(11), pp. 1632–40.

Soderberg, C. (1939) 'Factor of safety and working stress.', *Transactions of ASME*, 52, pp. 13–28.

Sotereanos, N.G., Sauber, T.J. and Tupis, T.T. (2013) 'Modular femoral neck fracture after primary total hip arthroplasty.', *The Journal of arthroplasty*, 28(1), p. 196.e7 – 9. doi: 10.1016/j.arth.2012.03.050.

Sowmianarayanan, S., Chandrasekaran, A., Krishnakumar, R. and International, A. (2013) 'Finite element analysis of proximal femur nail for subtrochanteric fractured femur.', International ANSYS conference proceedings 2006; [Online] Available at: http://bit.ly/1wvmtSh (Accessed on Aug 2013).

Speirs, A.D., Slomczykowski, M.A., Orr, T.E., Siebenrock, K. and Nolte, L.P. (2000) 'Three-dimensional measurement of cemented femoral stem stability: an in vitro cadaver study.', *Clinical biomechanics (Bristol, Avon)*, 15(4), pp. 248–55.

Sporer, S. and Paprosky, W. (2006) '(iii) Cementless femoral revision: The role of monoblock versus modular stems.', *Current Orthopaedics pp*, 20(3), pp. 171–178.

Stansfield, B.W. and Nicol, A.C. (2002) 'Hip joint contact forces in normal subjects and subjects with total hip prostheses: walking and stair and ramp negotiation.', *Clinical biomechanics (Bristol, Avon)*, 17(2), pp. 130–9.

Stiehl, J.B. (2009) 'Long-term periprosthetic remodeling in THA shows structural preservation.', *Clinical orthopaedics and related research*, 467(9), pp. 2356–61. doi: 10.1007/s11999-009-0722-0.

Stone, M.H., Wilkinson, R. and Stother, I.G. (1989) 'Some factors affecting the strength of the cement-metal interface.', *The Journal of bone and joint surgery. British volume*, 71(2), pp. 217–21.

Stryker. (2016) 'Exeter cemented hip joint implant design.', [Online] Available at: http://www.stryker.com (Accessed 2 Feb 2016).

Sugiyama, H., Whiteside, L.A., Engh, C.A. and Otani, T. (1994) 'Late mechanical stability of the proximal coated AML prosthesis.', *Orthopedics*, 17(7), pp. 583–8.

Sumner, D.R., Turner, T.M., Igloria, R., Urban, R.M. and Galante, J.O. (1998) 'Functional adaptation and ingrowth of bone vary as a function of hip implant stiffness.', *Journal of biomechanics,* 31(10), pp. 909–17.

Swedish NJR. (2014), Annual Report of Swedish Hip Arthroplasty Register, [Online] Available at: www.shpr.se/Libraries/Documents/Annual_Report_2014_Eng.sflb.ashx (Accessed Nov 2014).

Sychterz, C.J., Claus, A.M. and Engh, C.A. (2002) 'What we have learned about long-term cementless fixation from autopsy retrievals.', *Clinical orthopaedics and related research,* (405), pp. 79–91.

Szolwinski, M. and Farris, T. (1998) 'Observation, analysis and prediction of fretting fatigue in aluminum alloy.', *Wear 2436,* 221, pp. 2024–T351.

Tanner, K.E., Yettram, A.L., Loeffler, M., Goodier, W.D., Freeman, M.A. and Bonfield, W. (1995) 'Is stem length important in uncemented endoprostheses?', *Medical engineering & physics,* 17(4), pp. 291–6.

Tarala, M., Janssen, D. and Verdonschot, N. (2011) 'Balancing incompatible endoprosthetic design goals: A combined ingrowth and bone remodeling simulation.', *Medical engineering & physics,* 33(3), pp. 374-380. . doi: 10.1016/j.medengphy.2010.11.005.

Tarala, M., Janssen, D. and Verdonschot, N. (2013) 'Toward a method to simulate the process of bone ingrowth in cementless THA using finite element method.', *Medical engineering & physics,* 35(4), pp. 543–8. doi: 10.1016/j.medengphy.2012.10.010.

Theodorou, E.G., Provatidis, C.G., Babis, G.C., Georgiou, C.S. and Megas, P.D. (2011) 'Large diameter femoral heads impose significant alterations on the strains developed on femoral component and bone: a finite element analysis.', *The open orthopaedics journal,* 5, pp. 229–38. doi: 10.2174/1874325001105010229.

Tuke, P.W., Parry, R.P. and Appleton, H. (2010) 'Parvovirus PARV4 visualization and detection.', *The Journal of general virology,* 91(Pt 2), pp. 541–4. doi: 10.1099/vir.0.014852-0.

Turner, C.H., Cowin, S.C., Rho, J.Y., Ashman, R.B. and Rice, J.C. (1990) 'The fabric dependence of the orthotropic elastic constants of cancellous bone.', *Journal of biomechanics*, 23(6), pp. 549–61.

Tóth, K., Mécs, L. and Kellermann, P. (2010) 'Early experience with the Depuy Proxima short stem in total hip arthroplasty.', *Acta orthopaedica Belgica*, 76(5), pp. 613–8.

University of Victoria. (2014), Introduction to finite element analysis (FEA) or finite element method (FEM), [Online] Available at: http://www.engr.uvic.ca/~mech410/lectures/FEA_Theory.pdf (Accessed May 2014).

Viceconti, M., Brusi, G., Pancanti, A. and Cristofolini, L. (2006) 'Primary stability of an anatomical cementless hip stem: a statistical analysis.', *Journal of biomechanics*, 39(7), pp. 1169–79. doi: 10.1016/j.jbiomech.2005.03.024.

Viceconti, M., Monti, L., Muccini, R., Bernakiewicz, M. and Toni, A. (2001) 'Even a thin layer of soft tissue may compromise the primary stability of cementless hip stems.', *Clinical biomechanics (Bristol, Avon)*, 16(9), pp. 765–75.

Viceconti, M., Muccini, R., Bernakiewicz, M., Baleani, M. and Cristofolini, L. (2000) 'Large-sliding contact elements accurately predict levels of bone-implant micromotion relevant to osseointegration.', *Journal of biomechanics*, 33(12), pp. 1611–8.

Viceconti, M., Pancanti, A., Varini, E., Traina, F. and Cristofolini, L. (2006) 'On the biomechanical stability of cementless straight conical hip stems.', *Proceedings of the Institution of Mechanical Engineers. Part H, Journal of engineering in medicine*, 220(3), pp. 473–80.

Wang, X., Wang, T., Jiang, F. and Duan, Y. (2005) 'The hip stress level analysis for human routine activities.', *Biomed Eng Appl Basis Commun*, 17(3), pp. 43–48.

Weidenhielm, L.R., Mikhail, W.E., Nelissen, R.G. and Bauer, T.W. (1995) 'Cemented collarless (Exeter-CPT) versus cementless collarless (PCA) femoral components. A 2- to 14-year follow-up evaluation.', *The Journal of arthroplasty*, 10(5), pp. 592–7.

Weinans, H., Huiskes, R. and Grootenboer, H.J. (1992) ‘The behavior of adaptive bone-remodeling simulation models.’, *Journal of biomechanics*, 25(12), pp. 1425–41.

Wiles, P. (1958) ‘The surgery of the osteoarthritic hip.’, *British Journal of Surgery pp*, 45, pp. 488–497.

Wirth, A.J., Goldhahn, J., Flaig, C., Arbenz, P., Müller, R. and van Lenthe, G.H. (2011) ‘Implant stability is affected by local bone microstructural quality.’, *Bone*, 49(3), pp. 473–8. doi: 10.1016/j.bone.2011.05.001.

Wolff, J., Carl, P. and Crawford, M.E. (1892) ‘Epidural buprenorphine for postoperative analgesia. A controlled comparison with epidural morphine.’, *Anaesthesia*, 41(1), pp. 76–9.

Woolson, S.T. and Adler, N.S. (2002) ‘The effect of partial or full weight bearing ambulation after cementless total hip arthroplasty.’, *The Journal of arthroplasty*, 17(7), pp. 820–5.

Yan, W., Berthe, J. and Wen, C. (2011) ‘Numerical investigation of the effect of porous titanium femoral prosthesis on bone remodeling.’, *Materials & Design*, 32(4), pp. 1776–82.

Yildiz, H., Chang, F.K. and Goodman, S. (1998) ‘Composite hip prosthesis design. II. Simulation.’, *Journal of biomedical materials research*, 39(1), pp. 102–19.

Yildiz, H., Ha, S.K. and Chang, F.K. (1998) ‘Composite hip prosthesis design. I. Analysis.’, *Journal of biomedical materials research*, 39(1), pp. 92–101.

Zdero, R., Olsen, M., Bougherara, H. and Schemitsch, E.H. (2008) ‘Cancellous bone screw purchase: a comparison of synthetic femurs, human femurs, and finite element analysis.’, *Proceedings of the Institution of Mechanical Engineers. Part H, Journal of engineering in medicine*, 222(8), pp. 1175–83.

Zhang, T., Harrison, N.M., McDonnell, P.F., McHugh, P.E. and Leen, S.B. (2013) ‘A finite element methodology for wear–fatigue analysis for modular hip implants’, *Tribology International*, 65, pp. 113–127. doi: 10.1016/j.triboint.2013.02.016.

Appendix A

Formulas:

1. The number of cycles that will fail the hip implant.

$$(2N_f)^b = \left(\frac{\sigma_a}{\acute{\sigma_f} - \sigma_m}\right)$$

2. The Pearson linear correlation coefficient

$$r = \frac{n\sum xy - \left(\sum x\right)\left(\sum y\right)}{\sqrt{n\left(\sum x^2\right) - \left(\sum x\right)^2}\sqrt{n\left(\sum y^2\right) - \left(\sum y\right)^2}}$$

3. The stress value equation:

Strain values: $e_1 = 153 \times 10^{-6}$ $e_2 = 75 \times 10^{-6}$

Young's modulus: $E = 16.7 \times 10^{9}$

Poisson's ratio $\upsilon = 0.3$

Stress value: $$\sigma = \frac{E}{2}\left[\frac{e1 + e3}{1-\upsilon} + \frac{1}{1+\upsilon}\sqrt{(e1 + e3)^2 + (2e2 - e1 - e3)^2}\right]$$

4. Estimation of the error:

$$\frac{\text{Biggest value} - \text{Smallest value}}{\text{Biggest value}} \times 100$$

5. Trigonometric equations for three angles

$$F_x = F\cos(\alpha_x)$$
$$F_y = F\cos(\alpha_y)$$
$$F_z = F\cos(\alpha_z)$$

$$F_x = F\cos(\gamma)\cos(\beta)$$
$$F_y = F\cos(\gamma)\sin(\beta)$$
$$F_z = F\sin(\gamma)$$

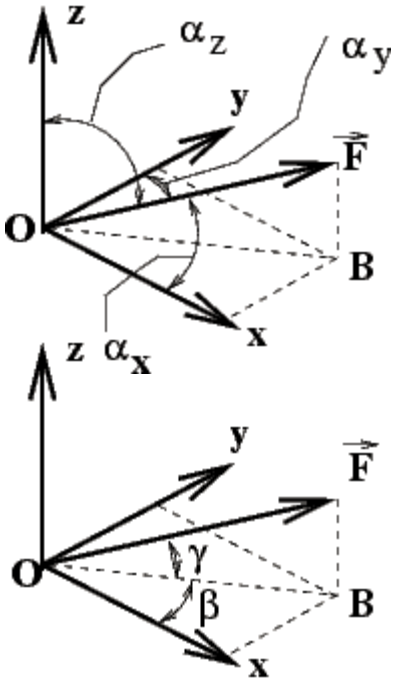

Tan α/cosβ =COT ɣ

ɣ =Arccotangent (Tan α/cosβ)

Appendix B

Data of nine different activities of daily living for dynamic loading analysis (Bergman et al. 2001)

Flexion and Abduction Angle, Femur System Relative to Pelvis System

Subject: Average Patient
Activity: Slow Walking WS
Trial number: 0

Time[s]	Flexion[deg]	Abduction[deg]	Meas. #	%Cycle	felx (z)	abd (x)
0	27.94	1.999	1	0	-201.475	14.99928
0.006	27.72	1.884	2	0.5	-200.015	14.13671
0.013	27.51	1.77	3	1	-198.618	13.28159
0.019	27.29	1.652	4	1.5	-197.153	12.3964
0.025	27.03	1.511	5	2	-195.416	11.33861
0.031	26.76	1.361	6	2.5	-193.609	10.21323
0.038	26.48	1.206	7	3	-191.731	9.05026
0.044	26.18	1.035	8	3.5	-189.713	7.767165
0.05	25.86	0.848	9	4	-187.555	6.363936
0.056	25.53	0.6534	10	4.5	-185.323	4.903606
0.062	25.18	0.447	11	5	-182.949	3.354663
0.069	24.82	0.2241	12	5.5	-180.501	1.681847
0.075	24.44	-0.0092	13	6	-177.908	-0.06905
0.081	24.06	-0.2542	14	6.5	-175.308	-1.90774
0.087	23.66	-0.5094	15	7	-172.563	-3.82295
0.094	23.25	-0.7776	16	7.5	-169.74	-5.83564
0.1	22.83	-1.055	17	8	-166.839	-7.91724
0.106	22.41	-1.339	18	8.5	-163.93	-10.0482
0.112	21.97	-1.636	19	9	-160.872	-12.2764
0.119	21.52	-1.941	20	9.5	-157.735	-14.5643
0.125	21.07	-2.25	21	10	-154.589	-16.8817
0.131	20.61	-2.566	22	10.5	-151.362	-19.2512
0.137	20.15	-2.888	23	11	-148.126	-21.665
0.144	19.68	-3.213	24	11.5	-144.81	-24.1007
0.15	19.2	-3.54	25	12	-141.413	-26.5505
0.156	18.72	-3.868	26	12.5	-138.006	-29.007
0.162	18.24	-4.196	27	13	-134.589	-31.4625
0.169	17.75	-4.522	28	13.5	-131.092	-33.902
0.175	17.26	-4.843	29	14	-127.585	-36.303
0.181	16.77	-5.161	30	14.5	-124.068	-38.6805
0.187	16.28	-5.475	31	15	-120.543	-41.0269
0.193	15.79	-5.779	32	15.5	-117.008	-43.2974
0.2	15.29	-6.075	33	16	-113.393	-45.507
0.206	14.8	-6.362	34	16.5	-109.842	-47.6482
0.212	14.3	-6.642	35	17	-106.21	-49.7361
0.218	13.81	-6.905	36	17.5	-102.642	-51.6961
0.225	13.32	-7.158	37	18	-99.0675	-53.5806
0.231	12.82	-7.401	38	18.5	-95.4122	-55.3895
0.237	12.34	-7.627	39	19	-91.8963	-57.0711

0.243	11.85	-7.839	40	19.5	-88.3006	-58.6477
0.25	11.36	-8.038	41	20	-84.6984	-60.1268
0.256	10.88	-8.223	42	20.5	-81.1636	-61.5013
0.262	10.4	-8.389	43	21	-77.6232	-62.734
0.268	9.927	-8.541	44	21.5	-74.1291	-63.8624
0.275	9.451	-8.683	45	22	-70.6077	-64.916
0.281	8.984	-8.803	46	22.5	-67.1482	-65.8062
0.287	8.522	-8.906	47	23	-63.7213	-66.57
0.293	8.06	-9.002	48	23.5	-60.2903	-67.2816
0.299	7.604	-9.08	49	24	-56.9	-67.8598
0.306	7.154	-9.138	50	24.5	-53.5508	-68.2896
0.312	6.706	-9.19	51	25	-50.2131	-68.6748
0.318	6.264	-9.231	52	25.5	-46.9172	-68.9786
0.324	5.83	-9.249	53	26	-43.6782	-69.1119
0.331	5.397	-9.263	54	26.5	-40.4442	-69.2156
0.337	4.967	-9.27	55	27	-37.2302	-69.2674
0.343	4.546	-9.259	56	27.5	-34.0816	-69.186
0.35	4.131	-9.243	57	28	-30.976	-69.0675
0.356	3.717	-9.222	58	28.5	-27.8762	-68.9119
0.362	3.308	-9.193	59	29	-24.8125	-68.6971
0.368	2.905	-9.157	60	29.5	-21.7924	-68.4303
0.374	2.505	-9.119	61	30	-18.7938	-68.1488
0.381	2.112	-9.079	62	30.5	-15.8468	-67.8523
0.387	1.723	-9.033	63	31	-12.929	-67.5114
0.393	1.337	-8.986	64	31.5	-10.0332	-67.163
0.399	0.9549	-8.939	65	32	-7.16611	-66.8146
0.406	0.5784	-8.891	66	32.5	-4.34077	-66.4587
0.412	0.2094	-8.843	67	33	-1.57153	-66.1028
0.418	-0.1592	-8.797	68	33.5	1.194781	-65.7617
0.424	-0.525	-8.752	69	34	3.940026	-65.4279
0.431	-0.8823	-8.708	70	34.5	6.621326	-65.1015
0.437	-1.237	-8.667	71	35	9.28286	-64.7973
0.443	-1.589	-8.628	72	35.5	11.92378	-64.508
0.449	-1.934	-8.59	73	36	14.51175	-64.226
0.456	-2.275	-8.555	74	36.5	17.0692	-63.9663
0.462	-2.615	-8.522	75	37	19.61854	-63.7213
0.468	-2.949	-8.489	76	37.5	22.12223	-63.4764
0.474	-3.274	-8.459	77	38	24.55772	-63.2537
0.481	-3.597	-8.429	78	38.5	26.97745	-63.031
0.487	-3.919	-8.401	79	39	29.38884	-62.8231
0.493	-4.231	-8.369	80	39.5	31.72445	-62.5855
0.499	-4.537	-8.338	81	40	34.01423	-62.3554
0.506	-4.842	-8.308	82	40.5	36.29556	-62.1326
0.512	-5.139	-8.271	83	41	38.51607	-61.8578
0.518	-5.427	-8.231	84	41.5	40.6683	-61.5607
0.524	-5.714	-8.191	85	42	42.81204	-61.2636
0.53	-5.994	-8.143	86	42.5	44.90246	-60.907
0.537	-6.261	-8.086	87	43	46.89482	-60.4835
0.543	-6.525	-8.025	88	43.5	48.86379	-60.0302
0.549	-6.783	-7.958	89	44	50.78702	-59.5323
0.555	-7.029	-7.875	90	44.5	52.61983	-58.9153

0.562	-7.265	-7.783	91	45	54.37723	-58.2313
0.568	-7.494	-7.686	92	45.5	56.08162	-57.5099
0.574	-7.714	-7.573	93	46	57.71818	-56.6694
0.58	-7.916	-7.442	94	46.5	59.22009	-55.6947
0.587	-8.113	-7.305	95	47	60.68412	-54.675
0.593	-8.297	-7.157	96	47.5	62.05089	-53.5731
0.599	-8.462	-6.982	97	48	63.27598	-52.2697
0.605	-8.615	-6.797	98	48.5	64.4115	-50.8913
0.612	-8.758	-6.604	99	49	65.4724	-49.4528
0.618	-8.88	-6.387	100	49.5	66.37717	-47.8347
0.624	-8.978	-6.152	101	50	67.10374	-46.0816
0.63	-9.068	-5.911	102	50.5	67.77082	-44.2829
0.637	-9.137	-5.651	103	51	68.28214	-42.3416
0.643	-9.176	-5.367	104	51.5	68.5711	-40.22
0.649	-9.204	-5.075	105	52	68.77854	-38.0377
0.655	-9.211	-4.773	106	52.5	68.8304	-35.7795
0.661	-9.188	-4.445	107	53	68.66001	-33.3259
0.668	-9.145	-4.105	108	53.5	68.34142	-30.7813
0.674	-9.082	-3.757	109	54	67.87458	-28.1758
0.68	-8.995	-3.392	110	54.5	67.22976	-25.4418
0.686	-8.879	-3.011	111	55	66.36976	-22.5869
0.693	-8.745	-2.625	112	55.5	65.37597	-19.6935
0.699	-8.592	-2.228	113	56	64.24083	-16.7167
0.705	-8.406	-1.815	114	56.5	62.86025	-13.6191
0.711	-8.197	-1.396	115	57	61.30816	-10.4758
0.718	-7.974	-0.9712	116	57.5	59.6512	-7.28843
0.724	-7.725	-0.5388	117	58	57.79999	-4.04359
0.73	-7.446	-0.0996	118	58.5	55.72444	-0.74749
0.736	-7.153	0.3435	119	59	53.54332	2.577923
0.743	-6.842	0.7894	120	59.5	51.22668	5.924193
0.749	-6.495	1.238	121	60	48.6401	9.290363
0.755	-6.139	1.686	122	60.5	45.98457	12.65146
0.761	-5.772	2.138	123	61	43.24514	16.04179
0.767	-5.365	2.584	124	61.5	40.20506	19.38613
0.774	-4.946	3.029	125	62	37.07323	22.7218
0.78	-4.52	3.473	126	62.5	33.88704	26.04861
0.786	-4.071	3.909	127	63	30.52681	29.31396
0.793	-3.6	4.337	128	63.5	26.99992	32.51775
0.799	-3.123	4.762	129	64	23.42625	35.69728
0.805	-2.636	5.179	130	64.5	19.77598	38.81505
0.811	-2.12	5.578	131	65	15.90679	41.79632
0.817	-1.603	5.968	132	65.5	12.02881	44.70839
0.824	-1.081	6.354	133	66	8.112333	47.58855
0.83	-0.5357	6.715	134	66.5	4.020325	50.28022
0.836	0.0165	7.062	135	67	-0.12383	52.86562
0.842	0.5685	7.399	136	67.5	-4.26647	55.37466
0.849	1.126	7.716	137	68	-8.44999	57.73305
0.855	1.701	8.008	138	68.5	-12.764	59.90389
0.861	2.273	8.286	139	69	-17.0542	61.9692
0.867	2.843	8.555	140	69.5	-21.3277	63.96625
0.874	3.428	8.781	141	70	-25.7115	65.64299

0.88	4.007	8.993	142	70.5	-30.0477	67.21493
0.886	4.585	9.194	143	71	-34.3733	68.70446
0.892	5.166	9.361	144	71.5	-38.7179	69.94139
0.899	5.748	9.506	145	72	-43.0659	71.01488
0.905	6.325	9.634	146	72.5	-47.3722	71.96214
0.911	6.894	9.741	147	73	-51.6141	72.75372
0.917	7.467	9.814	148	73.5	-55.8807	73.29362
0.924	8.033	9.871	149	74	-60.0897	73.7151
0.93	8.595	9.912	150	74.5	-64.2631	74.01823
0.936	9.151	9.92	151	75	-68.3859	74.07737
0.942	9.699	9.91	152	75.5	-72.443	74.00344
0.948	10.24	9.883	153	76	-76.4419	73.80383
0.955	10.78	9.837	154	76.5	-80.4265	73.4637
0.961	11.31	9.766	155	77	-84.3304	72.93863
0.967	11.83	9.68	156	77.5	-88.1537	72.30248
0.974	12.35	9.585	157	78	-91.9697	71.59956
0.98	12.85	9.462	158	78.5	-95.6317	70.68918
0.986	13.35	9.329	159	79	-99.2865	69.70442
0.992	13.84	9.188	160	79.5	-102.861	68.66001
0.998	14.32	9.03	161	80	-106.355	67.48919
1.005	14.78	8.862	162	80.5	-109.697	66.2437
1.011	15.24	8.689	163	81	-113.031	64.96055
1.017	15.7	8.508	164	81.5	-116.358	63.61743
1.023	16.13	8.318	165	82	-119.462	62.20684
1.03	16.57	8.128	166	82.5	-122.63	60.79556
1.036	16.99	7.936	167	83	-125.648	59.36876
1.042	17.39	7.743	168	83.5	-128.516	57.93385
1.048	17.8	7.55	169	84	-131.449	56.49828
1.055	18.19	7.359	170	84.5	-134.233	55.07695
1.061	18.57	7.172	171	85	-136.939	53.6848
1.067	18.94	6.991	172	85.5	-139.568	52.33678
1.073	19.3	6.812	173	86	-142.121	51.00313
1.079	19.66	6.638	174	86.5	-144.668	49.70626
1.086	19.99	6.476	175	87	-146.998	48.49842
1.092	20.32	6.318	176	87.5	-149.323	47.32002
1.098	20.64	6.164	177	88	-151.573	46.17112
1.105	20.94	6.023	178	88.5	-153.678	45.1189
1.111	21.23	5.889	179	89	-155.708	44.11867
1.117	21.52	5.759	180	89.5	-157.735	43.14807
1.123	21.79	5.638	181	90	-159.618	42.24446
1.13	22.03	5.529	182	90.5	-161.29	41.43031
1.136	22.28	5.423	183	91	-163.027	40.63842
1.142	22.51	5.322	184	91.5	-164.623	39.88375
1.148	22.7	5.236	185	92	-165.94	39.24107
1.154	22.89	5.153	186	92.5	-167.254	38.62072
1.161	23.07	5.072	187	93	-168.498	38.01524
1.167	23.22	5	188	93.5	-169.533	37.47697
1.173	23.34	4.934	189	94	-170.36	36.98351
1.179	23.46	4.867	190	94.5	-171.187	36.48251
1.186	23.56	4.803	191	95	-171.875	36.00391
1.192	23.62	4.745	192	95.5	-172.288	35.57013

1.198	23.67	4.684	193	96	-172.631	35.11388
1.204	23.7	4.621	194	96.5	-172.838	34.64263
1.211	23.7	4.558	195	97	-172.838	34.17134
1.217	23.67	4.489	196	97.5	-172.631	33.65511
1.223	23.63	4.416	197	98	-172.356	33.10891
1.229	23.58	4.34	198	98.5	-172.013	32.5402
1.235	23.48	4.248	199	99	-171.324	31.85168
1.242	23.37	4.153	200	99.5	-170.567	31.14063
1.248	23.26	4.059	201	100	-169.809	30.43698

Contact Forces in Hip Joint Relative to Femur

Subject: Average Patient
Activity: Slow Walking WS
Trial number: 0

Time[s]	-Fx[%BW]	-Fy[%BW]	-Fz[%BW]	Measurement		%Cycle
0	26.27	-1.112	65.39	70.48	1	0
0.006	27.09	-0.1128	70.34	75.37	2	0.5
0.013	27.93	0.8511	75.25	80.27	3	1
0.019	28.79	1.812	80.31	85.33	4	1.5
0.025	29.83	2.945	86.82	91.85	5	2
0.031	30.97	4.111	93.84	98.91	6	2.5
0.038	32.12	5.274	101	106.2	7	3
0.044	33.33	6.502	108.9	114.1	8	3.5
0.05	34.61	7.844	117.7	122.9	9	4
0.056	35.89	9.205	126.5	131.8	10	4.5
0.062	37.17	10.6	135.4	140.8	11	5
0.069	38.41	12.09	144.6	150.1	12	5.5
0.075	39.63	13.61	153.8	159.4	13	6
0.081	40.84	15.17	162.9	168.6	14	6.5
0.087	41.97	16.79	171.6	177.4	15	7
0.094	42.99	18.47	179.9	185.9	16	7.5
0.1	43.96	20.14	187.9	194	17	8
0.106	44.89	21.81	195.6	201.9	18	8.5
0.112	45.57	23.48	202.2	208.6	19	9
0.119	46.22	25.1	208.4	214.9	20	9.5
0.125	46.84	26.7	214.3	221	21	10
0.131	47.31	28.16	219.1	225.9	22	10.5
0.137	47.7	29.52	223	230	23	11
0.144	48.06	30.83	226.7	233.8	24	11.5
0.15	48.36	31.99	229.7	236.9	25	12
0.156	48.56	32.95	231.6	238.9	26	12.5
0.162	48.72	33.86	233.2	240.6	27	13
0.169	48.83	34.65	234.5	242	28	13.5
0.175	48.97	35.17	235	242.6	29	14
0.181	49.1	35.6	235.2	242.9	30	14.5
0.187	49.2	35.92	235.1	242.9	31	15
0.193	49.32	36.06	234.7	242.5	32	15.5
0.2	49.45	36.06	234	241.9	33	16
0.206	49.56	35.96	233.1	241	34	16.5
0.212	49.68	35.75	232	239.9	35	17
0.218	49.88	35.28	230.9	238.8	36	17.5
0.225	50.03	34.73	229.6	237.5	37	18
0.231	50.17	34.11	228.2	236.2	38	18.5
0.237	50.36	33.36	226.9	234.8	39	19
0.243	50.54	32.54	225.7	233.5	40	19.5
0.25	50.69	31.68	224.3	232.2	41	20
0.256	50.81	30.76	223.1	230.8	42	20.5

0.262	50.92	29.74	221.8	229.5	43	21
0.268	51.02	28.69	220.6	228.2	44	21.5
0.275	51.12	27.61	219.3	226.9	45	22
0.281	51.13	26.47	218.1	225.6	46	22.5
0.287	51.11	25.29	216.9	224.2	47	23
0.293	51.07	24.09	215.6	222.9	48	23.5
0.299	51.04	22.85	214.4	221.6	49	24
0.306	51.01	21.58	213.3	220.3	50	24.5
0.312	50.96	20.31	212.1	219.1	51	25
0.318	50.88	19.05	211	217.9	52	25.5
0.324	50.73	17.76	209.9	216.6	53	26
0.331	50.57	16.49	208.8	215.5	54	26.5
0.337	50.41	15.23	207.7	214.3	55	27
0.343	50.27	14.01	206.8	213.2	56	27.5
0.35	50.14	12.84	205.8	212.3	57	28
0.356	49.98	11.68	205	211.3	58	28.5
0.362	49.82	10.55	204.2	210.4	59	29
0.368	49.7	9.459	203.5	209.7	60	29.5
0.374	49.58	8.404	202.9	209	61	30
0.381	49.43	7.375	202.2	208.3	62	30.5
0.387	49.23	6.387	201.8	207.9	63	31
0.393	49.02	5.432	201.5	207.4	64	31.5
0.399	48.81	4.486	201.1	207	65	32
0.406	48.61	3.574	200.9	206.7	66	32.5
0.412	48.4	2.717	200.7	206.5	67	33
0.418	48.2	1.88	200.6	206.3	68	33.5
0.424	48	1.051	200.4	206.1	69	34
0.431	47.82	0.2801	200.4	206	70	34.5
0.437	47.64	-0.4695	200.4	206	71	35
0.443	47.47	-1.214	200.4	205.9	72	35.5
0.449	47.32	-1.883	200.4	205.9	73	36
0.456	47.15	-2.504	200.5	206	74	36.5
0.462	46.98	-3.109	200.6	206	75	37
0.468	46.78	-3.684	200.7	206.1	76	37.5
0.474	46.54	-4.202	200.8	206.2	77	38
0.481	46.28	-4.705	201	206.3	78	38.5
0.487	46.03	-5.174	201.2	206.4	79	39
0.493	45.78	-5.508	201.3	206.5	80	39.5
0.499	45.51	-5.788	201.5	206.6	81	40
0.506	45.23	-6.03	201.6	206.7	82	40.5
0.512	44.92	-6.164	201.8	206.8	83	41
0.518	44.61	-6.204	201.9	206.8	84	41.5
0.524	44.29	-6.213	201.9	206.8	85	42
0.53	43.94	-6.151	202	206.8	86	42.5
0.537	43.57	-6	201.9	206.7	87	43
0.543	43.21	-5.789	201.9	206.5	88	43.5
0.549	42.83	-5.504	201.7	206.3	89	44
0.555	42.47	-5.129	201.6	206.1	90	44.5
0.562	42.11	-4.699	201.3	205.7	91	45
0.568	41.74	-4.244	200.9	205.3	92	45.5
0.574	41.41	-3.728	200.4	204.7	93	46

0.58	41.1	-3.157	199.7	203.9	94	46.5
0.587	40.83	-2.541	198.9	203	95	47
0.593	40.56	-1.928	197.8	201.9	96	47.5
0.599	40.24	-1.254	196.5	200.5	97	48
0.605	39.95	-0.6152	194.9	199	98	48.5
0.612	39.67	-0.0132	193.2	197.3	99	49
0.618	39.41	0.5262	191.2	195.3	100	49.5
0.624	39.13	0.8988	188.8	192.9	101	50
0.63	38.88	1.226	186.4	190.4	102	50.5
0.637	38.66	1.496	183.6	187.6	103	51
0.643	38.44	1.714	180.3	184.4	104	51.5
0.649	38.24	1.857	176.9	181	105	52
0.655	38.07	1.882	173.3	177.4	106	52.5
0.661	37.95	1.794	169.2	173.4	107	53
0.668	37.84	1.54	164.8	169.1	108	53.5
0.674	37.75	1.182	160.3	164.7	109	54
0.68	37.67	0.7476	155.6	160.1	110	54.5
0.686	37.6	0.2111	150.6	155.2	111	55
0.693	37.57	-0.3447	145.6	150.3	112	55.5
0.699	37.54	-0.959	140.5	145.4	113	56
0.705	37.6	-1.671	135.2	140.3	114	56.5
0.711	37.66	-2.371	129.9	135.3	115	57
0.718	37.73	-3.045	124.8	130.4	116	57.5
0.724	37.79	-3.765	119.7	125.6	117	58
0.73	37.83	-4.457	114.7	120.9	118	58.5
0.736	37.85	-5.071	109.9	116.4	119	59
0.743	37.87	-5.691	105.3	112	120	59.5
0.749	37.84	-6.287	100.9	108	121	60
0.755	37.75	-6.756	96.88	104.2	122	60.5
0.761	37.64	-7.183	93.02	100.6	123	61
0.767	37.46	-7.628	89.51	97.33	124	61.5
0.774	37.24	-7.959	86.29	94.32	125	62
0.78	36.99	-8.229	83.26	91.48	126	62.5
0.786	36.61	-8.476	80.53	88.87	127	63
0.793	36.15	-8.693	78.06	86.46	128	63.5
0.799	35.64	-8.883	75.72	84.16	129	64
0.805	35.1	-9.065	73.58	82.03	130	64.5
0.811	34.52	-9.168	71.78	80.17	131	65
0.817	33.9	-9.24	70.06	78.38	132	65.5
0.824	33.24	-9.32	68.37	76.59	133	66
0.83	32.54	-9.352	66.91	74.99	134	66.5
0.836	31.83	-9.363	65.52	73.44	135	67
0.842	31.08	-9.37	64.13	71.88	136	67.5
0.849	30.32	-9.356	62.74	70.31	137	68
0.855	29.57	-9.275	61.34	68.73	138	68.5
0.861	28.83	-9.164	59.91	67.11	139	69
0.867	28.1	-9.03	58.46	65.49	140	69.5
0.874	27.31	-8.902	56.94	63.78	141	70
0.88	26.55	-8.774	55.43	62.08	142	70.5
0.886	25.8	-8.637	53.9	60.37	143	71
0.892	25.09	-8.465	52.32	58.64	144	71.5

0.899	24.41	-8.293	50.71	56.89	145	72
0.905	23.76	-8.128	49.11	55.16	146	72.5
0.911	23.15	-7.972	47.52	53.46	147	73
0.917	22.6	-7.779	45.92	51.76	148	73.5
0.924	22.08	-7.611	44.33	50.11	149	74
0.93	21.57	-7.447	42.77	48.48	150	74.5
0.936	21.12	-7.279	41.25	46.91	151	75
0.942	20.69	-7.117	39.76	45.38	152	75.5
0.948	20.28	-6.97	38.29	43.89	153	76
0.955	19.9	-6.817	36.89	42.46	154	76.5
0.961	19.53	-6.669	35.57	41.12	155	77
0.967	19.18	-6.545	34.25	39.8	156	77.5
0.974	18.85	-6.45	32.97	38.52	157	78
0.98	18.58	-6.331	31.9	37.45	158	78.5
0.986	18.32	-6.224	30.83	36.4	159	79
0.992	18.06	-6.118	29.78	35.36	160	79.5
0.998	17.78	-5.94	28.94	34.48	161	80
1.005	17.5	-5.726	28.23	33.7	162	80.5
1.011	17.23	-5.555	27.53	32.95	163	81
1.017	17.01	-5.386	26.93	32.3	164	81.5
1.023	16.85	-5.192	26.46	31.8	165	82
1.03	16.7	-4.991	26.03	31.33	166	82.5
1.036	16.55	-4.791	25.67	30.92	167	83
1.042	16.4	-4.558	25.51	30.67	168	83.5
1.048	16.27	-4.325	25.39	30.46	169	84
1.055	16.14	-4.095	25.35	30.33	170	84.5
1.061	16.08	-3.867	25.47	30.37	171	85
1.067	16.05	-3.648	25.69	30.51	172	85.5
1.073	16.03	-3.443	26	30.73	173	86
1.079	16.02	-3.237	26.43	31.07	174	86.5
1.086	16.03	-3.017	27.03	31.57	175	87
1.092	16.07	-2.81	27.7	32.14	176	87.5
1.098	16.11	-2.625	28.48	32.82	177	88
1.105	16.16	-2.515	29.44	33.68	178	88.5
1.111	16.22	-2.436	30.49	34.62	179	89
1.117	16.29	-2.351	31.59	35.62	180	89.5
1.123	16.4	-2.3	32.85	36.79	181	90
1.13	16.57	-2.321	34.28	38.14	182	90.5
1.136	16.75	-2.357	35.72	39.52	183	91
1.142	16.93	-2.431	37.25	40.99	184	91.5
1.148	17.13	-2.533	38.94	42.61	185	92
1.154	17.34	-2.652	40.63	44.25	186	92.5
1.161	17.56	-2.787	42.3	45.89	187	93
1.167	17.8	-2.969	44.02	47.57	188	93.5
1.173	18.04	-3.192	45.77	49.3	189	94
1.179	18.28	-3.411	47.49	51	190	94.5
1.186	18.55	-3.607	49.18	52.68	191	95
1.192	18.86	-3.745	50.86	54.37	192	95.5
1.198	19.18	-3.874	52.48	56.01	193	96
1.204	19.54	-3.979	54.09	57.65	194	96.5
1.211	19.92	-3.969	55.72	59.3	195	97

1.217	20.35	-3.856	57.4	61.02	196	97.5
1.223	20.81	-3.707	59.1	62.77	197	98
1.229	21.27	-3.532	60.88	64.58	198	98.5
1.235	21.76	-3.163	63	66.72	199	99
1.242	22.25	-2.757	65.18	68.93	200	99.5
1.248	22.75	-2.352	67.36	71.14	201	100

Moments of Contact Forces in Hip Joint Relative to Femur

Subject: Average Patient
Activity: Slow Walking WS
Trial number: 0

Time[s]	Mx[%BW*m]	My[%BW*m]	Mz[%BW*m]	Measurement		%Cycle
0	-0.05636	0.9969	-0.1133	1.005	1	0
0.006	-0.03149	1.099	-0.1551	1.11	2	0.5
0.013	-0.007554	1.2	-0.1957	1.216	3	1
0.019	0.01624	1.304	-0.2368	1.325	4	1.5
0.025	0.04409	1.44	-0.2873	1.469	5	2
0.031	0.07259	1.586	-0.3402	1.624	6	2.5
0.038	0.1009	1.737	-0.3936	1.784	7	3
0.044	0.1308	1.903	-0.4513	1.961	8	3.5
0.05	0.1633	2.09	-0.5149	2.159	9	4
0.056	0.1964	2.279	-0.5795	2.36	10	4.5
0.062	0.2303	2.47	-0.6454	2.564	11	5
0.069	0.2667	2.67	-0.715	2.776	12	5.5
0.075	0.3039	2.868	-0.7851	2.989	13	6
0.081	0.342	3.063	-0.8558	3.199	14	6.5
0.087	0.382	3.252	-0.9273	3.404	15	7
0.094	0.4238	3.433	-0.9991	3.6	16	7.5
0.1	0.4655	3.608	-1.07	3.792	17	8
0.106	0.5074	3.776	-1.14	3.977	18	8.5
0.112	0.5495	3.921	-1.206	4.138	19	9
0.119	0.5907	4.058	-1.269	4.292	20	9.5
0.125	0.6312	4.188	-1.331	4.439	21	10
0.131	0.6687	4.292	-1.386	4.559	22	10.5
0.137	0.7036	4.378	-1.435	4.661	23	11
0.144	0.7373	4.459	-1.482	4.757	24	11.5
0.15	0.7672	4.524	-1.522	4.834	25	12
0.156	0.7924	4.562	-1.554	4.884	26	12.5
0.162	0.8161	4.597	-1.583	4.93	27	13
0.169	0.8368	4.624	-1.608	4.967	28	13.5
0.175	0.8507	4.631	-1.623	4.98	29	14
0.181	0.8622	4.631	-1.634	4.986	30	14.5
0.187	0.8708	4.625	-1.641	4.984	31	15
0.193	0.8748	4.611	-1.643	4.973	32	15.5
0.2	0.8749	4.59	-1.64	4.952	33	16
0.206	0.8727	4.563	-1.633	4.925	34	16.5
0.212	0.8676	4.533	-1.623	4.892	35	17
0.218	0.8552	4.501	-1.605	4.854	36	17.5
0.225	0.841	4.466	-1.585	4.813	37	18
0.231	0.8248	4.429	-1.563	4.769	38	18.5
0.237	0.8053	4.394	-1.538	4.724	39	19
0.243	0.7839	4.359	-1.511	4.679	40	19.5
0.25	0.7612	4.325	-1.483	4.635	41	20
0.256	0.7368	4.292	-1.453	4.591	42	20.5

0.262	0.71	4.261	-1.421	4.548	43	21
0.268	0.6823	4.23	-1.389	4.505	44	21.5
0.275	0.6538	4.2	-1.356	4.461	45	22
0.281	0.6235	4.172	-1.321	4.42	46	22.5
0.287	0.5924	4.145	-1.286	4.381	47	23
0.293	0.5607	4.12	-1.25	4.342	48	23.5
0.299	0.5278	4.094	-1.213	4.303	49	24
0.306	0.494	4.07	-1.176	4.265	50	24.5
0.312	0.4603	4.047	-1.139	4.229	51	25
0.318	0.4269	4.025	-1.102	4.195	52	25.5
0.324	0.3928	4.005	-1.065	4.163	53	26
0.331	0.3589	3.987	-1.029	4.133	54	26.5
0.337	0.3254	3.969	-0.9928	4.104	55	27
0.343	0.2931	3.952	-0.9581	4.077	56	27.5
0.35	0.262	3.936	-0.9248	4.052	57	28
0.356	0.2313	3.922	-0.8922	4.029	58	28.5
0.362	0.2011	3.91	-0.8604	4.009	59	29
0.368	0.172	3.901	-0.8301	3.992	60	29.5
0.374	0.1439	3.892	-0.8009	3.976	61	30
0.381	0.1165	3.883	-0.7725	3.961	62	30.5
0.387	0.09011	3.883	-0.7464	3.955	63	31
0.393	0.06457	3.883	-0.7212	3.95	64	31.5
0.399	0.03928	3.883	-0.6962	3.945	65	32
0.406	0.01486	3.885	-0.6726	3.943	66	32.5
0.412	-0.008116	3.89	-0.6507	3.944	67	33
0.418	-0.03056	3.895	-0.6295	3.945	68	33.5
0.424	-0.05281	3.9	-0.6084	3.948	69	34
0.431	-0.07353	3.907	-0.5892	3.952	70	34.5
0.437	-0.09369	3.915	-0.5706	3.957	71	35
0.443	-0.1137	3.922	-0.5521	3.962	72	35.5
0.449	-0.1317	3.93	-0.5357	3.968	73	36
0.456	-0.1484	3.938	-0.5206	3.975	74	36.5
0.462	-0.1647	3.947	-0.5061	3.983	75	37
0.468	-0.1803	3.958	-0.4926	3.992	76	37.5
0.474	-0.1942	3.97	-0.4809	4.003	77	38
0.481	-0.2078	3.983	-0.4697	4.016	78	38.5
0.487	-0.2205	3.996	-0.4594	4.028	79	39
0.493	-0.2296	4.008	-0.4525	4.04	80	39.5
0.499	-0.2371	4.02	-0.4471	4.052	81	40
0.506	-0.2437	4.033	-0.4427	4.064	82	40.5
0.512	-0.2474	4.045	-0.4412	4.076	83	41
0.518	-0.2485	4.055	-0.4419	4.087	84	41.5
0.524	-0.2488	4.066	-0.4434	4.098	85	42
0.53	-0.2471	4.076	-0.4467	4.108	86	42.5
0.537	-0.243	4.084	-0.4522	4.117	87	43
0.543	-0.2373	4.092	-0.459	4.124	88	43.5
0.549	-0.2296	4.097	-0.4675	4.13	89	44
0.555	-0.2195	4.101	-0.4782	4.135	90	44.5
0.562	-0.2078	4.101	-0.4898	4.136	91	45
0.568	-0.1954	4.1	-0.5017	4.135	92	45.5
0.574	-0.1813	4.093	-0.5145	4.13	93	46

0.58	-0.1657	4.08	-0.5277	4.117	94	46.5
0.587	-0.1488	4.064	-0.5415	4.102	95	47
0.593	-0.1318	4.041	-0.5545	4.081	96	47.5
0.599	-0.1132	4.012	-0.5679	4.054	97	48
0.605	-0.09539	3.978	-0.5797	4.021	98	48.5
0.612	-0.07852	3.939	-0.5897	3.984	99	49
0.618	-0.06321	3.892	-0.5969	3.938	100	49.5
0.624	-0.05222	3.836	-0.5982	3.883	101	50
0.63	-0.04243	3.778	-0.598	3.825	102	50.5
0.637	-0.03404	3.711	-0.5949	3.759	103	51
0.643	-0.02687	3.632	-0.5886	3.679	104	51.5
0.649	-0.02163	3.548	-0.5796	3.596	105	52
0.655	-0.01948	3.459	-0.5665	3.505	106	52.5
0.661	-0.02018	3.357	-0.5485	3.401	107	53
0.668	-0.02526	3.248	-0.5251	3.29	108	53.5
0.674	-0.03307	3.135	-0.4984	3.175	109	54
0.68	-0.04283	3.017	-0.4686	3.053	110	54.5
0.686	-0.05523	2.891	-0.4352	2.924	111	55
0.693	-0.06815	2.765	-0.401	2.795	112	55.5
0.699	-0.08261	2.636	-0.3651	2.663	113	56
0.705	-0.09962	2.501	-0.3253	2.524	114	56.5
0.711	-0.1163	2.367	-0.2862	2.387	115	57
0.718	-0.1324	2.236	-0.2482	2.254	116	57.5
0.724	-0.1497	2.105	-0.2089	2.12	117	58
0.73	-0.1662	1.977	-0.171	1.991	118	58.5
0.736	-0.1808	1.855	-0.136	1.869	119	59
0.743	-0.1956	1.737	-0.1014	1.751	120	59.5
0.749	-0.2099	1.628	-0.0689	1.643	121	60
0.755	-0.2209	1.528	-0.04111	1.545	122	60.5
0.761	-0.2308	1.433	-0.01526	1.452	123	61
0.767	-0.2413	1.349	0.009429	1.37	124	61.5
0.774	-0.2489	1.273	0.02975	1.297	125	62
0.78	-0.255	1.202	0.04768	1.23	126	62.5
0.786	-0.2605	1.143	0.06316	1.174	127	63
0.793	-0.2653	1.092	0.07655	1.127	128	63.5
0.799	-0.2695	1.046	0.08845	1.084	129	64
0.805	-0.2735	1.006	0.09923	1.047	130	64.5
0.811	-0.2756	0.975	0.1065	1.019	131	65
0.817	-0.2768	0.9473	0.1124	0.9933	132	65.5
0.824	-0.2783	0.9216	0.1182	0.9699	133	66
0.83	-0.2786	0.9025	0.1217	0.9523	134	66.5
0.836	-0.2783	0.8857	0.1243	0.9367	135	67
0.842	-0.2779	0.8696	0.1266	0.9217	136	67.5
0.849	-0.277	0.8538	0.1284	0.9067	137	68
0.855	-0.2742	0.8373	0.1285	0.8904	138	68.5
0.861	-0.2707	0.8193	0.128	0.8723	139	69
0.867	-0.2665	0.8006	0.127	0.8533	140	69.5
0.874	-0.2624	0.782	0.1262	0.8344	141	70
0.88	-0.2584	0.7625	0.1255	0.8148	142	70.5
0.886	-0.2541	0.7424	0.1247	0.7945	143	71
0.892	-0.2488	0.7197	0.1233	0.7714	144	71.5

0.899	-0.2435	0.6955	0.1222	0.747	145	72
0.905	-0.2384	0.6707	0.1214	0.7222	146	72.5
0.911	-0.2336	0.6453	0.1209	0.6969	147	73
0.917	-0.2277	0.6177	0.1199	0.6691	148	73.5
0.924	-0.2226	0.59	0.1195	0.6418	149	74
0.93	-0.2175	0.5623	0.1192	0.6146	150	74.5
0.936	-0.2124	0.5342	0.1189	0.587	151	75
0.942	-0.2075	0.5066	0.1187	0.5601	152	75.5
0.948	-0.2029	0.4789	0.1189	0.5336	153	76
0.955	-0.1982	0.4524	0.1188	0.508	154	76.5
0.961	-0.1937	0.4274	0.1185	0.484	155	77
0.967	-0.1899	0.4021	0.119	0.4604	156	77.5
0.974	-0.1868	0.3776	0.1201	0.4381	157	78
0.98	-0.1831	0.3564	0.1201	0.4183	158	78.5
0.986	-0.1798	0.3354	0.1204	0.3992	159	79
0.992	-0.1766	0.3146	0.1207	0.3804	160	79.5
0.998	-0.1714	0.2997	0.1182	0.3649	161	80
1.005	-0.1654	0.2879	0.1142	0.3511	162	80.5
1.011	-0.1605	0.2765	0.1114	0.3385	163	81
1.017	-0.1557	0.2658	0.1085	0.3266	164	81.5
1.023	-0.1503	0.2573	0.1046	0.3158	165	82
1.03	-0.1447	0.2494	0.1004	0.3053	166	82.5
1.036	-0.1392	0.2434	0.09599	0.2963	167	83
1.042	-0.1329	0.2422	0.08997	0.2905	168	83.5
1.048	-0.1266	0.2416	0.08381	0.2854	169	84
1.055	-0.1204	0.2429	0.0775	0.2819	170	84.5
1.061	-0.1143	0.2469	0.07083	0.2811	171	85
1.067	-0.1085	0.2525	0.06417	0.2822	172	85.5
1.073	-0.1031	0.2601	0.05757	0.2857	173	86
1.079	-0.09772	0.2707	0.05047	0.2922	174	86.5
1.086	-0.09207	0.2851	0.04246	0.3026	175	87
1.092	-0.08678	0.3004	0.03465	0.3146	176	87.5
1.098	-0.08211	0.3187	0.02696	0.3302	177	88
1.105	-0.07955	0.3418	0.02052	0.3515	178	88.5
1.111	-0.07784	0.3671	0.01456	0.3755	179	89
1.117	-0.07599	0.3935	0.008265	0.4008	180	89.5
1.123	-0.07515	0.4229	0.002442	0.4295	181	90
1.13	-0.07629	0.4551	-0.001887	0.4615	182	90.5
1.136	-0.07784	0.4879	-0.0059	0.4941	183	91
1.142	-0.08043	0.5231	-0.009307	0.5293	184	91.5
1.148	-0.08386	0.5617	-0.01247	0.568	185	92
1.154	-0.08774	0.6001	-0.01516	0.6067	186	92.5
1.161	-0.09206	0.6381	-0.01734	0.6449	187	93
1.167	-0.09763	0.6768	-0.01839	0.684	188	93.5
1.173	-0.1043	0.7167	-0.01853	0.7245	189	94
1.179	-0.1109	0.7554	-0.01857	0.7637	190	94.5
1.186	-0.1169	0.7927	-0.01904	0.8015	191	95
1.192	-0.1213	0.8284	-0.02078	0.8375	192	95.5
1.198	-0.1254	0.8622	-0.02241	0.8715	193	96
1.204	-0.1289	0.8949	-0.02453	0.9045	194	96.5
1.211	-0.1293	0.9267	-0.02954	0.9362	195	97

1.217	-0.1269	0.9583	-0.03722	0.9674	196	97.5
1.223	-0.1236	0.9895	-0.04577	0.9983	197	98
1.229	-0.1196	1.023	-0.0553	1.031	198	98.5
1.235	-0.1105	1.063	-0.07105	1.071	199	99
1.242	-0.1005	1.105	-0.088	1.113	200	99.5

Flexion and Abduction Angle, Femur System Relative to Pelvis System

Subject: Average Patient
Activity: Normal Walking WN
Trial number: 0

Time[s]	Flexion[deg]	Abduction[deg]	Meas. #	%Cycle
0	26.43	1.883	1	0
0.005	26.32	1.749	2	0.5
0.011	26.21	1.616	3	1
0.017	26.09	1.481	4	1.5
0.022	25.96	1.334	5	2
0.028	25.79	1.176	6	2.5
0.033	25.62	1.017	7	3
0.039	25.44	0.8525	8	3.5
0.044	25.24	0.6741	9	4
0.05	25.02	0.4912	10	4.5
0.055	24.79	0.3066	11	5
0.061	24.55	0.1083	12	5.5
0.066	24.29	-0.0948	13	6
0.072	24.02	-0.3009	14	6.5
0.077	23.74	-0.5156	15	7
0.083	23.44	-0.7392	16	7.5
0.088	23.14	-0.9633	17	8
0.094	22.82	-1.193	18	8.5
0.099	22.5	-1.43	19	9
0.105	22.16	-1.671	20	9.5
0.11	21.82	-1.912	21	10
0.116	21.46	-2.162	22	10.5
0.121	21.1	-2.415	23	11
0.127	20.74	-2.666	24	11.5
0.132	20.36	-2.923	25	12
0.138	19.97	-3.181	26	12.5
0.143	19.58	-3.435	27	13
0.149	19.19	-3.696	28	13.5
0.154	18.79	-3.955	29	14
0.16	18.38	-4.208	30	14.5
0.166	17.97	-4.466	31	15
0.171	17.56	-4.722	32	15.5
0.176	17.14	-4.967	33	16
0.182	16.72	-5.211	34	16.5
0.188	16.3	-5.454	35	17
0.193	15.87	-5.689	36	17.5
0.199	15.45	-5.915	37	18
0.204	15.02	-6.137	38	18.5
0.21	14.59	-6.353	39	19
0.215	14.15	-6.558	40	19.5
0.221	13.72	-6.753	41	20
0.226	13.29	-6.941	42	20.5

0.232	12.86	-7.12	43	21
0.237	12.42	-7.286	44	21.5
0.243	11.99	-7.442	45	22
0.248	11.56	-7.59	46	22.5
0.254	11.13	-7.727	47	23
0.259	10.7	-7.85	48	23.5
0.265	10.27	-7.965	49	24
0.27	9.844	-8.071	50	24.5
0.276	9.421	-8.166	51	25
0.281	8.998	-8.249	52	25.5
0.287	8.578	-8.321	53	26
0.292	8.16	-8.386	54	26.5
0.298	7.742	-8.444	55	27
0.303	7.328	-8.49	56	27.5
0.309	6.918	-8.528	57	28
0.315	6.511	-8.558	58	28.5
0.32	6.107	-8.583	59	29
0.326	5.707	-8.6	60	29.5
0.331	5.308	-8.61	61	30
0.336	4.912	-8.616	62	30.5
0.342	4.521	-8.616	63	31
0.348	4.133	-8.61	64	31.5
0.353	3.746	-8.601	65	32
0.359	3.364	-8.587	66	32.5
0.364	2.987	-8.568	67	33
0.37	2.612	-8.545	68	33.5
0.375	2.239	-8.521	69	34
0.381	1.868	-8.491	70	34.5
0.386	1.501	-8.454	71	35
0.392	1.138	-8.418	72	35.5
0.397	0.7774	-8.377	73	36
0.403	0.4186	-8.331	74	36.5
0.408	0.067	-8.28	75	37
0.414	-0.2848	-8.227	76	37.5
0.419	-0.6333	-8.17	77	38
0.425	-0.9753	-8.106	78	38.5
0.43	-1.316	-8.037	79	39
0.436	-1.653	-7.965	80	39.5
0.441	-1.983	-7.888	81	40
0.447	-2.309	-7.804	82	40.5
0.452	-2.627	-7.714	83	41
0.458	-2.942	-7.621	84	41.5
0.463	-3.251	-7.52	85	42
0.469	-3.551	-7.412	86	42.5
0.474	-3.843	-7.297	87	43
0.48	-4.128	-7.177	88	43.5
0.486	-4.404	-7.051	89	44
0.491	-4.666	-6.916	90	44.5
0.496	-4.918	-6.772	91	45
0.502	-5.163	-6.624	92	45.5
0.507	-5.392	-6.47	93	46

0.513	-5.606	-6.303	94	46.5
0.519	-5.806	-6.129	95	47
0.524	-5.997	-5.951	96	47.5
0.53	-6.169	-5.763	97	48
0.535	-6.318	-5.565	98	48.5
0.541	-6.454	-5.362	99	49
0.546	-6.574	-5.149	100	49.5
0.552	-6.679	-4.93	101	50
0.557	-6.749	-4.699	102	50.5
0.563	-6.807	-4.463	103	51
0.568	-6.845	-4.219	104	51.5
0.574	-6.86	-3.967	105	52
0.579	-6.849	-3.708	106	52.5
0.585	-6.812	-3.439	107	53
0.59	-6.762	-3.17	108	53.5
0.596	-6.682	-2.89	109	54
0.601	-6.571	-2.601	110	54.5
0.607	-6.44	-2.309	111	55
0.612	-6.292	-2.012	112	55.5
0.618	-6.111	-1.709	113	56
0.623	-5.904	-1.401	114	56.5
0.629	-5.677	-1.09	115	57
0.634	-5.431	-0.7742	116	57.5
0.64	-5.154	-0.4553	117	58
0.645	-4.852	-0.1333	118	58.5
0.651	-4.53	0.1922	119	59
0.656	-4.192	0.5174	120	59.5
0.662	-3.824	0.8466	121	60
0.668	-3.432	1.176	122	60.5
0.673	-3.03	1.501	123	61
0.678	-2.61	1.831	124	61.5
0.684	-2.163	2.159	125	62
0.69	-1.696	2.482	126	62.5
0.695	-1.215	2.807	127	63
0.701	-0.7285	3.128	128	63.5
0.706	-0.2177	3.442	129	64
0.712	0.3123	3.752	130	64.5
0.717	0.8455	4.057	131	65
0.723	1.384	4.357	132	65.5
0.728	1.944	4.646	133	66
0.734	2.516	4.928	134	66.5
0.739	3.088	5.202	135	67
0.745	3.667	5.47	136	67.5
0.75	4.257	5.725	137	68
0.756	4.847	5.964	138	68.5
0.761	5.439	6.199	139	69
0.767	6.038	6.423	140	69.5
0.772	6.636	6.629	141	70
0.778	7.236	6.823	142	70.5
0.783	7.835	7.008	143	71
0.789	8.432	7.178	144	71.5

0.794	9.026	7.331	145	72
0.8	9.619	7.471	146	72.5
0.805	10.2	7.6	147	73
0.811	10.78	7.713	148	73.5
0.817	11.36	7.809	149	74
0.822	11.93	7.891	150	74.5
0.827	12.5	7.963	151	75
0.833	13.05	8.019	152	75.5
0.839	13.59	8.057	153	76
0.844	14.13	8.082	154	76.5
0.85	14.66	8.098	155	77
0.855	15.18	8.1	156	77.5
0.861	15.69	8.085	157	78
0.866	16.19	8.059	158	78.5
0.872	16.68	8.027	159	79
0.877	17.16	7.982	160	79.5
0.883	17.63	7.925	161	80
0.888	18.08	7.863	162	80.5
0.894	18.53	7.793	163	81
0.899	18.96	7.716	164	81.5
0.905	19.38	7.634	165	82
0.91	19.79	7.547	166	82.5
0.916	20.19	7.457	167	83
0.921	20.57	7.365	168	83.5
0.927	20.95	7.27	169	84
0.932	21.31	7.175	170	84.5
0.938	21.66	7.082	171	85
0.943	21.99	6.988	172	85.5
0.949	22.32	6.894	173	86
0.954	22.63	6.804	174	86.5
0.96	22.93	6.716	175	87
0.965	23.21	6.63	176	87.5
0.971	23.48	6.548	177	88
0.976	23.74	6.469	178	88.5
0.982	23.98	6.394	179	89
0.988	24.21	6.322	180	89.5
0.993	24.43	6.252	181	90
0.998	24.63	6.186	182	90.5
1.004	24.81	6.125	183	91
1.01	24.98	6.063	184	91.5
1.015	25.14	6.006	185	92
1.021	25.28	5.952	186	92.5
1.026	25.4	5.898	187	93
1.032	25.51	5.845	188	93.5
1.037	25.61	5.794	189	94
1.043	25.69	5.743	190	94.5
1.048	25.75	5.69	191	95
1.054	25.79	5.638	192	95.5
1.059	25.83	5.583	193	96
1.065	25.84	5.526	194	96.5
1.07	25.83	5.463	195	97

1.076	25.81	5.397	196	97.5
1.081	25.78	5.331	197	98
1.087	25.73	5.253	198	98.5
1.092	25.65	5.164	199	99
1.098	25.56	5.076	200	99.5

Contact Forces in Hip Joint Relative to Femur

Subject: Average Patient
Activity: Normal Walking WN
Trial number: 0

Time[s]	-Fx[%BW]	-Fy[%BW]	-Fz[%BW]	Measurement		%Cycle
0	20.26	1.027	74.96	77.65	1	0
0.005	21.01	1.676	79.55	82.3	2	0.5
0.011	21.77	2.297	84.09	86.89	3	1
0.017	22.54	2.914	88.7	91.57	4	1.5
0.022	23.39	3.609	93.94	96.87	5	2
0.028	24.42	4.392	99.82	102.9	6	2.5
0.033	25.47	5.171	105.8	108.9	7	3
0.039	26.56	5.964	111.9	115.1	8	3.5
0.044	27.77	6.83	118.4	121.8	9	4
0.05	29.1	7.759	125.3	128.9	10	4.5
0.055	30.45	8.678	132.2	135.9	11	5
0.061	31.85	9.595	139.1	143	12	5.5
0.066	33.32	10.59	146.2	150.3	13	6
0.072	34.88	11.65	153.3	157.7	14	6.5
0.077	36.39	12.69	160.3	164.8	15	7
0.083	37.83	13.76	167	171.8	16	7.5
0.088	39.27	14.9	173.7	178.7	17	8
0.094	40.63	16.09	180	185.3	18	8.5
0.099	41.88	17.26	185.9	191.4	19	9
0.105	43.07	18.47	191.7	197.3	20	9.5
0.11	44.16	19.73	196.8	202.7	21	10
0.116	45.19	21	201.5	207.6	22	10.5
0.121	46.11	22.22	205.7	212	23	11
0.127	47	23.45	209.7	216.2	24	11.5
0.132	47.77	24.66	212.9	219.6	25	12
0.138	48.45	25.8	215.6	222.5	26	12.5
0.143	49.08	26.89	218.1	225.1	27	13
0.149	49.64	27.94	220.2	227.5	28	13.5
0.154	50.11	28.85	221.7	229.2	29	14
0.16	50.54	29.67	222.9	230.5	30	14.5
0.166	50.92	30.45	223.9	231.6	31	15
0.171	51.26	31.13	224.6	232.4	32	15.5
0.176	51.58	31.58	224.9	232.8	33	16
0.182	51.91	31.98	224.9	233.1	34	16.5
0.188	52.21	32.31	224.9	233.2	35	17
0.193	52.46	32.46	224.6	232.9	36	17.5
0.199	52.72	32.42	224.2	232.6	37	18
0.204	52.96	32.22	223.6	232	38	18.5
0.21	53.18	31.94	222.9	231.4	39	19
0.215	53.38	31.51	222.1	230.6	40	19.5
0.221	53.57	30.99	221.3	229.8	41	20
0.226	53.72	30.34	220.3	228.8	42	20.5

0.232	53.88	29.63	219.3	227.8	43	21
0.237	54.01	28.8	218.2	226.6	44	21.5
0.243	54.12	27.88	217.1	225.4	45	22
0.248	54.21	26.86	215.8	224.2	46	22.5
0.254	54.29	25.79	214.6	222.9	47	23
0.259	54.33	24.64	213.3	221.5	48	23.5
0.265	54.37	23.45	212.1	220.2	49	24
0.27	54.41	22.22	210.9	218.9	50	24.5
0.276	54.41	20.97	209.6	217.6	51	25
0.281	54.4	19.69	208.4	216.3	52	25.5
0.287	54.39	18.4	207.3	215.1	53	26
0.292	54.37	17.09	206.2	213.9	54	26.5
0.298	54.33	15.78	205.1	212.8	55	27
0.303	54.29	14.49	204.1	211.7	56	27.5
0.309	54.26	13.21	203.2	210.8	57	28
0.315	54.21	11.92	202.3	209.8	58	28.5
0.32	54.14	10.66	201.5	208.9	59	29
0.326	54.05	9.445	200.8	208.1	60	29.5
0.331	53.96	8.232	200.1	207.4	61	30
0.336	53.85	7.042	199.5	206.7	62	30.5
0.342	53.73	5.897	198.9	206.1	63	31
0.348	53.61	4.804	198.4	205.5	64	31.5
0.353	53.49	3.738	197.9	205.1	65	32
0.359	53.37	2.722	197.5	204.6	66	32.5
0.364	53.24	1.777	197.2	204.2	67	33
0.37	53.09	0.899	196.9	203.9	68	33.5
0.375	52.89	0.0752	196.8	203.7	69	34
0.381	52.68	-0.7074	196.6	203.5	70	34.5
0.386	52.47	-1.405	196.5	203.4	71	35
0.392	52.23	-2.041	196.5	203.3	72	35.5
0.397	51.94	-2.614	196.6	203.4	73	36
0.403	51.64	-3.134	196.7	203.4	74	36.5
0.408	51.33	-3.56	196.9	203.5	75	37
0.414	50.98	-3.947	197.1	203.6	76	37.5
0.419	50.59	-4.267	197.3	203.8	77	38
0.425	50.17	-4.527	197.6	203.9	78	38.5
0.43	49.7	-4.713	197.9	204.1	79	39
0.436	49.19	-4.854	198.2	204.3	80	39.5
0.441	48.62	-4.906	198.6	204.5	81	40
0.447	47.98	-4.904	198.9	204.6	82	40.5
0.452	47.3	-4.842	199.2	204.8	83	41
0.458	46.58	-4.727	199.5	204.9	84	41.5
0.463	45.77	-4.519	199.7	204.9	85	42
0.469	44.88	-4.244	199.9	204.9	86	42.5
0.474	43.92	-3.887	200	204.8	87	43
0.48	42.94	-3.481	200.1	204.7	88	43.5
0.486	41.9	-2.985	200	204.4	89	44
0.491	40.84	-2.407	200	204.1	90	44.5
0.496	39.73	-1.793	199.7	203.7	91	45
0.502	38.62	-1.141	199.4	203.1	92	45.5
0.507	37.54	-0.4411	199	202.5	93	46

0.513	36.49	0.3358	198.5	201.8	94	46.5
0.519	35.44	1.11	197.7	200.9	95	47
0.524	34.44	1.891	196.9	199.9	96	47.5
0.53	33.52	2.67	195.9	198.8	97	48
0.535	32.7	3.396	194.7	197.4	98	48.5
0.541	31.92	4.092	193.3	195.9	99	49
0.546	31.27	4.76	191.8	194.4	100	49.5
0.552	30.73	5.375	190.1	192.7	101	50
0.557	30.36	5.825	188.1	190.6	102	50.5
0.563	30.1	6.234	186	188.5	103	51
0.568	30.01	6.586	183.6	186.2	104	51.5
0.574	30.05	6.814	181	183.6	105	52
0.579	30.22	6.876	178.2	180.9	106	52.5
0.585	30.55	6.826	175.1	177.9	107	53
0.59	30.94	6.715	171.9	174.8	108	53.5
0.596	31.5	6.465	168.4	171.5	109	54
0.601	32.18	6.038	164.7	167.9	110	54.5
0.607	32.95	5.506	160.8	164.2	111	55
0.612	33.75	4.909	156.8	160.5	112	55.5
0.618	34.62	4.209	152.7	156.7	113	56
0.623	35.49	3.392	148.4	152.7	114	56.5
0.629	36.39	2.525	144.1	148.6	115	57
0.634	37.29	1.658	139.8	144.7	116	57.5
0.64	38.1	0.7499	135.4	140.7	117	58
0.645	38.84	-0.164	131.1	136.7	118	58.5
0.651	39.53	-1.051	126.7	132.8	119	59
0.656	40.14	-1.93	122.5	128.9	120	59.5
0.662	40.58	-2.771	118.4	125.2	121	60
0.668	40.87	-3.524	114.4	121.5	122	60.5
0.673	41.02	-4.181	110.6	118	123	61
0.678	41.06	-4.811	106.9	114.6	124	61.5
0.684	40.9	-5.378	103.3	111.3	125	62
0.69	40.54	-5.821	100	108.1	126	62.5
0.695	40.08	-6.2	96.83	105	127	63
0.701	39.56	-6.565	93.75	102	128	63.5
0.706	38.82	-6.819	90.93	99.1	129	64
0.712	37.99	-6.995	88.25	96.33	130	64.5
0.717	37.12	-7.164	85.65	93.62	131	65
0.723	36.21	-7.324	83.14	90.98	132	65.5
0.728	35.23	-7.397	80.91	88.56	133	66
0.734	34.21	-7.424	78.75	86.18	134	66.5
0.739	33.18	-7.455	76.59	83.8	135	67
0.745	32.16	-7.466	74.52	81.51	136	67.5
0.75	31.2	-7.423	72.63	79.4	137	68
0.756	30.28	-7.359	70.82	77.37	138	68.5
0.761	29.36	-7.289	68.97	75.32	139	69
0.767	28.47	-7.19	67.17	73.31	140	69.5
0.772	27.63	-7.062	65.36	71.31	141	70
0.778	26.81	-6.93	63.52	69.3	142	70.5
0.783	26.01	-6.802	61.71	67.31	143	71
0.789	25.23	-6.655	59.89	65.32	144	71.5

0.794	24.47	-6.482	58.06	63.34	145	72
0.8	23.73	-6.298	56.23	61.36	146	72.5
0.805	23.01	-6.119	54.41	59.39	147	73
0.811	22.33	-5.919	52.58	57.43	148	73.5
0.817	21.66	-5.683	50.78	55.5	149	74
0.822	21	-5.423	49.04	53.62	150	74.5
0.827	20.35	-5.168	47.3	51.75	151	75
0.833	19.71	-4.917	45.58	49.9	152	75.5
0.839	19.12	-4.675	43.95	48.15	153	76
0.844	18.52	-4.455	42.34	46.43	154	76.5
0.85	17.95	-4.235	40.78	44.76	155	77
0.855	17.38	-4.016	39.3	43.16	156	77.5
0.861	16.81	-3.783	37.88	41.62	157	78
0.866	16.22	-3.517	36.56	40.15	158	78.5
0.872	15.63	-3.243	35.28	38.73	159	79
0.877	15.05	-2.977	34.11	37.4	160	79.5
0.883	14.46	-2.71	33.04	36.17	161	80
0.888	14.02	-2.441	32.06	35.08	162	80.5
0.894	13.58	-2.174	31.15	34.05	163	81
0.899	13.15	-1.911	30.33	33.11	164	81.5
0.905	12.73	-1.63	29.59	32.25	165	82
0.91	12.34	-1.361	28.9	31.45	166	82.5
0.916	11.97	-1.09	28.34	30.78	167	83
0.921	11.62	-0.8081	27.91	30.24	168	83.5
0.927	11.27	-0.5195	27.55	29.77	169	84
0.932	10.97	-0.2072	27.25	29.37	170	84.5
0.938	10.67	0.1143	27.12	29.14	171	85
0.943	10.42	0.4424	27.1	29.04	172	85.5
0.949	10.2	0.7688	27.15	29.02	173	86
0.954	9.995	1.091	27.32	29.11	174	86.5
0.96	9.82	1.41	27.71	29.43	175	87
0.965	9.692	1.679	28.18	29.85	176	87.5
0.971	9.574	1.957	28.73	30.35	177	88
0.976	9.444	2.288	29.44	31	178	88.5
0.982	9.377	2.616	30.42	31.94	179	89
0.988	9.335	2.934	31.47	32.95	180	89.5
0.993	9.305	3.272	32.62	34.08	181	90
0.998	9.406	3.484	33.92	35.37	182	90.5
1.004	9.648	3.572	35.43	36.89	183	91
1.01	9.948	3.613	36.97	38.45	184	91.5
1.015	10.29	3.625	38.6	40.11	185	92
1.021	10.71	3.432	40.4	41.94	186	92.5
1.026	11.28	3.094	42.36	43.95	187	93
1.032	11.86	2.728	44.38	46.02	188	93.5
1.037	12.45	2.336	46.44	48.14	189	94
1.043	13.05	1.876	48.6	50.35	190	94.5
1.048	13.63	1.347	50.9	52.71	191	95
1.054	14.19	0.8388	53.26	55.13	192	95.5
1.059	14.74	0.3914	55.63	57.55	193	96
1.065	15.31	-0.0272	58.04	60.03	194	96.5
1.07	15.89	-0.3708	60.61	62.66	195	97

1.076	16.47	-0.6474	63.22	65.33	196	97.5
1.081	17.04	-0.8883	65.84	68.02	197	98
1.087	17.64	-0.9407	68.62	70.85	198	98.5
1.092	18.31	-0.8921	71.58	73.89	199	99
1.098	18.96	-0.8255	74.57	76.95	200	99.5

Moments of Contact Forces in Hip Joint Relative to Femur

Subject: Average Patient
Activity: Normal Walking WN
Trial number: 0

Time[s]	Mx[%BW*m]	My[%BW*m]	Mz[%BW*m]	Measurement		%Cycle
0	-0.0027	1.395	-0.2336	1.414	1	0
0.005	0.01288	1.491	-0.2652	1.514	2	0.5
0.011	0.02776	1.586	-0.2959	1.613	3	1
0.017	0.04248	1.682	-0.3267	1.714	4	1.5
0.022	0.05906	1.792	-0.3616	1.829	5	2
0.028	0.07772	1.913	-0.4006	1.956	6	2.5
0.033	0.09627	2.036	-0.4397	2.085	7	3
0.039	0.1151	2.161	-0.4795	2.217	8	3.5
0.044	0.1358	2.295	-0.5224	2.358	9	4
0.05	0.158	2.434	-0.5679	2.504	10	4.5
0.055	0.1799	2.573	-0.613	2.651	11	5
0.061	0.2017	2.71	-0.6578	2.796	12	5.5
0.066	0.2258	2.849	-0.705	2.944	13	6
0.072	0.2512	2.989	-0.7537	3.093	14	6.5
0.077	0.2763	3.124	-0.8014	3.237	15	7
0.083	0.3024	3.256	-0.8494	3.378	16	7.5
0.088	0.3304	3.386	-0.8991	3.519	17	8
0.094	0.3598	3.509	-0.9489	3.653	18	8.5
0.099	0.389	3.624	-0.997	3.778	19	9
0.105	0.4192	3.735	-1.046	3.901	20	9.5
0.11	0.4508	3.835	-1.094	4.013	21	10
0.116	0.4832	3.923	-1.141	4.114	22	10.5
0.121	0.5142	4.003	-1.185	4.206	23	11
0.127	0.5456	4.078	-1.228	4.293	24	11.5
0.132	0.5771	4.135	-1.269	4.364	25	12
0.138	0.6065	4.181	-1.306	4.422	26	12.5
0.143	0.6348	4.224	-1.341	4.477	27	13
0.149	0.6623	4.261	-1.374	4.526	28	13.5
0.154	0.6861	4.284	-1.402	4.559	29	14
0.16	0.7078	4.299	-1.426	4.584	30	14.5
0.166	0.7282	4.311	-1.448	4.606	31	15
0.171	0.7463	4.317	-1.467	4.62	32	15.5
0.176	0.7584	4.314	-1.478	4.623	33	16
0.182	0.7691	4.307	-1.487	4.621	34	16.5
0.188	0.7779	4.297	-1.494	4.615	35	17
0.193	0.782	4.282	-1.496	4.602	36	17.5
0.199	0.7812	4.264	-1.492	4.585	37	18
0.204	0.7759	4.243	-1.483	4.561	38	18.5
0.21	0.7687	4.22	-1.472	4.535	39	19
0.215	0.7574	4.197	-1.457	4.507	40	19.5
0.221	0.7438	4.172	-1.44	4.476	41	20
0.226	0.7268	4.145	-1.418	4.441	42	20.5

0.232	0.708	4.118	-1.395	4.405	43	21
0.237	0.6862	4.09	-1.369	4.367	44	21.5
0.243	0.6619	4.061	-1.34	4.327	45	22
0.248	0.6349	4.031	-1.308	4.285	46	22.5
0.254	0.6066	4.002	-1.275	4.244	47	23
0.259	0.5764	3.972	-1.241	4.201	48	23.5
0.265	0.5448	3.943	-1.205	4.159	49	24
0.27	0.5122	3.915	-1.168	4.118	50	24.5
0.276	0.4792	3.888	-1.131	4.078	51	25
0.281	0.4451	3.863	-1.093	4.039	52	25.5
0.287	0.411	3.839	-1.055	4.003	53	26
0.292	0.3763	3.816	-1.017	3.968	54	26.5
0.298	0.3415	3.794	-0.9791	3.933	55	27
0.303	0.3071	3.775	-0.942	3.903	56	27.5
0.309	0.2731	3.758	-0.9056	3.875	57	28
0.315	0.2388	3.741	-0.8689	3.848	58	28.5
0.32	0.2052	3.726	-0.8333	3.824	59	29
0.326	0.1728	3.715	-0.7994	3.804	60	29.5
0.331	0.1404	3.705	-0.7658	3.786	61	30
0.336	0.1087	3.696	-0.7331	3.77	62	30.5
0.342	0.07813	3.689	-0.7017	3.756	63	31
0.348	0.04895	3.683	-0.672	3.744	64	31.5
0.353	0.02046	3.679	-0.6432	3.735	65	32
0.359	-0.006701	3.676	-0.6159	3.727	66	32.5
0.364	-0.03197	3.674	-0.5907	3.721	67	33
0.37	-0.05548	3.675	-0.5676	3.719	68	33.5
0.375	-0.07757	3.679	-0.5466	3.72	69	34
0.381	-0.09855	3.684	-0.5268	3.723	70	34.5
0.386	-0.1173	3.69	-0.5094	3.727	71	35
0.392	-0.1344	3.699	-0.494	3.734	72	35.5
0.397	-0.1498	3.711	-0.4808	3.745	73	36
0.403	-0.1638	3.724	-0.4691	3.757	74	36.5
0.408	-0.1754	3.738	-0.4601	3.77	75	37
0.414	-0.1859	3.754	-0.4525	3.785	76	37.5
0.419	-0.1946	3.773	-0.4471	3.804	77	38
0.425	-0.2017	3.792	-0.4434	3.823	78	38.5
0.43	-0.2068	3.813	-0.4419	3.844	79	39
0.436	-0.2107	3.834	-0.4417	3.865	80	39.5
0.441	-0.2122	3.859	-0.4443	3.89	81	40
0.447	-0.2123	3.884	-0.4485	3.915	82	40.5
0.452	-0.2108	3.909	-0.4543	3.941	83	41
0.458	-0.2078	3.935	-0.4617	3.968	84	41.5
0.463	-0.2023	3.962	-0.4716	3.995	85	42
0.469	-0.195	3.99	-0.4835	4.023	86	42.5
0.474	-0.1854	4.017	-0.4975	4.052	87	43
0.48	-0.1745	4.043	-0.5126	4.079	88	43.5
0.486	-0.1612	4.067	-0.53	4.105	89	44
0.491	-0.1456	4.091	-0.5493	4.131	90	44.5
0.496	-0.129	4.113	-0.5694	4.154	91	45
0.502	-0.1113	4.131	-0.5899	4.175	92	45.5
0.507	-0.09237	4.147	-0.6113	4.193	93	46

0.513	-0.07126	4.158	-0.6339	4.206	94	46.5
0.519	-0.05013	4.163	-0.6556	4.215	95	47
0.524	-0.02879	4.165	-0.677	4.22	96	47.5
0.53	-0.00746	4.161	-0.6973	4.219	97	48
0.535	0.01256	4.148	-0.7148	4.209	98	48.5
0.541	0.03185	4.13	-0.7308	4.194	99	49
0.546	0.05042	4.106	-0.745	4.173	100	49.5
0.552	0.06764	4.075	-0.7567	4.145	101	50
0.557	0.08054	4.031	-0.762	4.103	102	50.5
0.563	0.09241	3.98	-0.7652	4.054	103	51
0.568	0.1028	3.921	-0.7654	3.997	104	51.5
0.574	0.11	3.852	-0.7608	3.928	105	52
0.579	0.1128	3.774	-0.7503	3.849	106	52.5
0.585	0.1127	3.685	-0.7351	3.759	107	53
0.59	0.111	3.592	-0.7178	3.665	108	53.5
0.596	0.1057	3.489	-0.6951	3.559	109	54
0.601	0.09577	3.376	-0.6661	3.442	110	54.5
0.607	0.08302	3.257	-0.6334	3.319	111	55
0.612	0.06859	3.136	-0.5986	3.193	112	55.5
0.618	0.05141	3.01	-0.5605	3.062	113	56
0.623	0.03116	2.88	-0.5184	2.926	114	56.5
0.629	0.009601	2.747	-0.4747	2.788	115	57
0.634	-0.01196	2.615	-0.4311	2.651	116	57.5
0.64	-0.03462	2.485	-0.3867	2.515	117	58
0.645	-0.05742	2.356	-0.3424	2.381	118	58.5
0.651	-0.07954	2.23	-0.2992	2.251	119	59
0.656	-0.1014	2.108	-0.2569	2.126	120	59.5
0.662	-0.1224	1.993	-0.2168	2.008	121	60
0.668	-0.141	1.885	-0.1803	1.899	122	60.5
0.673	-0.1572	1.786	-0.1475	1.799	123	61
0.678	-0.1726	1.69	-0.1162	1.703	124	61.5
0.684	-0.1864	1.606	-0.08825	1.619	125	62
0.69	-0.197	1.532	-0.06531	1.546	126	62.5
0.695	-0.2059	1.463	-0.04481	1.478	127	63
0.701	-0.2145	1.399	-0.0255	1.415	128	63.5
0.706	-0.2201	1.346	-0.01101	1.364	129	64
0.712	-0.2238	1.3	4.51E-04	1.319	130	64.5
0.717	-0.2273	1.257	0.01121	1.277	131	65
0.723	-0.2306	1.217	0.02122	1.238	132	65.5
0.728	-0.2316	1.185	0.02762	1.208	133	66
0.734	-0.2315	1.156	0.03234	1.18	134	66.5
0.739	-0.2314	1.128	0.03708	1.152	135	67
0.745	-0.2309	1.102	0.04102	1.126	136	67.5
0.75	-0.229	1.078	0.04308	1.103	137	68
0.756	-0.2265	1.056	0.0445	1.08	138	68.5
0.761	-0.2239	1.032	0.04588	1.057	139	69
0.767	-0.2205	1.008	0.04654	1.033	140	69.5
0.772	-0.2164	0.9838	0.04663	1.008	141	70
0.778	-0.212	0.9575	0.04683	0.9818	142	70.5
0.783	-0.2079	0.9313	0.04716	0.9554	143	71
0.789	-0.2032	0.9044	0.04711	0.9281	144	71.5

0.794	-0.1978	0.8764	0.04651	0.8996	145	72
0.8	-0.1921	0.8481	0.0457	0.8708	146	72.5
0.805	-0.1866	0.8195	0.04509	0.8416	147	73
0.811	-0.1804	0.7896	0.0441	0.8112	148	73.5
0.817	-0.1734	0.76	0.04215	0.7807	149	74
0.822	-0.1657	0.7312	0.03943	0.7508	150	74.5
0.827	-0.1581	0.7028	0.03681	0.7213	151	75
0.833	-0.1507	0.6741	0.03433	0.6915	152	75.5
0.839	-0.1435	0.6468	0.03187	0.6633	153	76
0.844	-0.1369	0.6202	0.02992	0.6358	154	76.5
0.85	-0.1304	0.5943	0.02786	0.6091	155	77
0.855	-0.1239	0.57	0.02558	0.5838	156	77.5
0.861	-0.1171	0.5478	0.02259	0.5607	157	78
0.866	-0.1094	0.5281	0.01835	0.5397	158	78.5
0.872	-0.1015	0.5098	0.01367	0.52	159	79
0.877	-0.09385	0.4939	0.008853	0.5028	160	79.5
0.883	-0.08624	0.4807	0.00359	0.4884	161	80
0.888	-0.07861	0.466	-0.001453	0.4726	162	80.5
0.894	-0.07107	0.453	-0.006674	0.4586	163	81
0.899	-0.06366	0.4423	-0.01216	0.447	164	81.5
0.905	-0.05579	0.4332	-0.01838	0.4372	165	82
0.91	-0.04828	0.4245	-0.02431	0.428	166	82.5
0.916	-0.04078	0.4189	-0.03076	0.4221	167	83
0.921	-0.03302	0.4161	-0.03793	0.4192	168	83.5
0.927	-0.02511	0.4146	-0.04547	0.4179	169	84
0.932	-0.01659	0.4137	-0.05371	0.4175	170	84.5
0.938	-0.007897	0.4171	-0.06286	0.4219	171	85
0.943	9.33E-04	0.4221	-0.0724	0.4283	172	85.5
0.949	0.009691	0.4277	-0.08198	0.4356	173	86
0.954	0.01829	0.4364	-0.09193	0.4463	174	86.5
0.96	0.02671	0.4497	-0.1025	0.462	175	87
0.965	0.03375	0.4641	-0.1119	0.4786	176	87.5
0.971	0.041	0.4804	-0.1218	0.4973	177	88
0.976	0.04962	0.5009	-0.1337	0.5208	178	88.5
0.982	0.05803	0.5267	-0.1464	0.5497	179	89
0.988	0.06616	0.5536	-0.1589	0.5797	180	89.5
0.993	0.07478	0.5829	-0.1724	0.6124	181	90
0.998	0.07998	0.6128	-0.1826	0.6444	182	90.5
1.004	0.08172	0.645	-0.1898	0.6773	183	91
1.01	0.08221	0.6768	-0.1956	0.7092	184	91.5
1.015	0.08188	0.7097	-0.2009	0.7421	185	92
1.021	0.07595	0.7458	-0.2012	0.7762	186	92.5
1.026	0.06608	0.7828	-0.1977	0.81	187	93
1.032	0.0554	0.821	-0.1936	0.8453	188	93.5
1.037	0.04404	0.8602	-0.1891	0.8818	189	94
1.043	0.03078	0.9018	-0.1831	0.9207	190	94.5
1.048	0.01562	0.9479	-0.1759	0.9642	191	95
1.054	0.001011	0.9961	-0.1697	1.01	192	95.5
1.059	-0.01198	1.044	-0.1651	1.057	193	96
1.065	-0.02421	1.093	-0.1613	1.105	194	96.5
1.07	-0.03449	1.146	-0.16	1.157	195	97

1.076	-0.04298	1.199	-0.1606	1.21	196	97.5
1.081	-0.05052	1.252	-0.1623	1.264	197	98
1.087	-0.05305	1.308	-0.1693	1.32	198	98.5
1.092	-0.05295	1.367	-0.1793	1.38	199	99
1.098	-0.05236	1.426	-0.19	1.44	200	99.5

Flexion and Abduction Angle, Femur System Relative to Pelvis System

Subject: Average Patient
Activity: Fast Walking WF
Trial number: 0

Time[s]	Flexion[deg]	Abduction[deg]	Meas. #	%Cycle
0	28.76	4.481	1	0
0.005	28.58	4.331	2	0.5
0.009	28.4	4.179	3	1
0.014	28.22	4.027	4	1.5
0.019	28.05	3.871	5	2
0.024	27.84	3.681	6	2.5
0.029	27.62	3.484	7	3
0.033	27.4	3.285	8	3.5
0.038	27.18	3.078	9	4
0.043	26.94	2.854	10	4.5
0.048	26.68	2.617	11	5
0.052	26.42	2.378	12	5.5
0.057	26.16	2.129	13	6
0.062	25.89	1.873	14	6.5
0.067	25.6	1.608	15	7
0.072	25.3	1.333	16	7.5
0.076	25	1.053	17	8
0.081	24.69	0.7707	18	8.5
0.086	24.36	0.4802	19	9
0.09	24.03	0.1864	20	9.5
0.095	23.69	-0.1162	21	10
0.1	23.35	-0.4151	22	10.5
0.105	22.99	-0.7205	23	11
0.11	22.63	-1.027	24	11.5
0.114	22.27	-1.337	25	12
0.119	21.89	-1.645	26	12.5
0.124	21.51	-1.952	27	13
0.129	21.12	-2.259	28	13.5
0.133	20.73	-2.569	29	14
0.138	20.34	-2.872	30	14.5
0.143	19.93	-3.174	31	15
0.148	19.53	-3.469	32	15.5
0.152	19.12	-3.766	33	16
0.157	18.71	-4.059	34	16.5
0.162	18.29	-4.341	35	17
0.167	17.87	-4.616	36	17.5
0.171	17.45	-4.89	37	18
0.176	17.03	-5.161	38	18.5
0.181	16.6	-5.418	39	19
0.186	16.17	-5.662	40	19.5
0.191	15.74	-5.905	41	20
0.195	15.32	-6.14	42	20.5

0.2	14.88	-6.365	43	21
0.205	14.45	-6.573	44	21.5
0.21	14.02	-6.774	45	22
0.214	13.59	-6.969	46	22.5
0.219	13.15	-7.153	47	23
0.224	12.72	-7.319	48	23.5
0.229	12.28	-7.473	49	24
0.233	11.85	-7.621	50	24.5
0.238	11.42	-7.759	51	25
0.243	10.99	-7.882	52	25.5
0.248	10.55	-7.985	53	26
0.252	10.12	-8.082	54	26.5
0.257	9.685	-8.17	55	27
0.262	9.254	-8.246	56	27.5
0.267	8.823	-8.303	57	28
0.271	8.392	-8.349	58	28.5
0.276	7.96	-8.387	59	29
0.281	7.536	-8.416	60	29.5
0.286	7.107	-8.429	61	30
0.291	6.685	-8.431	62	30.5
0.295	6.26	-8.42	63	31
0.3	5.839	-8.406	64	31.5
0.305	5.421	-8.38	65	32
0.31	5.002	-8.345	66	32.5
0.314	4.588	-8.297	67	33
0.319	4.178	-8.241	68	33.5
0.324	3.769	-8.177	69	34
0.329	3.365	-8.107	70	34.5
0.333	2.959	-8.028	71	35
0.338	2.566	-7.94	72	35.5
0.343	2.176	-7.844	73	36
0.348	1.789	-7.741	74	36.5
0.352	1.405	-7.634	75	37
0.357	1.026	-7.522	76	37.5
0.362	0.6629	-7.398	77	38
0.367	0.3025	-7.27	78	38.5
0.372	-0.0563	-7.137	79	39
0.376	-0.4061	-7.001	80	39.5
0.381	-0.7466	-6.857	81	40
0.386	-1.071	-6.709	82	40.5
0.391	-1.395	-6.556	83	41
0.395	-1.71	-6.399	84	41.5
0.4	-2.015	-6.238	85	42
0.405	-2.306	-6.073	86	42.5
0.41	-2.585	-5.905	87	43
0.414	-2.855	-5.733	88	43.5
0.419	-3.117	-5.556	89	44
0.424	-3.362	-5.378	90	44.5
0.429	-3.595	-5.196	91	45
0.433	-3.81	-5.013	92	45.5
0.438	-4.016	-4.824	93	46

0.443	-4.205	-4.634	94	46.5
0.448	-4.377	-4.441	95	47
0.452	-4.532	-4.246	96	47.5
0.457	-4.672	-4.048	97	48
0.462	-4.789	-3.848	98	48.5
0.467	-4.893	-3.644	99	49
0.472	-4.971	-3.44	100	49.5
0.476	-5.043	-3.231	101	50
0.481	-5.079	-3.024	102	50.5
0.486	-5.1	-2.811	103	51
0.491	-5.096	-2.597	104	51.5
0.495	-5.083	-2.381	105	52
0.5	-5.038	-2.164	106	52.5
0.505	-4.967	-1.943	107	53
0.51	-4.875	-1.721	108	53.5
0.515	-4.768	-1.496	109	54
0.519	-4.635	-1.271	110	54.5
0.524	-4.474	-1.04	111	55
0.529	-4.288	-0.8107	112	55.5
0.534	-4.09	-0.5772	113	56
0.538	-3.866	-0.3431	114	56.5
0.543	-3.613	-0.1044	115	57
0.548	-3.338	0.1353	116	57.5
0.553	-3.051	0.3764	117	58
0.557	-2.746	0.6191	118	58.5
0.562	-2.403	0.8681	119	59
0.567	-2.046	1.116	120	59.5
0.572	-1.676	1.368	121	60
0.576	-1.298	1.619	122	60.5
0.581	-0.8848	1.876	123	61
0.586	-0.4518	2.134	124	61.5
0.591	-0.0135	2.394	125	62
0.595	0.4299	2.653	126	62.5
0.6	0.8948	2.917	127	63
0.605	1.384	3.181	128	63.5
0.61	1.882	3.447	129	64
0.614	2.376	3.71	130	64.5
0.619	2.884	3.978	131	65
0.624	3.408	4.242	132	65.5
0.629	3.944	4.507	133	66
0.633	4.479	4.769	134	66.5
0.638	5.016	5.032	135	67
0.643	5.564	5.292	136	67.5
0.648	6.117	5.548	137	68
0.653	6.672	5.798	138	68.5
0.657	7.229	6.05	139	69
0.662	7.783	6.294	140	69.5
0.667	8.346	6.532	141	70
0.672	8.899	6.761	142	70.5
0.676	9.457	6.989	143	71
0.681	10.01	7.208	144	71.5

0.686	10.56	7.414	145	72
0.691	11.11	7.613	146	72.5
0.696	11.65	7.806	147	73
0.7	12.18	7.987	148	73.5
0.705	12.72	8.151	149	74
0.71	13.24	8.308	150	74.5
0.715	13.76	8.458	151	75
0.719	14.26	8.591	152	75.5
0.724	14.76	8.703	153	76
0.729	15.26	8.807	154	76.5
0.734	15.75	8.905	155	77
0.738	16.22	8.987	156	77.5
0.743	16.68	9.044	157	78
0.748	17.13	9.092	158	78.5
0.753	17.59	9.133	159	79
0.757	18.02	9.161	160	79.5
0.762	18.44	9.167	161	80
0.767	18.85	9.163	162	80.5
0.772	19.26	9.151	163	81
0.776	19.66	9.13	164	81.5
0.781	20.03	9.092	165	82
0.786	20.4	9.043	166	82.5
0.791	20.76	8.987	167	83
0.795	21.11	8.924	168	83.5
0.8	21.45	8.85	169	84
0.805	21.76	8.766	170	84.5
0.81	22.08	8.677	171	85
0.814	22.38	8.585	172	85.5
0.819	22.66	8.484	173	86
0.824	22.93	8.376	174	86.5
0.829	23.19	8.264	175	87
0.834	23.44	8.151	176	87.5
0.838	23.68	8.034	177	88
0.843	23.9	7.912	178	88.5
0.848	24.1	7.785	179	89
0.853	24.3	7.659	180	89.5
0.857	24.48	7.529	181	90
0.862	24.65	7.398	182	90.5
0.867	24.81	7.264	183	91
0.872	24.96	7.131	184	91.5
0.877	25.09	6.994	185	92
0.881	25.2	6.855	186	92.5
0.886	25.3	6.714	187	93
0.891	25.4	6.572	188	93.5
0.896	25.48	6.426	189	94
0.9	25.54	6.279	190	94.5
0.905	25.59	6.125	191	95
0.91	25.63	5.969	192	95.5
0.915	25.66	5.809	193	96
0.919	25.66	5.644	194	96.5
0.924	25.65	5.473	195	97

0.929	25.64	5.298	196	97.5
0.934	25.62	5.118	197	98
0.938	25.57	4.926	198	98.5
0.943	25.5	4.727	199	99
0.948	25.44	4.531	200	99.5

Contact Forces in Hip Joint Relative to Femur

Subject: Average Patient
Activity: Fast Walking WF
Trial number: 0

Time[s]	-Fx[%BW]	-Fy[%BW]	-Fz[%BW]	Measurement		%Cycle
0	33.29	1.216	115.7	120.4	1	0
0.005	34.19	2.131	120.8	125.6	2	0.5
0.009	35.11	3.047	126	130.9	3	1
0.014	36.02	3.941	131.2	136.1	4	1.5
0.019	36.95	4.843	136.4	141.4	5	2
0.024	38.01	5.909	142.4	147.5	6	2.5
0.029	39.11	7.037	148.7	153.9	7	3
0.033	40.21	8.16	155	160.3	8	3.5
0.038	41.32	9.285	161.3	166.8	9	4
0.043	42.42	10.44	167.8	173.4	10	4.5
0.048	43.51	11.69	174.5	180.2	11	5
0.052	44.57	12.95	181.1	187	12	5.5
0.057	45.63	14.21	187.8	193.8	13	6
0.062	46.62	15.46	194.3	200.4	14	6.5
0.067	47.54	16.73	200.6	206.8	15	7
0.072	48.35	18.01	206.7	213	16	7.5
0.076	49.13	19.26	212.6	219.1	17	8
0.081	49.82	20.49	218.1	224.6	18	8.5
0.086	50.38	21.7	222.9	229.6	19	9
0.09	50.81	22.85	227.3	234	20	9.5
0.095	51.16	23.97	231.3	238.1	21	10
0.1	51.41	25.05	234.8	241.7	22	10.5
0.105	51.51	26.07	237.5	244.4	23	11
0.11	51.56	27.04	239.8	246.8	24	11.5
0.114	51.5	27.93	241.5	248.5	25	12
0.119	51.38	28.79	242.8	249.9	26	12.5
0.124	51.14	29.51	243.2	250.3	27	13
0.129	50.91	30.21	243.5	250.6	28	13.5
0.133	50.65	30.86	243.4	250.5	29	14
0.138	50.35	31.4	242.7	249.9	30	14.5
0.143	49.96	31.79	241.5	248.6	31	15
0.148	49.55	32.16	240.1	247.3	32	15.5
0.152	49.13	32.49	238.6	245.8	33	16
0.157	48.72	32.71	236.8	243.9	34	16.5
0.162	48.37	32.72	234.6	241.7	35	17
0.167	48.07	32.67	232.3	239.4	36	17.5
0.171	47.78	32.61	229.9	237.1	37	18
0.176	47.53	32.48	227.5	234.7	38	18.5
0.181	47.36	32.11	225	232.1	39	19
0.186	47.22	31.64	222.4	229.5	40	19.5
0.191	47.1	31.12	219.7	226.9	41	20
0.195	46.99	30.57	217.2	224.3	42	20.5

0.2	46.93	29.85	214.6	221.7	43	21
0.205	46.93	28.97	212.1	219.1	44	21.5
0.21	46.95	28.04	209.5	216.5	45	22
0.214	46.97	27.07	207	214	46	22.5
0.219	47.01	26.03	204.7	211.6	47	23
0.224	47.04	24.89	202.4	209.3	48	23.5
0.229	47.07	23.67	200.2	207	49	24
0.233	47.12	22.45	198.1	204.8	50	24.5
0.238	47.17	21.15	196	202.7	51	25
0.243	47.2	19.86	194.2	200.9	52	25.5
0.248	47.23	18.48	192.4	199	53	26
0.252	47.26	17.08	190.6	197.1	54	26.5
0.257	47.27	15.68	189	195.4	55	27
0.262	47.26	14.29	187.6	194	56	27.5
0.267	47.21	12.86	186.2	192.5	57	28
0.271	47.15	11.43	184.9	191.1	58	28.5
0.276	47.1	10.01	183.8	190	59	29
0.281	47.05	8.686	182.8	189	60	29.5
0.286	46.99	7.365	182	188.1	61	30
0.291	46.95	6.082	181.2	187.3	62	30.5
0.295	46.92	4.833	180.6	186.7	63	31
0.3	46.9	3.67	180.2	186.2	64	31.5
0.305	46.89	2.573	179.9	185.9	65	32
0.31	46.89	1.479	179.6	185.6	66	32.5
0.314	46.91	0.4538	179.5	185.6	67	33
0.319	46.92	-0.4967	179.6	185.6	68	33.5
0.324	46.96	-1.364	179.8	185.8	69	34
0.329	47	-2.206	180	186.1	70	34.5
0.333	47.03	-3.023	180.3	186.4	71	35
0.338	47.05	-3.738	180.8	186.8	72	35.5
0.343	47.05	-4.354	181.4	187.5	73	36
0.348	47.05	-4.962	182.1	188.1	74	36.5
0.352	47.05	-5.547	182.7	188.8	75	37
0.357	47.05	-6.1	183.5	189.5	76	37.5
0.362	47.03	-6.519	184.4	190.4	77	38
0.367	46.99	-6.923	185.4	191.3	78	38.5
0.372	46.94	-7.305	186.3	192.3	79	39
0.376	46.89	-7.647	187.3	193.3	80	39.5
0.381	46.82	-7.891	188.4	194.2	81	40
0.386	46.72	-8.102	189.4	195.2	82	40.5
0.391	46.59	-8.292	190.4	196.2	83	41
0.395	46.44	-8.423	191.5	197.3	84	41.5
0.4	46.27	-8.499	192.5	198.2	85	42
0.405	46.05	-8.498	193.5	199.1	86	42.5
0.41	45.81	-8.464	194.4	199.9	87	43
0.414	45.55	-8.358	195.2	200.7	88	43.5
0.419	45.26	-8.208	196	201.3	89	44
0.424	44.95	-8.004	196.7	201.9	90	44.5
0.429	44.62	-7.747	197.2	202.3	91	45
0.433	44.29	-7.446	197.5	202.5	92	45.5
0.438	43.94	-7.082	197.7	202.6	93	46

0.443	43.57	-6.675	197.7	202.5	94	46.5
0.448	43.21	-6.233	197.5	202.3	95	47
0.452	42.88	-5.808	197.1	201.8	96	47.5
0.457	42.58	-5.383	196.4	201.1	97	48
0.462	42.29	-4.955	195.5	200	98	48.5
0.467	42.07	-4.485	194.4	198.9	99	49
0.472	41.9	-4.091	192.9	197.4	100	49.5
0.476	41.76	-3.696	191.4	195.9	101	50
0.481	41.67	-3.378	189.4	193.9	102	50.5
0.486	41.68	-3.034	187.2	191.8	103	51
0.491	41.77	-2.783	184.7	189.4	104	51.5
0.495	41.9	-2.549	182.2	186.9	105	52
0.5	42.07	-2.399	179.2	184.1	106	52.5
0.505	42.36	-2.285	176	181.1	107	53
0.51	42.73	-2.269	172.6	177.8	108	53.5
0.515	43.12	-2.293	169.2	174.6	109	54
0.519	43.54	-2.395	165.6	171.2	110	54.5
0.524	44.03	-2.567	161.7	167.6	111	55
0.529	44.53	-2.781	157.8	164	112	55.5
0.534	45.06	-3.023	153.9	160.4	113	56
0.538	45.58	-3.284	150	156.9	114	56.5
0.543	46.12	-3.579	146.1	153.3	115	57
0.548	46.68	-3.901	142.3	149.8	116	57.5
0.553	47.22	-4.223	138.5	146.4	117	58
0.557	47.75	-4.574	134.9	143.1	118	58.5
0.562	48.24	-4.956	131.4	140.1	119	59
0.567	48.68	-5.332	128.1	137.2	120	59.5
0.572	49.11	-5.701	124.9	134.3	121	60
0.576	49.48	-6.061	121.8	131.6	122	60.5
0.581	49.78	-6.361	119	129.2	123	61
0.586	49.93	-6.643	116.4	126.8	124	61.5
0.591	50.02	-6.908	113.9	124.6	125	62
0.595	50.06	-7.198	111.5	122.5	126	62.5
0.6	49.97	-7.4	109.4	120.5	127	63
0.605	49.73	-7.599	107.4	118.6	128	63.5
0.61	49.42	-7.79	105.5	116.8	129	64
0.614	49.04	-8.005	103.7	115	130	64.5
0.619	48.59	-8.151	102	113.3	131	65
0.624	47.97	-8.262	100.4	111.6	132	65.5
0.629	47.27	-8.354	98.71	109.8	133	66
0.633	46.51	-8.462	97.04	107.9	134	66.5
0.638	45.72	-8.526	95.42	106.1	135	67
0.643	44.83	-8.54	93.78	104.3	136	67.5
0.648	43.87	-8.516	91.96	102.2	137	68
0.653	42.88	-8.482	90.09	100.1	138	68.5
0.657	41.87	-8.431	88.19	97.98	139	69
0.662	40.84	-8.347	86.25	95.79	140	69.5
0.667	39.78	-8.228	84.14	93.43	141	70
0.672	38.71	-8.099	81.94	90.99	142	70.5
0.676	37.65	-7.954	79.71	88.51	143	71
0.681	36.62	-7.776	77.44	86.01	144	71.5

0.686	35.61	-7.564	75.06	83.42	145	72
0.691	34.59	-7.335	72.62	80.77	146	72.5
0.696	33.63	-7.106	70.25	78.21	147	73
0.7	32.73	-6.87	67.86	75.65	148	73.5
0.705	31.88	-6.603	65.42	73.07	149	74
0.71	31.04	-6.336	63	70.52	150	74.5
0.715	30.23	-6.049	60.61	68	151	75
0.719	29.51	-5.78	58.35	65.64	152	75.5
0.724	28.83	-5.519	56.11	63.32	153	76
0.729	28.16	-5.258	53.91	61.05	154	76.5
0.734	27.51	-5.01	51.75	58.82	155	77
0.738	26.9	-4.795	49.71	56.72	156	77.5
0.743	26.34	-4.587	47.84	54.8	157	78
0.748	25.8	-4.368	46.04	52.95	158	78.5
0.753	25.27	-4.144	44.25	51.12	159	79
0.757	24.79	-3.947	42.61	49.45	160	79.5
0.762	24.32	-3.761	41.16	47.95	161	80
0.767	23.9	-3.576	39.87	46.62	162	80.5
0.772	23.49	-3.379	38.62	45.33	163	81
0.776	23.09	-3.21	37.45	44.11	164	81.5
0.781	22.73	-3.074	36.56	43.16	165	82
0.786	22.4	-2.938	35.82	42.35	166	82.5
0.791	22.11	-2.794	35.19	41.66	167	83
0.795	21.84	-2.655	34.72	41.1	168	83.5
0.8	21.62	-2.53	34.55	40.84	169	84
0.805	21.45	-2.401	34.6	40.78	170	84.5
0.81	21.3	-2.265	34.78	40.85	171	85
0.814	21.18	-2.14	35.08	41.03	172	85.5
0.819	21.12	-2.067	35.81	41.63	173	86
0.824	21.12	-1.996	36.81	42.49	174	86.5
0.829	21.14	-1.928	37.92	43.46	175	87
0.834	21.21	-1.864	39.14	44.55	176	87.5
0.838	21.32	-1.789	40.79	46.06	177	88
0.843	21.46	-1.701	42.68	47.8	178	88.5
0.848	21.65	-1.64	44.79	49.77	179	89
0.853	21.85	-1.591	46.99	51.84	180	89.5
0.857	22.08	-1.561	49.55	54.27	181	90
0.862	22.33	-1.548	52.32	56.91	182	90.5
0.867	22.62	-1.568	55.23	59.71	183	91
0.872	22.93	-1.642	58.28	62.65	184	91.5
0.877	23.25	-1.728	61.53	65.8	185	92
0.881	23.6	-1.798	64.94	69.11	186	92.5
0.886	23.98	-1.896	68.44	72.54	187	93
0.891	24.42	-2.015	72.03	76.08	188	93.5
0.896	24.86	-2.103	75.72	79.73	189	94
0.9	25.34	-2.147	79.49	83.46	190	94.5
0.905	25.85	-2.191	83.33	87.27	191	95
0.91	26.36	-2.221	87.08	91.01	192	95.5
0.915	26.89	-2.215	90.93	94.84	193	96
0.919	27.43	-2.122	94.9	98.81	194	96.5
0.924	28	-2.004	98.83	102.7	195	97

0.929	28.59	-1.868	102.7	106.6	196	97.5
0.934	29.19	-1.687	106.6	110.6	197	98
0.938	29.85	-1.309	110.9	114.8	198	98.5
0.943	30.53	-0.8741	115.1	119.1	199	99
0.948	31.2	-0.4455	119.3	123.3	200	99.5

Moments of Contact Forces in Hip Joint Relative to Femur

Subject: Average Patient
Activity: Fast Walking WF
Trial number: 0

Time[s]	Mx[%BW*m]	My[%BW*m]	Mz[%BW*m]	Measurement		%Cycle
0	-0.0141	2.101	-0.342	2.129	1	0
0.005	0.00842	2.206	-0.3819	2.239	2	0.5
0.009	0.03095	2.312	-0.4221	2.351	3	1
0.014	0.05292	2.418	-0.4617	2.462	4	1.5
0.019	0.07507	2.524	-0.5015	2.575	5	2
0.024	0.1013	2.647	-0.5481	2.705	6	2.5
0.029	0.1291	2.775	-0.5972	2.841	7	3
0.033	0.1567	2.904	-0.6462	2.979	8	3.5
0.038	0.1844	3.033	-0.6955	3.117	9	4
0.043	0.2129	3.167	-0.7461	3.261	10	4.5
0.048	0.2439	3.307	-0.8004	3.411	11	5
0.052	0.2751	3.446	-0.8546	3.561	12	5.5
0.057	0.306	3.586	-0.9088	3.712	13	6
0.062	0.337	3.721	-0.9624	3.859	14	6.5
0.067	0.3687	3.855	-1.016	4.003	15	7
0.072	0.4007	3.985	-1.07	4.146	16	7.5
0.076	0.4319	4.113	-1.122	4.285	17	8
0.081	0.4628	4.231	-1.173	4.414	18	8.5
0.086	0.4933	4.336	-1.221	4.532	19	9
0.09	0.5224	4.432	-1.265	4.639	20	9.5
0.095	0.551	4.522	-1.309	4.74	21	10
0.1	0.5786	4.602	-1.35	4.831	22	10.5
0.105	0.6049	4.665	-1.386	4.904	23	11
0.11	0.63	4.719	-1.42	4.968	24	11.5
0.114	0.6534	4.761	-1.45	5.02	25	12
0.119	0.676	4.795	-1.478	5.063	26	12.5
0.124	0.6952	4.809	-1.5	5.085	27	13
0.129	0.7139	4.819	-1.52	5.103	28	13.5
0.133	0.7315	4.821	-1.537	5.113	29	14
0.138	0.7463	4.81	-1.55	5.108	30	14.5
0.143	0.7573	4.786	-1.557	5.09	31	15
0.148	0.7676	4.76	-1.563	5.069	32	15.5
0.152	0.7772	4.731	-1.567	5.044	33	16
0.157	0.7838	4.694	-1.567	5.01	34	16.5
0.162	0.7849	4.646	-1.56	4.963	35	17
0.167	0.7847	4.594	-1.551	4.912	36	17.5
0.171	0.7839	4.542	-1.542	4.861	37	18
0.176	0.7815	4.488	-1.53	4.806	38	18.5
0.181	0.7726	4.427	-1.511	4.741	39	19
0.186	0.7608	4.366	-1.489	4.675	40	19.5
0.191	0.7481	4.303	-1.466	4.607	41	20
0.195	0.7342	4.241	-1.442	4.54	42	20.5

0.2	0.7159	4.18	-1.414	4.471	43	21
0.205	0.6931	4.117	-1.38	4.398	44	21.5
0.21	0.6694	4.055	-1.347	4.325	45	22
0.214	0.6442	3.994	-1.311	4.252	46	22.5
0.219	0.6173	3.937	-1.275	4.184	47	23
0.224	0.5874	3.883	-1.237	4.117	48	23.5
0.229	0.5556	3.829	-1.196	4.05	49	24
0.233	0.5236	3.777	-1.156	3.984	50	24.5
0.238	0.4895	3.729	-1.114	3.922	51	25
0.243	0.4556	3.686	-1.073	3.866	52	25.5
0.248	0.4192	3.644	-1.03	3.81	53	26
0.252	0.3823	3.602	-0.9869	3.755	54	26.5
0.257	0.3452	3.565	-0.9441	3.704	55	27
0.262	0.3084	3.534	-0.9025	3.661	56	27.5
0.267	0.2706	3.505	-0.8603	3.62	57	28
0.271	0.2325	3.48	-0.8185	3.582	58	28.5
0.276	0.1948	3.458	-0.7776	3.549	59	29
0.281	0.1596	3.44	-0.7399	3.522	60	29.5
0.286	0.1245	3.425	-0.7026	3.498	61	30
0.291	0.09026	3.411	-0.6667	3.477	62	30.5
0.295	0.05688	3.403	-0.6323	3.461	63	31
0.3	0.02579	3.396	-0.6006	3.449	64	31.5
0.305	-0.003566	3.393	-0.5711	3.441	65	32
0.31	-0.03288	3.39	-0.5417	3.433	66	32.5
0.314	-0.06042	3.391	-0.5148	3.431	67	33
0.319	-0.086	3.396	-0.4904	3.433	68	33.5
0.324	-0.1094	3.404	-0.4687	3.438	69	34
0.329	-0.1321	3.413	-0.4477	3.444	70	34.5
0.333	-0.1542	3.422	-0.4275	3.452	71	35
0.338	-0.1736	3.436	-0.4108	3.465	72	35.5
0.343	-0.1905	3.455	-0.3974	3.483	73	36
0.348	-0.2071	3.475	-0.3844	3.502	74	36.5
0.352	-0.2231	3.495	-0.3719	3.521	75	37
0.357	-0.2383	3.516	-0.3606	3.542	76	37.5
0.362	-0.2499	3.542	-0.3535	3.568	77	38
0.367	-0.2612	3.569	-0.347	3.595	78	38.5
0.372	-0.2718	3.597	-0.3412	3.623	79	39
0.376	-0.2814	3.626	-0.3367	3.652	80	39.5
0.381	-0.2884	3.655	-0.3347	3.682	81	40
0.386	-0.2945	3.686	-0.3339	3.712	82	40.5
0.391	-0.3	3.716	-0.3337	3.743	83	41
0.395	-0.304	3.749	-0.3353	3.776	84	41.5
0.4	-0.3064	3.78	-0.3382	3.808	85	42
0.405	-0.3068	3.811	-0.3431	3.839	86	42.5
0.41	-0.3062	3.84	-0.3485	3.868	87	43
0.414	-0.3037	3.868	-0.3557	3.896	88	43.5
0.419	-0.3	3.895	-0.364	3.924	89	44
0.424	-0.2948	3.92	-0.3733	3.948	90	44.5
0.429	-0.2881	3.941	-0.3835	3.97	91	45
0.433	-0.2801	3.955	-0.3938	3.985	92	45.5
0.438	-0.2704	3.969	-0.4056	3.999	93	46

0.443	-0.2595	3.977	-0.4177	4.007	94	46.5
0.448	-0.2475	3.98	-0.4302	4.011	95	47
0.452	-0.2359	3.976	-0.4409	4.007	96	47.5
0.457	-0.2242	3.966	-0.4507	3.998	97	48
0.462	-0.2123	3.947	-0.4592	3.979	98	48.5
0.467	-0.1992	3.923	-0.4679	3.955	99	49
0.472	-0.188	3.888	-0.4731	3.921	100	49.5
0.476	-0.1768	3.85	-0.4778	3.884	101	50
0.481	-0.1674	3.8	-0.4785	3.834	102	50.5
0.486	-0.1573	3.743	-0.4788	3.776	103	51
0.491	-0.1496	3.675	-0.4749	3.708	104	51.5
0.495	-0.1422	3.605	-0.4703	3.638	105	52
0.5	-0.137	3.523	-0.4616	3.556	106	52.5
0.505	-0.1326	3.432	-0.4505	3.464	107	53
0.51	-0.1309	3.335	-0.4358	3.366	108	53.5
0.515	-0.1301	3.235	-0.4196	3.265	109	54
0.519	-0.1314	3.132	-0.4009	3.16	110	54.5
0.524	-0.1344	3.019	-0.3787	3.045	111	55
0.529	-0.1386	2.906	-0.3556	2.931	112	55.5
0.534	-0.1435	2.792	-0.3314	2.815	113	56
0.538	-0.149	2.68	-0.307	2.702	114	56.5
0.543	-0.1554	2.566	-0.2814	2.586	115	57
0.548	-0.1625	2.452	-0.2552	2.471	116	57.5
0.553	-0.1696	2.342	-0.2295	2.359	117	58
0.557	-0.1776	2.236	-0.2036	2.252	118	58.5
0.562	-0.1864	2.135	-0.1778	2.15	119	59
0.567	-0.1952	2.039	-0.153	2.054	120	59.5
0.572	-0.2038	1.946	-0.1287	1.961	121	60
0.576	-0.2123	1.859	-0.1055	1.874	122	60.5
0.581	-0.2192	1.78	-0.08543	1.796	123	61
0.586	-0.2257	1.709	-0.067	1.725	124	61.5
0.591	-0.2319	1.644	-0.04985	1.661	125	62
0.595	-0.2387	1.582	-0.0327	1.6	126	62.5
0.6	-0.2432	1.53	-0.01945	1.55	127	63
0.605	-0.2478	1.486	-0.007513	1.507	128	63.5
0.61	-0.2522	1.446	0.003616	1.468	129	64
0.614	-0.2572	1.41	0.01466	1.434	130	64.5
0.619	-0.2605	1.379	0.0231	1.404	131	65
0.624	-0.2628	1.354	0.02969	1.38	132	65.5
0.629	-0.2646	1.329	0.03562	1.356	133	66
0.633	-0.2668	1.307	0.04162	1.335	134	66.5
0.638	-0.2679	1.286	0.04618	1.315	135	67
0.643	-0.2676	1.267	0.0491	1.296	136	67.5
0.648	-0.2662	1.246	0.05138	1.275	137	68
0.653	-0.2645	1.224	0.05351	1.253	138	68.5
0.657	-0.2624	1.201	0.0552	1.231	139	69
0.662	-0.2594	1.178	0.0561	1.208	140	69.5
0.667	-0.2553	1.151	0.05664	1.181	141	70
0.672	-0.2509	1.122	0.05726	1.151	142	70.5
0.676	-0.2461	1.092	0.05762	1.121	143	71
0.681	-0.2404	1.06	0.05742	1.089	144	71.5

0.686	-0.2338	1.025	0.05688	1.052	145	72
0.691	-0.2266	0.9876	0.0561	1.015	146	72.5
0.696	-0.2195	0.951	0.05527	0.9776	147	73
0.7	-0.2122	0.9121	0.05466	0.938	148	73.5
0.705	-0.204	0.8708	0.05361	0.8959	149	74
0.71	-0.1959	0.8293	0.05259	0.8537	150	74.5
0.715	-0.1872	0.7882	0.05101	0.8117	151	75
0.719	-0.179	0.7476	0.04983	0.7704	152	75.5
0.724	-0.1711	0.7068	0.04893	0.7289	153	76
0.729	-0.1632	0.6666	0.04796	0.688	154	76.5
0.734	-0.1557	0.6273	0.04719	0.648	155	77
0.738	-0.1491	0.5898	0.04702	0.6102	156	77.5
0.743	-0.1427	0.5556	0.04653	0.5755	157	78
0.748	-0.1361	0.5223	0.04566	0.5416	158	78.5
0.753	-0.1293	0.4893	0.04461	0.5081	159	79
0.757	-0.1234	0.4591	0.04385	0.4774	160	79.5
0.762	-0.1178	0.433	0.04274	0.4508	161	80
0.767	-0.1123	0.4102	0.04119	0.4273	162	80.5
0.772	-0.1065	0.3881	0.03923	0.4043	163	81
0.776	-0.1015	0.3678	0.03771	0.3834	164	81.5
0.781	-0.09746	0.354	0.0361	0.3689	165	82
0.786	-0.09351	0.3427	0.03412	0.3569	166	82.5
0.791	-0.08936	0.334	0.03151	0.3472	167	83
0.795	-0.08545	0.3281	0.02865	0.3403	168	83.5
0.8	-0.08201	0.3292	0.02507	0.3402	169	84
0.805	-0.07856	0.3346	0.02076	0.3443	170	84.5
0.81	-0.07498	0.3427	0.01586	0.3512	171	85
0.814	-0.07173	0.353	0.01091	0.3604	172	85.5
0.819	-0.07007	0.3731	0.005882	0.3796	173	86
0.824	-0.06856	0.3988	3.23E-05	0.4047	174	86.5
0.829	-0.06717	0.4264	-0.006012	0.4317	175	87
0.834	-0.06596	0.4559	-0.01219	0.4608	176	87.5
0.838	-0.0646	0.4955	-0.02025	0.5002	177	88
0.843	-0.063	0.5403	-0.0294	0.5447	178	88.5
0.848	-0.06223	0.5894	-0.03849	0.594	179	89
0.853	-0.06178	0.6407	-0.04762	0.6455	180	89.5
0.857	-0.06203	0.7007	-0.05752	0.7058	181	90
0.862	-0.06279	0.7653	-0.06772	0.7709	182	90.5
0.867	-0.06451	0.833	-0.07749	0.8391	183	91
0.872	-0.06774	0.904	-0.08633	0.9106	184	91.5
0.877	-0.07137	0.9796	-0.09555	0.9868	185	92
0.881	-0.0746	1.059	-0.1058	1.067	186	92.5
0.886	-0.07866	1.139	-0.1154	1.148	187	93
0.891	-0.08332	1.221	-0.1247	1.23	188	93.5
0.896	-0.08717	1.305	-0.1351	1.315	189	94
0.9	-0.08989	1.39	-0.1468	1.4	190	94.5
0.905	-0.09263	1.476	-0.1586	1.487	191	95
0.91	-0.09496	1.559	-0.1705	1.571	192	95.5
0.915	-0.09636	1.644	-0.1835	1.657	193	96
0.919	-0.09544	1.732	-0.1993	1.746	194	96.5
0.924	-0.09388	1.818	-0.2154	1.833	195	97

0.929	-0.09178	1.903	-0.2318	1.919	196	97.5
0.934	-0.08851	1.987	-0.2493	2.005	197	98
0.938	-0.08004	2.077	-0.2729	2.096	198	98.5
0.943	-0.07007	2.167	-0.2979	2.189	199	99
0.948	-0.06024	2.256	-0.3226	2.279	200	99.5

Flexion and Abduction Angle, Femur System Relative to Pelvis System

Subject: Average Patient
Activity: Up Stairs SU
Trial number: 0

Time[s]	Flexion[deg]	Abduction[deg]	Meas. #	%Cycle
0	56.26	-4.761	1	0
0.008	55.87	-4.719	2	0.5
0.016	55.47	-4.677	3	1
0.024	55.06	-4.634	4	1.5
0.032	54.62	-4.579	5	2
0.04	54.18	-4.529	6	2.5
0.048	53.71	-4.47	7	3
0.056	53.22	-4.409	8	3.5
0.064	52.73	-4.348	9	4
0.072	52.2	-4.282	10	4.5
0.08	51.67	-4.214	11	5
0.088	51.12	-4.145	12	5.5
0.096	50.54	-4.071	13	6
0.104	49.96	-3.998	14	6.5
0.112	49.35	-3.921	15	7
0.119	48.72	-3.843	16	7.5
0.127	48.08	-3.764	17	8
0.135	47.42	-3.685	18	8.5
0.143	46.74	-3.604	19	9
0.151	46.05	-3.526	20	9.5
0.159	45.34	-3.451	21	10
0.167	44.61	-3.376	22	10.5
0.175	43.87	-3.306	23	11
0.183	43.12	-3.242	24	11.5
0.191	42.36	-3.178	25	12
0.199	41.59	-3.123	26	12.5
0.207	40.8	-3.069	27	13
0.215	40.01	-3.02	28	13.5
0.223	39.21	-2.979	29	14
0.231	38.4	-2.937	30	14.5
0.239	37.58	-2.905	31	15
0.247	36.76	-2.875	32	15.5
0.255	35.93	-2.846	33	16
0.263	35.1	-2.826	34	16.5
0.271	34.27	-2.807	35	17
0.279	33.43	-2.79	36	17.5
0.287	32.6	-2.777	37	18
0.295	31.76	-2.764	38	18.5
0.303	30.92	-2.752	39	19
0.311	30.09	-2.741	40	19.5
0.319	29.25	-2.728	41	20
0.327	28.42	-2.715	42	20.5

0.335	27.59	-2.698	43	21
0.343	26.77	-2.679	44	21.5
0.35	25.96	-2.65	45	22
0.359	25.14	-2.614	46	22.5
0.366	24.34	-2.571	47	23
0.374	23.54	-2.517	48	23.5
0.382	22.75	-2.458	49	24
0.39	21.98	-2.386	50	24.5
0.398	21.21	-2.301	51	25
0.406	20.45	-2.207	52	25.5
0.414	19.7	-2.097	53	26
0.422	18.97	-1.969	54	26.5
0.43	18.24	-1.829	55	27
0.438	17.52	-1.67	56	27.5
0.446	16.82	-1.488	57	28
0.454	16.12	-1.298	58	28.5
0.462	15.44	-1.082	59	29
0.47	14.77	-0.8491	60	29.5
0.478	14.1	-0.6065	61	30
0.486	13.45	-0.3346	62	30.5
0.494	12.81	-0.0543	63	31
0.502	12.18	0.239	64	31.5
0.51	11.56	0.5513	65	32
0.518	10.95	0.8684	66	32.5
0.526	10.34	1.194	67	33
0.534	9.749	1.524	68	33.5
0.542	9.164	1.855	69	34
0.55	8.587	2.183	70	34.5
0.558	8.014	2.51	71	35
0.566	7.448	2.832	72	35.5
0.574	6.893	3.146	73	36
0.582	6.345	3.448	74	36.5
0.59	5.808	3.741	75	37
0.598	5.278	4.022	76	37.5
0.605	4.758	4.286	77	38
0.613	4.249	4.537	78	38.5
0.621	3.746	4.77	79	39
0.629	3.255	4.985	80	39.5
0.637	2.773	5.185	81	40
0.645	2.3	5.368	82	40.5
0.653	1.839	5.532	83	41
0.661	1.388	5.681	84	41.5
0.669	0.9452	5.816	85	42
0.677	0.517	5.932	86	42.5
0.685	0.0949	6.041	87	43
0.693	-0.312	6.136	88	43.5
0.701	-0.7077	6.219	89	44
0.709	-1.095	6.298	90	44.5
0.717	-1.463	6.368	91	45
0.725	-1.824	6.434	92	45.5
0.733	-2.167	6.5	93	46

0.741	-2.494	6.565	94	46.5
0.749	-2.808	6.631	95	47
0.757	-3.102	6.704	96	47.5
0.765	-3.377	6.78	97	48
0.773	-3.634	6.865	98	48.5
0.781	-3.871	6.956	99	49
0.789	-4.084	7.057	100	49.5
0.797	-4.275	7.167	101	50
0.805	-4.444	7.285	102	50.5
0.813	-4.585	7.412	103	51
0.821	-4.7	7.546	104	51.5
0.828	-4.79	7.687	105	52
0.836	-4.848	7.833	106	52.5
0.845	-4.88	7.983	107	53
0.852	-4.879	8.133	108	53.5
0.86	-4.841	8.284	109	54
0.868	-4.776	8.434	110	54.5
0.876	-4.674	8.58	111	55
0.884	-4.536	8.724	112	55.5
0.892	-4.361	8.86	113	56
0.9	-4.152	8.988	114	56.5
0.908	-3.905	9.109	115	57
0.916	-3.617	9.217	116	57.5
0.924	-3.299	9.316	117	58
0.932	-2.935	9.4	118	58.5
0.94	-2.537	9.469	119	59
0.948	-2.102	9.526	120	59.5
0.956	-1.621	9.563	121	60
0.964	-1.112	9.586	122	60.5
0.972	-0.5607	9.593	123	61
0.98	0.0317	9.577	124	61.5
0.988	0.6512	9.551	125	62
0.996	1.314	9.502	126	62.5
1.004	2.003	9.44	127	63
1.012	2.728	9.365	128	63.5
1.02	3.486	9.27	129	64
1.028	4.268	9.168	130	64.5
1.036	5.078	9.052	131	65
1.044	5.913	8.924	132	65.5
1.052	6.77	8.793	133	66
1.06	7.645	8.652	134	66.5
1.067	8.536	8.509	135	67
1.076	9.443	8.363	136	67.5
1.084	10.36	8.215	137	68
1.091	11.28	8.072	138	68.5
1.099	12.21	7.929	139	69
1.107	13.15	7.792	140	69.5
1.115	14.08	7.66	141	70
1.123	15.01	7.531	142	70.5
1.131	15.93	7.411	143	71
1.139	16.84	7.296	144	71.5

1.147	17.73	7.189	145	72
1.155	18.61	7.084	146	72.5
1.163	19.47	6.987	147	73
1.171	20.31	6.89	148	73.5
1.179	21.13	6.796	149	74
1.187	21.93	6.705	150	74.5
1.195	22.69	6.61	151	75
1.203	23.43	6.516	152	75.5
1.211	24.14	6.417	153	76
1.219	24.81	6.316	154	76.5
1.227	25.46	6.21	155	77
1.235	26.07	6.097	156	77.5
1.243	26.65	5.979	157	78
1.251	27.19	5.854	158	78.5
1.259	27.7	5.725	159	79
1.267	28.17	5.589	160	79.5
1.275	28.61	5.447	161	80
1.283	29.01	5.306	162	80.5
1.291	29.39	5.161	163	81
1.299	29.73	5.012	164	81.5
1.306	30.03	4.863	165	82
1.314	30.3	4.71	166	82.5
1.322	30.52	4.56	167	83
1.33	30.72	4.41	168	83.5
1.338	30.87	4.262	169	84
1.346	30.99	4.12	170	84.5
1.354	31.09	3.976	171	85
1.362	31.15	3.84	172	85.5
1.37	31.19	3.709	173	86
1.378	31.19	3.586	174	86.5
1.386	31.16	3.472	175	87
1.394	31.1	3.364	176	87.5
1.402	31.01	3.267	177	88
1.41	30.9	3.18	178	88.5
1.418	30.76	3.104	179	89
1.426	30.59	3.037	180	89.5
1.434	30.4	2.984	181	90
1.442	30.19	2.94	182	90.5
1.45	29.95	2.908	183	91
1.458	29.69	2.887	184	91.5
1.466	29.41	2.875	185	92
1.474	29.12	2.872	186	92.5
1.482	28.81	2.88	187	93
1.49	28.48	2.897	188	93.5
1.498	28.14	2.918	189	94
1.506	27.79	2.947	190	94.5
1.514	27.43	2.98	191	95
1.522	27.06	3.015	192	95.5
1.53	26.69	3.052	193	96
1.538	26.31	3.09	194	96.5
1.546	25.92	3.124	195	97

1.554	25.54	3.155	196	97.5
1.561	25.15	3.179	197	98
1.569	24.76	3.197	198	98.5
1.577	24.37	3.204	199	99
1.585	23.99	3.199	200	99.5